Development of E-Sense: a Flexible *in vitro* Platform to Detects Cardiovascular Risk

R A Smith

PhD 2022

Development of E-Sense: a Flexible *in vitro* Platform to Detect Cardiovascular Risk

Rhys Alexander Smith PhD 2022

A thesis submitted in partial fulfilment of the requirements of Manchester Metropolitan University for the degree of Doctor of Philosophy

Department of Life Sciences Manchester Metropolitan University 2022

COVID-19 IMPACT STATEMENT

The progress of this PhD project was greatly impacted by the COVID-19 pandemic, which coincided with a nation-wide lockdown of the UK from March 2020. During this time, MMU adhered to the measures put in place by the government and closed all campuses, including research labs to all members of staff and students. As easing of restrictions began in late July/early August 2020, MMU began with gradual reopening of research labs to PGR students and technical staff. During this time there was a great hindrance to lab user time with a maximum of 4 hour time slots given to students and only half capacity labs in place. Hours in which labs were open was also severely reduced with advice that students should utilise around 3 days of lab time per week. In addition, university resources were unavailable such as offices which had key pieces equipment such as GraphPad which were not available to PGR students elsewhere. During this time, any and all symptoms of COVID-19 such as sore throat or temperature resulted in mandatory isolation and no access to labs until successive negative tests by way of lateral flow were undertaken. During this time, there was a worldwide shortage in fundamental lab equipment such as plasticware, which resulted in periods which tissue culture as well as some molecular techniques was limited. This culminated in a restricted number of experiments that could have been undertaken in the same timeframe and resulted in a negative impact on the project.

Acknowledgements

First and foremost, I would like to thank my supervisory team for all their help, guidance and support during my project. As well as the COVID-19 pandemic, I experienced personal health issues and would not have been able to progress without the help and understanding of my supervisor Dr Stephen White. His patience and encouragement has helped me beyond measure. In addition, I would like to thank Prof. Tristan McKay who has always been available to help, especially during early development of our TFARs.

Outside of my supervisory team, there are almost too many people to thank at MMU. Firstly, a massive thank you to the inaugural members of Chaka Khan, Ryan Riley (my twin) and Rob Beal, who not only helped to support me but also made my experience all the better on a personal level. Some of my best memories will always be our daily 'fishing trips', not only are they incredible colleagues, but more importantly, better friends. A special thank you to my amazing friends outside the White lab group; Alysha Burrows, Lorna Fitzpatrick, Chip Thornton, Toby Aarons, Fran Bartoli-Leonard, Liam Evans-Hanson (the world's greatest DM). They have been incredible friends since I undertook my master's degree in 2017 all through until now and wouldn't be here without them! A special thank you to Dr Alex Langford-Smith, who maintains he is my lab Mum, who was incredible for helping me during my first year before moving on to greener pastures. The technical team at MMU deserve a note of appreciation, namely Dr Stuart Fielding who has been a great support throughout my time at MMU (I will always remember joke of the day and week).

Finally, a special thank you to my family. I dedicate my thesis to my parents who

have supported me throughout my education and academic career. From a

young age I have had medical issues, which led to me losing most of school years. My parents supported me all the way through and whilst many people may not have been able to, they pushed me to work hard, as they said, “your body might not work but your brain does”. Without them I wouldn’t be where I am today.

Manuscripts and Publications:

R. Smith, R. Beal, S. Satta, A. Langford-Smith, G. Ferris, T. McKay and S.J. White. BMI1 and hTERT Extend the proliferative potential of human coronary artery endothelial cells while maintaining key aspects of endothelial function and mechanosensitivity. Target Journal Scientific Reports. Manuscript in preparation.

R. Smith, R. Beal, A. Langford-Smith, T. McKay and S.J. White. Microplastic BPA Activates a Multifactorial Stress Response and Downregulates Protective Pathways Known to Affect Cardiovascular Risk. Target Journal ATVB. Manuscript in preparation.

S. Satta, R. Beal, **R. Smith**, A. Langford-Smith, G. Ferris, J.E Teasdale, A.T. Tanjeko, J. Serre, G.G. Hazell, G. Sala-Newby, P. Wang, J.L. Johnson, M.J. Humphries, G. Gayan-Ramirez, P. Libby, F. Crea, H. Degens, H.Jia, T.J. Johnson, Y. Alexander, A.C. Newby and S.J. White. *A Nrf2-OSGIN1&2-HSP70 axis mediates cigarette smoke-induced endothelial detachment – implications for plaque erosion.* In press. Cardiovascular Research.

R.Beal, **R. Smith**, S. Satta, A. Langford-Smith, G. Ferris, J. Humphries, M.J. Humphries and S.J. White. Regulation of the endothelial adhesome by pathological and physiological flow, in preparation, target Journal Circ Res.

Bartoli-Leonard F, *Edwards N, Langford-Smith AWW, Tandel S, **Smith RA** , Moreno-Martinez D, Barraclough M, , McCarthy E, Parker B, , , Bruce , Alexander MY, , Wilkinson FL, . Increased miRNA-3148 in Systemic Lupus Erythematosus regulates vascular calcification via RUNX2; a potential vascular protective mechanism? Target Journal ATVB

Conference Participation:

- **2022 -** Northern Vascular Biology Forum meeting (Oral Presentation)
- **2022 –** 17th International Symposium on Biomechanics in Vascular Biology and Cardiovascular Disease (Oral Presentation)
- **2019** – Northern Vascular Biology Forum meeting (Poster Presentation)
- **2019** – Manchester Metropolitan University Symposium (Oral presentation)
- **2019** – NC3Rs Award Winners Summer School (Oral presentation)
- **2019** – BAS/BSCR at the BCS Annual Conference (Poster Presentation)
- **2018 -** BAS/BSCR at the BCS Annual Conference (Poster Presentation)
- **2018** – Manchester Metropolitan University Symposium (Poster Presentation)

Awards:

- **2018** – NC3Rs/BHF 2017 Studentship Competition
- **2018** – Manchester Metropolitan University Symposium image competition prize winner

  2019 – Manchester Metropolitan University Symposium oral presentation prize

winner

Abstract

Coronary heart disease (CHD) is one of the leading causes of mortality and morbidity worldwide. Atherosclerosis (AS), a key mechanism in the potentiation of CHD, is often defined as a chronic inflammatory disease provoked by the oxidation of lipids retained in the arterial wall which results in the formation of atherosclerotic lesions and plaques.

Atherosclerotic plaques preferentially form at predilected sites of bifurcations and branch points exposed to disturbed flow patterns. In contrast, straight sectional regions of the arterial wall which are subjected to laminar flow are relatively spared, implicating the response of endothelial cells to their flow environment in the initiation of the disease. There are a variety of signalling pathways and shear responsive transcription factors known to regulate these processes such as NFκB, AP1 (inflammatory and cytokine response), IRF3 (toll-like receptor signalling), XBP1 (unfolded protein response/ER stress) and KLF2 and Nrf2 (protective signalling pathways).

The understanding of these pathways is built upon decades of research using *in vivo* animal models. This study culminated in the development and validation of a novel endothelial cell-based *in vitro* platform, able to monitor the activity of atherosclerosis-related transcription factors. To facilitate this, a novel human coronary artery endothelial cell line with an extended proliferative potential, reduced senescence and mechanosensitive was created (HCAECPro) in order to circumvent one of the major drawbacks of *in vitro* modelling- the relative short lifespan of primary HCAECs. Transcription factor activator reporters with a novel binding response element, were incorporated into this HCAECPro cell line to create novel ‘E-Sense lines’, which upon validation, exhibited a dynamic range,

several orders of magnitude greater than previously available reporters. Quantification of transcription factor reporter activity with these E-Sense lines allowed for screening of novel compounds to assess their potentiation for atherosclerosis.

The use of plastics in everyday life has steadily increased over the previous few decades, in particular; the use of microplastic, Bisphenol A (BPA). The plastic has come under scrutiny in recent years, with circulating concentrations in the human body significantly higher than previously expected. Although currently considered safe for human consumption, recent studies have suggested it plays a role in the potentiation of endocrine and neurodegenerative disorders. Its potential impact on cardiovascular health is still unknown.

However, the findings within this project demonstrate that exposure to microplastic, Bisphenol A (BPA), exerts a significant effect on several of the key TFARs related to cardiovascular disease progression. Indeed, these findings suggest that BPA causes a reduction of key protective signalling transcription factors KLF2 and Nrf2 under flow, whilst increasing the induction of the stress response possibly via TLR signalling.

List of Figures

List of Tables

Abbreviations

ACS	Acute coronary syndrome
ANOVA	Analysis of variance
AP1	Activating Protein-1
ARE	Antioxidant response element
ATP	Adenosine Triphosphate
BMI1	B lymphoma Mo-MLV insertion region 1
BPA	Bisphenol A
CAD	Coronary artery disease
CDK	Cyclin dependent kinase
cDNA	Complementary Deoxyribonucleic Acid
CSE	Cigarette smoke extract
CVD	Cardiovascular disease
DAPI	4,6'-diamidino-2-phenylindole
DAMP	Damage-associated molecular pattern
DMEM	Dulbecco's modified eagle's medium
DNA	Deoxyribonucleic Acid
EC	Endothelial cell
ECM	Extracellular matrix
ER	Endoplasmic reticulum
ESS	Elevated shear stress
ET	Endothelin
FACS	Fluorescent activated cell sorting
FBS	Foetal bovine serum
FITC	Fluorescein isothiocyanate
HCAEC	Human coronary artery endothelial cell
HDL	High-density lipoprotein
hTERT	Human telomerase reverse transcriptase
IFN	Interferon
IRF3	Interferon regulatory factor 3
KLF	Kruppel-like factor
LDL	Low-density lipoprotein
LPS	Lipopolysaccharide
LSS	Laminar shear stress

MAPK	Mitogen-activated protein kinase
MI	Myocardial infarction
NFkB	Nuclear factor-kappa-B
NO	Nitric oxide
Nrf2	Nuclear factor erythroid 2-related factor 2
OSS	Oscillatory shear stress
Ox-LDL	Oxidised Low-density lipoprotein
PAMPS	Pathogen-associated molecular pattern
PBS	Phosphate buffered saline
PCR	Polymerase chain reaction
PERK	PKR-like ER kinase
PFA	Paraformaldehyde
PI	Propidium Iodide
PRR	Pathogen recognition receptor
PVC	Polyvinyl chloride
qPCR	Quantitative polymerase chain reaction
RNA	Ribonucleic acid
ROS	Reactive oxygen species
RT-PCR	Reverse transcription polymerase chain reaction
SA-β-GAL	Senescence-associated β-galactosidase
SEM	Standard error of mean
TBP	TATA-binding protein
TBS	Tris-buffered saline
TF	Transcription factor
TFAR	Transcription factor activator reporter
THBD	Thrombomodulin
TLR	Toll-like receptor
TNFa	Tumour necrosis factor-α
UPR	Unfolded protein response
VLDL	Very-low-density lipoprotein
VLDLR	Very-low-density lipoprotein receptor
vWF	Von-Willebrand Factor
XBP1	X-box binding protein 1

Chapter 1:

General Introduction

1.0 Cardiovascular Disease and Atherosclerosis

Cardiovascular disease (CVD) is one of the leading causes of morbidity and mortality worldwide. In 2015, it was estimated that 17.9 million people died as a result of cardiovascular disease, with ischaemic heart disease being the leading cause of death. This number is set to rise, with an estimated 22.2 million annual deaths expected by 2030 (World Health Organization, 2022). The incidence of mortality from CVD has steadily increased over the previous few centuries, becoming the world's leading cause of death by the start of the twentieth century, coinciding with the industrial revolution. Originally seen as a predominantly developed world issue, with a high incidence in progressive countries in Western Europe and the USA, recent studies have highlighted its increasing prevalence in developing nations, with around 75% CVD-related deaths occurring in low- and middle-income countries (Gaziano *et al.*, 2010).

Of all the presentations of cardiovascular disease, coronary artery disease and cerebrovascular disease relating to atherosclerosis are at the forefront. Acute coronary syndrome (ACS) is the most threatening manifestation of coronary artery disease (CAD), with events such as myocardial infarction (MI), ischemic sudden death and unstable angina all potentially life-threatening events with poor prognosis (Fuster and Kovacic, 2014). MI is clinically defined by the presence of acute myocardial injury, with abnormal cardiac biomarkers and evidence of acute myocardial ischaemia (Thygesen *et al.*, 2019). MI can be categorised into type I and type II, with type I MI is precipitated by atherothrombotic coronary artery disease (CAD), initiated by atherosclerotic plaque disruption such as erosion and rupture (Thygesen *et al.*, 2019). Type II MI does not present with atherothrombotic plaque

disruption and is caused by an acute mismatch of blood supply and demand (Thygesen *et al.*, 2019).

Atherosclerosis, the major underlying pathological process in the potentiation of CAD; is often described as a chronic inflammatory disease affecting medium and large-sized arteries (Weber and Noels, 2011). In the absence of major predisposing genetic mutation, atherosclerosis is a slow, often clinically silent, process with plaque formation taking decades (Bentzon *et al.*, 2014) (Lieb and Vasan, 2013). Thrombi formation is initiated via disruption of an atherosclerotic plaque, through plaque rupture, plaque erosion or eruption of a calcified nodule (Roberts, 2014)(Silvestre- Roig *et al.*, 2014). Plaque disruption and thrombosis may cause tissue ischemia, leading to MI, stroke or limb ischemia, depending on the location of the occlusion. Atherosclerotic plaque formation may remain clinically silent, or limit tissue perfusion precipitating intermittent hypoxia and symptoms observed in unstable angina; however, atherothrombosis triggering severe myocardial or cerebral ischemia remains the most serious life-threatening complication of atherosclerosis (Virmani, Burke and Farb, 1999). Plaque erosion or rupture are the major substrates for thrombosis within coronary arteries (White, Newby and Johnson, 2016). White et. al. reviewed the available histopathology studies from a variety of countries with differing study criteria, reported a total of 1119 cases to demonstrate that 66% cases of fatal atherothrombosis resulted from ruptured atherosclerotic plaques while 31% were due to plaque erosion (White, Newby and Johnson, 2016). Figure 1.1 (below) demonstrates key differences between typical features of eroded and ruptured atherosclerotic plaques.

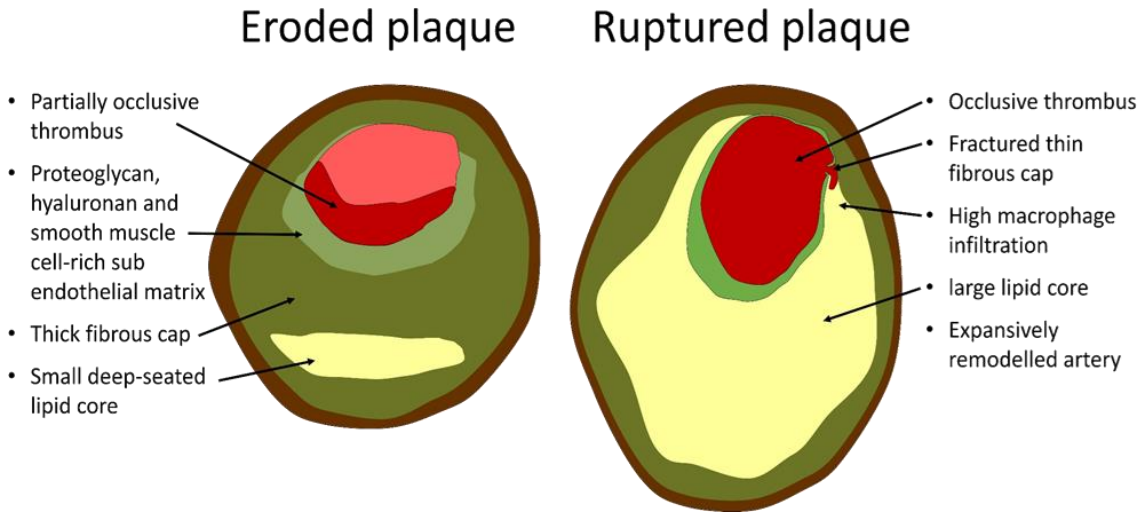

Figure 1.1 Typical differences between eroded and ruptured plaques. Eroded plaques display morphological alterations of matrix below site of erosion with an increase in versican, hyaluronic acid and vascular smooth muscle cells. Eroded plaques contain thick fibrous caps, either containing a deep seated or non-existent necrotic core with less frequent occlusive thrombi. Ruptured plaques however, contain a thin fibrous cap with a proportion of underlying macrophages and extensive lipid core (White, Newby and Johnson, 2016).

1.1 How Shear Stress Confers an Athero-protective or Pro-atherogenic Environment

The arterial endothelium in subjected to three distinct types of hemodynamic forces; (i) hydrostatic pressure (produced via the force acting upon vessel wall), (ii) circumferential tension (produced by traction forces applied by the intracellular connections produced during vascular motility and the pulsatile nature of blood flow) and (iii) shear stress (resulting from the biomechanical forces produced during frictional dragging by blood flow exerted on the arterial wall) (D'Auria *et al.*, 2015). Shear stress is determined by three principal components; blood viscosity, blood flow and vessel geometry, measured in Pascals (Pa) or dynes per square centimetre (dyne/cm^2).

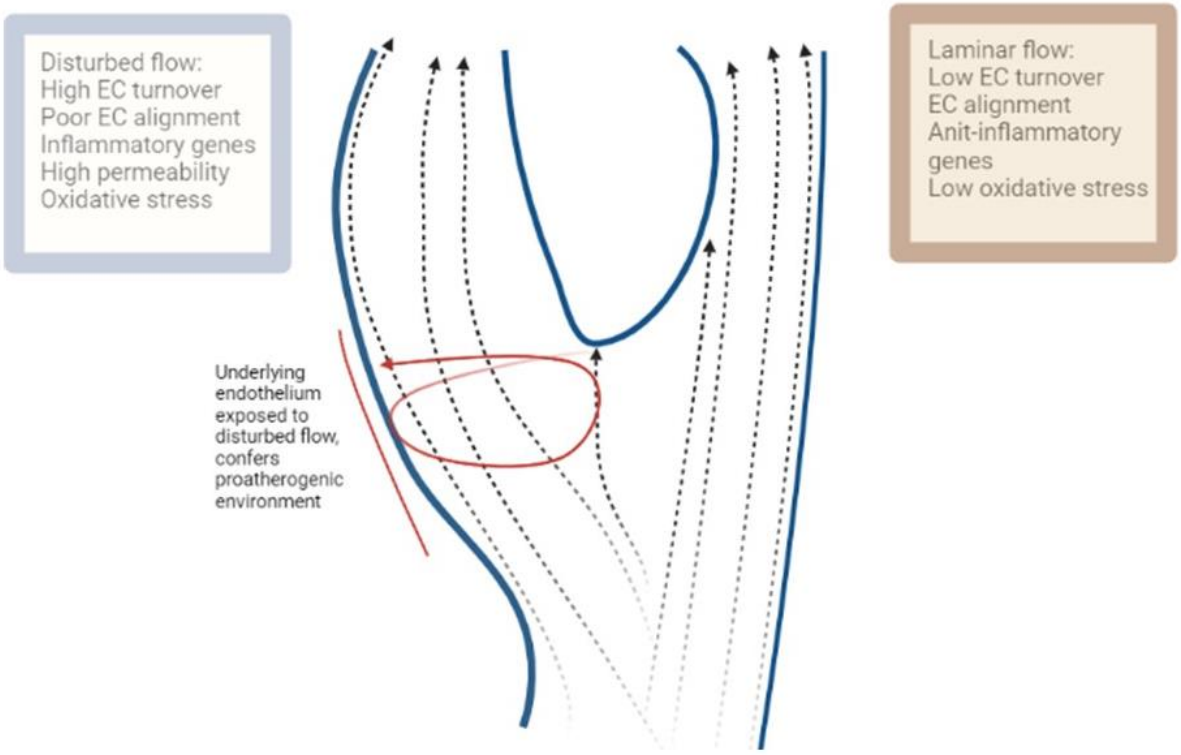

F**igure 1.2: Effects of Flow Environment on the Endothelium.** Straight sectional areas of the arteries are protected from protected from plaque development. These areas result in unidirectional high shear stress, which confer a quiescent, anti-inflammatory phenotype with endothelial alignment in direction of flow. Areas of disturbed flow result in endothelial insult and activation and confer a pro- inflammatory phenotype. These areas have a high EC turnover and present with poor EC alignment and an increase in oxidative stress, resulting in atherosclerosis susceptible areas (Hahn and Schwartz, 2009).

Recent studies have demonstrated the pathological processes leading to atherosclerotic plaque development preferentially occur at sites where the endothelium is exposed to disturbed flow, such as bifurcations leading to focal development of disease, whilst areas subjected to stable laminar flow are more resistant to atherogenesis (D'Auria *et al.*, 2015)(Chistiakov, Orekhov and Bobryshev, 2017). The endothelium in straight sections of arteries that experience laminar flow adopt an athero-protective phenotype, controlled by a

laminar shear activation of transcription factors Nrf2, KLF2, KLF4 and the suppression of the inflammatory response via downregulation of NFκB activity (Nayak, Lin and Jain,

2011). At regions exposed to laminar shear stress, endothelial cells adopt a quiescent, anti-inflammatory phenotype of the endothelium, accompanied with characteristic directional flow alignment, expression of anti-inflammatory genes and a reduction in oxidative stress with low cell turnover and permeability (Zhang and Friedman, 2013)(Chistiakov, Orekhov and Bobryshev, 2017). By contrast, the endothelium at the inner walls of bifurcations and curved sections of artery, where the endothelium experiences multidirectional 'disturbed' blood flow, with a low net time averaged wall shear stress over the cardiac cycle, do not adopt the athero- protective phenotype, rendering these sections of artery athero-prone (Hoogendoorn *et al.*, 2019). Regions experiencing disturbed flow result in a reduced bioavailability of nitric oxide, leading to an increase in neointimal hyperplasia accompanied by infiltration, trapping and oxidation of low-density lipoprotein (LDL) (White, Newby and Johnson, 2016)(Vergallo *et al.*, 2013). These regions are primed for inflammation, experience increased oxidative stress, display no alignment with flow and have increased rates of apoptosis. This amplifies the response to pro- atherosclerotic risk factors and influences the underlying vascular smooth muscle cells (D'Auria *et al.*, 2015).

The response of the endothelium to its haemodynamic environment demonstrates that endothelial cells possess mechanosensitive shear stress transducers, capable of converting physical force to biomechanical signals. Indeed, many EC mechanotransducers have been proposed as a functional flow sensor, however, the exact mechanisms of how they orchestrate shear stress responsiveness is still unclear. So far putative mechanotransducers including ion

channels, integrins, glycocalyx etc have been an area proposed as flow sensors (Hahn and Schwartz, 2009). The glycocalyx, which is carbohydrate rich, resides upon the upper surface of the endothelium, extending 0.4-0.5µM into vessel wall. Some cells in low shear stress regions have a primary cilium, measuring several micrometres. Lateral cell

membrane contains the adhesion receptors platelet/endothelial cell-adhesion molecule 1 (PECAM1) and vascular endothelial (VE)-cadherin, together binding to adjacent ECs. Actin stress fibres, actin cytoskeleton and intermediate filaments, connect mechanically varying cellular regions. Adhesion receptors such integrins and PECAM1 experience tension, which is transmitted to basal membrane (Hahn and Schwartz, 2009). The current school of thought is that under different shear stress patterns, the glycocalyx experiences mechanical tension via drag transmitted to cortical skeleton, concurrently, if present the primary cilium is defected and bends, transmitting force to the membrane and cytoskeleton. Membrane tension and or direct transmission of force to mechanosensors alters ion channel activity and intracellular signalling. Under flow, ATP release and transport near cell surface is also modulated (Hahn and Schwartz, 2009).

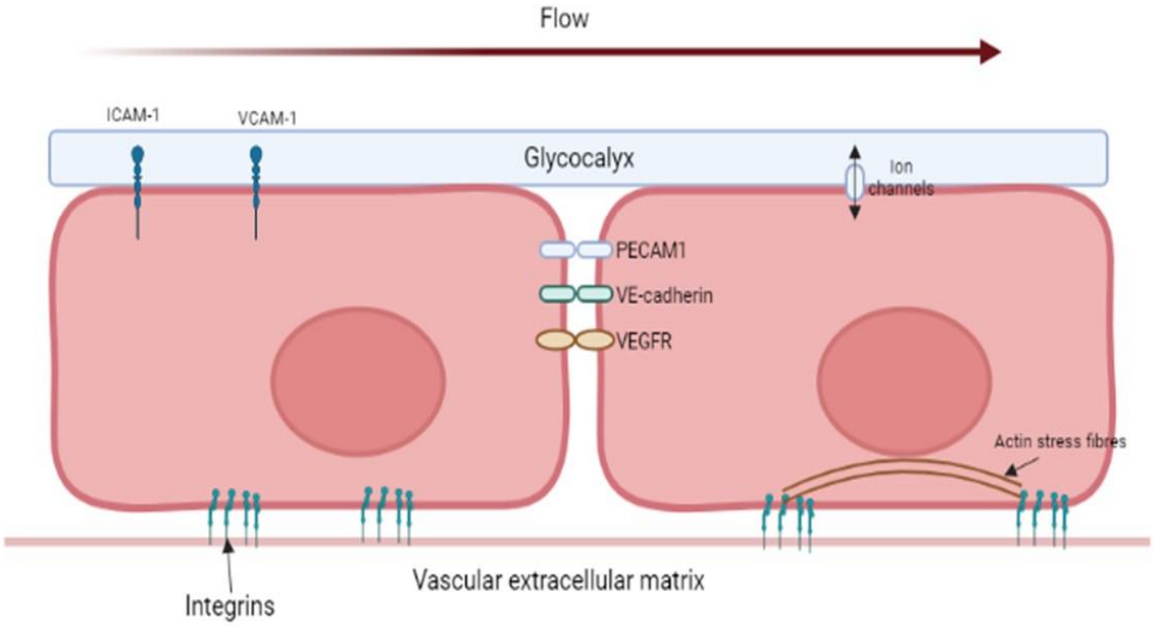

Figure 1.3: Endothelial Cell Mechanotransducers. When experiencing shear stress, the glycocalyx recognises mechanical drag of the blood flow and transmits this to the cortical cytoskeleton. Cilium is deflected top the direction of flow, in addition the mechanical tension is transmitted to the lateral borders and basal membrane, where adhesion receptors PECAM1, VE-cadherin and integrins experience the changes in tension. Ion channels have been show to open in response to alterations of shear stress (Hahn and Schwartz, 2009).

The regulatory action of flow on endothelial cells has been well established, leading to the induction of a plethora of genes due to transcriptional activity of shear- sensitive TFs (White, Newby and Johnson, 2016). Although mechanisms are relatively well understood, the time course of transcriptional activation of these TFs is vital in understanding the initiation and progression of atherosclerosis (Conway *et al.*, 2013). *In vitro* models have revealed what appears to be an initial induction of proatherogenic transcription factors in both laminar and disturbed flow. Indeed, when exposing an endothelial cell monolayer to laminar shear stress that had previously been cultured under static conditions, there is an immediate cascade of signalling events. This initial signalling cascade results in the opening of ion channels release of prostacyclin and NO, increase

ROS signalling and kinase/GTPase activation. In the first hour of laminar shear stress exposure under *in vitro* conditions, proatherogenic transcription factors NFκB and AP1 are activated as well as protective signalling transcription factor KLF2 (White, Newby and Johnson, 2016). However, these events are transient under physiological laminar flow *in vitro*, with the majority of endothelial cell adaptation occurring within the first 24 hours (figure 1.4). When exposing endothelial cells to disturbed flow, these events occur in a similar fashion, however, unlike under laminar shear stress, the induction of proatherogenic pathways is sustained, suggesting that endothelial cell's ability to adapt to their flow environments and downregulate proatherogenic pathways under laminar flow, may be a major difference between the atheroprotective effects of laminar shear stress and the proatherogenic effects of disturbed flow (Jo *et al.*, 1997)(Zakkar *et al.*, 2009)

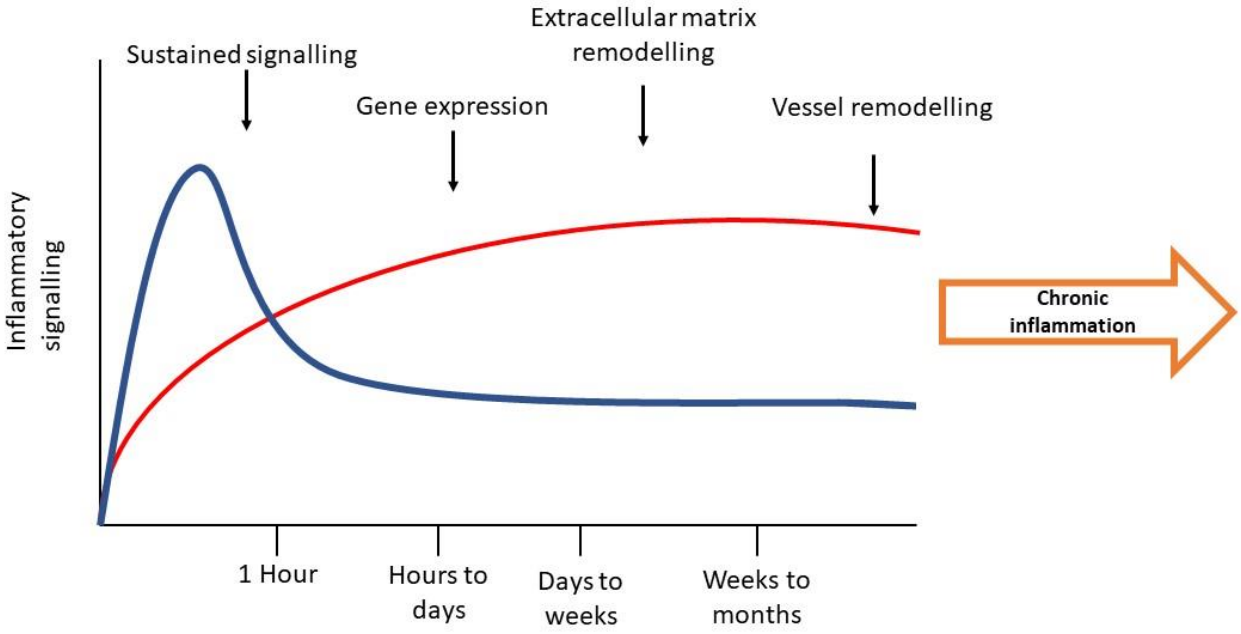

Figure 1.4 Endothelial Activation Timepoints Under Laminar and Disturbed Flow. Initial induction of laminar flow (blue line), results in transient activity of proinflammatory pathways which return to baseline in the first 1-24 hours, concurrently with cellular remodelling and adaptation. Disturbed flow (red line) results in an initial induction of proinflammatory pathways which is subsequently sustained, resulting in alterations in the extracellular matrix (ECM) and integrin engagement which can enhance proinflammation (Hahn and Schwartz, 2009).

1.1.2 Physiological Function of Endothelial Cells

The endothelium plays a major role in the potentiation of atherosclerosis and vascular homeostasis. Composed of a single layer of endothelial cells, the endothelium can be thought of as a dynamic organ, functioning as a regulator of vascular tone, maintenance of blood fluidity and angiogenesis, whilst providing a physical barrier between the blood and the surrounding tissues (Chiu and Chien, 2011). Additionally, the endothelium provides essential functions in regulating immune responses and platelet adhesion. Although it is essential that blood flow remains within the vessels, it also vital that macromolecules and ions must have free passage to the underlying interstitium and cells (Galley and Webster, 2004). This transport of molecules is mediated via the tight junction complex and adherens, which in turn act as a selective barrier to the egress of molecules from circulation. Glucose presents a key molecule required for the underlying tissues and cells of the endothelium. The facilitative glucose transporters, *GLUT-1* and *GLUT-4* have been shown to be expressed on endothelial cells, with *GLUT-1* the most abundant isoform found in the endothelial cells (Galley and Webster, 2004).

As previously mentioned, endothelial cells play a major role in vascular tone, primarily through the production and release of vasoactive mediators such as nitric oxide (NO), prostacyclin and endothelin (ET) (Ait-Oufella *et al.*, 2010). These vasoactive substances are released from the endothelium in response to humoral and mechanical stimuli, resulting in functional and structural changes of the underlying vascular smooth muscle. Nitric oxide is a major vasodilator and the constitutive production by endothelial cells maintains the vasculature in a state of vasodilation. In parallel to the dilatory effects of NO produced by the

endothelium, endothelin (ET) is responsible for vasoconstriction effects, with ET-1 only produced by vascular endothelial cells (Davignon and Ganz, 2004). ET-1 has been demonstrated to exert vasoconstrictive actions via ET_A receptor stimulation in vascular smooth muscle cells, whilst stimulation of ET_B in endothelial cells produced vasodilation effects. ET-1 is known to stimulate cell proliferation and increasing the expression of collagenase, prostaglandin endoperoxidase synthase and platelet-derived growth factor (Galley and Webster, 2004).

As well as passage of molecules, the endothelium regulates leukocyte trafficking and its movement into the underlying tissues, through tightly regulated processes involving adhesion molecules (Chiu and Chien, 2011). These adhesion molecules mediate the adhesion of leukocytes by binding to specific ligands thus binding them to the endothelium. Some of the notable adhesion molecules expressed in endothelial cells are P-selectin, E-selectin, vascular cell adhesion molecule (VCAM) and intracellular adhesion molecule-1 (ICAM-1) (Sung *et al.*, 2007). ICAM-1 and VCAM are able to interact with activated lymphocytes due to the expression of leukocyte function-associated antigen-1 (LFA-1). Lymphocytes are also able to interact with endothelial cells under basal conditions due to L-selectin receptor (Sung *et al.*, 2007). Adhesion molecules of L-selectin such as LFA-1 are involved in the transient adherence of endothelial cells and leukocytes. The movement of the adherent cells between tightly adjacent endothelial cells and the underlying interstitium is regulated by sequential activation steps, thus allowing for the integrity of the endothelium to be maintained whilst simultaneously allowing for the movement of activated inflammatory cells at site of infection and disturbance (Ait-Oufella *et al.*, 2010).

The endothelium provides an essential role in vascular homeostasis, with endothelial cells and vascular smooth muscle cells expressing a variety of proteins which directly participate in homeostasis. The engagement of these proteins, in particular coagulation proteins by their specific receptors on the vascular wall results in cellular activation and gene expression of coagulation, angiogenesis, adhesion and regulation vascular wall tone. The signals which induce these gene expressions are mediated by protease-activated receptors (Chistiakov, Orekhov and Bobryshev, 2017).

1.1.3 Endothelial Senescence

A major drawback of current endothelial *in vitro* modelling is the relative short lifespan of primary endothelial cells in culture. In current cellular models, anecdotal evidence demonstrates human umbilical venous cells (HUVECs) and human coronary artery endothelial cells (HCAECs) are able to be passaged to ~p6 before induction of cellular senescence and phenotypic alterations. *In vivo*, endothelial cells are constantly exposed to damaging stimuli such haemodynamic forces, which can result in telomeric and non-telomeric DNA damage, mitochondrial damage, and sensory pathway alterations (Sun and Feinberg, 2021). These damage-induced stimuli can result in the activation of tumour suppressor pathways p53-p21 and $p16^{INK4A}$, whereby proliferative arrest and senescence occurs (He *et al.*, 2005). In culture, the induction of cellular senescence results in observable changes in an endothelial cell's morphology, such as enlarged, elongated and refractory changes with diminished or abolished mechanosensing properties (Rossman *et al.*, 2017). The cells remain metabolically active, however, secrete a variety of inflammatory molecules which

can directly interact with healthy endothelial cells resulting in an increase in the signalling cascade which induces cell cycle arrest. The secretion of these inflammatory factors has been linked with in an increase in arterial dysfunction and cardiometabolic diseases (Erusalimsky, 2009).

A primary endothelial cell's lifespan presents an issue for continued *in vivo* modelling, particularly in terms of economical and labour-intensive costs. Researchers are presented with a small window in order to produce data which is not impacted due to an increase in inflammatory signalling or reduced proliferative potential of the cell. In order to circumvent this, strides have been made in extending an endothelial cell's lifespan beyond natural constraints. Currently, commercially available hTERT-immortalized dermal microvascular endothelial cells are able to be purchased from ATCC. This method of proliferation-extension focuses on telomere attrition related senescence. During human development and aging, senescence is engaged in tissue in response to varying types of damage. Telomere damage in one of the key aspects of senescence, with these highly repetitive DNA structures located on the ends of chromosomes (Erusalimsky, 2009)(Kuilman *et al.*, 2010). Telomeres are made of a simple double-stranded DNA repeat, (TTAGGG)n, with a repeat sequence occurring for 2-30kbp, containing a guanidine-rich single-stranded 3'-overhang (50-200 nucleotides in length) (Meyne, Ratliff and Moyzis, 1989). This single strand repeat results in the formation of a T-loop (hairpin loop structure), accompanied with proteins that enable telomeres to cap chromosomal ends thus protecting from deterioration or fusion with neighbouring chromosomes (Victorelli and Passos, 2017). Telomere driven senescence is induced via DNA polymerase α's inability to fully replicate the ends of linear DNA molecules, resulting in

telomere length shortening during each DNA replication (McHugh and Gil, 2018). Once repetitive DNA replication occurs, the telomere length shortens excessively, resulting in critical telomere shortening (~12.8 repeats of repetitive clusters) (Victorelli and Passos, 2017). Once this threshold has been exceeded, telomere length shortens to an extent in which they are unable to 'cap' chromosomal ends, resulting in progressive DNA erosion and eventual cell-cycle arrest (Nandakumar and Cech, 2013).

Telomeres are protected by shelterin, a multiprotein complex able to prevent the DNA damage response by coating the telomere, thus inhibiting end-to-end chromosome fusions which result in telomere crisis (Palm and de Lange, 2008). In conjunction, cells lacking critical shelterin components such as POT1 and TRF2 have been shown to exhibit an atypical DNA damage response, consequently resulting in premature senescence (Denchi and De Lange, 2007). These cells are advertised as expressing specific endothelial surface proteins and undergo tubule formation in culture with morphology similar to that of a primary cell counterpart. It should be noted, ATCC does not appear to have demonstrated that hTERT-Immortalized cells remain mechanosensitive. Additionally, although advertised as 'immortal', it is expressed the cells have an extended lifespan rather than continue to proliferate indefinitely, with a passage limit not stated.

In addition, other routes have been implemented in order to extend the proliferative capacity of cells in culture, namely BMI1. The BMI1-encoding gene is a key epigenetic regulator and has been shown to be involved in the proliferative and senescent cellular pathways (Yadirgi *et al.*, 2011). BMI1 in a known repressor of the p16 encoding locus, INK^{4a} thus inducing an extended

proliferative effect. Currently, BMI1 overexpression has been implemented and has successfully extended the proliferative capacity of human epithelial cells, however, has not been previously implemented in the use case of primary endothelial cells(Tan *et al.*, 2020).

1.2 Transcriptional Regulation of Atherosclerosis

Intracellular signalling cascades from diverse shear-sensors, can converge to modulate key transcription factors. As previously stated, the vascular endothelium controls vascular homeostasis through modulation of these transcriptional programmes, resulting in a pro-atherogenic or athero-protective environment (Virmani, Burke and Farb, 1999)(White, Newby and Johnson, 2016). Cardiovascular research in previous decades has allowed us to discern how a wide array of disease relevant signalling pathways can be funnelled down to a few transcription factors that modulate many aspects relating to atherosclerosis progression by regulating the expression of thousands of that control athero-protection, inflammation and cell stress.

1.2.1 Transcriptional Mechanisms of Atheroprotection

Atherosclerosis is a focal inflammatory disease of the cardiovascular arterial system, involving the dysregulation of a number of different cell types, principally endothelial cell dysregulation (Davignon and Ganz, 2004). Endothelial cells in regions of normal and disturbed flow experience different haemodynamic environments, conferring opposing alterations in transcriptional regulation. In straight sections of arteries, endothelial cells experience an atheroprotective environment of normal laminar flow, with these areas usually spared from disease (Chien, 2008). In these areas, shear-sensors cascade and modulate key athero- protective programmes, predominantly through the increase in activity of transcription factors NF-E2-related factor 2 (NRF2), Kruppel-like factor 2 (KLF2) and

4 (KLF4). For example, KLF2 regulates the expression of over 1000 genes in endothelial cells, demonstrating the potential influence of this single shear-regulated transcription factor in regulating endothelial phenotype (Boon *et al.*, 2010).

1.2.2 Transcriptional Mechanisms of Atheroprotection by NRF2

NRF2 is a ubiquitously expressed antioxidant transcription factor, regulating the expression of cytoprotective genes in response to exogenous and in-situ signals. The transcription factor belongs to the bZIP factors within the CNC family proteins, which regulate gene expression, tissue differentiation and development in a plethora of organisms. Six highly conserved NRF2-ECH homology (Neh)

domains, Neh1- Neh6, comprise the NRF2 protein (He, Ru and Wen, 2020) (Satta *et al.*, 2017). Each of these domains play a crucial role in the interaction and activation of NRF2, Neh contains the CNC-type bZIP region, crucial for DNA binding and dimerization with other transcription factors. Additionally, Neh1 is essential for the homo- or heterodimerisation with Maf proteins and leucine zipper containing protein domains. Neh2 presents in the N-terminal region of NRF2, possessing two motifs; DLG and ETGE which are responsible for direct interaction with Keap1 which is plays an essential role in homeostatic condition regulation via NRF2 degradation (Tebay *et al.*, 2015) (Ahmed *et al.*, 2017). As the Neh2 domain lies in the N-terminal, Neh3 resides within the C-terminal region of NRF2 and acts as a transactivation domain which enables the transcription of the antioxidant response element (ARE)- dependent genes via interaction with chromo-ATPase/helicase DNA binding protein, CHD6 (Ahmed *et al.*, 2017). Domains Neh4 and Neh5 coordinate with the co-activators CREB/ATF4 (CBP) and brahma-related gene 1 (BRG1). Finally, the Neh6 domain, as with the Neh2 domain is responsible for the interaction with the Keap1 pathway for NRF2 degradation, with the NRF2 expression in cells exposed to oxidative insults, mediated by redox-insensitive Neh6 (Deshmukh *et al.*, 2017).

There are several defence strategies in order to prevent endothelial cell dysfunction, resulting in atherogenesis, one of which involves prevention of free radical toxicity via excessive ROS production and dysregulation of the antioxidant defence system. Vascular endothelial cells require reactive oxygen species (ROS) signalling in order to maintain vascular homeostasis (Alhayaza *et al.*, 2020). Although ROS signalling is vital to maintain the endothelium, excessive production, or ineffective quenching promotes endothelial dysfunction, atherogenesis and decreased NO availability (Xu and Zou, 2009). This delicate homeostatic balance in the endothelium has been shown to be primarily

mediated by the antioxidant response, a programme of gene expression controlled by Nrf2, through biding to the antioxidant response element (ARE) (Satta *et al.*, 2017). The ARE, commonly referred to the electrophile response element is a cis-acting regulatory element involved in the modulation of gene activity resulting in antioxidant protein production and phase II detoxifying enzymes such as NQO1 (NADPH: quinone oxidoreductase), ferritin, GPx (glutathione peroxidase) and HO-1/ HMOX1 (heme oxygenase). Both constitutive and inducible expression of these ARE-regulated genes has been shown to be modulated by transcriptional activity of NRF2 (Chen *et al.*, 2015). These phase II enzymes mediate the protective mechanism against electrophile and oxidative stress due to their ability to conjugate redox-cycling chemicals. The antioxidant defensive mechanism of the ARE has been extensively studied in hepatic detoxification studies, however, the role of the ARE in antioxidant defence of the vascular system via induction of HO-1 and ferritin has been a major area of research (Chen *et al.*, 2015). A considerable amount of evidence suggests HO-1 plays a vital role in the pathogenesis of diseases regulated by oxidative stress and has served as a possible therapeutic target. Indeed, studies have shown that the induction of HO-1 in vascular cells results in the suppression of oxidised low-density lipoprotein-induced monocyte transmigration and results in atherosclerotic lesion formation inhibition in *Ldlr*$^{-/-}$ mice. The significance of HO-1 in the protection against atherogenesis has been further demonstrated. The hypercholesterolemic mouse model, *ApoE*$^{-/-}$ containing *HMOX1*$^{-/-}$ displayed an enhanced development of atherosclerosis in comparison to *ApoE*$^{-/-}$ only mice (Ishikawa *et al.*, 2001). HO-1 signalling and expression in macrophages, exhibits protective roles in atherosclerosis. *HMOX1*$^{-/-}$ mice display an upregulation of ROS generation, increase in inflammatory cytokines and treatment with TNFα results in increased foam cell formation – this has been attributed to the increase

in expression of scavenger receptor A (SR-A). In addition, smooth muscle cells in *HMOX1*$^{-/-}$ mice have an increase in neointimal formation and greater cell death due to enhanced oxidative stress susceptibility (Kishimoto, Kondo and Momiyama, 2019). The iron sequestrant, ferritin, which protects endothelial cells from oxidative- mediated cytolysis, is known to be upregulated in response to oxidative stress, providing an additional defence mechanism to protect the endothelium from dysregulation (Juckett *et al.*, 1995).

NRF2/ARE signalling is highly conserved amongst all species across the biosphere, known to be in control of a wide variety of genes such as those mentioned previously (Satta *et al.*, 2017). The relationship between NRF2 and the antioxidant response element was first highlighted in 1994 by Moi et al and a study by Chan et al in 2001 revealed NRF2-null mice displayed decreased basal and inducible expression of ARE-regulated genes in addition to an increase in oxidative stress and antioxidant capacity (Chan, Han and Kan, 2001)(Moi *et al.*, 1994).

NRF2 activation in the endothelium can be initiated by an increase in ROS production and PI3K-Akt signalling when endothelial cells are exposed to laminar shear stress (Chen *et al.*, 2015). Endothelial cells which have been infected via adenoviral overexpression of NRF2, demonstrated a significant reduction in several inflammatory genes. The inducible expression of VCAM1, TNFα, monocyte chemoattractant protein-1 (MCP1) and IL-1β are known to be regulated by redox mechanisms, which are, as previously mentioned, regulated by the expression of NRF2 (Saha *et al.*, 2020).

NRF2-regulated gene expression is primarily controlled by Kelch-like erythroid cell derived protein with CNC homology-associated protein 1 (KEAP1), resulting in NRF2 degradation (Deshmukh *et al.*, 2017). Under homeostatic conditions,

NRF2 is sequestered by KEAP1 which promotes it ubiquitination and degradation. Pro- oxidant electrophilic attack of the cystines in KEAP1, releases NRF2 from KEAP1 allowing translocation of NRF2 to the nucleus (Wardyn, Ponsford and Sanderson, 2015). Heterodimerisation of Nrf2, predominantly with MAF proteins, facilitates binding to ARE's and transcriptional activation of genes (Baird and Yamamoto, 2020)(figure 1.5, below).

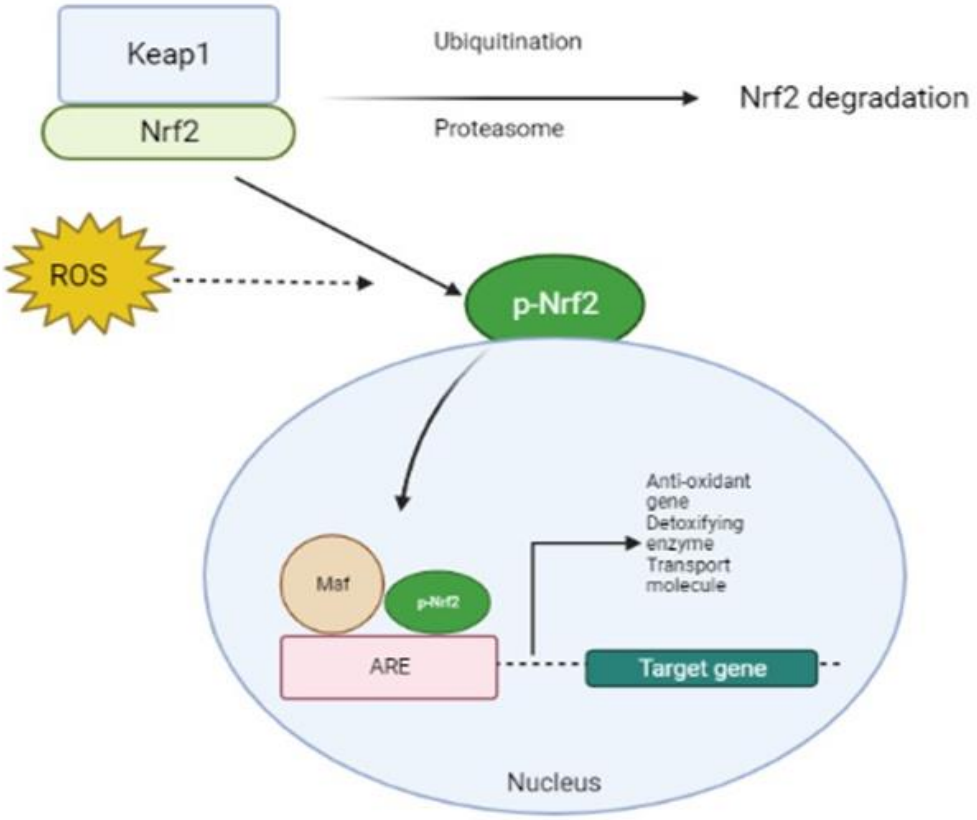

Figure 1.5: NRF2-Keap1-ARE Signalling. NRF2 is ubiquitinated via Keap1 and degraded within the proteosome. After ROS insults, NRF2 is activated via phosphorylation (p-NRF2) thus inactivating Keap1. P-NRF2 then accumulates within the nucleus, binding to the ARE resulting in downstream signalling of antioxidant genes (Oh and Jun, 2

1.2.3 Transcriptional Mechanisms of Atheroprotection by KLF2 and KLF4

The expression of Kruppel-like factor 2 (KLF2) and KLF4 are upregulated by laminar shear stress in endothelial cells. This modulation results in the induction of profound change in endothelial gene expression, altering >1000 genes, with concomitant anti- inflammatory and atheroprotective effects (Teasdale *et al.*, 2017). While there is significant overlap in the genes regulated by KLF2 and KLF4, there are some distinctions between them. KLF2 & KLF4 are vital mediators of vascular protective effects, induced through physiological and pharmacological stimuli. The transcription factors are essential for the induction of anti-inflammatory, anti- thrombotic and vasodilatory factors such as thrombomodulin (THBD), endothelial nitric oxide synthase (eNOS) and c-type natriuretic peptide (CNP) under laminar flow (Lago *et al.*, 2011).

The Kruppel-like factor family of transcription factors (KLFs) are a subclass of the zinc finger family of DNA-binding TFs(Dang, Pevsner and Yang, 2000). Although KLFs are part of the zinc finger family of transcription factors, there are a variety of features which distinguish them apart. KLF proteins contain 3 Cys2/His2 zinc terminus at the C terminus with the interfinger space sequence containing a highly conserved 7-aa sequence, TGEKP(Y/F)X. Most of the KLFs are able to bind with other similar DNA sequences, for example the 'CACCC' sequence or 'GT' box (Jain, Sangwung and Hamik, 2014). Structural studies revealed that the DNA-binding specificity is dictated by 3 critical residues within each zinc finger, although these zinc finger domains are similar, the non-binding domains are highly divergent (Jain, Sangwung and Hamik, 2014).

The first subset of the KLF family identified in mammals in 1993, which were observed in red blood cells, subsequently identified as the erythroid Kruppellike

factor – EKLF/KLF1 (Haldar, Ibrahim and Jain, 2007). KLF1 was shown to play an essential role in the synthesis of the β-globin gene and erythrocyte development. Since the initial discovery, 17 mammalian KLFs have been identified and subsequently designated KLF1-17 based on chronological date of discovery (Haldar, Ibrahim and Jain, 2007). The members of the KLF family that have currently been discovered have been shown to play key roles in the regulation of various cellular process in several distinct cell types. Indeed, it has been demonstrated that KLF2, 4 and 6 are expressed in endothelial cells and play essential roles in EC biology and regulation (Suzuki *et al.*, 2005).

The transcription factor KLF2 has been demonstrated to be specifically induced by laminar shear stress in endothelial cells, whilst disturbed flow negatively regulates KLF2 (figure 1.6) (Lago *et al.*, 2011). Laminar shear stress induced KLF2 activation through the increase in protein levels via activation of the *KLF2* promoter and mRNA stabilisation. The myocyte enhancer binding factor 2 (MEF2), which binds to the MEF2 binding site, is implicated in *KLF2* promoter transcriptional activation, which is activated via upstream mitogen activated protein kinase (MAPK) signalling cascade (Boon *et al.*, 2010). Within this induction of signalling, consists of MAPK kinase-5 (MEK5) as well as extracellular-signal-regulated kinase-5 (ERK5, official gene name MAPK7). KLF2 expression in endothelial cells confers regulation of endothelial cell quiescence and gene expression during vasculogenesis. The deletion of KLF2 in endothelial cells has been demonstrated to have detrimental effects on vascular homeostasis, leading to complications in vascular tone cardiac dysfunction and induction of bleeding (Sangwung *et al.*, 2017). The induction of KLF2 via laminar shear stress results in the inhibition of proinflammatory cytokine expression, with KLF2 overexpression shown to highly induce and

eNOS (Boon and Horrevoers, 2009). In addition, KLF2 is known to modulate the transcriptional activity of proinflammatory TF, NFκB.

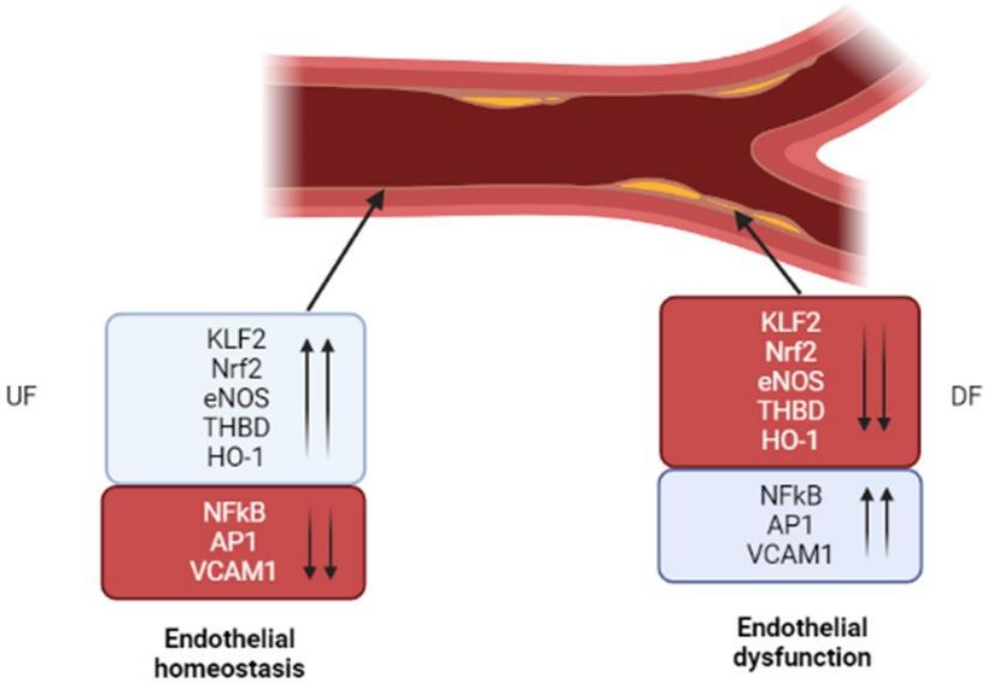

Figure 1.6: KLF2 expression in regions of laminar and disturbed flow. In areas of the arterial wall exposed to laminar shear stress (unidirectional flow- UF), KLF2 is upregulated conferring an increase in activity of downstream anti-thrombotic genes whilst inhibiting pro-inflammatory genes. Conversely, predilected sites under disturbed flow inhibits KLF2 expression and upregulates proinflammatory targets (Dabravolski *et al.*, 2022)(Huang *et al.*, 2021).

There is direct competition between KLF2 and NFκB activity, through competition for a shared co-factor p300 and PCAF. KLF2 diminishes NFκB activity by sequestering p300/PCAF from NFκB. KLF2 is also able to transcriptionally regulate NFκB subunit, p65 via p300/PCAF recruitment and reduced histone 3 lysine 9 (H3K9) and H4K8 acetylation, conversely NFκB recruitment of p300 cofactor results in an inhibitory effect on KLF2 activity (Jha and Das, 2017).

Endothelial cells demonstrate various defence mechanisms in increased inflammatory events, with the expression of adhesion molecules such as vascular cell adhesion molecule-1 (VCAM-1) and E-selectin, initial events for endothelial cell health defence against pro-inflammation and leukocyte attachment induction (Jha and Das, 2017). During KLF2 overexpression, VCAM-1 is observed to be strongly inhibited as well as the inhibition of tissue factor, thus suggesting KLF2 strongly attenuates the expression of cellular adhesion molecules in endothelial cells. A study in 2015 by Doddaballapur et al, showed that the atheroprotective mechanism produced when the endothelium is exposed to laminar shear stress results in the alteration of endothelial cell metabolism via KLF2-mediated repression of 6- phosphofructo-2-kinase/fructose-2,6-biphosphatase-3 (PFKB3). It was shown that there was reduction in the mitochondrial glucose uptake of endothelial cells under laminar shear stress, which was reversed by silencing *KLF2* (Doddaballapur *et al.*, 2015).

1.3 Transcriptional Mechanisms of Pro-Inflammation

The atheroprotective mechanisms induced by laminar flow are absent at regions of disturbed flow, thus priming for endothelium activation (Gimbrone and García-Cardeña, 2016). Many of the lifestyle factors associated with atherosclerosis risk mediate their effect through the increase in the inflammatory, oxidative and cellular stress pathways, modulated through the transcription factors; NFκB, AP1, XBP1 and IRF3 as described below.

1.3.1 TLR4 Signalling

Atherosclerosis, often regarded as a chronic, oxidised lipid-induced inflammatory disease, associated with endothelial dysfunction resulting in accumulation of atherogenic lipoproteins (Linton *et al.*, 2019). Endothelial cells recognise danger- and pathogen-associated molecular patterns (DAMPS & PAMPS), with lipopolysaccharide one of the most widely studied PAMPs. DAMPs and PAMPs are able to bind to pattern recognition receptors (PRR) such as Toll-like receptors (TLRs) (Zhu, Huang and Zhao, 2022). Oxidised LDL is recognised as a DAMP and binds to and activates TLR4 resulting in a signalling cascade that results in the activation of both IRF3 and NFκB, via two discreet pathways; MyD88-independent and MyD88-dependent (Figure 1.7) (Kumar, 2020) (Ve *et al.*, 2017). TLR4 MyD88- independent pathway results TIR-domain-containing adapter-inducing interferon-β (TRIF) activation (den Dekker *et al.*, 2010). TRIF activates transcription factor Interferon (IFN)-Regulated Factor 3 (IRF3), leading to transcriptional regulation of IRF3 target genes. MyD88-dependent, TLR activation results in binding of MyD88 to the intracellular TIR domain of TLR4, facilitating the phosphorylation of IL-1R Associated Kinase 1 (IRAK1) by IRAK4 (Verstak *et al.*, 2014). Tumour necrosis factor associated receptor 6 (TRAF6) is then able to bind to the IRAK4-IRAK1 phosphorylated complex, with subsequent

IRAK1-TRAF6 dissociation from TLR to activate complex of transforming growth factor β activated kinase (TAK1), TAK1- binding protein 1 (TAB1) and TAB2/3. TAK1 activates NFκB inhibitor IκB kinase complex (IKK), resulting in IκB protein phosphorylation (Park *et al.*, 2014). These IκB protein sequester NFκB factors within the cytoplasm in an inactive form, however, upon phosphorylation of IκB's they are degraded resulting in nuclear translocation of NFκB leading to transcription of pro-inflammatory genes (Mankan *et al.*, 2009).

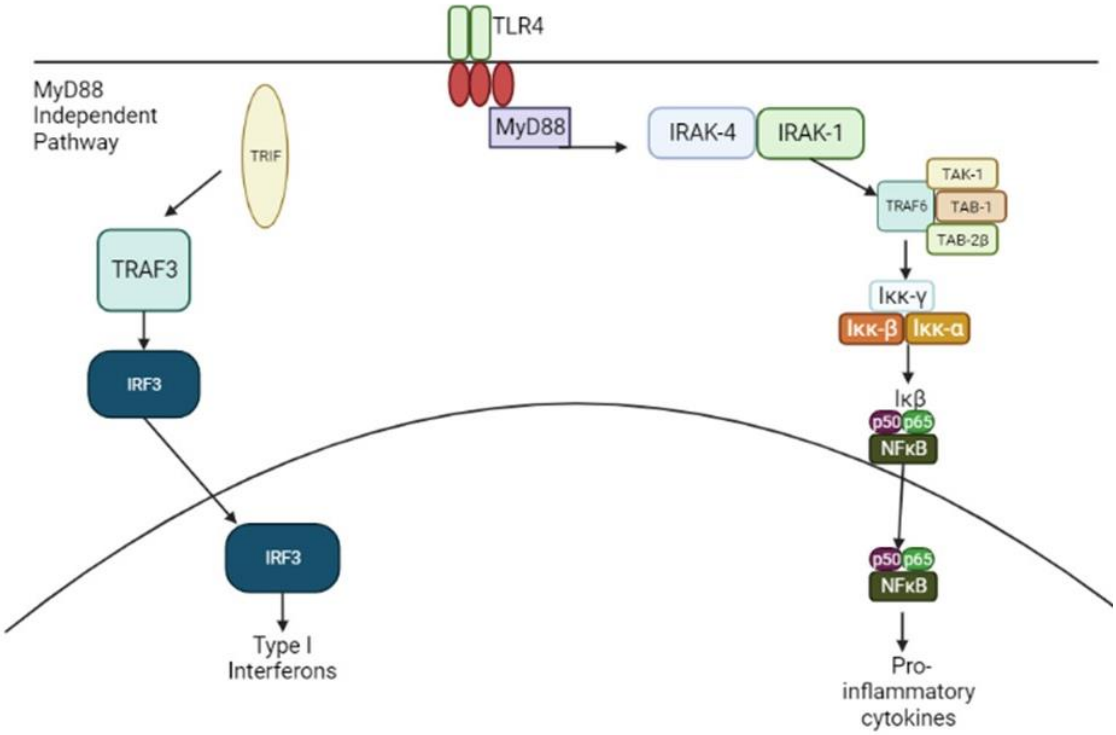

Figure 1.7: Downstream TLR4 signalling cascades via MyD88-dependent and independent pathways. (den Dekker *et al.*, 2010) Schematic diagram of the differential induction of IRF3 via the MyD88-independent pathway utilising TRIF and TRAF6 vs induction of the NFkB and the inflammatory cytokine response via the MyD88-dependent pathway.

The role of IRF3 in regulating atherosclerosis and plaque stability has been investigated. Lieu et al, in 2017 demonstrated that IRF3 was more abundant in the coronary arteries of CHD patients as well aortic root in hyperlipidaemic mice, especially in endothelial cells, implying an important role of IRF3 in endothelial homeostasis and CVD. Knockout of IRF3 (*IRF3*$^{-/-}$) significantly reduced atherogenesis in hyperlipidaemic mice. From their study it was deduced that IRF3 directly increased ICAM1/VCAM1 expression and promoted monocyte-macrophage infiltration which results in cytokine production and accelerated endothelial cell injury (Liu *et al.*, 2017). They also demonstrated an increase in markers of plaque stability in *IRF3*$^{-/-}$ mice, deducing IRF3 promotes plaque instability (see figure 1.8).

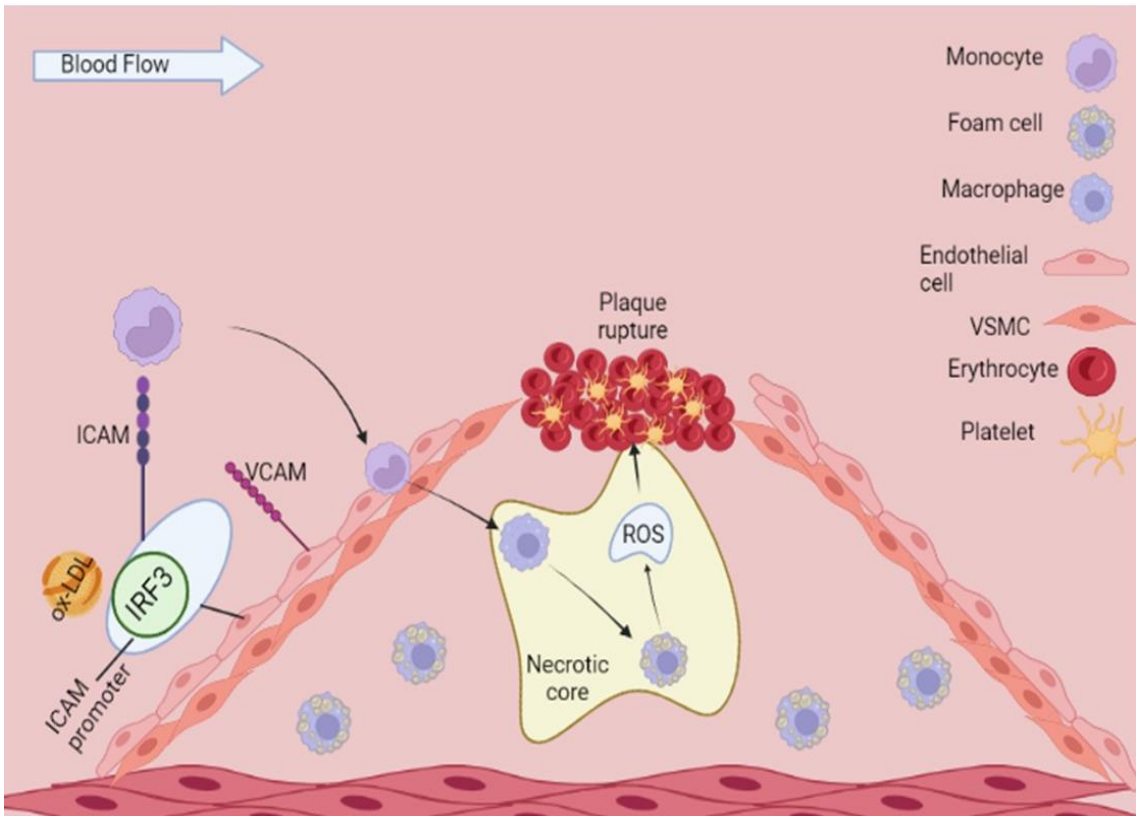

Figure 1.8: IRF3 Promotes Plaque Instability. In hyperlipidaemic environments, IRF3 promotes transcriptional induction of ICAM and subsequently VCAM within endothelial cells resulting in an increase macrophage migration and subsequently increasing inflammation (Liu *et al.*, 2017).

1.3.2 MAPK and NFκB Inflammation

Two, key proinflammatory pathways; mitogen-activated protein kinase (MAPK) and nuclear-factor-kappa-B (NFκB), have been shown to be differentially modulated at protected and susceptible sites within the arterial tree (Warboys *et al.*, 2011). It is most likely that the activation of both contributes to inflammation and lesion development in predilected sites, as proinflammatory genes such as VCAM-1, E- Selectin and IL-8 require both for transcription to be induced. There are three well characterised MAPK pathways; c-Jun N-terminal Kinase (JNK), p38 and extracellular signal-regulated kinase (ERK). MAPK activation leading to a proinflammatory response has been linked to atherogenesis and plaque formation (Warboys *et al.*, 2011). Indeed, this proinflammatory signalling has been demonstrated to induce MAPK phosphatase-1 (MKP-1), which results in a negative regulation of MAPK via p38 and JNK inactivation. Inflammatory cytokines and stress preferentially activate the JNK and p38 pathways, whilst growth factors induce ERK activation (Zakkar *et al.*, 2008). The activation of JNK and p38 is dependent on the upstream activity of MAPK kinases (MAPKKs – MKK3 and MKK6). The phosphorylated forms of JNK and p38 results in the induction of transcription factor activating protein-1 (AP1) and subsequent family of activators, c-Jun and activating transcription factor 2 (ATF2) (see figure 1.9 below) (Gangnuss *et al.*, 2004). The activity of JNK/p38 has been shown in subsequent studies to be negatively regulated by shear stress, with unidirectional shear stress inhibiting JNK activity via blocking the cleavage of protein kinase C epsilon (Magid and Davies, 2005). This MKP-1 activation has been shown to be significantly induced in cultured endothelial cells exposed to unilateral flow, thus laminar flow induces an atheroprotective phenotype by reducing MAPK activity. MKP-1 was also shown to increase p38 activation and increase VCAM-1 expression through its silencing in endothelial cells. This has been shown to be

intrinsically linked with protective signalling pathway, Nrf2, which is proposed to suppress endothelial cell activation by reducing MAPK Kinases 3/6 (MKK3/6) signalling to p38 and induces enhanced activation of MKP-1 (Pua *et al.*, 2022)(Zakkar *et al.*, 2008).

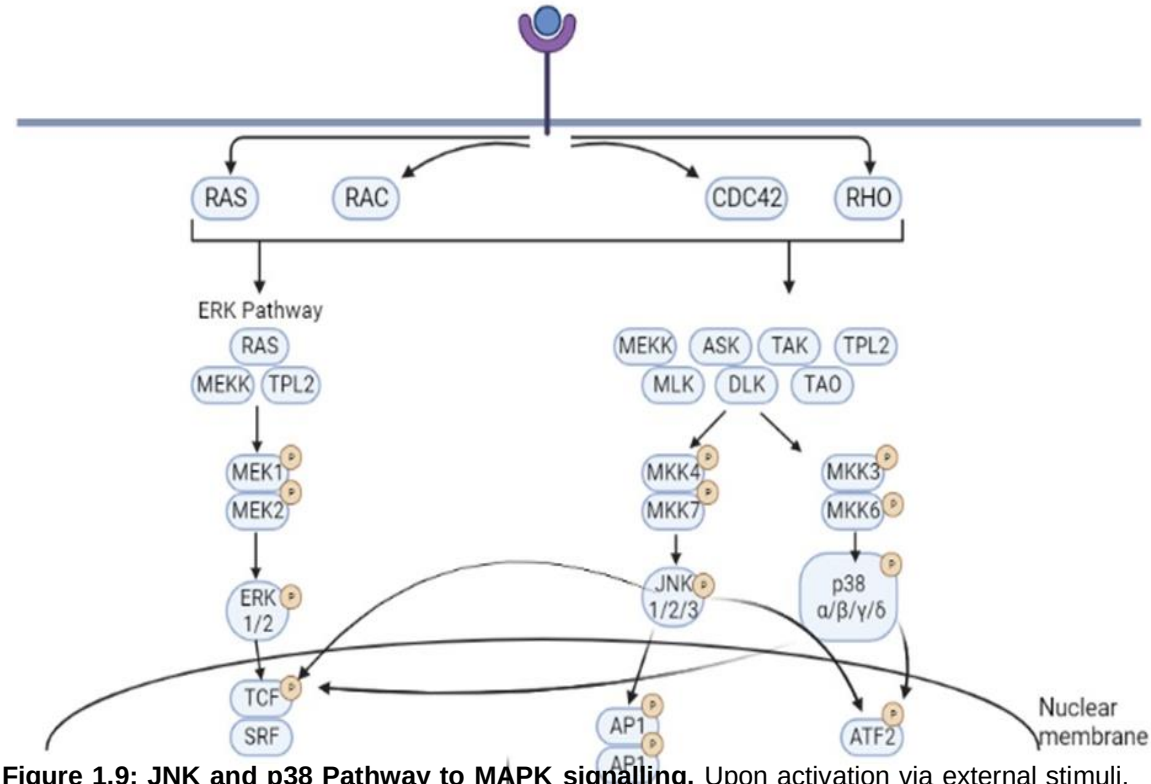

Figure 1.9: JNK and p38 Pathway to MAPK signalling. Upon activation via external stimuli, ERK, JNK and p38 MAPK pathways are activated with sequential protein phosphorylation. These activated MAPK translocate to the nucleus and trigger cellular response, inducing AP1 transcriptional activity (Pua *et al.*, 2022).

NFκB modulates a variety of processes such as immunity, inflammation and cell survival, which have closely linked it to cardiovascular health. The induction and subsequent signalling of NFκB in endothelial cells typically leads to an increase in the expression of genes which regulate the recruitment of inflammatory cells to vessel wall e.g. TNFα, IL-1, ICAM-1. NFκB is a dimeric transcription factor, part of the Rel family which constitutes a highly conserved Rel-homology domain (RHD). This RHD is the primary mediator of inhibitor kappa B (IκB) protein interaction, NFκB translocation to the nucleus and DNA-binding (Mankan *et al.*, 2009). The IκB regulatory proteins, consisting of IκBα, IκBβ and IκBγ bind to NFκB via ankyrin repeats, thus preventing the nuclear translocation leading to transcriptional induction. The NFκB family of proteins is made of five dsicreet monomers; p65 (RelA), RelB, c-Rel, p50/p105 (NFκB1) and p52/p100 (NFκB2), which exist as homo/heterodimers bound to IκB family proteins (Wan and Lenardo, 2010). The major signalling pathways of NFκB activation have been characterised into two 52athogen cascades; canonical/classical pathways (mediated by IκB degradation) and the non-canonical/alternative pathway (mediated by p100) (Warboys *et al.*, 2011). The activation of the canonical pathway is typically due to inflammatory stimuli such interleukins, tumour necrosis factor-α (TNFα) or lipopolysaccharides (LPS) which results in IκB kinase (IKK) activation complex containing IKKKα, β and γ subunits. Upon stimulation by proinflammatory cytokines, this signalling results in activation of β subunit of IKK, leading to the phosphorylation of IκB proteins on two N-terminal serine residues (Harhaj and Dixit, 2011). The alternative pathway of activation is mediated through IKKα activation leading to p100 phosphorylation. The ubiquitin ligase machinery recognises phosphorylated IκB resulting in polyubiquitination and subsequent degradation, in the case of p100 this processing occurs in the proteosome. Freed NFκB dimers translocate to the nucleus whereby

they bind to the promoter and enhancer regions of target genes at specific sequences (Warboys *et al.*, 2011). Once activated, NFκB can then be downregulated by a variety of mechanisms, including the feedback mechanism which results in newly synthesised IκBα proteins binding to nuclear NFκB and subsequent exportation out to cytosol (Oeckinghau and Sankar, 2009)

Active NFκB and its regulated molecules have been identified in atherosclerotic plaques and early lesions, highlighting its role in atherogenesis. It has been demonstrated that mice lacking the IKKγ expression, fed on a high-fat, cholesterol rich diet, demonstrated reduced inflammation and plaque formation, supporting NFκB's mediated proinflammatory gene expression is crucial in lesion formation (Gareus *et al.*, 2008). In addition, *in vivo* studies found in healthy mice and pigs, that the expression of NFκB subunits p65, IκBα and Iκβ3 was significantly increased in regions of the aortic wall in predilected sites which experiences low shear stress in compariaons to regions experiencing normal unidirectional flow. *In vivo* pig studies also described the expression of NFκB negative regulator, Cezanne in these athero-prone regions, demonstrating a marked expression (Passerini *et al.*, 2004). Cezanne (Cellular Zinc-finger Anti-NFκB) has been previously shown to be induced via TNFα and IL-1, functioning as an inhibitor of NFκB. This inhibition results in a negative feedback loop for inflammatory cytokine signalling. The anti-inflammatory effects of Cezanne were demonstrated, with a suppression in NFκB activation in response to TNFα via the cleaving of polyubiquitin chains from RIP1- a member of the TNFR complex (Luong *et al.*, 2013). The expression of Cezanne has been subsequently shown to be increased in areas of laminar flow by Warboys et al.

1.3.3 The Unfolded Protein Response

Work over the last two decades has elucidated several factors in the pathological processes of atherosclerosis. This work has revealed that endoplasmic reticulum (ER) stress and the subsequent induction of the unfolded protein response, is a major event for the initiation and progression of atherosclerosis. Insults that can impair ER function such as oxidative stress, ischemic insults and enhanced expression of normal/folding defective protein leads to the accumulation of unfolded proteins resulting in ER function abnormalities (Zeng *et al.*, 2009). The unfolded protein response (UPR) is an adaptive response activated to ensure ER homeostasis maintenance. The UPR is known to triggered in mammalian cells by protein kinase RNA-like ER kinase (PERK), inositol-requiring protein 1α (IRE1α) and activating transcription factor 6 (ATF6) (Tsuru *et al.*, 2016). A critical role UPR signalling is to reduce protein synthesis in order to re-establish ER homeostasis. Activated ERK inhibits protein synthesis by phosphorylating IRE1α and eukaryotic initiation factor 2α (eIF2α), which could result in mRNAs degradation via IRE1-dependent decay (RIDD). A co- ordinated regulatory transcriptional network is then activated, containing transcription factors ATF4, ATF6 and X-box binding protein 1 (XBP1), which regulate genes which modulate ER homeostasis (De Nisco *et al.*, 2021) (Tsuru *et al.*, 2016). Upon activation. ATF4 translocates to the nucleus, resulting in induction of genes that encode amino acid transporters and oxidative stress protectors. Active ATF6, by way of limited proteolysis post translocation from ER to golgi apparatus, regulates ER chaperone and XBP1 expression (Park, Kang and So, 2021)(Tsuru *et al.*, 2016). In order to exist in its activated form, XBP1 undergoes mRNA splicing, controlled by IRE1α, which then undergoes nuclear translocation and modulates transcriptional regulation of ER chaperones and components of ER-

associated

degradation (ERAD) (Tsuru *et al.*, 2016). X-box binding protein 1 (XBP1) is a key mechanosensitive signal transducer relating to endoplasmic reticulum stress response. XBP1 has been shown to be highly expressed in atherosclerotic plaque predilection sites such as bifurcations where the underlying endothelium experiences disturbed flow. In *ApoE*$^{-/-}$ mice, these sites where XBP1 activity was highest, correlated with an increase in lesion size and severity (Zeng *et al.*, 2009). *In vitro* models have indicated that sustained experience to disturbed flow results in an increase in XBP1 splicing in endothelial cells, which in turn induces an increase in apoptosis and endothelial loss (Zeng *et al.*, 2009). Additionally, a study by Civelek et al., highlighted the increased ER stress activation in predilected sites. Indeed, using a nonatherosclerotic pig model, they were able to demonstrate an increase in IRE1α, ATF6 and XBP1 in athero-susceptible regions of coronary and non-coronary arterial regions (Civelek *et al.*, 2009).

The UPR presents as a major adaptive response in order to maintain ER integrity, with unresolved UPR leading to apoptotic cell death. Inflammation and apoptosis represent two well documented processes in atherosclerosis initiation and development with evidence suggesting UPR activation occurs during early and advanced atherosclerotic lesions (Zhou and Tabas, 2013). Figure 1.10 below outlines the role of the UPR and XBP1 activation in predilected sites of atherosclerosis development.

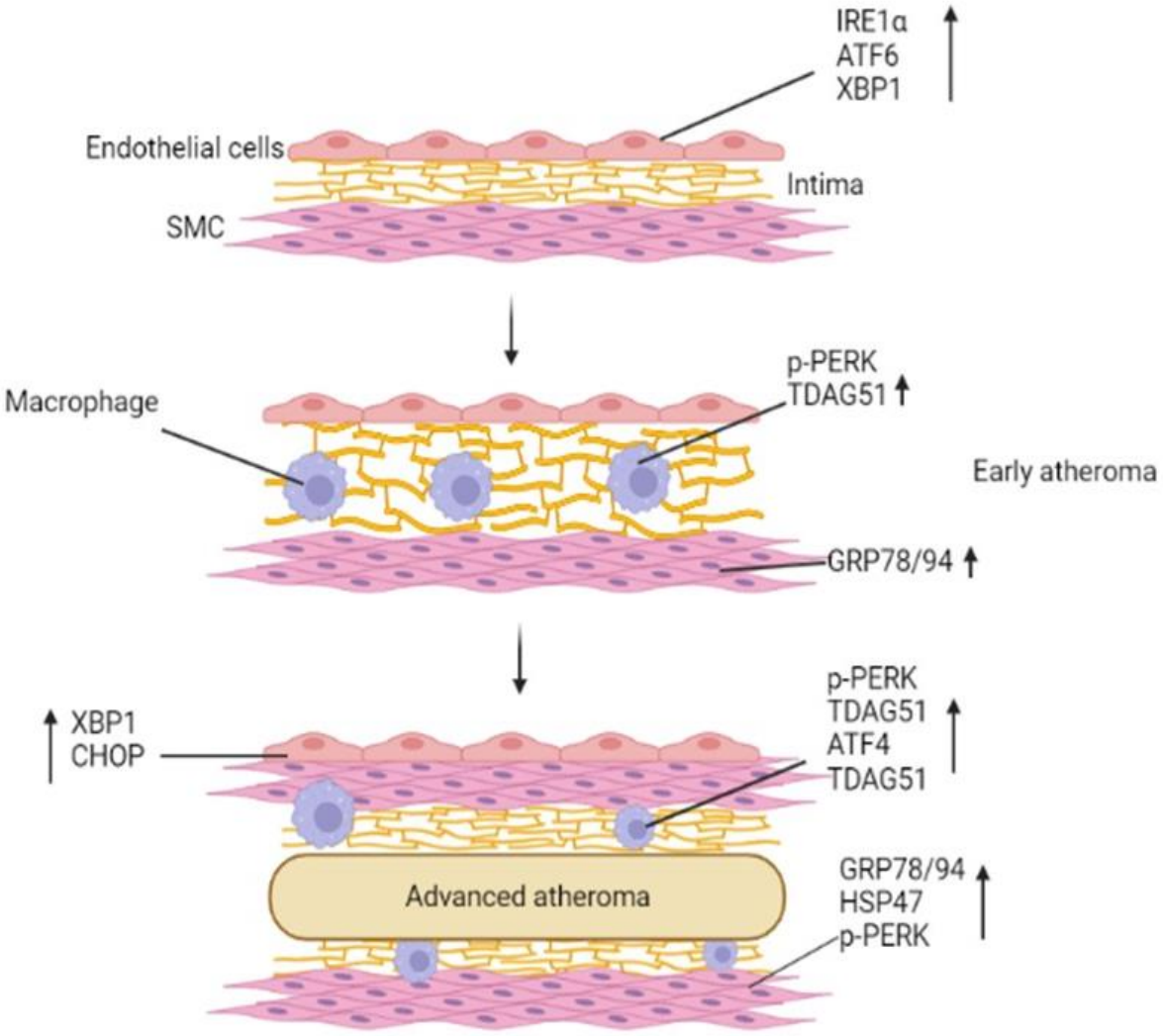

Figure 1.10: UPR Signalling in Atherosclerosis Development. Endothelial cells in predilected sites such as bifurcations which experience disturbed flow, are primed ER chaperone expression, resulting in an induction of ATF6, IRE1α and XBP1. PERK is activated in macrophages, endothelial cells and smooth muscle cells in lesions associated with advanced atherosclerosis. Sustained PERK induces CCAAT/enhancer binding protein homologous protein (CHOP) which induces apoptosis. Early expression of endothelial XBP1 results in EC chaperone expression, which is thought to become detrimental in advanced lesions. Resulting increase in XBP1 splicing to activated form through IRE1α activation may result in increased apoptosis activity (Zhou and Tabas, 2013).

1.4 *In* Vitro platforms of Atherosclerosis Disease Modelling

As previously mentioned, atherosclerosis is characterised as a chronic immune disease and remains asymptomatic until plaque formation becomes extensive enough to cause a stenosis leading to eventual rupture or erosion leading to myocardial infarction, ischemic stroke and subsequent morbidity or mortality (Lichtman *et al.*, 2013). In the earlier stages, the disease is driven by an increase in cholesterol-rich, apolipoprotein B-containing lipoproteins being retained at specific predilection sites (i.e., bifurcations). These mechanisms, in most part have required the use of animal models to mimic human disease, however, discerning an appropriate species has proved challenging. Recapitulating human disease perfectly is animal models is unrealistic, with best fit the current methodology, with different species chosen based on a specific area of research. The use of non-human primates provides the most appropriate in terms of similarities to human physiology and clinical significance, however, they are difficult to maintain due to costs, ethical issues and time consumption, with disease developing over a longer period.

Current *in vitro* Cell Models of Atherosclerosis

Although atherosclerosis disease is still predominantly examined in animal models, great strides have been made in *in vitro* modelling over the previous few decades. *In vitro* platforms are generally classified into 2D and 3D models (Chen *et al.*, 2022).

2D *in vitro models*

Currently, the most widely used *in vitro* modelling system are 2D models, which have proven essential for studying the pathology and drug evaluation for a variety of diseases and cell types. The most common variant of 2D modelling is the use of single-cell culture systems, containing one type of cell component, in the case of atherosclerosis endothelial cells, smooth muscle cells and macrophages are

the most common cell types utilised (Chen *et al.*, 2022). These single-cell cultures have been extensively used to assess new types of therapeutics such as microRNA, exosomes, and mechanistic atherosclerotic studies. Although extensively used in these therapeutic approaches, more recently they have been increasingly used for the evaluation of drug-loaded delivery systems efficacy in the treatment of atherosclerosis, due to issues observed in free drug administration (Jensen and Teng, 2020). However, despite the widespread use of single-cell models, single-cell models present a drawback for the prediction of therapeutic efficacy in patients with models unable to mimic native features in human plaque formation. For example, under static conditions, endothelial cells are not considered 'active' due to the lack of a shear stress environment with many key shear-sensing genes downregulated (Simmons, Kumar and Jo, 2016).

Microfluidic Chips

As mentioned earlier, the lack of a shear-regulated environment such as that found within human blood vessels presents a challenge in atherosclerosis research. More recently, there has been an increase in the development in *in vitro* systems which incorporate vascular flow, in order to reduce the reliance on *in vivo* and *ex vivo* animal models. The emergence of microfluidic chip models, such as an endothelium on a chip, have become ever more present in atherosclerosis modelling (Pattanayak *et al.*, 2021). Microfluidic chip models present with several advantages over conventional 2D single cell models, such as an enhanced sensitivity, ability to subject endothelial cells to a variety of flow environments and continuous monitoring (Liao *et al.*, 2018).

An endothelium on a chip model was created by Zheng et al in order to evaluate early atherosclerosis formation (Zheng *et al.*, 2016). The model investigated the effects of shear stress, glucose transport, LDL and ROS production on

endothelial function in the earlier stages of the disease. For this particular model, endothelial cells were seeded into the chip in order to form a monolayer, later treated with glucose or low-density lipoproteins (LDL) under low fluid shear stress and cyclic stress in order to mimic a hyperglycaemic or hyperlipidaemic environment. Results from this model demonstrated the novel finding that endothelial cells seeded and exposed to the hyperlipidaemic chip model, displayed significantly sharper decreases in VE-Cadherin levels than compared to static culture counterparts, demonstrating the advantages of models that incorporate shear stress comparable to that found in the vasculature (Zheng *et al.*, 2016).

The effect of differential flow patterns and endothelial orientation and realignment is a crucial area of endothelial biology that has to be considered when using *in vitro* models (Conway *et al.*, 2013). Conventional 2D models cannot recapitulate this reassembly of the endothelial cytoskeletal structures and stress fibres. A recent study by Baratichi et al., introduced the concept of microfluidic chip system which allowed for the generation of disturbed flow and low wall shear stress between the ridges on the chip (Tovar-Lopez *et al.*, 2019). This system was able to demonstrate the effects of the flow environment on endothelial cells. In addition to the opposing realignment of the cytoskeletal structure under disturbed flow, it was also demonstrated that the nucleus circularity index of cells increased under disturbed flow with a decrease in nuclear area coverage (Tovar-Lopez *et al.*, 2019).

3D Models

Similarly, to the 2D endothelium-on-a-chip, a major area in *in vitro* modelling has been the creation of the 3D vessel-on-a-chip, a form of an organ-on-a-chip (OOC). OOC systems is classed as a biomimetic *in vitro* microfluidic platform developed through the combination of cell biology, microfluidic technology and

tissue engineering, including biomaterial science applications (Liao *et al.*, 2018). The advancements of vessel-on-a-chip systems have been developed through the seeding of cells on a fibre scaffold. An example of the implementation of this type of model was created by the Li group, in which endothelial cells were seeded on a highly oriented electorspun poly-scaffold (Xu *et al.*, 2021). Under perfusion, the endothelial cells realigned to the direction of flow in a similar geometry to natural vessel endothelium and displayed improved endothelialisation (Xu *et al.*, 2021).

Although greatly increasing in the generation in more developed systems, vessels-on-a-chip have focussed on the creation of non-diseased systems, and limited application on atherosclerotic vessels-on-a-chip, with the technology still in its infancy. One such study, investigated by Joore et al., looked at the biological processes associated with atherosclerosis by studying monocyte adhesion to the endothelium utilising tubular vessels-on-a-chip (Poussin *et al.*, 2019). These tubular vessels were created by seeding human coronary artery endothelial cells onto collagen and culturing the cell-collagen complex under perfused flow. Using this approach, the authors demonstrated that when treated with TNFα, the vessels expressed significant ICAM-1 proteins with an increase in monocyte recruitment (Poussin *et al.*, 2019).

Chapter 2

Methods and Materials

2.1 Cell culture

HCAECs

Human coronary artery endothelial cells (supplied by Promocell) and HCAECPro were continually cultured using Endothelial cell growth medium, MV2 (Promocell) supplemented with 100 U/ml penicillin/streptomycin and Promocell supplement pack at 37^{O}C with 5% CO_2. Once cells had reached a confluency >80%, cells were passaged at a 1 in 3 ratio utilising standard trypsin technique, Trypsin-EDTA (Lonza). When passaging, cell pellet was obtained by centrifugation for 5 minutes at 300g.

HEK293T

HEK293T cells were maintained in Dulbecco's Modified Eagle's Medium (DMEM) (Lonza) see table 2.1 supplemented with 10% foetal bovine serum (FBS), 1% L-glutamine, and 1% Pen/Strep.. Cells were passaged when reaching 90-100% confluency at a 1:6 ratio (high split ratio due to high proliferative rate of HEK293Ts).

Table 2.1: HEK293T Cell Culture Media

Component	Volume
DMEM	435mL
FBS	50mL
L-Glutamine (200mM)	10mL
PenStrep (100x)	5mL (1x)

Parallel Plate Flow

Primary HCAECs and HCAECPro were seeded onto glass side, previously gelatin coated, within a silicon gasket with 9.3cm^2 growth area at a density of 2.5x10^5 cells/slide for three days to ensure confluency and contact inhibition of replication to mirror in vivo conditions. Cells were maintained under three different types of flow; oscillatory (± 5 dynes/cm^2, 1 HZ), laminar (15 dynes/cm^2) and elevated (75 dynes/cm^2). Endothelial culture media MV2 without ascorbic acid and hydrocortisone supplementation was supplemented with 3.35% dextran in order to establish comparable viscosity with plasma (see table 2.2). Cells were maintained under varying flow conditions for 72 hours in order to allow full adaptation to their flow environment. Figure 2.1 (below demonstrates parallel plate flow setup).

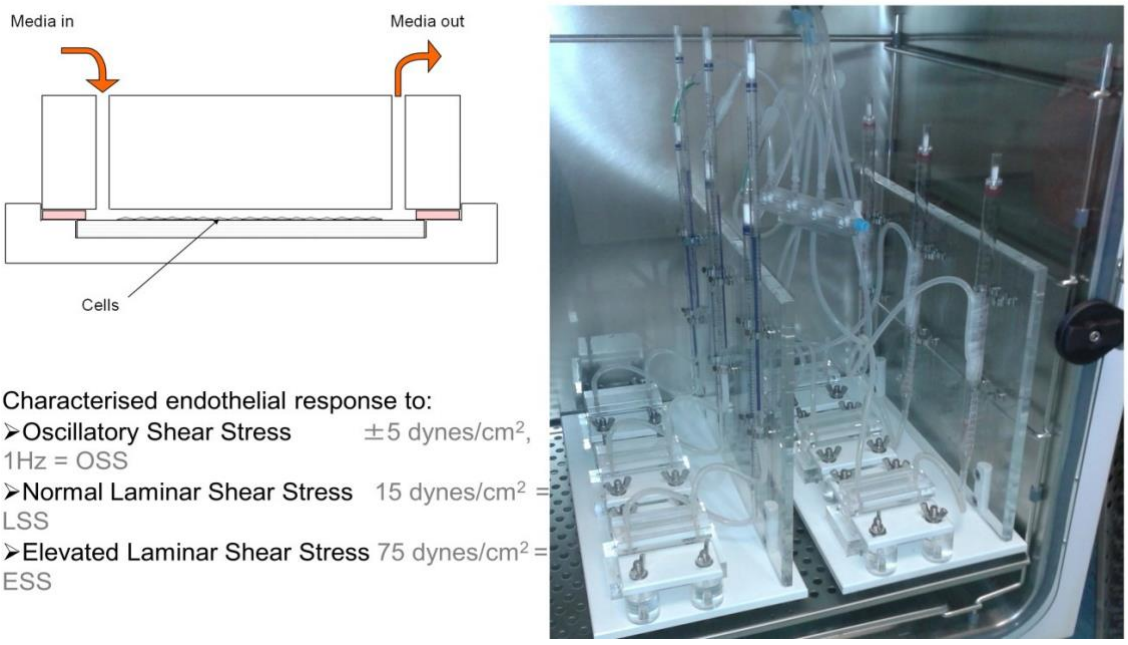

Figure 2.1 Schematic diagram of in-house parallel plate flow chambers.

Primary HCAECs and HCAECPro cells were seeded onto a 0.1% gelatine coated slide at a density of 2.5x10^5 cells/slide and allowed to adhere for three days before induction of flow. Cells were exposed to either OSS, LSS or ESS for 72 hours in order to adapt and induce changes relating to flow environment. After 72 hours, flow system was disassembled, where chamber slides were either fixed for immunofluorescence or lysed in order to extract RNA.

Table 2.2: Culture Media for HCAECs Under Flow

Component	Volume/Concentration
Endothelial Cell Medium MV2	500mL
Foetal Calf Serum	(As supplied) To final conc of 0.05mL/mL
Epidermal Growth Factor	(As supplied) To final conc of 5ng/mL
Basic Fibroblast Growth Factor	(As supplied) To final conc of 10ng/mL
Insulin Like Growth Factor	(As supplied) To final conc of 20ng/mL
Vascular Endothelial Growth Factor	(As supplied) To final conc of 0.5ng/mL
Dextran	3.146g/100mL

2.2 Lentiviral production and Transduction

293T cells were transfected with 3rd generation lentiviral vector constructs to create HIV-based self-inactivating (SIN) lentiviral vectors, for generation of BMI1 and hTERT.

Day 1: HEK293T cells were split into a 6-well plate at a $2.5x10^5$ cells/well. Day 2: cells transfected using Viafect (Promega) using White Lab packaging: envelope ratio (see table 2.3). Day 3: media change to target media of choice (MV2). Day 4: Viral supernatant was collected and filtered through 0.45µM filter, supernatant can be added directly onto target cells with the addition of DEA-Dextran or stored at $-80^{O}C$.

Table 2.3: Lentiviral Production Components

Component	Concentration/Volume
Δ8.9	0.55µg
VSV-G	0.075µg
Backbone (target vector)	0.625µg
Viafect	10µL
Optimem	125µL

(Δ8.9 and VSV-G at a ratio of 8:1 by mass, mix well and incubate at room temperature for 20 minutes),

Once viral supernatant had been collected, HCAEC and HCAECPro cells were seeded in a 12-well delta plate at a seeding density of $2x10^5$ cells/well. Once cells had reached ~50% confluency, 0.5mL of viral supernatant was added per well for 12-18 hours. The following day, the viral supernatant was aspirated off and replenished with 0.5mL Promocell MV2 media. Cells were then continually passaged as normal.

2.3 Senescence-Associated β-galactosidase Staining

Initially cells were fixed with PEM (PIPES, EGTA and Magnesium) buffer at 37^OC for 15minutes (see immunocytochemistry), washed x2 with phosphate buffered saline (PBS) containing $MgCl_2$ (1mM) (pH 6.0) and stained for 2-4 hours (see table 2.4). Stain was then washed twice using PBS + $MgCl_2$ and imaged utilising phase contrast of Zeiss brightfield microscope. Quantitative image analysis was performed utilising ImageJ Fiji software.

Table 2.4: SA-β-Galactosidase Staining

Potassium Ferrocyanide	5mM
Potassium Ferricyanide	5mM
X-Gal	1mg/mL (used from 20mg/mL stock)

***Made up 1M $MgCl_2$ and dilute in 1/1000 in PBS.**

2.4 RNA Isolation and Purification

Cells of interest were lysed in 350μL buffer RL containing 1% β-mercaptoethanol. Isolation and purification of RNA was performed using the Total RNA Purification Plus kit provided by Norgen Biotek. RNA purification was carried out according to user manual.

2.5 Reverse Transcription Reaction (cDNA Generation)

Throughout the project, cDNA was generated using the commercially available QuantiNova Reverse Transcription kit supplied by Qiagen. Generation was accomplished by following user manual. Each reaction used RNA at a concentration of 250ng. Reverse transcription steps were carried out using Qunata Biotech Thermocycler using settings set out in Qiagen user's manual.

2.6 Quantifying mRNA Expression via RT-qPCR

Prior to qPCR analysis, cDNA was generated by reverser transcription as set out previously, using 250ng RNA. qPCR was carried out using Qiagen QuantiNova SYBR Green RT-PCR Kit. For each reaction, a mastermix was made by combining forward and reverse primers (final concentration of 2nM), cDNA (final concentration of 1ng/mL) and SYBR mastermix (supplied by Qiagen), mix was created using user manual guidelines. PCR reactions were conducted using the CFX connect RT PCR thermocycler supplied by Bio-Rad in 96-well, semi-skirted plates. Reaction conditions performed: 95^{O}C for 5 minutes (one step), 95^{O}C for 20 minutes (40 cycles), 62^{O} for 20 seconds and 72^{O}C for 25 seconds. Each reaction was carried out in triplicate for technical repeats. Ct values of target genes were normalised to housekeeper, RPLP0. mRNA expression was analysed using $2^{-\Delta\Delta Ct}$ method. Primers used can be found in appendix.

2.7 Flow Cytometry- Cell Cycle

In order to assess the differing cell cycle phases of our iHCAECs compared to primary HCAECs, FACS analysis was implemented.

Day 1: Once cells had reached a desired confluency level (~90%), they were trypsinised and centrifuged at 300g for 5 minutes in order for a pellet to form. Residual supernatant was then aspirated, and pellet was gently resuspended in 500μL of PBS via pipetting. 3mL of **ice cold** 75% ethanol was then added to the tube wall in dropwise manner, whilst mixing via vortexing. The resulting suspension was then mixed again by syringe and vortex before being stored at -20^{O}C overnight.

Day 2: Stored cells suspended in PBS and ethanol were centrifuged at 500g for 10 minutes at 4^{O}C. Residual ethanol was aspirated off before cells were washed and resuspended in 2mL of PBS. Cells suspended in PBS were then again centrifuged at 500g for 10 minutes at 4^{O}C. PBS was then aspirated from cell pellet. Cell pellet was then re-suspended in 500μL of PBS. 25μL of propidium iodide (PI) (1mg/mL) stain and 10μL Rnase A (20mg/mL in PBS) was then added and briefly vortexed before incubated in the dark for 30 minutes at 37^{o}C (once 30 minutes have passed samples can be stored on ice or immediately proceed to next step). Samples were then centrifuged at 500g for 10 minutes at 4^{o}C, the staining solution was then aspirated from cells and resuspended in 500μL FACs solution and transferred to a FACs tube. Samples were then analysed utilising BD FACS calibur flow cytometer.

2.8 Flow Cytometry: Apoptosis

Flow cytometry was carried out using commercially available BD Annexin V FITC apoptosis detection kit. Cells were initially washed twice with sterile PBS, trypsinised and centrifuged at 300g for 5 minutes. Cells were then resuspended in 500μL PBS in which cell count was then measured using a haemocytometer, with cells diluted to 1x10^{6} cells /mL. 100μL was then aliquoted into separate Eppendorf tubes, with 500μL 1X binding buffer added to each sample. Incubation of apoptotic and cell viability dyes, annexin V and propidium iodide (PI) was then carried out as follows:

- PI 1:200 added to 1x10^{5} cells
- FITC Annexin V 1:200 added to 1 tube containing 1x10^{5} cells

- Annexin V (1:200) and PI (1:200) added to $1x10^5$ cells

Mix was then gently vortexed and incubated for 15 minutes at room temperature in the dark. Post incubation period, 400μL 1X binding buffer was then added to each tube and mixture was transferred to a FACS tube. Samples were then taken to BD FACS Verse Flow cytometer and analysed. Further analysis was carried out using FlowJo software.

2.9 Gateway Cloning

The gateway cloning reaction took place in a one tube format, however, can be broken down into its constituent reactions; BP reaction, LR reaction.

In a 1.5mL microcentrifuge tube the following was prepared for the BP reaction:

- attB DNA (entry clone) (50-100ng) 1.0-5.0μL
- attp DNA (pDONR supplied by Invitrogen, 150ng/μL) 1.3μL
- BP Clonase II enzyme mix 3.0 μL (supplied by Invitrogen)
- TE buffer, pH 8.0 add to a final volume of 15μL

All constituents were mixed well via brief vortexing and incubated at 25°C for 18 hours. Following incubation period, 5μL of the reaction was removed and placed in a separate tube, this was then used and transformed into NEB Stable competent cells in order assess BP reaction efficiency. To the remaining 10μL reaction the following was added:

- Destination vector (NLuc/VLuc backbone) (150ng/μL) 2.0μL
- LR Clonase II enzyme mix supplied by Invitrogen 3.0μL
- Final volume 15μL

The constituents were once again mixed well by briefly vortexing and incubated for 2 hours at 25°C. Following incubation period, 2μL proteinase K solution was added and

incubated for 10 minutes at 37^{O}C. Finally, 1μL of the final gateway reaction was then transformed in 50μL NEB Stable competent cells and spread LB plates containing appropriate antibiotic to select for expression clones.

2.10 Immunofluorescent Cell Staining

HCAECs were seeded into 8-well chamber slides at a density of 1x10^{5}/well. Cells were allowed to adhere and proliferate for two days, upon which cells were washed with PBS containing calcium and magnesium and fixed with PEM buffer (table 2.5) and incubated at 37^{O}C for 15 minutes. Cells were then permeabilised using Triton-x100 (0.1% in PBS) for 10 mins at room temperature. Cells were then washed in PBS (Ca^{+} + Mg^{+}) with 0.1% Tween® 20 (PBST) and blocked using appropriate block (BSA 1% or Goat serum 5% in PBST) for 1 hour at room temperature. Cells were then incubated with primary antibodies with appropriate concentration (see appendix) for 4 hours at room temperature. Cells were washed with PBS (Ca^{+} + Mg^{+}) and incubated with Alexa fluor secondary antibodies at 1:400 dilution (note, cell stain such as Phalloidin was also incubated at secondary antibody stage 1:200 dilution) in the dark at room temperature for 1 hour. Cells were washed once more with PBST (Ca^{+} + Mg^{+}) and mounted with Vectorshield Antifade with DAPI, addition of coverslip was then sealed using standard nail varnish and left to dry for 1 hour.

Table 2.5 PEM (PIPES, EGTA & Magnesium) Fixation Buffer

Reagent	Quantity	Final Concentration
EGTA (500mM)	0.8mL	10mM
$MgSO_4$ (1M)	40µL	1mM
PIPES (500mM, pH 6.9)	8mL	100mM
Sucrose (2M)	1.5mL	75mM
Triton X-100 (10%)	400µL	0.1%
ddH_2O	19.86mL	

*Just before use add 10mL Paraformaldehyde (16%) to buffer to a final concentration of 4%.

*Store PEM at 4^{O}C indefinitely *without* Paraformaldehyde.

2.11 Conventional Cloning

DNA insert vector previously ordered were transformed (see below) into 50µL commercial Invitrogen DH5α competent cells, spread onto ampicillin agar plates and incubated overnight at 37^{O}C. Colonies formed were inoculated and picked the following day post incubatory period, DNA was isolated using the Qiagen QIAprep spin miniprep kit. Backbone vectors (Vluc and Nluc) were grown overnight following retrieval of cells from glycerol stock. 15µg of backbone and DNA insert vectors were digested using *BamH1* and *XHO1* restriction enzymes. Resultant reaction was separated via gel electrophoresis. Once correct bands identified, mix containing digested DNA and enzyme was purified utilising the GFX PCR DNA and gel band purification kit by GE healthcare. The total product from purification of the DNA was then separated via gel electrophoresis. Bands of interest were then physically cut from gel and purified utilising (insert kit name). DNA from backbone and vector inserts were then ligated utilising the T4 ligase kit commercially available from Invitrogen, at a ratio of backbone 1:3 vector insert. As a result, ligated DNA was then transformed into NEB Stable competent cells

(in order to reduce recombination issues). DNA was once again isolated using the Qiagen QIAprep spin miniprep kit, with 500ng of DNA then digested, again using *BamH1* and *XHO1* restriction enzymes. Digested DNA was then separated using gel electrophoresis. Samples which contained the correct band sizes were then sent for sequencing for confirmatory purposes.

2.12 Transforming Competent cells

1-5μL (1pg-100ng) of plasmid DNA was pipetted into 50μL of appropriate competent cells, with the tube carefully flicked 4-5 times in order to mix the cells and DNA. Important note: do not vortex. The mixture was then incubated on ice for 30 minutes. The DNA and cell mixture were then heat shocked at exactly 42^{o}C for exactly 30 seconds and placed immediately back on ice for 30 minutes. 950μL of 37^{o}C SOC media (DH5α competent cells) or 950μL room temperature NEB 10-beta/Stable Outgrowth Medium (NEB Stable competent cells) was pipetted into the mixture and placed at 37^{o}C on a shaker at 225-250rpm for 60 minutes. Finally, 50-100μL of each mixture was spread onto pre-warmed selection plates containing appropriate antibiotics and incubated overnight at 37^{o}C.

2.13 Restriction Digest

500ng-1μg of plasmid DNA was digested with 1μL of appropriate enzyme and 3μL of appropriate buffer, e.g. CutSmart, made up to a total volume of 30μL with Rnase/Dnase free water for 1 hour at 37^{O}C. Enzymes are then inactivated at temperatures between 60^{O}C- 70^{O}C for 20 minutes and DNA is then separated via agarose gel electrophoresis.

2.14 Bacterial Maintenance

Bacteria containing target plasmid DNA were spread onto sterile LB agar plates containing selective antibiotic resistance. Colonies formed thus displayed resistance to antibiotic and were selected and used for inoculation of sterile LB broth containing selected antibiotic, grown overnight at 37^{O}C. Plasmid DNA was isolated using either the Qiagen QIAprep spin miniprep kit, or the Sigma GenElute HP Endotoxin-Free Plasmid Maxiprep Kit.

2.15 BPA Stimulation

Bisphenol A (97%) was purchased from ThermoFisher Scientific. BPA is available in solid form and therefore must be reconstituted prior to use. BPA is soluble in alkaline, acidic and alcohol solutions. However, to ensure vehicle had no effect, BPA was solubilised in ddH_2O. As BPA is weakly soluble in water, BPA was sonicated for 24 hours in ddH_2O to a concentration of 1000 parts per million (ppm) or 0.1%. BPA solution was then added to Promocell MV2 media to required concentrations.

2.16 Measuring Luciferase Activity

Luciferase activity of cells containing either Nluc or Vluc, were using enzyme reaction-based kits. For cells containing Nluc, reaction mix containing luciferase buffer and luciferin enzyme using Promega Nano-glo dual luciferase assay kit at a dilution of 1:100 was created. For cells containing Vluc, reaction mix containing luciferase buffer and Vargulin enzyme (1:100 dilution) using Pierce Cypridina Luciferase flash assay kit supplied by Thermo Fisher scientific was created Following stimulation, 20μL of media

collected from TFAR containing cells was added in triplicate to a 96-well white bottom plate, to the media 20µL of enzyme containing mixture for either Nluc or Vluc was added to appropriate wells, culminating in 40µL total volume per well. Luminescence of plates was immediately measured using the Promega GloMax Explorer plate reader. Cells containing Nluc were measured using pre-set Nano-glo luciferase settings. Cells containing Vluc were measured using 'Luciferase assay' pre-set settings.

2.17 Statistical Analysis

Data sets produced were analysed using GraphPad Prism software v9.4.0 (GraphPad, San Diego, CA, USA). Prior to statistical significance analysis, normal distribution and homoscedasticity was analysed using a Shapiro-Wilk test performed using GraphPad. Utilising an unpaired T-test for normally distributed data between two independent groups, we measured the statistical significance. In a data set containing three or more groups with one independent variable, a one-way analysis of variance (ANOVA) was implemented to compare the variance of the group means. Finally, we utilised a Two-way ANOVA in order to determine the variance of normally distributed sets. These sets have three or more groups, containing two independent, defined groups. Post hoc analysis was implemented on ANOVA analysis using Bonferroni or Tukey. Finally, data sets that were not normally distributed and unpaired, a non-parametric Mann-Whitney test was used to confirm significance. Summary of p value significance is as follows: *$p<0.05$, **$p<0.01$, ***$p<0.001$ and ****$p<0.0001$, all expressed with ± standard error of mean (SEM).

Chapter 3:

Overexpressing BMI1 and hTERT Results in an Extended Proliferative Lifespan and a Reduction in Senescence in Human Coronary Artery Endothelial Cells.

3.0 Introduction

To create the E-sense platform, a stable endothelial cell platform that could be expanded beyond the normal restraints of primary endothelial cells was required to allow genetic manipulation, with insertion of TFARS, and reproducible quantification of cell signalling and transcription factor activity. In addition, the creation of a stable endothelial cell line will reduce costs and eliminate donor variability. However, for the E-sense system to work, the cell platform must retain key endothelial features, especially mechanosensitivity, to allow the quantification of protective as well as inflammatory and cell stress pathways involved in atherosclerosis. To achieve this, we opted to overexpress two anti-senescent factors, rather than create an immortalised cell line, and also to use primary human coronary artery endothelial cells (HCAECs) as the cell origin due to its relevance in disease processes. This contrasts with the currently available immortalised cell lines that have been derived from endothelial cells.

Cellular senescence is known to be controlled by a variety of mechanisms, resulting in permanent cell cycle arrest. One of these mechanisms of cell cycle arrest is regulated by $p16^{INK4a}$/Rb and $p53/p21^{CIP1}$ (McHugh and Gil, 2018) (Salama *et al.*, 2014). This arrest is dependent on the activation of the cyclin-dependent kinase (CDK) inhibitors p21 and p16, with p53 upregulating expression of p21, resulting in initial cell cycle arrest (He *et al.*, 2005). $P16^{INK4a}$ has been shown to mediate permanent cell cycle arrest via CDK4 and CD6 inhibition, thus resulting in RB phosphorylation, blocking entry to S phase (Baker *et al.*, 2016).

In addition, telomere attrition is a key driver of replicative senescence, with erosion of these highly repetitive DNA structures located on the ends of chromosomes with each round of cell replication. Telomeres are made of a simple double-stranded DNA repeat, (TTAGGG)n, with a repeat sequence

occurring for 2-30kbp, containing a guanidine-rich single-stranded 3'-overhang (50-200 nucleotides in length) (Meyne, Ratliff and Moyzis, 1989). Each round of DNA replication in the absence of telomerase results in telomer shortening, eventually resulting in critical telomere shortening (~12.8 repeats of repetitive clusters) (Victorelli and Passos, 2017). Once this threshold, the Hayflick limit, has been exceeded, telomere length shortens to an extent in which they are unable to 'cap' chromosomal ends, resulting in progressive DNA erosion initiating cell-cycle arrest (Nandakumar and Cech, 2013).

In order to circumvent the induction of cell cycle arrest and senescence, HCAECs were transduced with lentiviral vectors overexpressing both BMI1 and hTERT. BMI1, an anti-senescence polycomb protein, is a known repressor of the *INK4a* locus, encoding the tumour suppressor p16, thus suppressing p16-controlled cellular senescence. hTERT overexpression leads to maintenance of telomere integrity with shelterin-forming protein complexes, thus preventing telomere erosion during successive replication and senescence being induced due to reaching the Hayflick limit.

Aims and objectives:

Aim: Establish an endothelial cell line with increased capacity for proliferation and reduction in senescence without inducing transformation.

This will be addressed in the following objectives:

- Using lentiviral overexpression, we will create a human coronary artery endothelial cell line with elevated expression of both BMI1 and hTERT (HCAECPro) to increase proliferative capacity.
- Use established molecular and immunological staining techniques to monitor any phenotypic changes as well expression senescence and proliferation alteration of HCAECPro cells.
- Utilise in-house parallel plate flow apparatus to establish retainment of mechanosensing properties of HCAECPro cells.

3.1 Overexpressing BMI1 + hTERT Results in Extended Proliferation and Reduced Senescence in Human Coronary Artery Endothelial Cells

Previous work within the White lab had demonstrated that overexpressing with BMI1 alone had increased the proliferative potential of HCAECs by several passages, however, quiescence and subsequent senescence was induced in a high proportion of cells by passage 10. In order to increase the proliferative potential further, primary HCAECs were transduced with lentiviral vectors overexpressing either BMI1, hTERT or both (HCAECPro cell line) (fig 3.1 & 3.1.2). We selected passage 3 (p3) primary HCAECs from a 23-year-old male that were observed to grow particularly well for this approach. Following this, each cell line was concurrently passaged (primary HCAECs, BMI1 only, hTERT only and both BMI1 and hTERT overexpression) assaying key markers of senescence, proliferation, apoptosis and morphology at regular intervals (p4, 6, 9, 12 and 15). Figure 3.1 demonstrates the process of lentiviral overexpression of the primary HCAECs.

One key phenotypic trait of a HCAEC is its ability to remain mechanosensitive. Using the White lab in house parallel plate flow apparatus (see fig 2.1), we were able to monitor the response to flow of our transduced cell lines and incorporated molecular techniques to measure the activity of flow regulated genes.

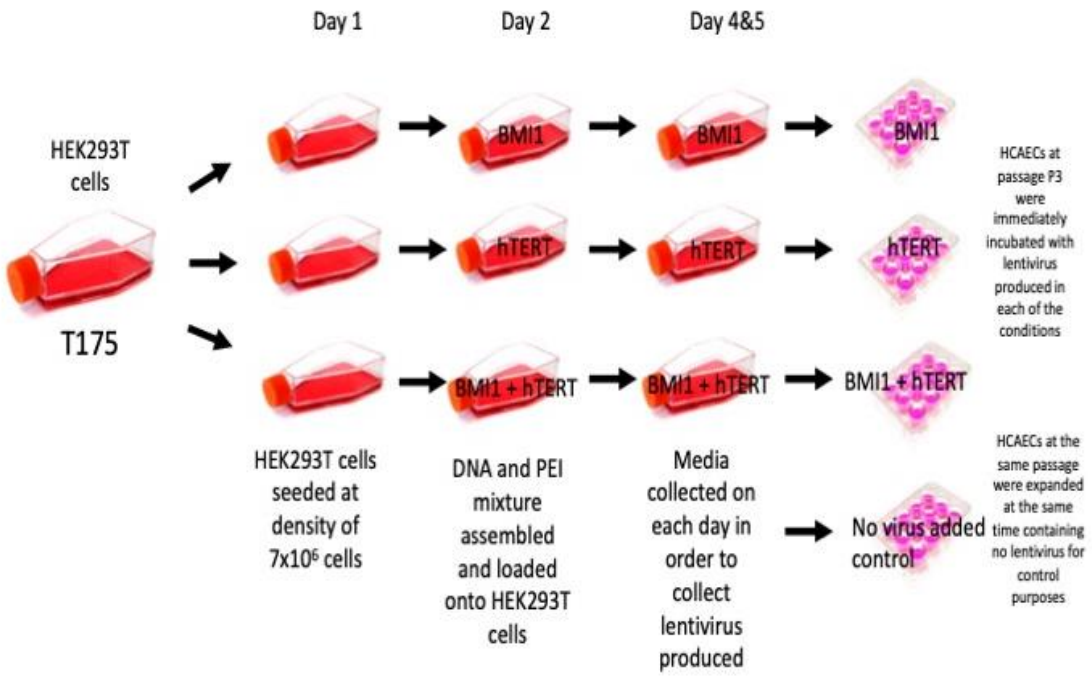

Figure 3.1. Lentiviral Transduction of HCAECs with BMI1 + hTERT.

Lentiviral vectors overexpressing BMI1 and hTERT were prepared by co-transfection of vector and packaging plasmids into HEK293T cells. Media was replaced with Promocell MV2 HCAEC media on day 3 and collected on day 4 and added directly to primary HCAECs. Fresh MV2 media was added to the transduced HEK293T cells and collected on day 5, this was used to replace the media on the primary HCAECs, ensuring the maximum amount of lentiviral vectors from the HEK293T were added to the primary HCAECs. As there were no selectable markers for either BMI1 and hTERT vectors, continued passage will self-select HCAECs overexpressing each transgene.

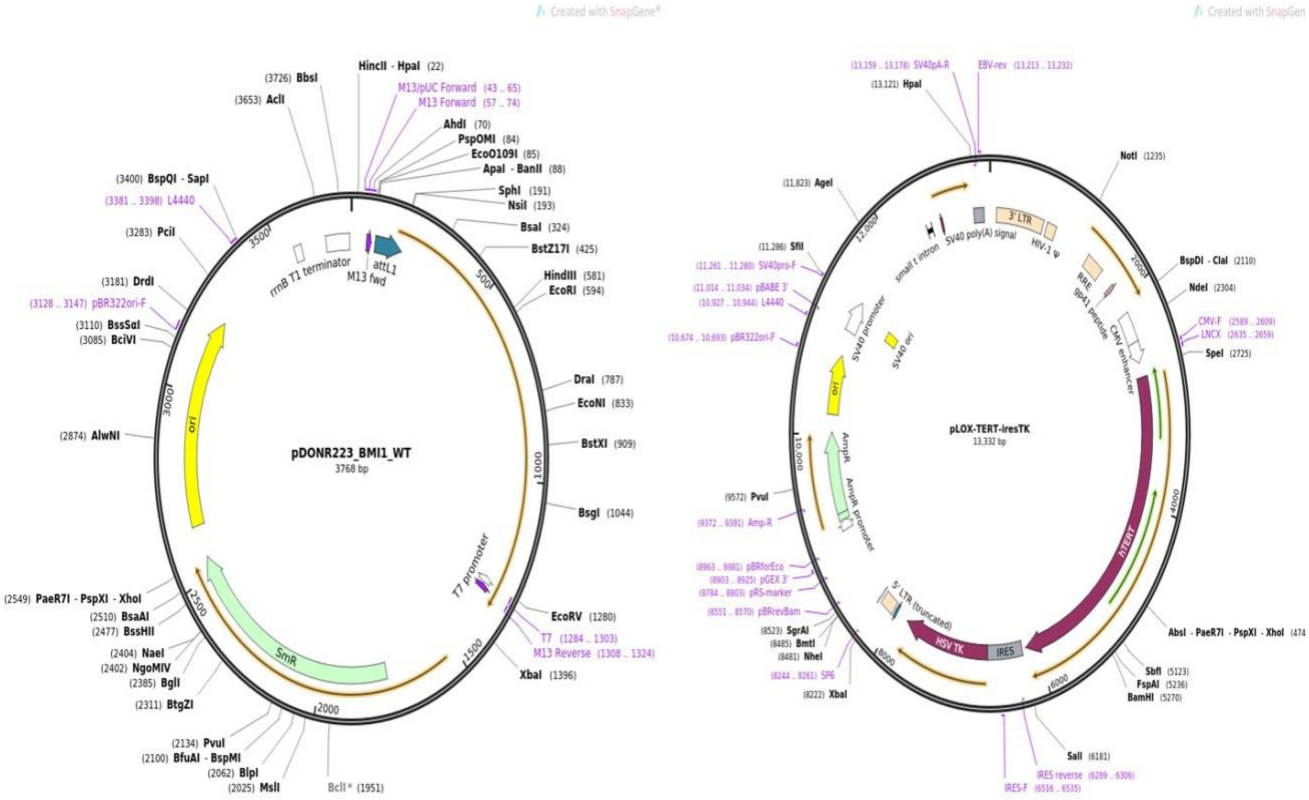

Figure 3.1.2: BMI1 and hTERT Plasmid maps

BMI1 pENTR plasmid map cloned into backbone vector supplied by McKay collaborating lab group in addition to hTERT overexpressing plasmid. Plasmids were incorporated into HCAECs at passage p3 utilising lentiviral overexpression (see figure 3.1).

HCAECs overexpressing BMI1 + hTERT continued to proliferate beyond complete replicative exhaustion which was observed at passage 14 in HCAECs. In order to quantify senescence in each cell line, transduced cells were stained for Senescence-associated β-galactosidase activity (SA-β-Gal), utilising a classical stain (pH6.0) (fig 3.1.3).

It was observed that there was a significant reduction in the percentage of positively stained cells of our HCAECPro cell line (BMI1+hTERT) at p4, p9 and p15 compared to primary cells of the same passage (fig 3.1.3). Under the staining conditions used, 31.4% of primary HCAECs stained positively for β galactosidase activity at p4, which increased 2.6-fold between p4 to p9 (82.03%, $p<0.0001$ compared to p4) and 95.2%

cells positively stained at p14 ($p<0.0001$ to p4) (fig 3.1.4). Conversely there was no significant change in the percentage of HCAECPro cells positively stained between p4 and p15 (26.7% ➔ 27.8%, p 0.95) whereas the percentage of positively stained HCAECPro p4 cells was significantly reeuced compared to primary cells at p14 (26.7% ➔ 95.2%, $p<0.0001$). It is to be noted primary HCAECs underwent complete cell cycle arrest at p14 and could not be cultured past this point. BMI1 only and hTERT only cells also demonstrated a marked reduction in senescent cells compared to controls, demonstrating both BMI1 and hTERT's ability to individually inhibit senescence.

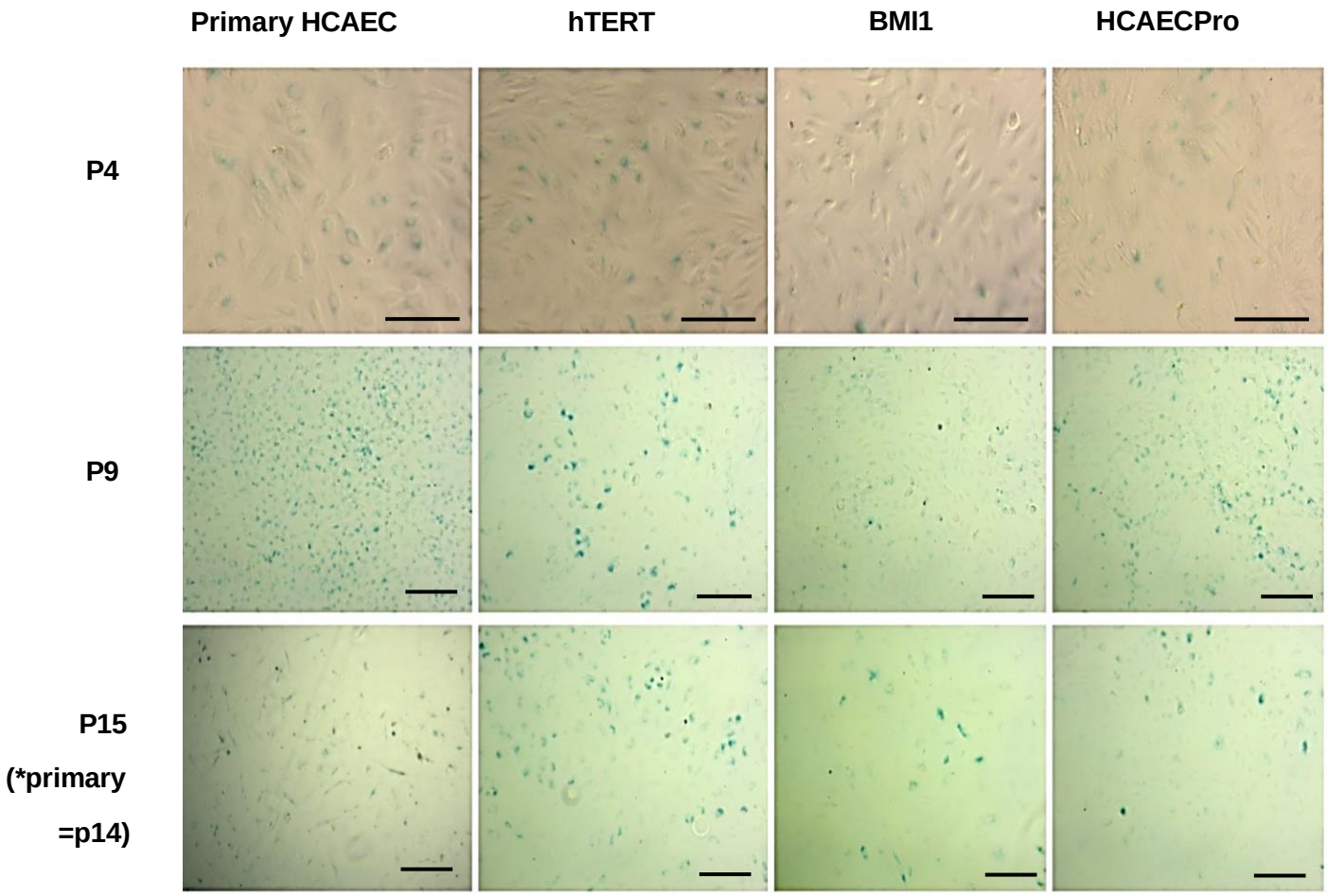

Figure 3.1.3: Images of SA-β-Gal activity in Primary HCAECs and Transduced HCAECs.

Senescence-associated β-galactosidase staining of primary HCAECs, transduced lines with BMI1, hTERT or BMI1+hTERT (HCAECPro) and passaged to p4, p9 and p15 (primary cells underwent full cell cycle arrest at p14 therefore final β-galactosidase activity was performed at this passage). Cells were fixed in PEM buffer and subsequently stained with Senescence-associated β- galactosidase for 6 hours at 37^{O}C. Images taken using a light microscope. Scale bar = 500µM.

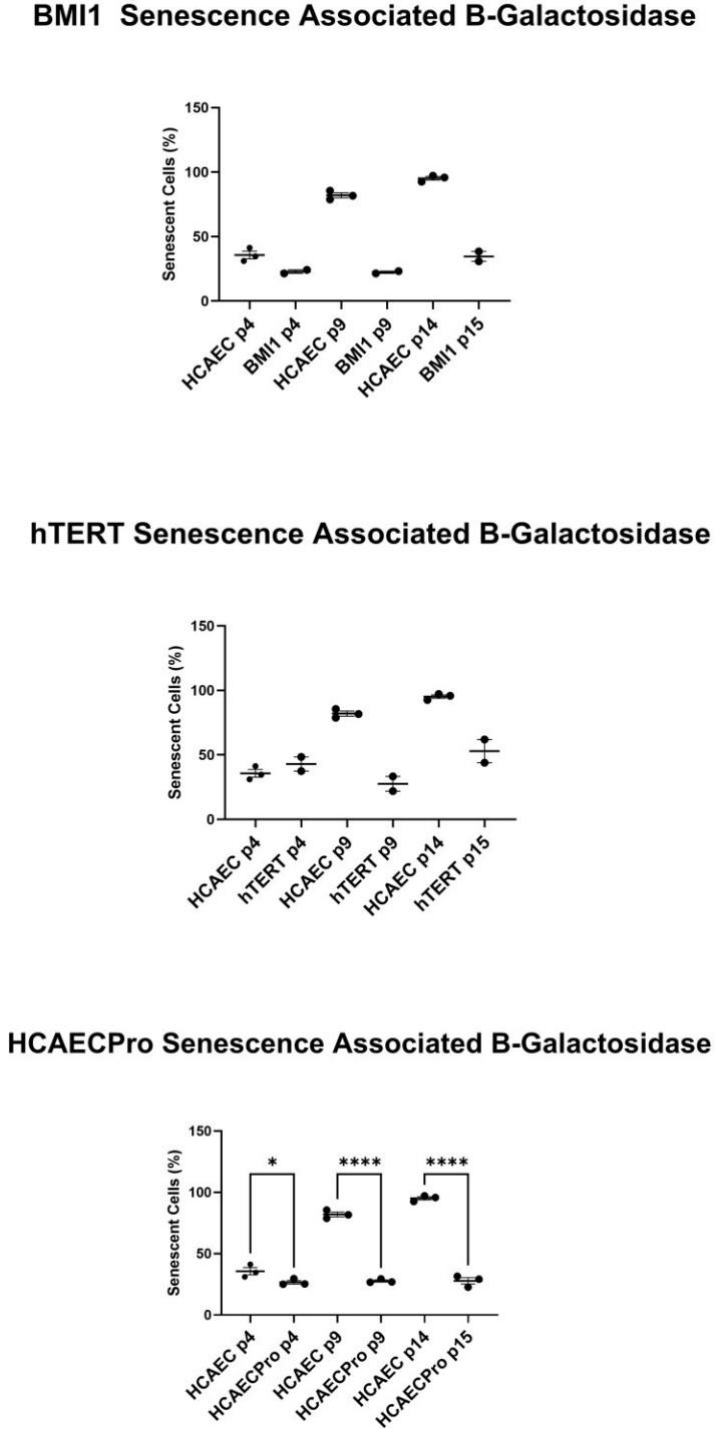

Figure 3.1.4: Quantification of SA-β-Gal Activity

Senescence-associated β-galactosidase staining of primary HCAECs, transduced lines with BMI1, hTERT or BMI1+hTERT (HCAECPro) and passaged to p4, p9 and p15 (primary cells underwent full cell cycle arrest at p14 therefore final β-galactosidase activity was performed at this passage. Cells were stained with Senescence-associated β- galactosidase for 6 hours at 37^{O}C. BMI1 n=2, hTERT n=2, HCAECPro and primary HCAECs n=3, ANOVA. *p= <0.05, **p<0.01, ***p<0.001, ±SEM). Images taken using a light microscope. Quantification carried out using ImageJ/Fiji software.

As previously stated, activation of the $p16^{INK4A/pRB}$ and $p53/p21^{WAF1/CIP1}$ pathways play vital roles in the induction of cellular senescence. qPCR quantification of p16, p21 and p53 mRNA expression was performed at p4, p9 and p15 to further investigate the induction of senescence.

qPCR analysis supported the observation that SA β-galactosidase activity increased

with passage in primary HCAECs, but was suppressed by the overexpression of anti-senescent factors (fig 3.1.5→ 3.1.7). Overexpression of BMI1 prevented the increase of p16 and p21 expression observed in primary HCAECs between p4 and p9 (5.64-fold increase, $p<0.0001$) (fig 3.1.5).

qPCR analysis demonstrated a similar trend in p16, p21 and p53 mRNA expression in BMI1 only transduced cells at each passage (figure 3.1.5). In each of the senescent modulators we see a decrease in expression in BMI1 cells in comparison to primary cells counterparts of the same passage. We see a small increase in expression of p16, p21 and p53 at p15 of our HCAECPro cells with levels of mRNA expression comparable to primary HCAECs at p4 (fig 3.1.7). Results suggest overexpression of BMI1 has the greatest impact on the expression of both p16 and p21, with less noticeable impact on p53 mRNA expression.

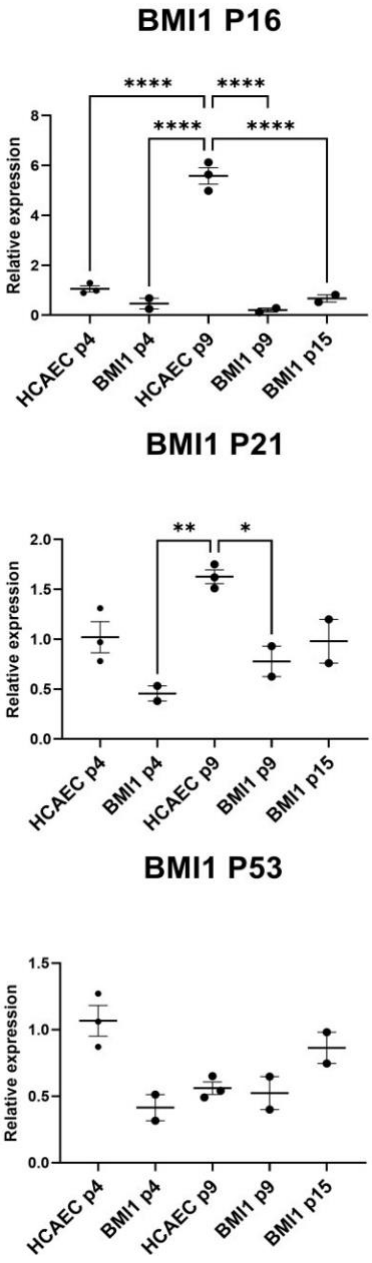

Figure 3.1.5: mRNA Expression of p16, p21 and p53 in BMI1 HCAECs.

Activity of key senescent modulators p16, p21 and p53 in BMI1 transduced HCAECs. RNA was extracted from BMI1 only cells at passages p4, p5 and p15 and subsequently assessed against expression in primary cells (HCAEC) at p4 and p9. BMI1 only cells n=2, primary HCAECs n=3, ANOVA. *p= <0.05, **p<0.01, ***p<0.001, ±SEM.

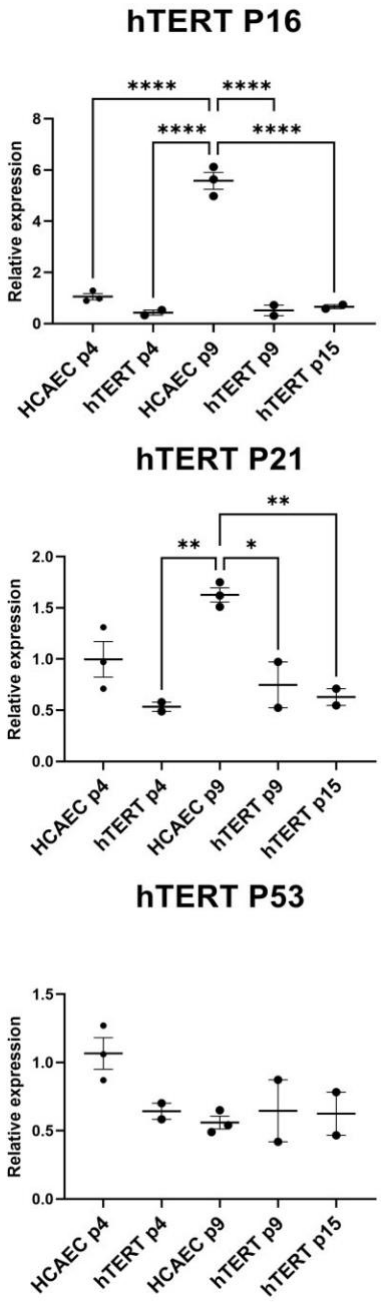

Figure 3.1.6: mRNA Expression of p16, p21 and p53 in hTERT HCAECs.

Activity of key senescent modulators p16, p21 and p53 in hTERT transduced HCAECs.. RNA was extracted from hTERT only cells at passages p4, p5 and p15 and subsequently assessed against expression in primary cells (HCAEC) at p4 and p9. BMI1 only cells n=2, primary HCAECs n=3, ANOVA. *p= <0.05, **p<0.01, ***p<0.001, ±SEM.

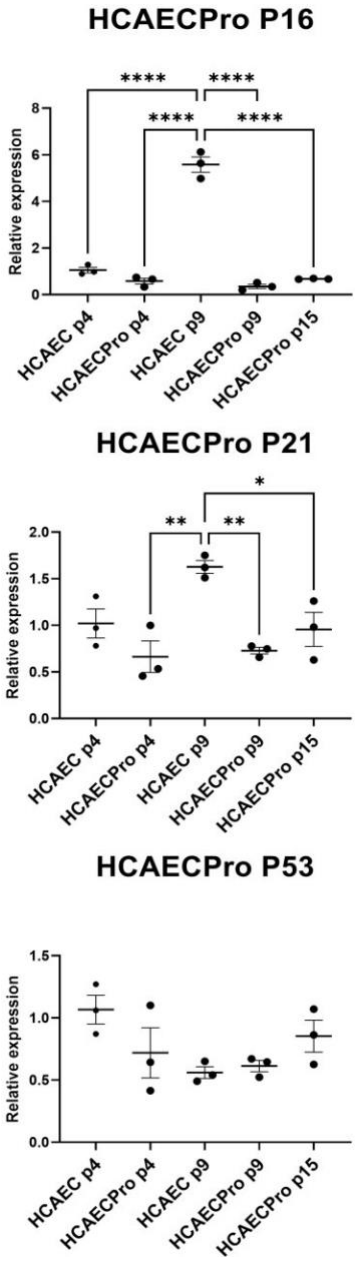

Figure 3.1.7: mRNA Expression of p16, p21 and p53 in HCAECPro cells.

Activity of key senescent modulators p16, p21 and p53 in HCAECPro cells. RNA was extracted from HCAECPro cells at passages p4, p5 and p15 and subsequently assessed against expression in primary cells (HCAECs) at p4 and p9. HCAECPro and primary HCAECs n=3, ANOVA. *p= <0.05, **p<0.01, ***p<0.001, ±SEM.

3.2 BMI1 and hTERT transduced cells demonstrate an increased rate of proliferation and reduced levels of apoptosis

In addition to evaluating the rate of senescence in each of our transduced cell lines, we monitored the proportion of transduced cells undergoing apoptosis at p9 and p15 and compared them to primary HCAECs at a low passage of p6 (fig 3.2.1 → 3.2.3). Representative analysis demonstrated that both BMI1 only and hTERT only cells had a lower proportion of cells undergoing apoptosis at p6 and p15 compared to primary counterparts (fig 3.2.1 & 3.2.2). BMI1 apoptotic activity decreased from p6 to p15, however the number of viable cells also decreased, with a 7.3-fold increase in necrotic cells between p6 and p15 (fig 3.2.1). hTERT only cells mirrored this trend with a decrease in apoptotic cells from p6 to p15 but a 4.76-fold increase in necrotic cells in this same passage range (fig 3.2.2). HCAECPro cells displayed a significant decrease in the proportion of cells undergoing apoptosis from p6 to p15 compared to primary cell controls, with the smallest Increase in necrotic cells of 3.9-fold (fig 3.2.3). All three cell lines displayed a decrease in viable cells as they progressed to p15, with 47.32% HCAECPro cells viable. In contrast, in culture it was observed that at p14 primary cells underwent full cell cycle arrest (see figure 3.3.1) and complete senescence induced.

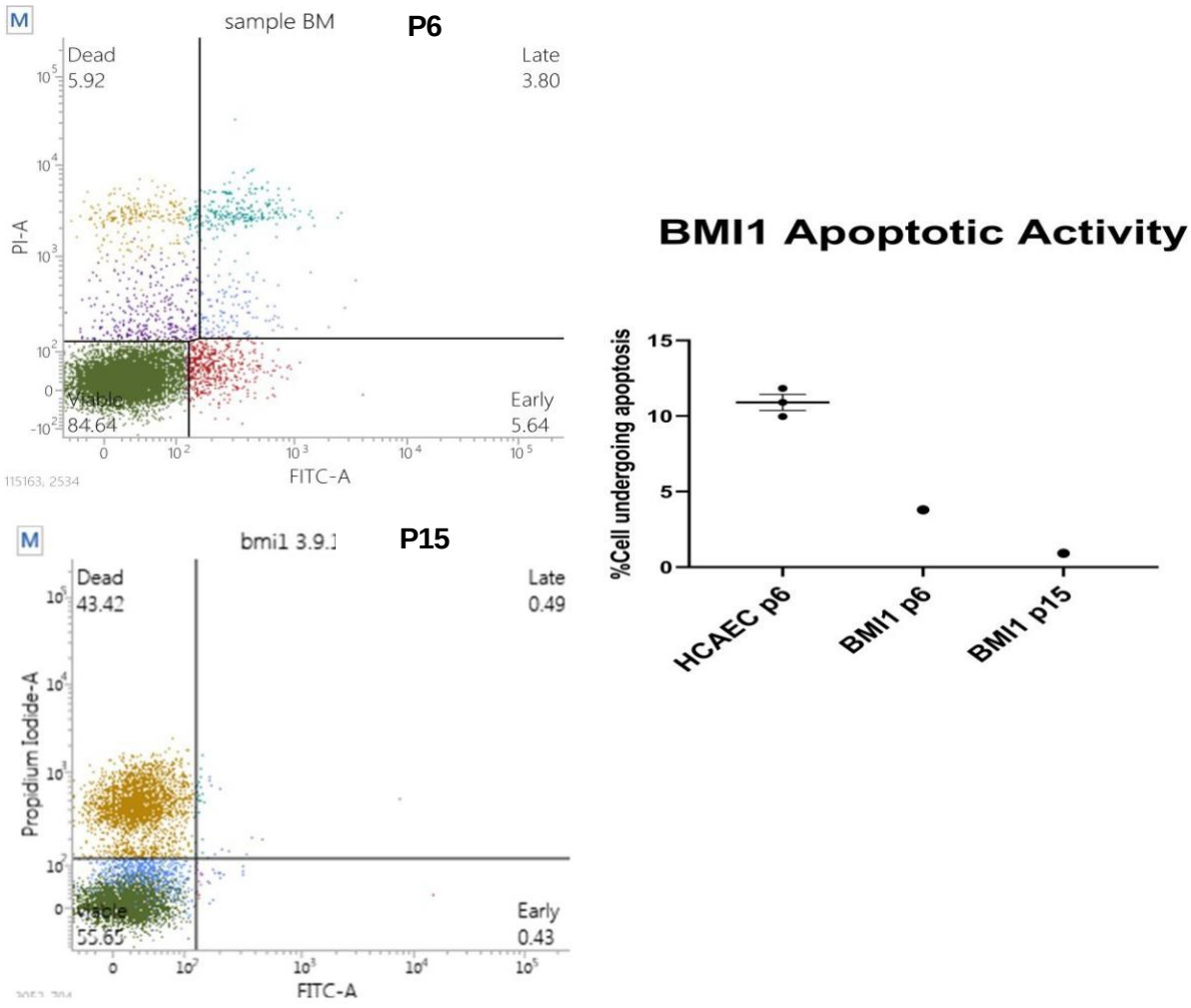

Figure 3.2.1: Apoptosis Activity in BMI1 HCAECs Measured by FACS.

BMI1 transduced HCAECs were passaged to p9 and p15 and apoptosis activity was measured in comparison to primary HCAECs at p6 by flow cytometry. Cells were treated using Annexin V and PI for 15 minutes. Cells positive for Annexin V visible in right quadrants signifying early and late apoptosis. BMI1 representative n=1, primary HCAECs n=3.

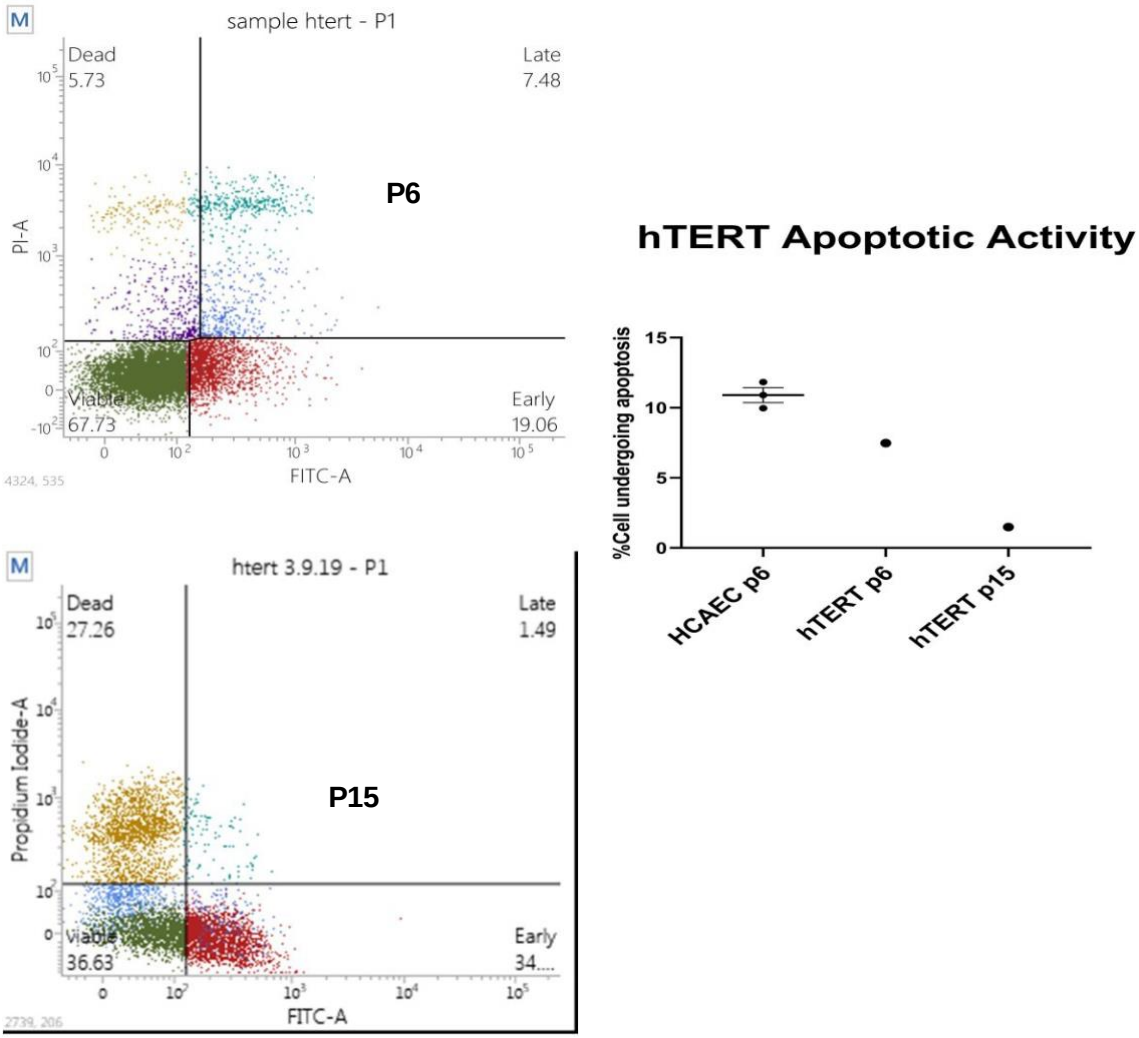

Figure 3.2.2: Apoptosis Activity in hTERT HCAECs Measured by FACS.

hTERT transduced HCAECs were passaged to p9 and p15 and apoptosis activity and viability was measured in comparison to primary HCAECs at p6 by flow cytometry. Cells were treated using Annexin V and PI for 15 minutes. Cells positive for Annexin V visible in right quadrants signifying early and late apoptosis. hTERT representative n=1, primary HCAECs n=3.

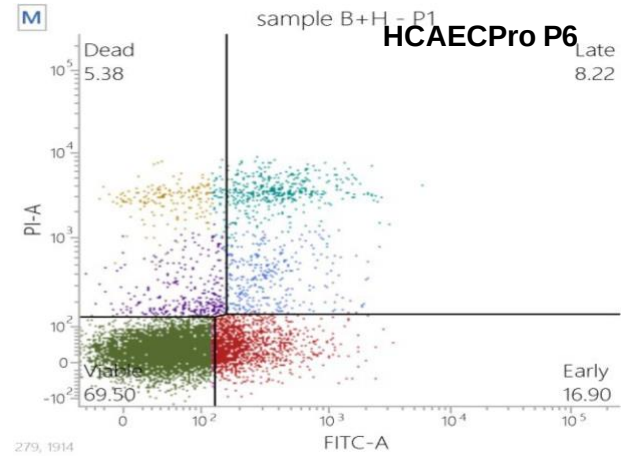

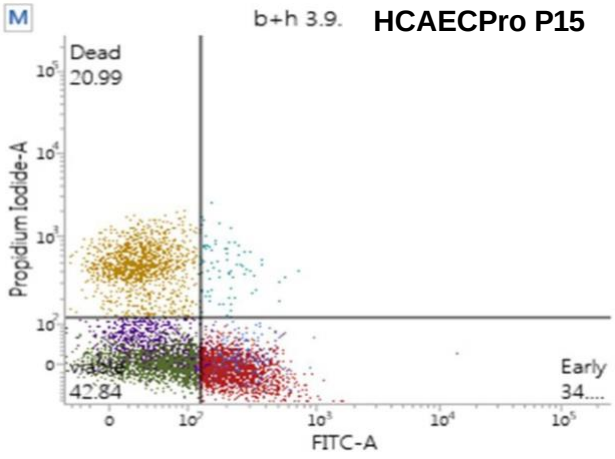

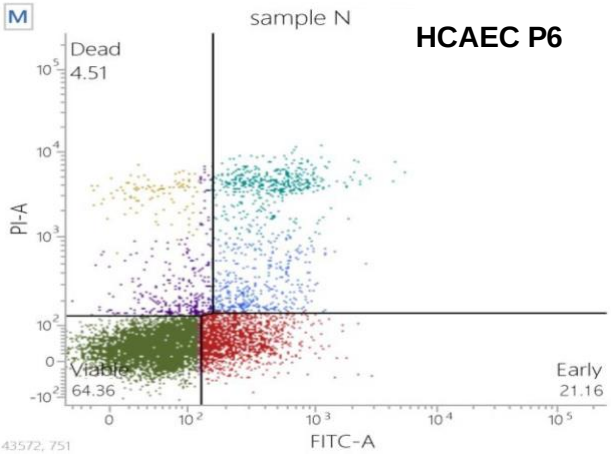

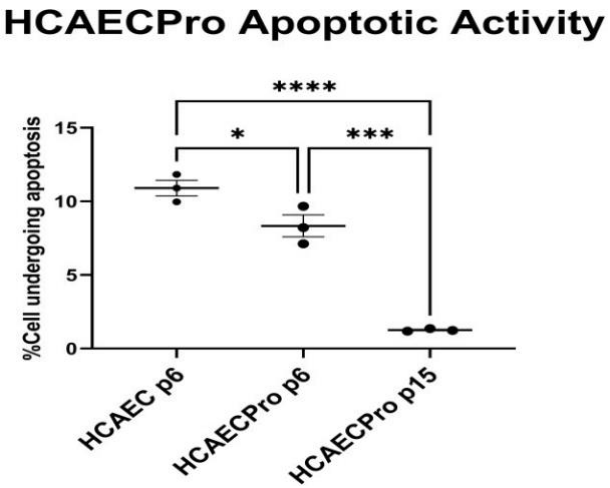

Figure 3.2.3: Apoptosis Activity in HCAECs and HCAECPro Cells Measured by FACS.

HCAECPro cells were passaged to p9 and p15 and apoptosis activity and viability was measured in comparison to primary HCAECs at p6 by flow cytometry. Cells were treated using Annexin V and PI for 15 minutes. Cells positive for Annexin V visible in right quadrants signifying early and late apoptosis HCAECPro and primary HCAECs n=3, ANOVA.3 *p= <0.05, **p<0.01, ***p<0.001, ±SEM

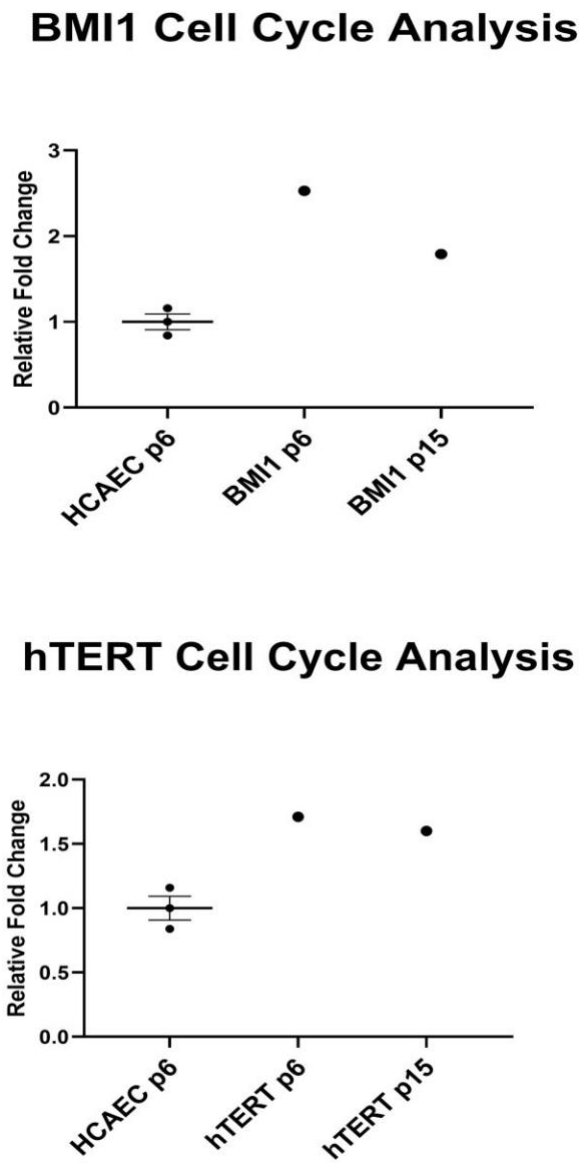

Figure 3.2.4: Cell Cycle Analysis of BMI1 and hTERT only HCAECs Measured by FACS.

Cell cycle quantification of BMI1 only transduced cells and hTERT only transduced cells at passages p9 and p15 in comparison to primary HCAEC at p6 by flow cytometry. Flow cytometry is able to distinguish between each stage of cell cycle other than G0 and G1. Peaks relating to G2 and S phase were analysed in order to assess cells ability to divide. Cells were treated with PI and RNAse A at 37^{O}C for 30 minutes. BMI1 n=1, primary HCAEC n=3.

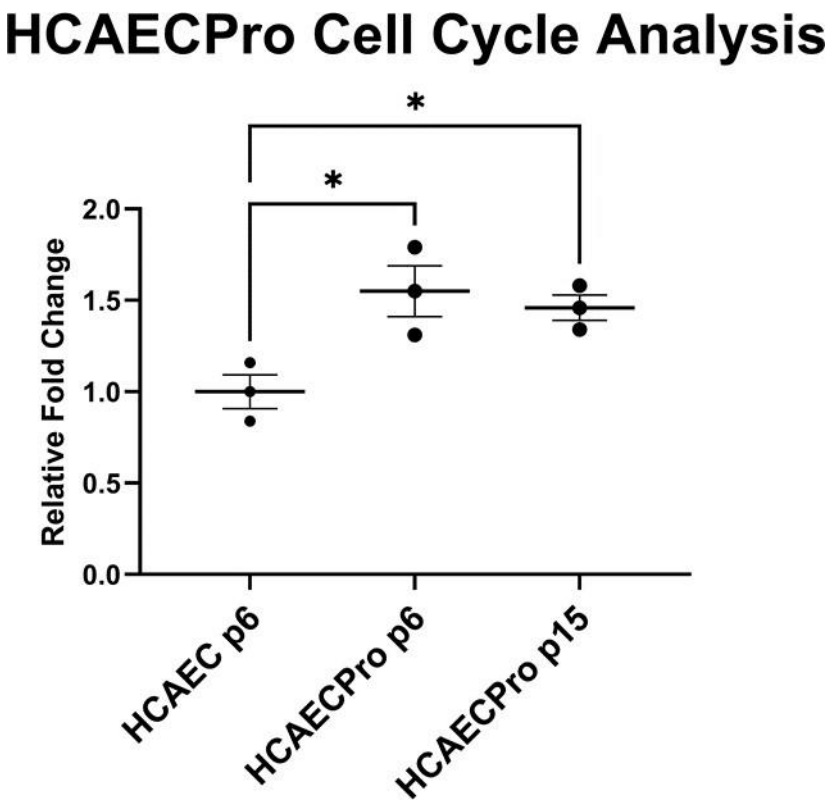

Figure 3.2.5: Cell Cycle Analysis of HCAECPro cells Measured by FACS.

Cell cycle quantification of HCAECPro cells at passages p9 and p15 in comparison to primary HCAEC at p6 by flow cytometry. Flow cytometry is able to distinguish between each stage of cell cycle other than G0 and G1. Peaks relating to G2 and S phase were analysed in order to assess cells ability to divide. Cells were treated with PI and RNAse A at 37^{O}C for 30 minutes. HCAECPro and primary HCAECs n=3, ANOVA. *p= <0.05, **p<0.01, ***p<0.001, ±SEM

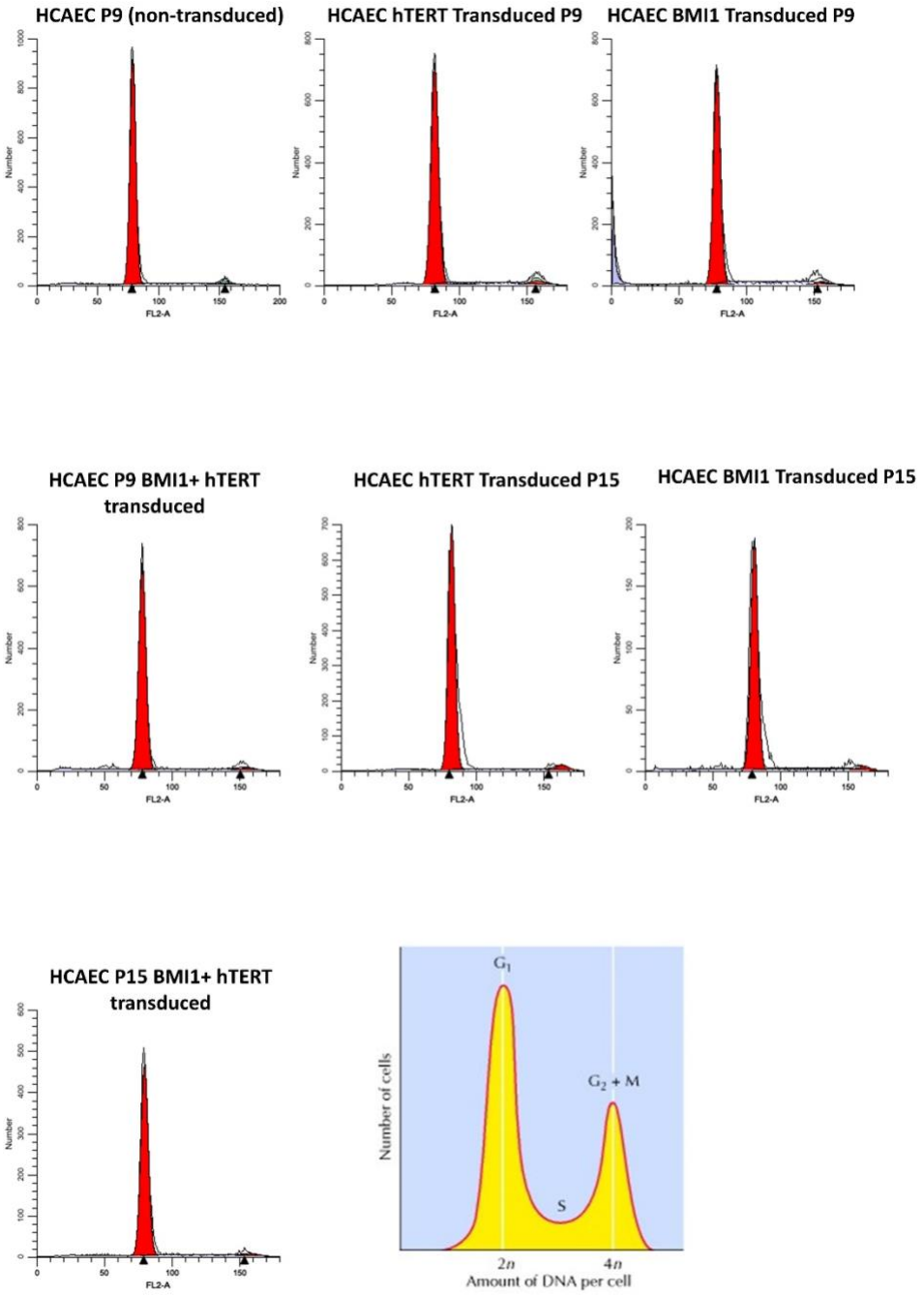

Figure 3.2.6: Cell cycle analysis DNA content density graphs.

FACS cell cycle analysis DNA content density graphs of non-transduced HCAECs at P9 in comparison to hTERT, BMI1 and BMI1 + hTERT transduced cells at P9 and P15. Analysis of non-transduced cells at P15 was unable to be carried due to cells senescing at earlier passages, future work will aim to analyse cells at earlier passages in order to compare against transduced cell lines. Results are representative of a single experiment with each sample representing 10,000 events. Graph obtained typically displays two peaks correlating with DNA contents of 2n and 4n; cells in G_1 and G_2/M respectively (Hiscox, 2006).

3.3 HCAECPro Cells retain key endothelial morphological traits

On balance, doubly transduced HCAECs containing both BMI1 and hTERT (HCAECPro) appeared to have modestly better rates of proliferation (fig 3.2.5), and lower levels of senescence, without observed detrimental effects, therefore we proceeded with this cell line. As we were unable to select for expression of transduced cells, we compared HCAECPro at passage 15 (one passage beyond the point where HCAECs underwent full cell cycle arrest) with low passage HCAECs to ensure that continued passage hadn't resulted in loss of key endothelial traits, or significant changes in morphology. Continued passage effectively selects for HCAECs transduced by BMI and hTERT, as non-transduced cells would undergo senescence and be lost from the culture.

Visually, HCAECPro cells appear indistinguishable from primary HCAEC cell types, whilst retaining the classical "cobblestone" phenotype even at a late passage of p15 (fig 3.3.1). As primary cells move towards a higher passage of p9, it was observed that there is a change in morphology in some of cells, now becoming enlarged and elongated (see red arrows). As primary cells move towards p14, they lose all morphological features associated with HCAECs I culture. At this passage, cells could no longer be passaged. Due to this induction of cell cycle arrest, it can be assumed at p15 remaining cells in culture have been selected out as transduced cells.

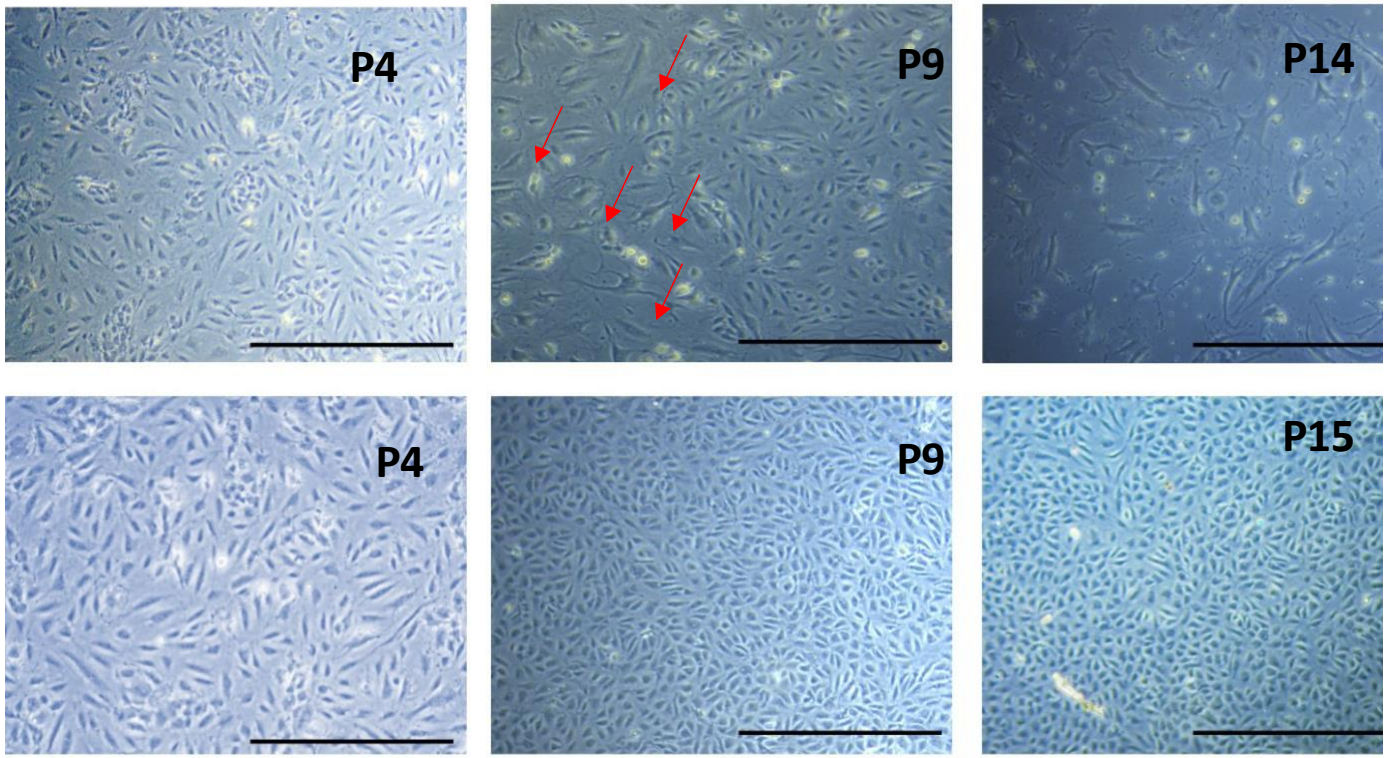

Figure 3.3.1: Phase Contrast Images of HCAECs and HCAECPro cells In Culture.

Primary HCAECs (top row) and HCAECPro cells (bottom row) were continually passaged concurrently with one another in PromoCell MV2 endothelial cell media, at $37^{O}C$, 5% CO_2. Both cell lines were passaged until >90% confluency, at which point cells were split 1 in 3 using standard filtered $75cm^2$ flasks. Primary cells were cultured until full cell cycle arrest at p14, HCAECPro cells remained proliferative and retained "cobblestone" phenotype even at a high passage of p15. Images taken on standard table top light microscope. Scale bar = 500µM

We examined p15 HCAECPro for a range of endothelial and morphological markers and compared them to HCAECs at p4. We examined the distribution of the actin cytoskeleton and focal adhesions using vinculin as a key component of the endothelial adhesome (Figure 3.3.2), no differences in the actin cytoskeleton or number/location of focal adhesions were observed. Similarly, immunofluorescence of VE-cadherin (Figure 3.3.3) and βcatenin (Figure 3.3.4) was identical in both p15 HCAECPro and p4 HCAECs, showing intercellular localisation and perinuclear staining indicative of the endoplasmic reticulum/Golgi staining. Primary endothelial cells store von Willebrand Factor (vWF) in Weibel Palade bodies, resulting in a punctate staining of vWF, which was similar in number and size between HCAECPro and p4 HCAECs (Figure 3.3.5).

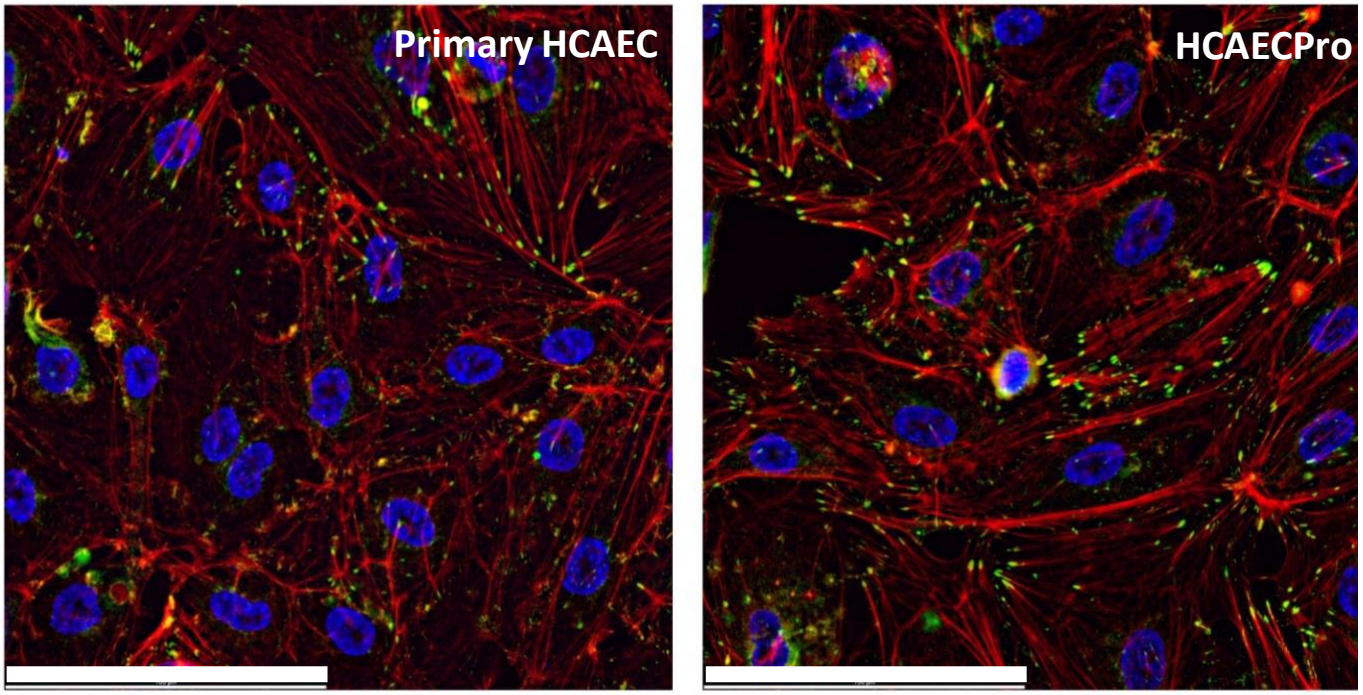

Figure 3.3.2: ICC Staining of Vinculin and Phalloidin.

Immunofluorescent images of primary HCAECs and HCAECPro cells stained for focal adhesion marker Vinculin (green) and cytoskeletal actin filament marker Phalloidin (red). Cells were incubated overnight at $4^{O}C$ with Vinculin at 1:200 in TBST containing 1% BSA. Cells were washed and incubated with Alexa fluor 488 goat-anti mouse antibody 1:400 and 568-phalloidin 1:100 at room temperature in TBST containing 1% BSA in the dark for 1 hour. Slides were mounted in Vectershield antifade mounting media containing DAPI. Images taken using Thunder Imaging system x40. Scale bar = 100µM.

.

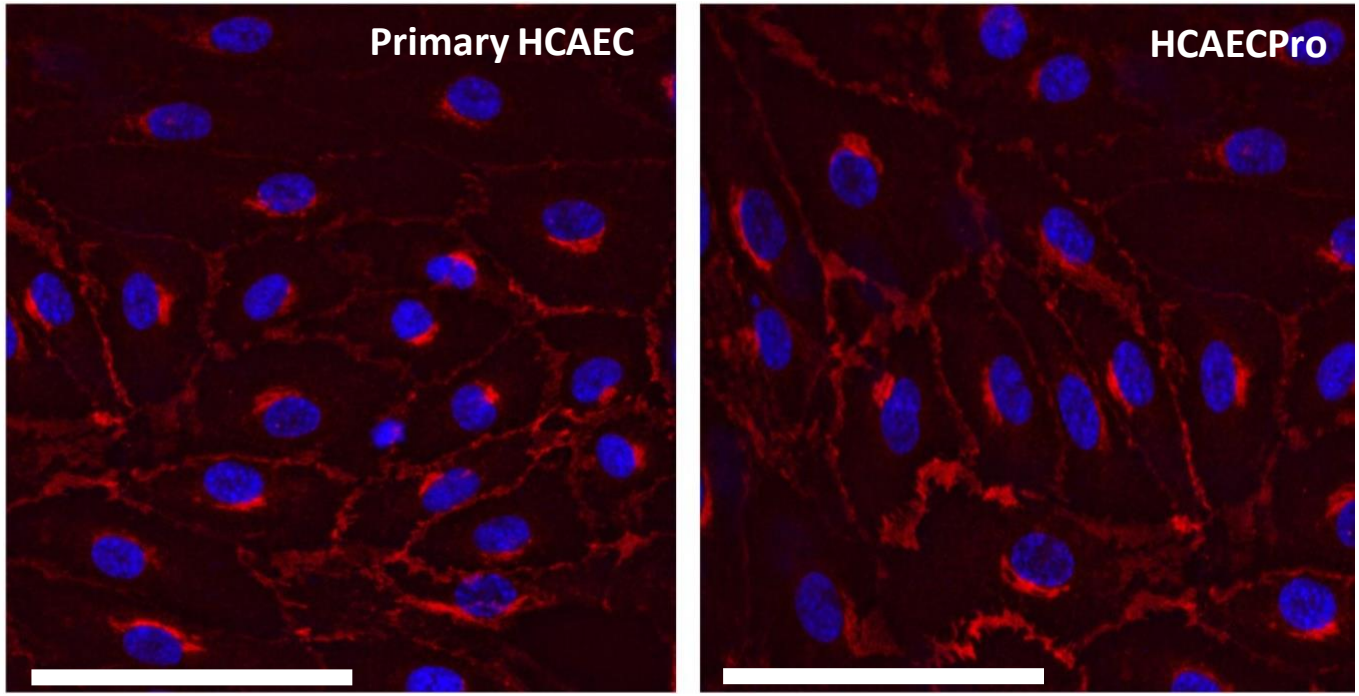

Figure 3.3.3: ICC Staining of VE-Cadherin

Immunofluorescent images of primary HCAECs and HCAECPro endothelial specific adhesion molecule, VE-cadherin (red) and DAPI (blue). Cells were incubated overnight at $4^{O}C$ with Ve-Cadherin at 1:200 in TBST containing 1% BSA. Cells were washed and incubated with Alexa fluor 594 goat-anti rabbit antibody 1:400 at room temperature in TBST containing 1% BSA in the dark for 1 hour. Slides were mounted in Vectershield antifade mounting media containing DAPI. Images taken using Thunder Imaging system x40. Scale bar = 100µM.

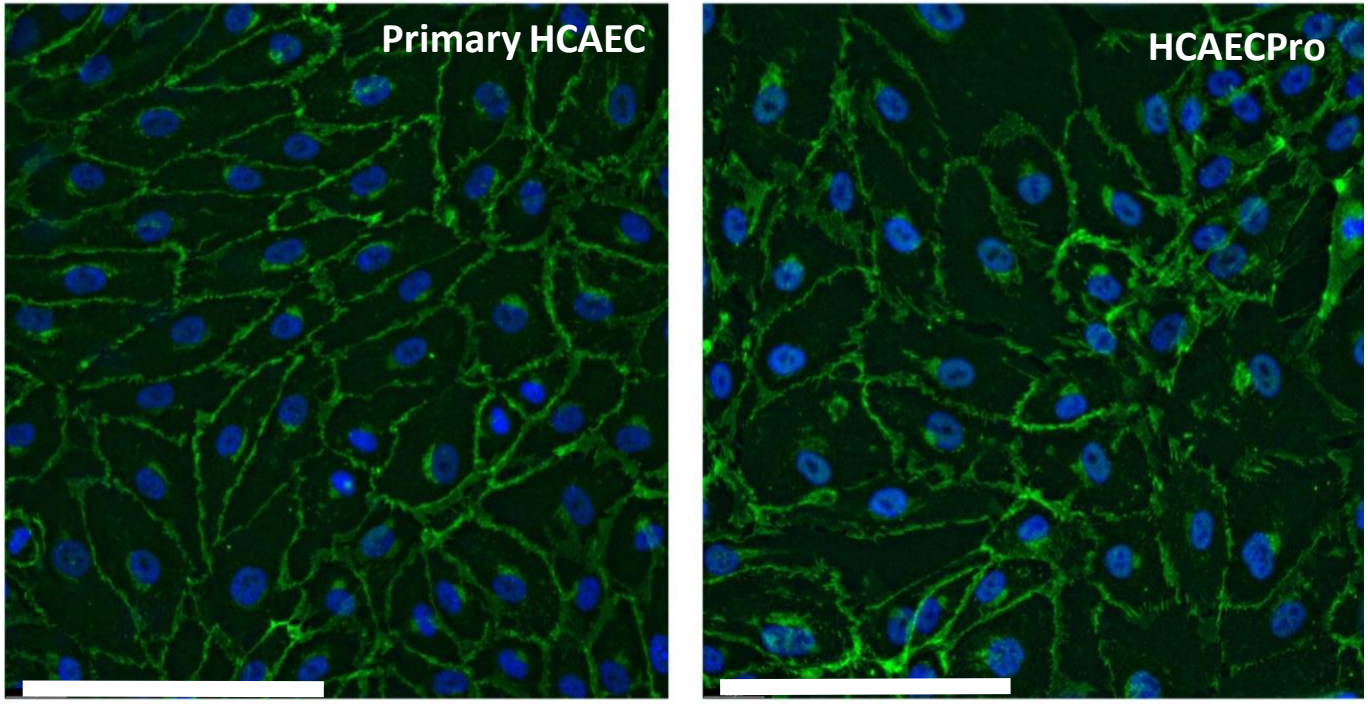

Figure 3.3.4: ICC Staining of β-Catenin Immunofluorescent images of primary HCAECs and HCAECPro stained for endothelial adheren junctional complex β-catenin (green) and DAPI (blue). Cells were incubated overnight at $4^{O}C$ with β-catenin at 1:200 in TBST containing 1% BSA. Cells were washed and incubated with Alexa fluor 488 goat-anti rabbit antibody 1:400 at room temperature in TBST containing 1% BSA in the dark for 1 hour. Slides were mounted in Vectershield antifade mounting media containing DAPI. Images taken using Thunder Imaging system x40. Scale bar = 100µM.

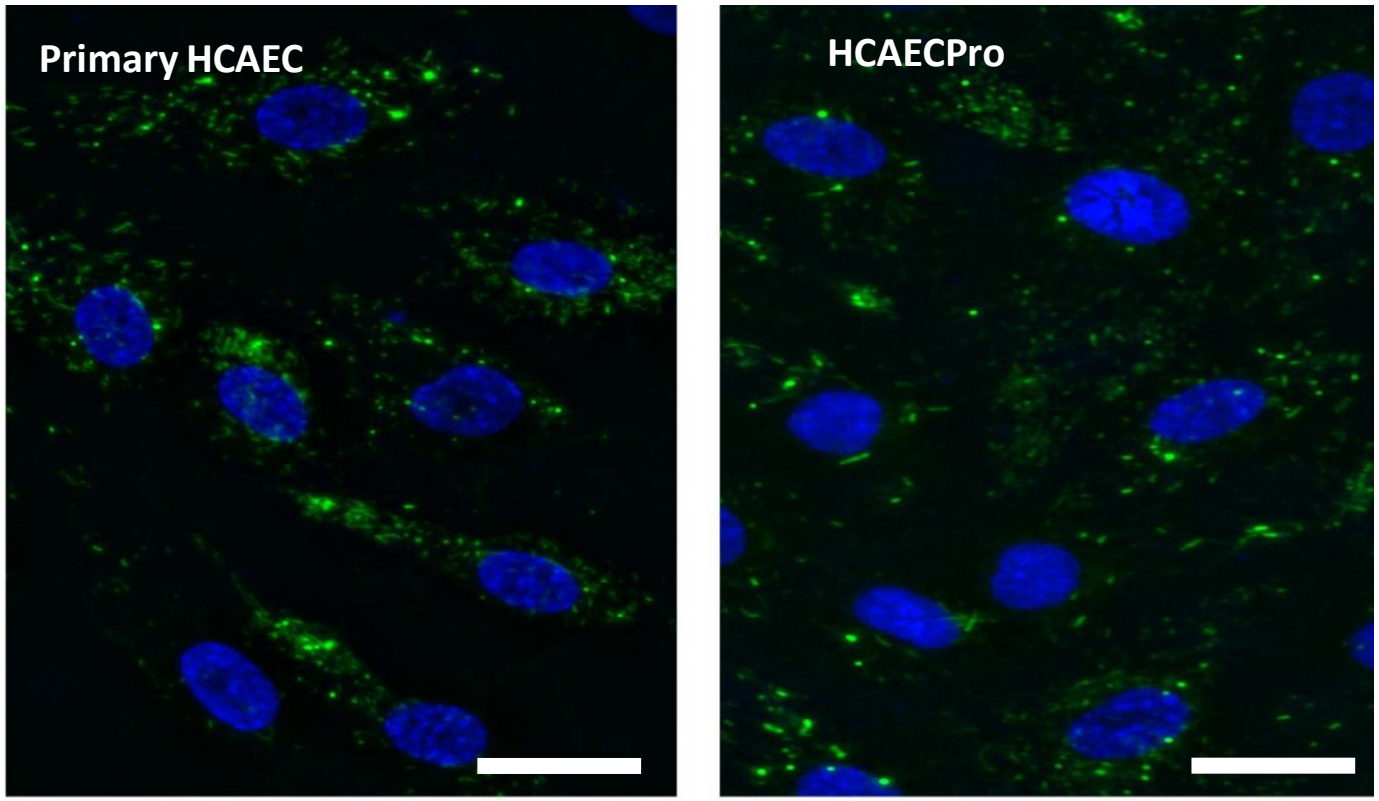

Figure 3.3.5: ICC Staining of vWF

Immunofluorescent images of primary HCAECs and HCAECPro stained for endothelial Von Willebrand Factor (green) and DAPI (blue). Cells were washed and incubated with Alexa fluor 488 goat-anti rabbit antibody 1:400 at room temperature in TBST containing 1% BSA in the dark for 1 hour. Slides were mounted in Vectershield antifade mounting media containing DAPI. Images taken using Thunder Imaging system x60. Scale bar = 100µM.

3.4 HCAECPro Cells Retain Response to Shear Stress Comparable to Primary HCAECs

Results have demonstrated that lentiviral overexpression leads to an increase in the proliferative potential and reduced senescence of HCAECPro cells, morphological studies have shown that HCAECPro cells, even at a high passage remain endothelial-like with little to distinguish them from primary cell counterparts.

Although results appear to demonstrate an increase in proliferation without inducing transformation, it was imperative that HCAECPro cells retain key mechanosensitive properties. The key hallmark of an endothelial cell is its ability to realign in direction of mechanical force, i.e., blood flow within the arteries. Utilising our in-house parallel plate flow system (see figure 2.1), we are able to able to expose our cell lines to oscillatory, normal laminar and elevated shear stress to mimic the different physiological flow environments seen with coronary arteries.

Observational images under phase contrast, as well as immunofluorescent staining of actin realignment with phalloidin and focal adhesion marker vinculin revealed realignment in direction of flow under OSS (fig 3.4.2→3.4.4).

Previous work within the White lab has developed the use of this model. Utilising this method, we were able to expose HCAECPro late passage cells and primary cell counterparts to three distinct flow environments and thus measure the mRNA expression of already established flow regulated genes (fig 3.4.5→3.4.12). Observing conformational changes in addition to regulation of these genes allowed us to identify properties of the transduced cell line comparable to primary cells.

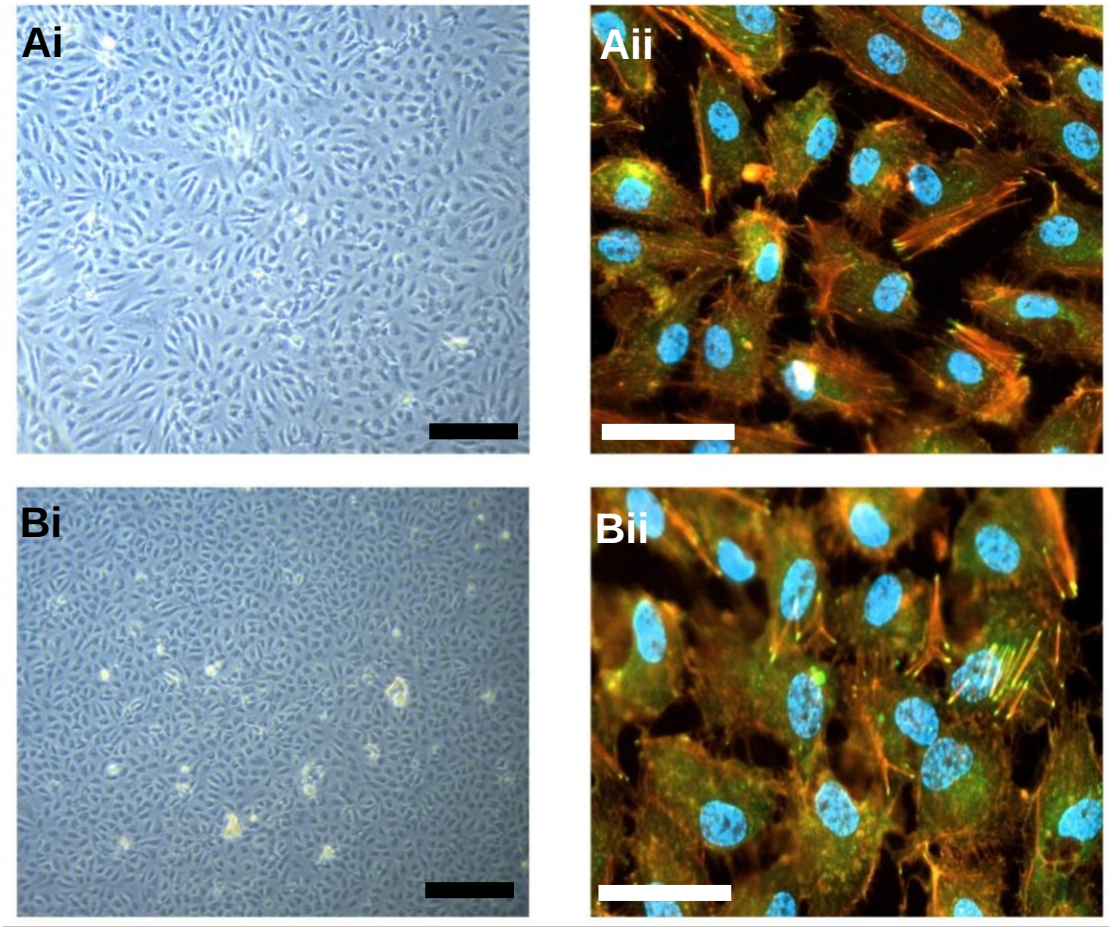

Figure 3.4.2: HCAECs and HCAECPro cells Exposed to OSS

Phase contrast images of primary HCAECs (Ai & Aii) and HCAECPro cells (Bi & Bii) exposed to OSS (±0.5Pa) for 72 hours using in house parallel plate flow apparatus. Phase contrast images taken using standard table top light microscope. Following flow, both cell lines were subsequently fixed using PEM buffer. Cells were incubated overnight at $4^{O}C$ with Vinculin at 1:200 in TBST containing 1% BSA. Cells were washed and incubated with Alexa fluor 488 goat-anti mouse antibody 1:400 and 568-phalloidin 1:100 at room temperature in TBST containing 1% BSA in the dark for 1 hour. Slides were mounted in Vectershield antifade mounting media containing DAPI. Images taken using Zeiss M2 fluorescent microscope. White Scale bar = 100µM, black scale bar = 500µM.

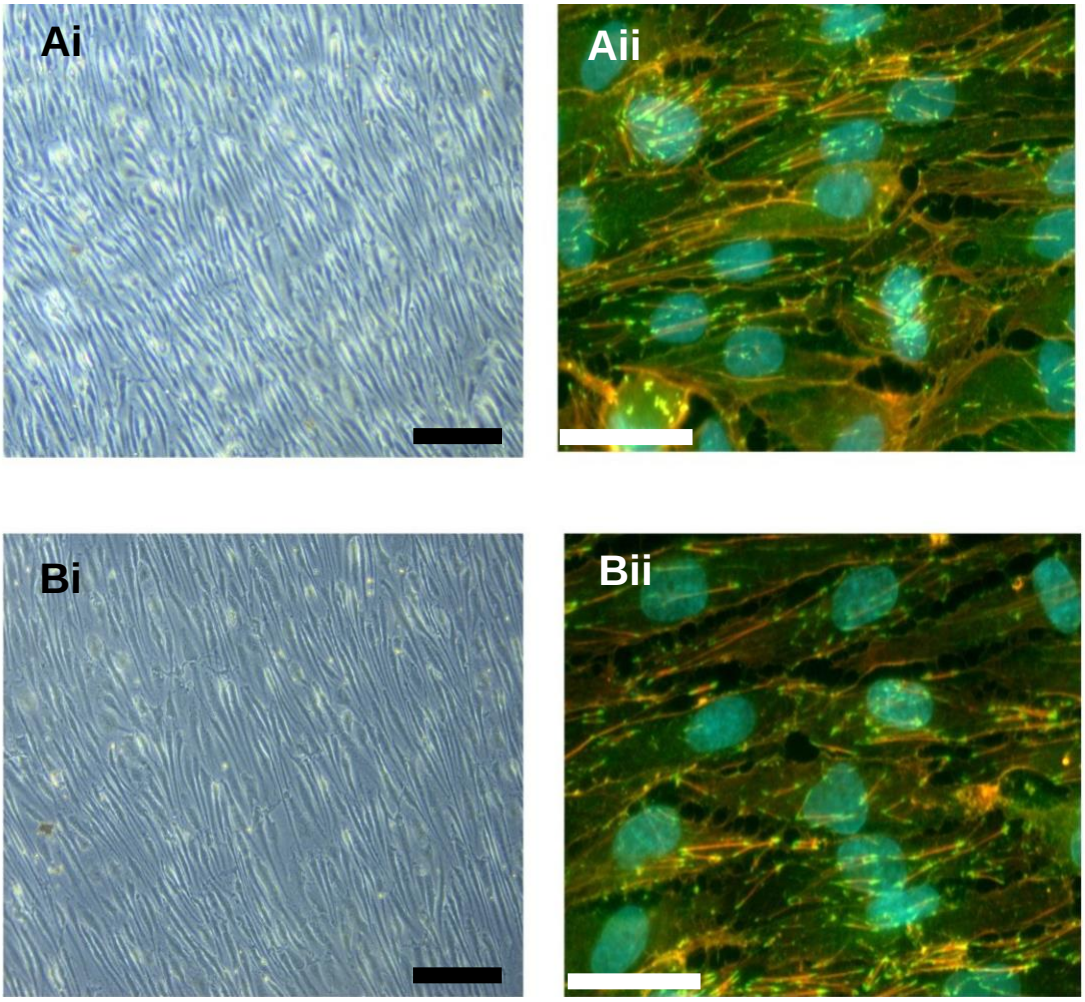

Figure 3.4.3: HCAECs and HCAECPro cells Exposed to LSS

Phase contrast images of primary HCAECs (Ai & Aii) and HCAECPro cells (Bi & Bii) exposed to LSS (1.5Pa) for 72 hours using in house parallel plate flow apparatus. Phase contrast images taken using standard table top light microscope. Following flow, both cell lines were subsequently fixed using PEM buffer. Cells were incubated overnight at $4^{O}C$ with Vinculin at 1:200 in TBST containing 1% BSA. Cells were washed and incubated with Alexa fluor 488 goat-anti mouse antibody 1:400 and 568-phalloidin 1:100 at room temperature in TBST containing 1% BSA in the dark for 1 hour. Slides were mounted in Vectershield antifade mounting media containing DAPI. Images taken using Zeiss M2 fluorescent microscope. Scale bar = 100µM, black scale bar= 300µM.

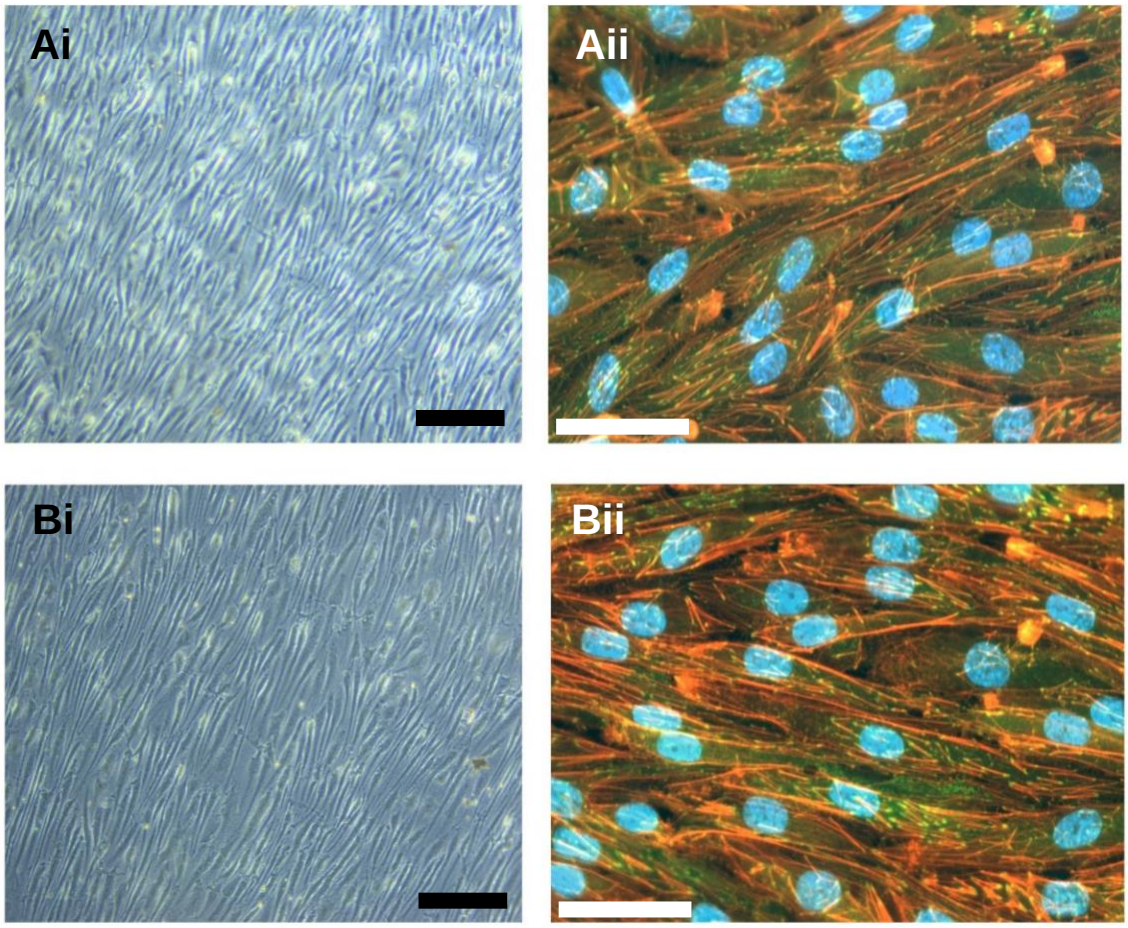

Figure 3.4.4: HCAECs and HCAECPro cells Exposed to ESS

Phase contrast images of primary HCAECs (Ai & Aii) and HCAECPro cells (Bi & Bii) exposed to ESS (7.5Pa) for 72 hours using in house parallel plate flow apparatus. Phase contrast images taken using standard table top light microscope. Following flow, both cell lines were subsequently fixed using PEM buffer. Cells were incubated overnight at $4^{O}C$ with Vinculin at 1:200 in TBST containing 1% BSA. Cells were washed and incubated with Alexa fluor 488 goat-anti mouse antibody 1:400 and 568-phalloidin 1:100 at room temperature in TBST containing 1% BSA in the dark for 1 hour. Slides were mounted in Vectershield antifade mounting media containing DAPI. Images taken using Zeiss M2 fluorescent microscope. Scale bar = 100µM, black scale bar = 300µM.

In addition, we performed qPCR for the major transcription factors that are responsible for modifying the >1000 genes that are flow sensitive in HCAECs (KLF2 and KLF4) and KLF-regulated genes (eNOS-NOS3, NOV, PI16 and IκBα) and Nrf2

regulated genes (OSGIN1 and OSGIN2), comparing their expression in p4 HCAECs and p15 HCAECPro in response to flow (Fig 3.4.5 ➔ 3.4.12). All of the genes analysed showed shear responsiveness, indicating that HCAECPro maintain the ability to sense shear stress and regulate the main transcription factors (KLF2/4 and Nrf2) and downstream genes. This was further confirmed using our TFARs in Chapter 4.

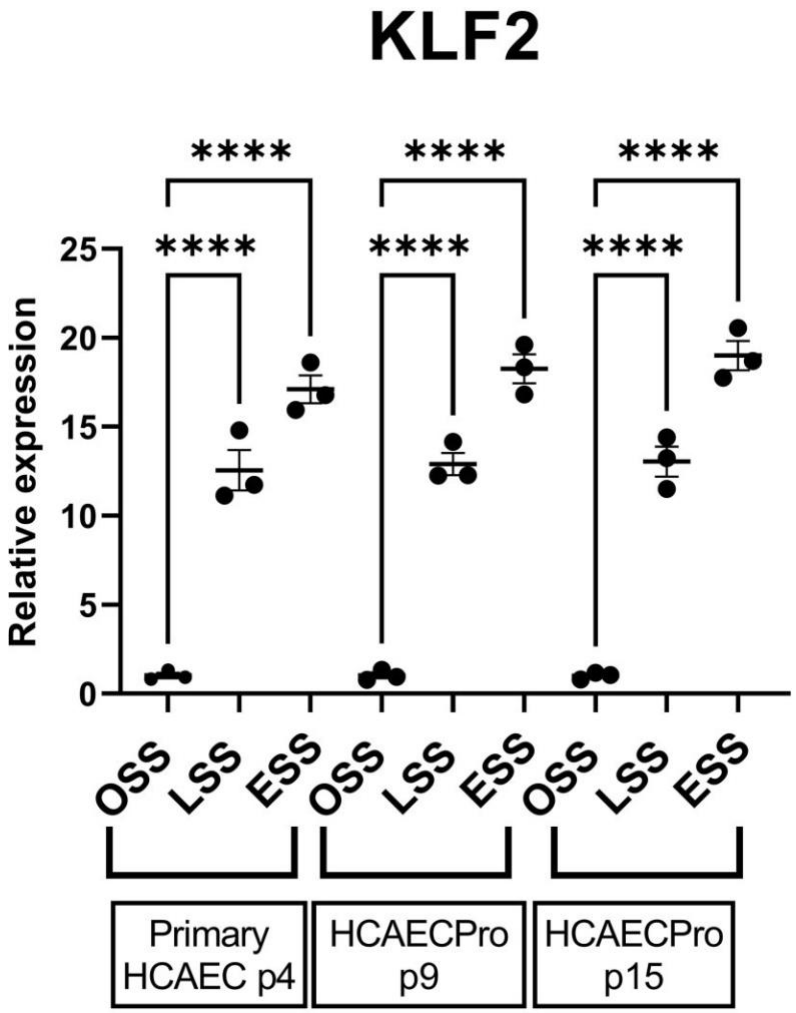

Figure 3.4.5: KLF2 mRNA expression in primary HCAECs and HCAECPro.

Cells were cultured for 72hr under oscillatory shear stress (±0.5Pa -OSS), normal laminar (1.5Pa – LSS) and elevated shear stress (7.5Pa – ESS). Primary HCAECs and HCAECPro cells were seeded onto a 0.1% gelatine coated slide at a density of $2.5x10^5$ cells/slide and allowed to adhere for three days before induction of flow. HCAECPro cells response to flow was monitored at higher passages of p9 and p15 in order to assess retained mechanosensitivity. n=3, ANOVA. *p= <0.05, **p<0.01, ***p<0.001, ±SEM.

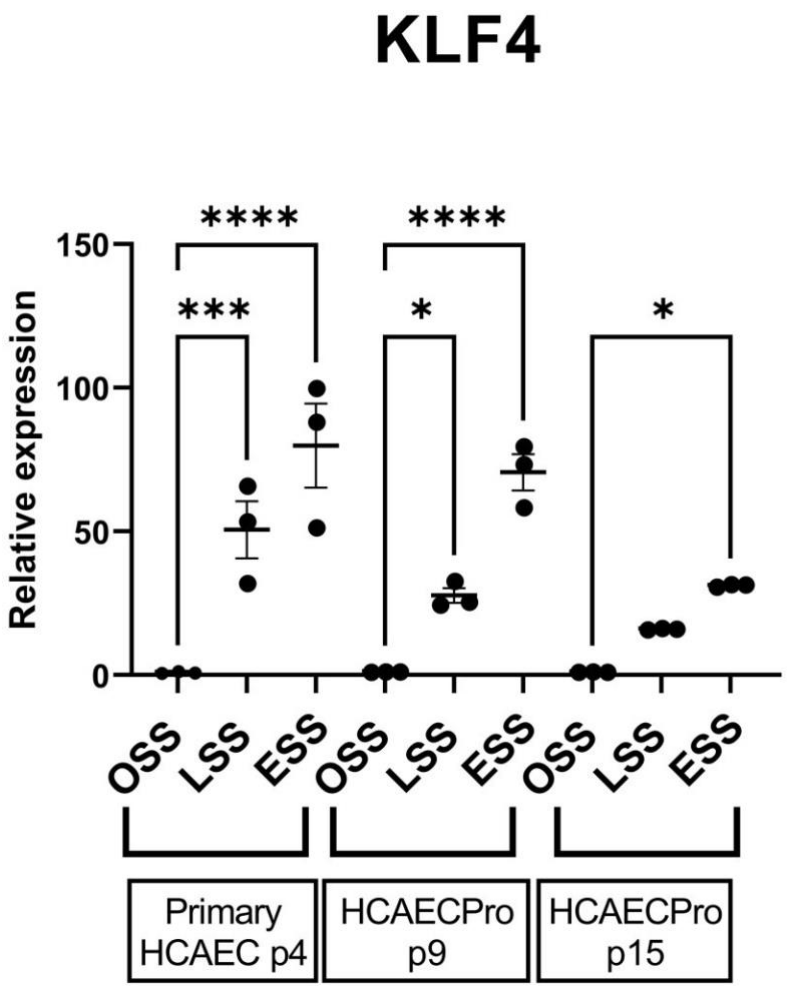

v

Figure 3.4.6: KLF4 mRNA expression in primary HCAECs and HCAECPro.

Cells were cultured for 72hr under oscillatory shear stress (±0.5Pa -OSS), normal laminar (1.5Pa – LSS) and elevated shear stress (7.5Pa – ESS). Primary HCAECs and HCAECPro cells were seeded onto a 0.1% gelatine coated slide at a density of $2.5x10^5$ cells/slide and allowed to adhere for three days before induction of flow. HCAECPro cells response to flow was monitored at higher passages of p9 and p15 in order to assess retained mechanosensitivity. n=3, ANOVA. *p= <0.05, **p<0.01, ***p<0.001, ±SEM.

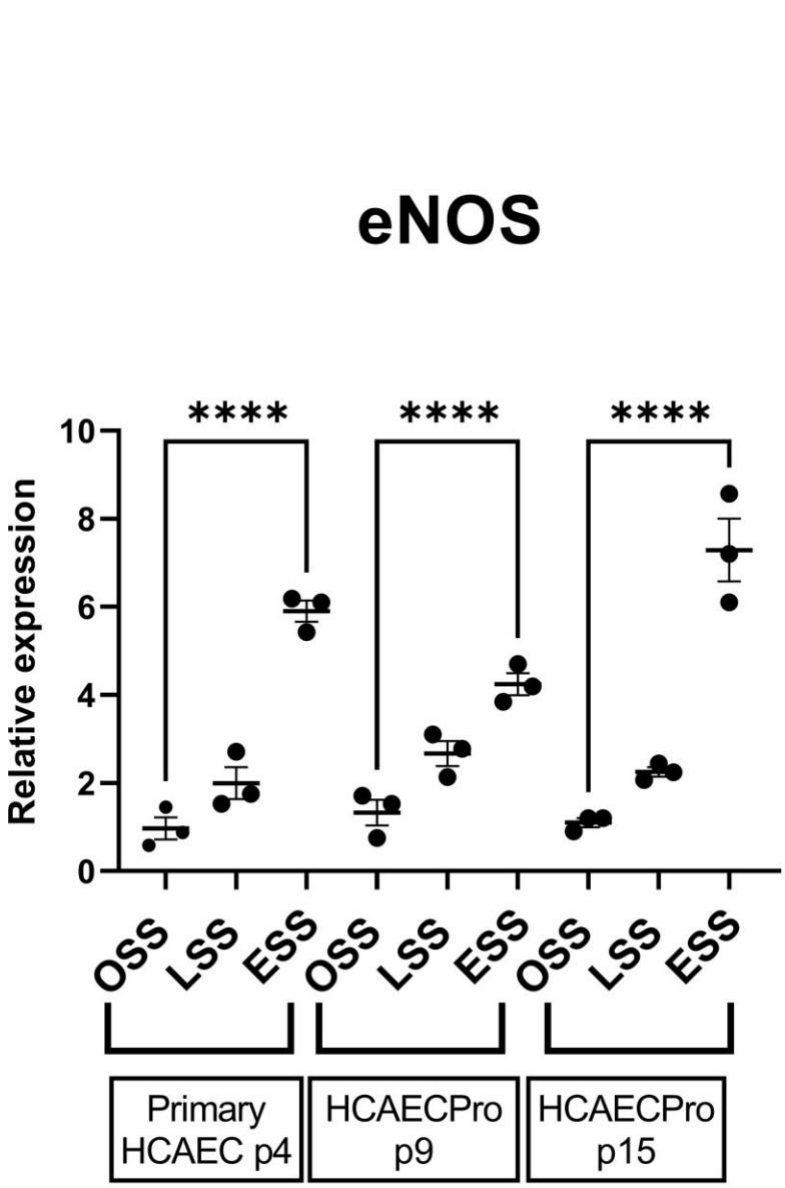

Figure 3.4.7: eNOS mRNA expression in primary HCAECs and HCAECPro.

Cells were cultured for 72hr under oscillatory shear stress (±0.5Pa -OSS), normal laminar (1.5Pa – LSS) and elevated shear stress (7.5Pa – ESS). Primary HCAECs and HCAECPro cells were seeded onto a 0.1% gelatine coated slide at a density of $2.5x10^5$ cells/slide and allowed to adhere for three days before induction of flow. HCAECPro cells response to flow was monitored at higher passages of p9 and p15 in order to assess retained mechanosensitivity. n=3, ANOVA. *p= <0.05, **p<0.01, ***p<0.001, ±SEM.

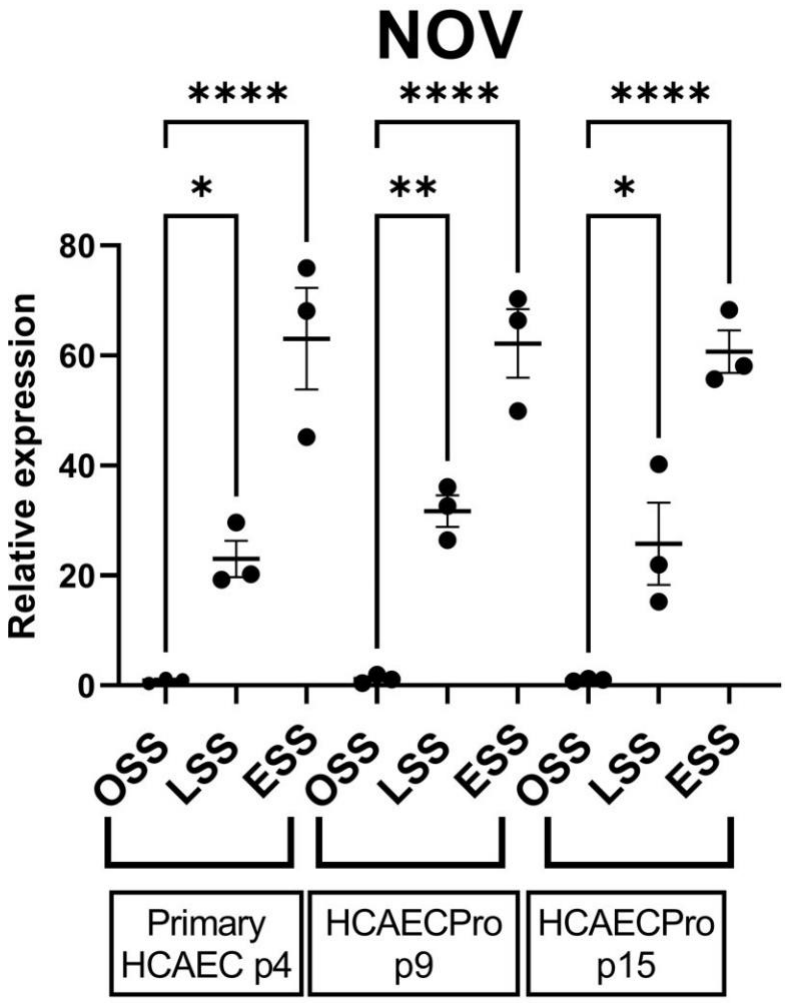

Figure 3.4.8: NOV mRNA expression in primary HCAECs and HCAECPro

Cells were cultured for 72hr under oscillatory shear stress (±0.5Pa -OSS), normal laminar (1.5Pa – LSS) and elevated shear stress (7.5Pa – ESS). Primary HCAECs and HCAECPro cells were seeded onto a 0.1% gelatine coated slide at a density of $2.5x10^5$ cells/slide and allowed to adhere for three days before induction of flow. HCAECPro cells response to flow was monitored at higher passages of p9 and p15 in order to assess retained mechanosensitivity. n=3, ANOVA. *p= <0.05, **p<0.01, ***p<0.001, ±SEM.

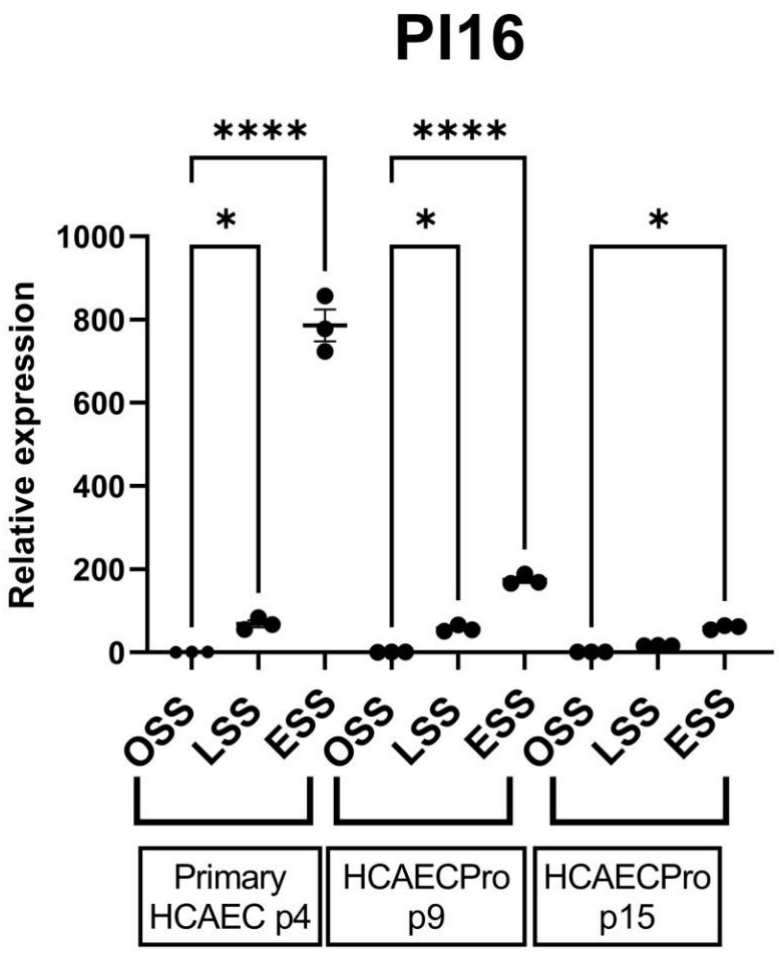

Figure 3.4.9: PI16 mRNA expression in primary HCAECs and HCAECPro

Cells were cultured for 72hr under oscillatory shear stress (±0.5Pa -OSS), normal laminar (1.5Pa – LSS) and elevated shear stress (7.5Pa – ESS). Primary HCAECs and HCAECPro cells were seeded onto a 0.1% gelatine coated slide at a density of $2.5x10^5$ cells/slide and allowed to adhere for three days before induction of flow. HCAECPro cells response to flow was monitored at higher passages of p9 and p15 in order to assess retained mechanosensitivity. n=3, ANOVA. *p= <0.05, **p<0.01, ***p<0.001, ±SEM.

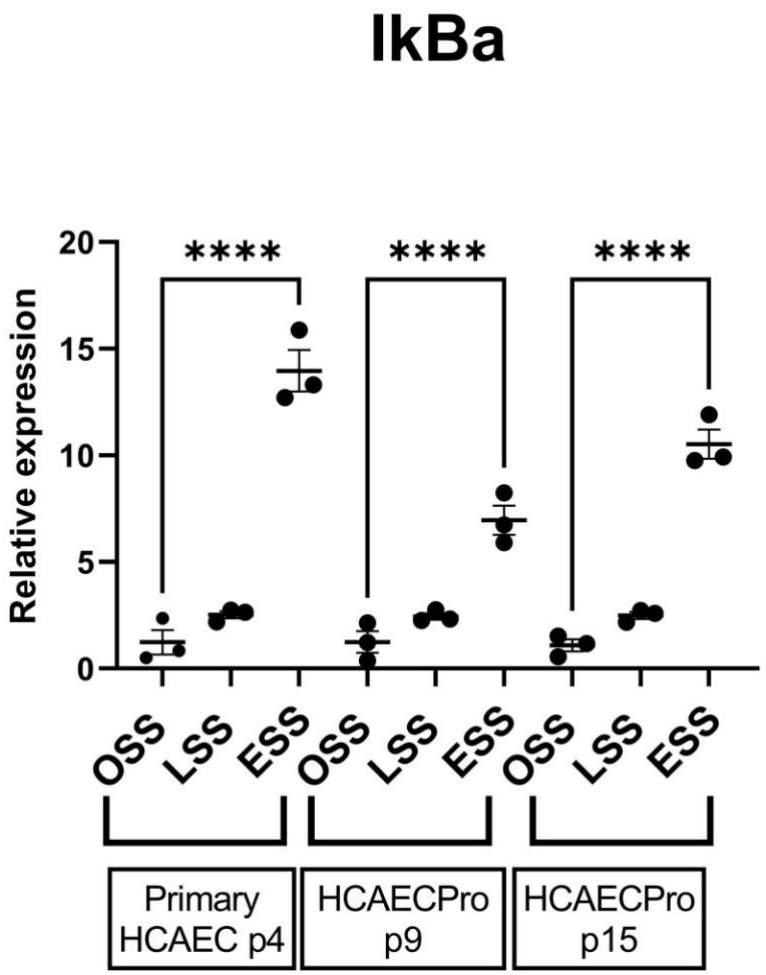

Figure 3.4.10: IkBα mRNA expression in primary HCAECs and HCAECPro

Cells were cultured for 72hr under oscillatory shear stress (±0.5Pa -OSS), normal laminar (1.5Pa – LSS) and elevated shear stress (7.5Pa – ESS). Primary HCAECs and HCAECPro cells were seeded onto a 0.1% gelatine coated slide at a density of $2.5x10^5$ cells/slide and allowed to adhere for three days before induction of flow. HCAECPro cells response to flow was monitored at higher passages of p9 and p15 in order to assess retained mechanosensitivity. n=3, ANOVA. *p= <0.05, **p<0.01, ***p<0.001, ±SEM.

.

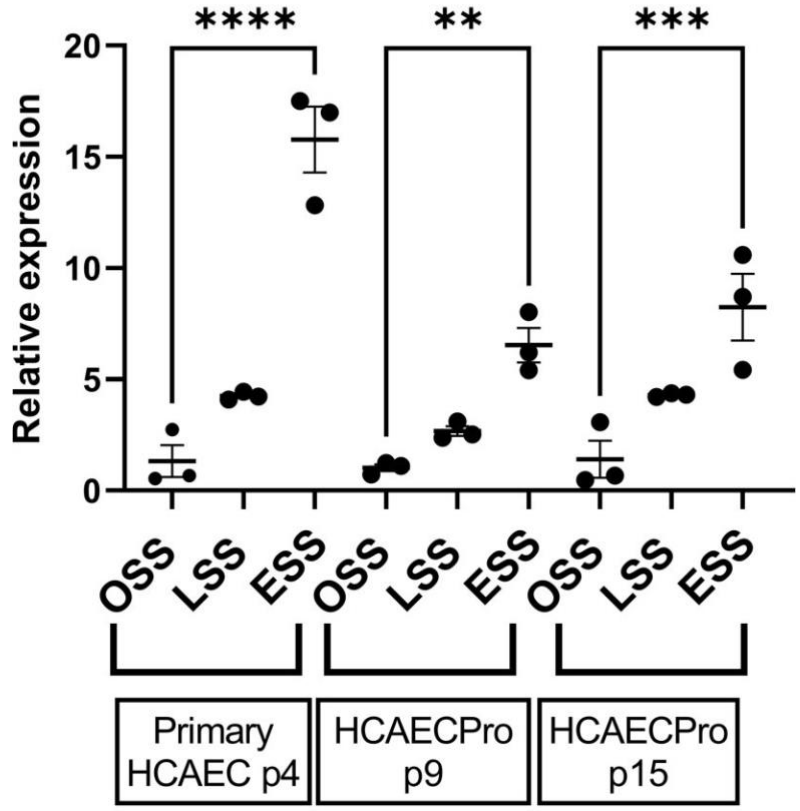

Figure 3.4.11: OSGIN1 mRNA expression in primary HCAECs and HCAECPro

Cells were cultured for 72hr under oscillatory shear stress (±0.5Pa -OSS), normal laminar (1.5Pa – LSS) and elevated shear stress (7.5Pa – ESS). Primary HCAECs and HCAECPro cells were seeded onto a 0.1% gelatine coated slide at a density of $2.5x10^5$ cells/slide and allowed to adhere for three days before induction of flow. HCAECPro cells response to flow was monitored at higher passages of p9 and p15 in order to assess retained mechanosensitivity. n=3, ANOVA. *p= <0.05, **p<0.01, ***p<0.001, ±SEM.

.

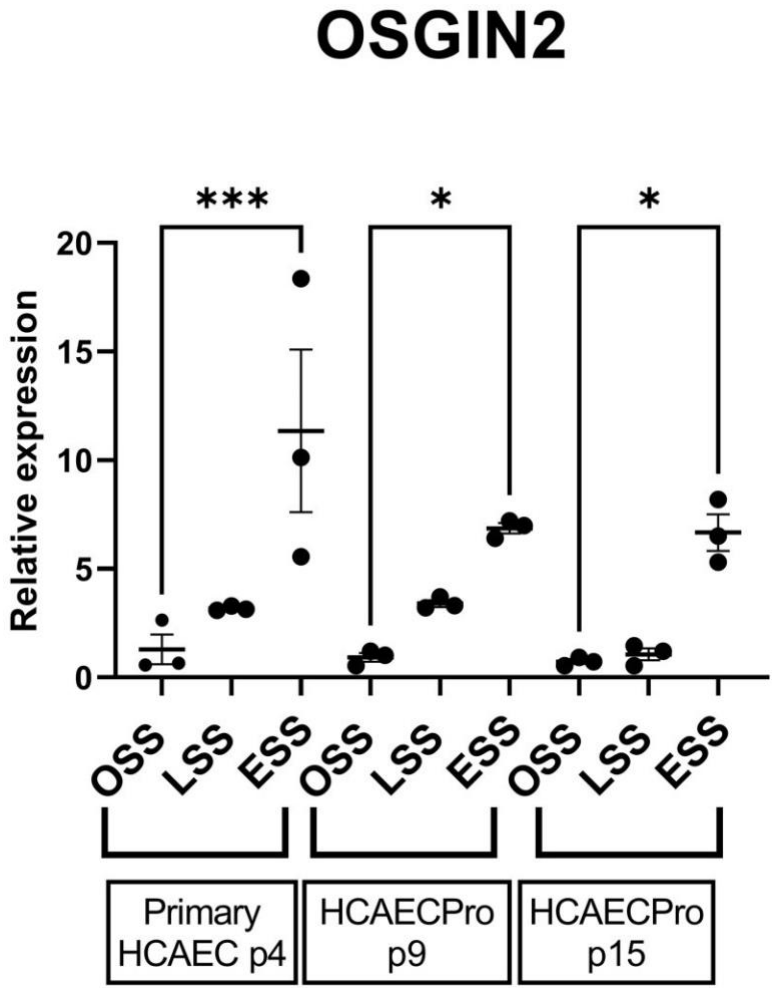

Figure 3.4.12 OSGIN2 mRNA expression in primary HCAECs and HCAECPro

Cells were cultured for 72hr under oscillatory shear stress (±0.5Pa -OSS), normal laminar (1.5Pa – LSS) and elevated shear stress (7.5Pa – ESS). Primary HCAECs and HCAECPro cells were seeded onto a 0.1% gelatine coated slide at a density of $2.5x10^5$ cells/slide and allowed to adhere for three days before induction of flow. HCAECPro cells response to flow was monitored at higher passages of p9 and p15 in order to assess retained mechanosensitivity. n=3, ANOVA. *p= <0.05, **p<0.01, ***p<0.001, ±SEM.

3.5 Discussion

This chapter describes the creation of an endothelial cell line to enable the formation of the E-Sense system. While many cell types participate in the development of atherosclerotic plaques, the observation that plaques form at focal points within arteries, exposed to low laminar and disturbed shear stress (Bentzon *et al.*, 2014) identified endothelial cells as key players in regulating atherosclerosis. In addition, plaque growth also localises to regions exposed to disturbed flow (Chien, 2008)(Warboys *et al.*, 2011). For a cell-based system for detecting cardiovascular risk, endothelial cells are ideal as they can respond to the proinflammatory and cell stress pathways implicated in atherosclerosis (described in chapter 1) and protective signalling induced by exposure to laminar flow that spares straighter sections of artery from plaque development (Wong *et al.*, 2016). The ideal cell line would be able to be sequentially passaged without undergoing replicative senescence, maintain similar phenotype to primary HCAECs, and importantly retain the response to flow, to allow the protective effects of laminar flow to be quantified and measured. This was considered important as any compound that reduced the response to laminar flow has the capacity to advance plaque formation and plaque growth by reducing the expression of protective genes.

Replicative senescence was assessed by quantification of senescent-associated β- galactosidase activity, and upregulation of $p16^{ink}$ and p21 by qPCR. β-galactosidase hydrolyses monosaccharides and the observed increase in activity is linked to an increase in senescent cells (Juers, Matthews and Huber, 2012). Figure 3.1.3 demonstrates that with continued passage, the percentage of HCAECs that stain positive for β-galactosidase activity increases as expected,

which was prevented by overexpression of BMI1 and hTERT in HCAECPro and also by transduction of eachseparately (Figures 3.1.3 + 3.1.4). These observations were supported by changes in expression of p16ink and p21 (figure 3.1.5➔3.1.7)., both of which significantly increased in HCAECs between p4 and p9, but remained at basal levels in HCAECPro. Taken together, they provide strong evidence that overexpression of BMI1 and hTERT prevent replicative senescence as would be expected given their known function within the cell. It was not possible to passage HCAECs beyond p14 as they underwent complete cell cycle arrest that was also associated with a significant change in their morphology.

Both proliferation and apoptosis were assessed by flow cytometry. We observed a small increase in the number of cells in G2/S phase with BMI1 and hTERT overexpression compared to HCAECs p4 (Figure 3.2.5) that might be linked with reduced number of senescent cell that would be present at low number in p4 primary cells. Importantly, this number did not change between p9 and p15 in HCAECPro, which might be expected if cellular transformation was occurring. Furthermore, we didn't see any induction of apoptosis with extended passage in HCAECPro (Figure 3.2.3).

Although our data demonstrated that we had successfully extended proliferative capacity of HCAECPro, by preventing replicative senescence, it was important to show that BMI1/hTERT transduced cells maintained key endothelial features such as morphology and mechanosensitivity (Ishii, Warabi and Mann, 2021). Phase contrast images and immunocytochemical analysis demonstrated that morphology and gene expression and protein location showed no discernible differences between p4 HCAECs and p15 HCAECPro cultured under static conditions (Figures 3.3.2➔3.3.6). HCAECPro retain the 'cobblestone' endothelial cell morphology, similar numbers and distribution of focal adhesion

marker, vinculin and F-actin marker phalloidin as p4 HCAECs. Stable cell-cell junctions labelled with VE- cadherin and associated intracellular ligand β catenin similarly were not changed in HCAECPro p15. Staining for endothelial specific vWF show that HCAECPro cells exhibit the Weibel Palade bodies distinct to endothelial cells containing VWF. The immunocytochemistry we performed indicates that even at a high passage of p15, our HCAECPro cell line displays morphological features which are both comparable and indiscriminate to low passage primary HCAECs, therefore indicating maintenance of endothelial phenotype even at p15.

Finally, a key endothelial trait is its ability to detect and respond to changes in the haemodynamic environment (Dolan, Kolega and Meng, 2013). Using our in-house parallel plate flow, we exposed both primary HCAECs and HCAECPro to laminar flow (1.5 Pa), oscillatory flow (0.5 Pa) and elevated flow (7.5 Pa) for 72 hours and assessed both morphological and gene expression changes in response to the different flow environments. Fundamentally, p15 HCAECPro adopted the same morphology as p4 HCAECs in all 3 flow environments, with cobblestone appearance under OSS, and alignment with the direction of flow in both LSS and ESS (figure 3.4.2➔3.4.4)

Changes in gene expression on culture under flow were also similar. All flow responsive genes were significantly changed between OSS and laminar flow. Some evidence for a blunted KLF4 induction was observed, with lower upregulation in response to LSS and ESS observed at p15 compared to HCAECs p4 (LSS 51-fold at p4 in HCAECs, 16.4-fold in HCAECPro p15. ESS 79.2-fold in HCAEC p4, 31.7- fold in HCAECPro p15). This was also mirrored by PI16, which is one of the most laminar flow-responsive genes in HCAECs and potentially indicates a predominant role for KLF4 in this response (Hazell *et al.*, 2016). However, KLF2 and the other flow sensitive genes eNOS, NOV and IκBα showed

comparable responses to laminar flow compared to oscillatory flow between HCAECPro and p4 HCAECs (Figures 3.4.5➔3.4.10). Similarly, both OSGIN1 and OSGIN2 (Nrf2 regulated genes) (figure 3.4.11 and 3.4.12), also responded to the flow environment in an identical pattern to HCAECs p4. Taken together, the data demonstrates that HCAECPro retain mechanosensitivity and a similar response to laminar flow that would allow the protective pathways induced by laminar flow to be assessed within the E-Sense system.

3.6 Summary

Key Findings of HCAECPro Cells in Comparison to Primary HCAECs:

	Expression of senescent markers	Apoptosis	G2/S Phase	Flow-regulated genes
HCAECPro p9	**Reduced**	**Reduced**	**Increased**	**Comparable**
HCAECPro p15	**Reduced**	**Reduced**	**Increased**	**Comparable**

Conclusion

The results in this chapter demonstrate that transduction of HCAECs with hTERT and BMI1 (termed HCAECPro) extend the proliferative capacity of HCAECs beyond their natural capacity and at least to p15. No significant changes in morphology or gene expression was observed and HCAECPro retain the key feature of mechanosensitivity that is required for the E-Sense system. Therefore, HCAECPro provide a suitable cell platform to create E-Sense.

Chapter 4

Creation and Assessment of Novel TFARs in Response to Known Agonists in HCAECPro

4.0 Introduction

Modulation of signalling cascades or gene expression in response to external factors can be measured through the use of standard molecular techniques such as western blotting and PCR. Although typically robust methods, one main drawback is the need to lyse cells, resulting in only single timepoints and time-intensive preparation. When drug or compound screening, repeated or continuous measurements may provide additional insights on kinetics that are useful for elucidating the mechanisms of action of test compounds. Transcription Factor Activator Reporters (TFARs) are particularly useful in analysing signalling cascades that result in alterations of transcription factor activity and can result in a large dynamic range of signal, making quantification easier (Xu *et al.*, 2013). In addition, the use of secreted luciferases have become increasingly popular as they allow repeated sampling and kinetic studies to be performed.

Eukaryotic genes include enhancer and promoter regions that regulate transcriptional activity through the recruitment of transcription factors and RNA polymerase machinery to initiate transcription. Transcriptional factors (TFs) recognise and bind to specific DNA sequences with key bases forming interactions with the transcription factor, creating “transcriptional switches”, which regulate gene expression (Lin, Xu and Leaman, 2016). There is some tolerance for mismatches between an ideal binding site for a transcription factor and functional sequences found in promoters and enhancers, leading to the definition of a ‘consensus’ binding sequence, with greater affinity for binding observed to sequences that are closer the consensus (Xu *et al.*, 2013). One of the key components in the transcriptional initiation machinery associated with RNA polymerase II (RNA Pol II) promoters is the presence of a TATA box, which recruits TATA-binding protein (TBP) just upstream of the site of transcription initiation (Ponjavic *et al.*, 2006) (Trifonov, 2016).

However, binding of TBP to the TATA box is insufficient for the recruitment of RNA Pol II rand initiation of transcription. This results in the need for additional TFs, to be recruited to a promoter to trigger the formation of the pre-initiation complex (PIC), which includes TBP and 14 additional TBP-associated factors and RNA Pol II around the TATA box and initiator (Inr) sequence to allow transcription to occur (Papadakis *et al.*, 2005).

TFARs combine multimerised transcription factor binding sites, frequently using a repeat of the same consensus sequence upstream of a minimal promoter containing a TATA box and Inr sequence (Minchin and Busby, 2013). This forms a basic and inducible promoter that is responsive to just the transcription factor that bind the inserted consensus sequence. Downstream of the inducible minimal promoter, TFARs contain a reporter gene to allow quantification of promoter activity (Ghim *et al.*, 2010). For this project we combined both a secreted luciferase (Nano-luciferase, or Vargula-luciferase) and green fluorescent protein to allow visual assessment of TFAR activity. Secreted luciferases allow continuous measurement of TF activity with assay systems that are highly specific allowing more than one TFAR to be included in a single cell line, increasing the capacity to concurrently assess different signalling pathways. Figure 4.1 below describes the structure of a TFAR used in this project. Our TFARs contained six repeated binding sequences of transcription factors, containing transcript variants spaced 10.5bp apart, upstream of the inducible minimal promoter. The minimal promoter is comprised of a short sequence, allowing for the formation of the initiation complex. This inducible promoter has a downstream luciferase (either nLuc or vLuc), which is secreted upon binding of TF consensus sequence and subsequent transcriptional activation, with an additional GFP tag attached (Yariv Greenshpan, Omri Sharabi , Ksenia M Yegodayev, Ofra Novoplansky , Moshe Elkabets, 2022).

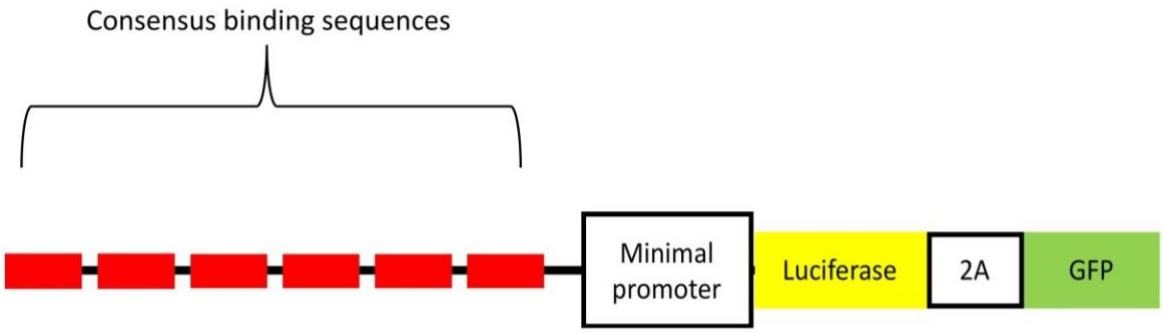

Figure 4.1: TFAR design – We used 6 TF binding sites upstream of a minimal promoter to create the TFARs used in this study. If the consensus binding sequence contained multiple options, we included these variations within the 6 repeated consensus binding sites spaced 10.5bp apart upstream of a minimal promoter, which upon activation drives luciferase secretion.

In this study, we employed a novel approach in our TFAR design that increased the dynamic range of our reporters. Firstly, we incorporated potential variation found in transcription factor binding motifs (TFBMs)–- the DNA sequence which form the recognition site for TF binding. TFBM consensus sequences contain variations in DNA sequence (e.g., Fig 4.2), indicating some 'wobble' in base preference at particular sites within the consensus sequence.

A

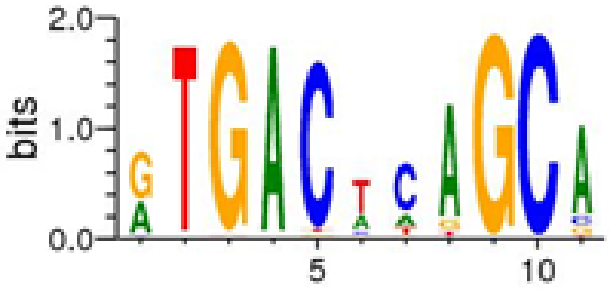

B T(A/C)Ann(A/G)TGA(C/T)nnnGC(A/G)

C

TAAnnATGACTCAGCA
TCAnnGTGACACAGCA
TAAnnGTGACTCAGCA
TCAnnATGACTCAGCA
TAAnnATGACTCAGCA
TCAnnGTGACACAGCA

Figure 4.2: Construction of Nrf2 (NFE2L2) TFAR. A) consensus binding site for Nrf2 from Motifmap (https://motifmap.ics.uci.edu/). B) ARE consensus sequence from…. C) combining the available data from different sources, we designed a series of TF binding sites that include a range of potential binding preferences of Nrf2.

Secondly, most TFAR design simply concatemerized the consensus binding sequences, however we hypothesised that this may be suboptimal, due to the rotational constraints of the DNA double helix, preventing the activation domains of adjacently bound TFs from interacting as they would be positioned on different rotational planes of the helix. It is a common observation that within human promoters, TF binding sites cluster over short stretches of DNA, but these are often regularly spaced to align with the rotational frequency of the DNA double helix (10.5 bp). This was specifically investigated by Vsevolod et al in 2003 to uncover the spacing preference of five transcription factors; Bicoid (Bcd), Kruppel, Hunchback (Hb), Knirps and Caudal. They identified a striking periodic preference of 10bp or

11bp, suggesting a preferential position of binding site combinations on the same side of the DNA helix (Makeev *et al.*, 2003). Furthermore, they discerned a high amplitude of Hb-Hb and Bcd-Bcd signalling corresponding to the double helical period of 22bp. To further this point, a study in 2012 by Huang et al, sort to establish whether TFBM spacing resulted in a more effective activation of TFs (Huang *et al.*, 2012). Prior to this study the importance of the spatial and stereospecific relationship exhibited between transcription factor activators and transcription factor pre- initiation complex; TATA-box bound TFIIA/TBP had not been defined. In their analysis, they showed that their transcription factor templates which contained a proximal GAL4 binding site 22bp from TFIIA/TBP/TATA-box complex resulted in more effective activation of target transcription factors (Huang *et al.*, 2012).

With studying the literature surrounding optimal transcription factor design, we incorporated a sequential spacing of TF binding sites 21bp apart, in order to alter the spatial and stereospecificity of our TFARs. This approach leads to an even space of TF dimers on the same rotational plane, allowing the TF activation domains to align and interact**.**

Aims and objectives

Aim: to construct and test the sensitivity of six transcription factor activator reporters, known to either positively or negatively regulate gene expression that influences atherosclerosis; and quantify their response to known agonists, in order to create the E-Sense Platform

This will be addressed in the following objectives:

- Design, clone and transduce, TFARs for Nrf2 (NFE2L2), KLF2, XBP1 and IRF3 into HCAECPro cells to complement existing TFARs for NFκB and AP1, available from the McKay lab to create 'E-Sense lines'.
- Undertake dose-response experiments utilising known agonists in order to establish the minimal and maximal induction (dynamic range) of our TFARs under static conditions.
- Use each E-Sense line under both oscillatory and laminar flow in addition to agonists in order to quantify TFAR activity and the interaction in response to flow.

4.1 Design and construction of TFARs for Nrf2, KLF2, IRF3 and XBP1

TFARs were designed containing multimerised repeats of our target genes; NRF2, KLF2, IRF3, and XBP1 based on publications and defined motifs from MotifMap. The repeating binding sites were spaced every 21bp, ensuring that repeated units were spaced on alternating double helix repeats.

Initially, gateway cloning was employed to clone inserts into the lentiviral vectors containing either N-Luc or V-luc, with TFAR sequences produced by synthetic gene sequencing with *attB*1/2 flanking sequences; however, despite multiple attempts and significant troubleshooting, it was not possible to isolate clones with correctly inserted TF binding sites.

This resulted in a redesign, using the design illustrated in Fig 4.3 below. These sequences were again generated by synthetic DNA gene construction by Eurofins and sequenced to confirm fidelity. An example of a complete TFAR is included below, along with the consensus sequences for each transcription factor in below. This replaced the KLF2-specific sequences in the given example below. See appendix for TF binding site transcript variants.

KLF2

GGATCCGCTAGCGAATTCCTCCCCACACCCCCATTCCTGGCCCCCACACCCC
CATAACCGGGCCCCACACCCCCATGGGTGGGCCCCACACCCCCATAATCCG
TCCCCACACCCCCATCACATATCCCCACACCCCCATGATCGAGGGGCTATAA
AAAGGGGGTGGGGGCGCGTTCGTCCTCACTCTCTTCCCTCGCCTCGAGTCTA GAAAGCTT

Figure 4.3 – example of the designed TFAR. Each TFAR was flanked by 3 different restriction sites at each end to facilitate cloning into the intended recipient plasmid and future proof if required to clone into a different plasmid. The TF binding consensus highlighted in yellow were spaced 21bp apart, with the minimal promoter in pink (TATAAA box and Inr underlined – consensus YYANWYY; Y=C/T, W=A/T).

Conventional restriction enzyme digestion of both donor plasmid containing the

TFAR sequence and recipient lentiviral vectors containing vLuc or nLuc, with *BamH1* and *XHO1* restriction enzymes created fragments with compatible overhangs for orientation-specific ligation. The recipient vectors were treated with calf intestinal phosphatase to remove the 5’ phosphates to prevent self-re-ligation of any single-cut vector. TFAR sequence and nLuc or vLuc vectors were separated via gel electrophoresis. The appropriate bands were cut and purified from the gel (see fig 4.7).

Inserts and vectors were ligated via ligation reaction utilising T4 ligase enzyme. Resultant DNA ligations were transformed into NEB Stable3 competent cells with Ampicillin selection. Three colonies from the resulting from each ligation were picked grown up and miniprepped to extract the plasmid DNA. Successful ligation of the TFAR was confirmed using *BamH1* and *XHO1* digestion to release the inserted TFAR sequence and compared against pLNT-AP1-vLuc-GFP-2A and pLNT-NFkB- vLuc-GFP-2A control. Sequence fidelity was confirmed by sanger sequencing

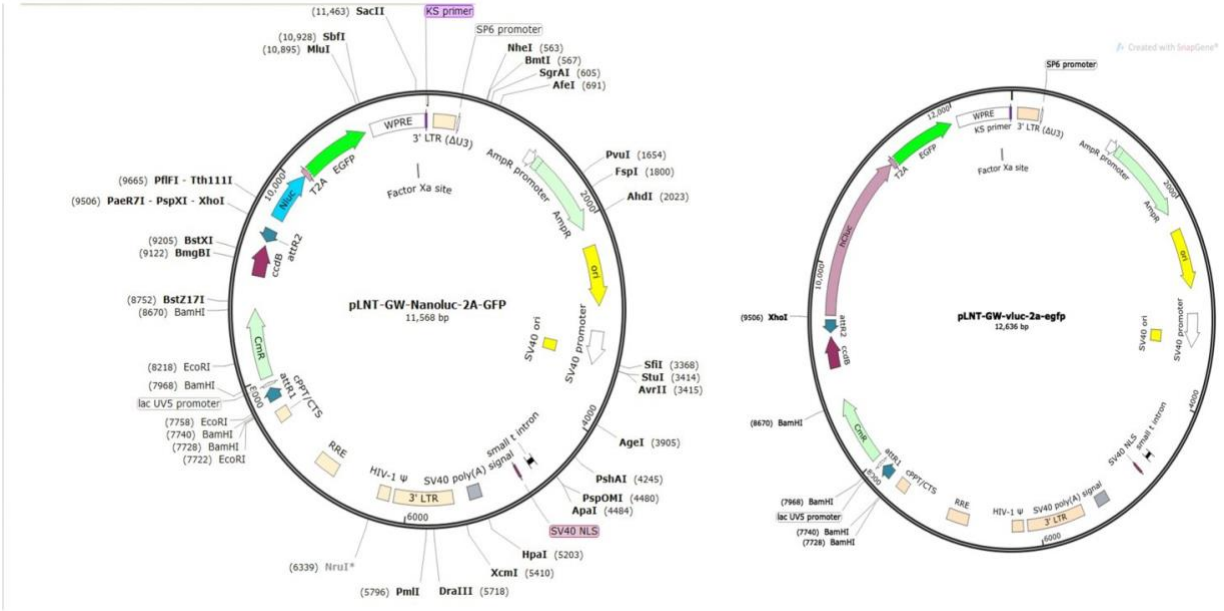

Figure 4.4: nLuc and vLuc backbone for TFAR development. Plasmid maps of backbone vector supplied by McKay collaborating lab group which transcription factors containing minimal promoter constructs were cloned into containing either a nLuc or vLuc luciferase, with GFP attached.

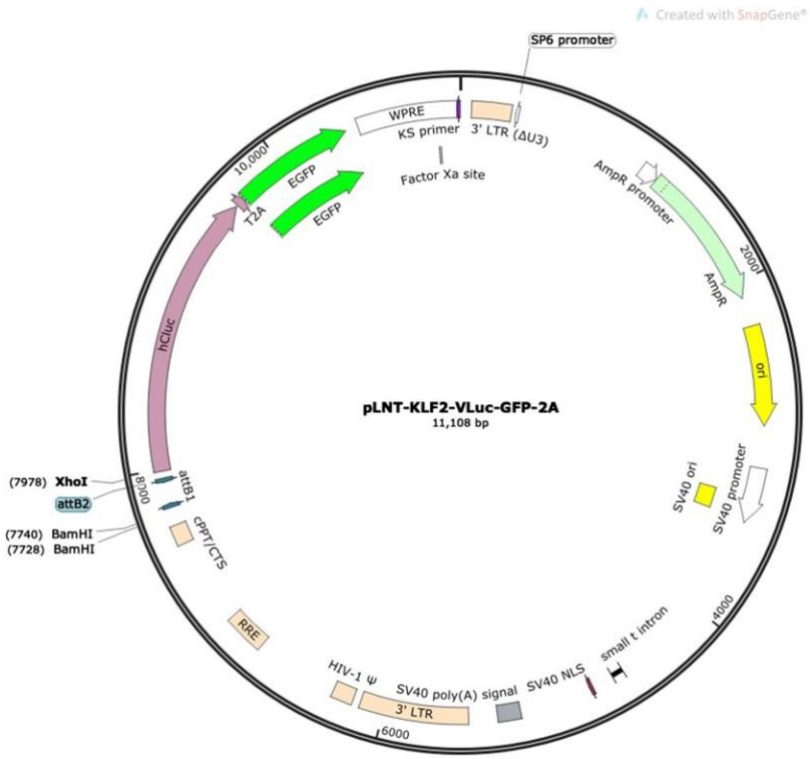

Figure 4.5 KLF2-vLuc . Example of plasmid map of final TFAR. Transcription factor constructs were cloned into either a nLuc or vLuc backbone with GFP attached.

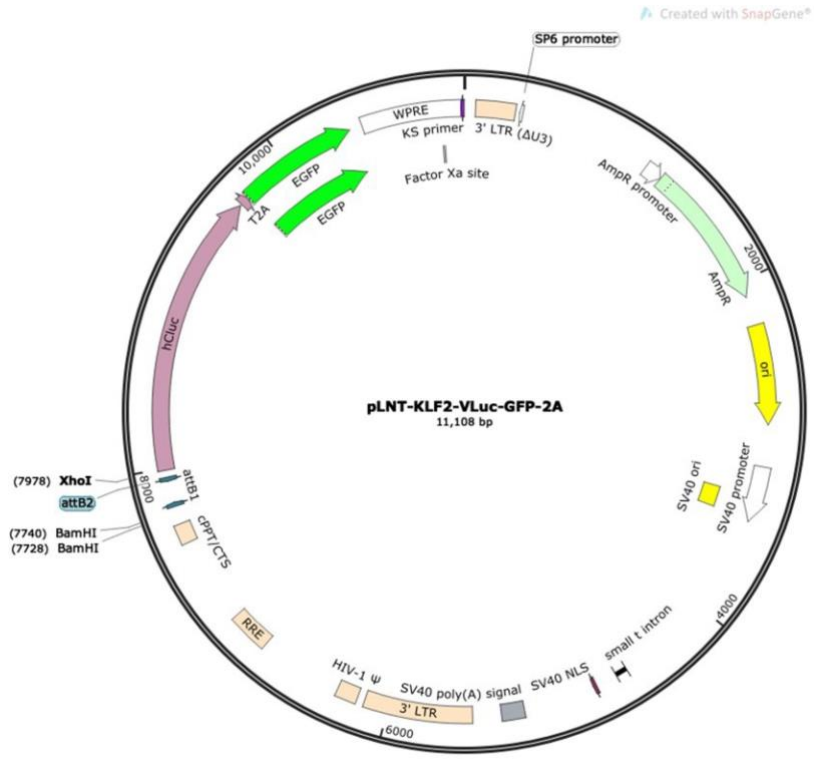

Figure 4.6: Cloned in TFAR into Luciferase Backbone. Example of KLF2 target gene cloned into vLuc backbone. Plasmid map demonstrates final product after ligation.

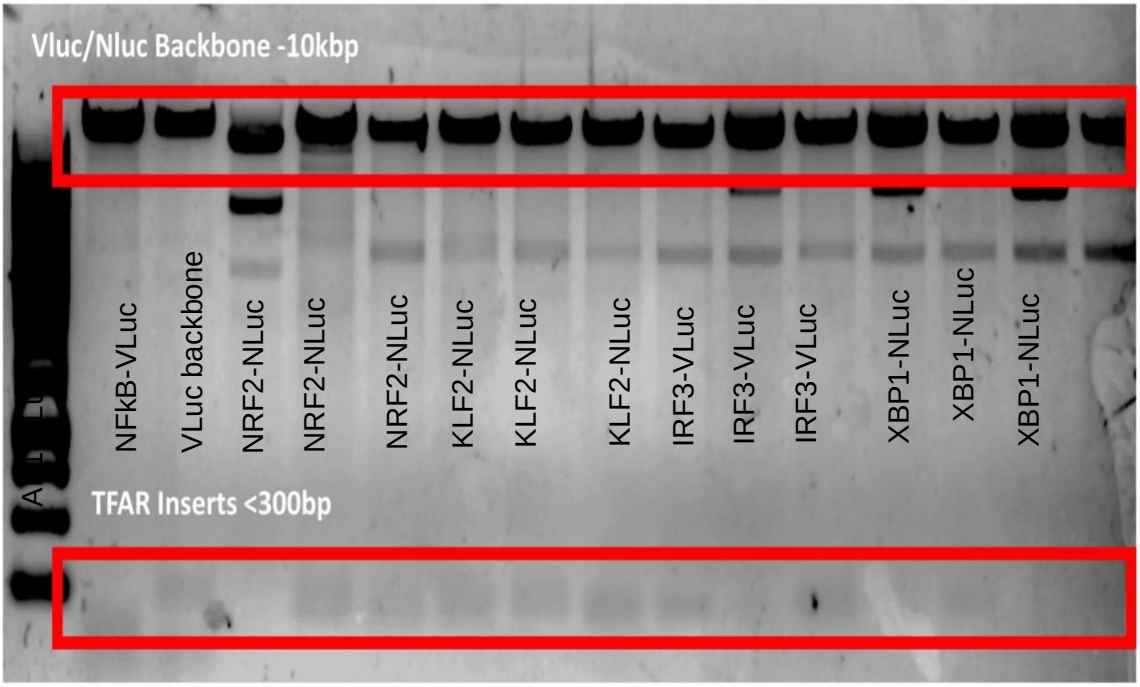

***Figur*e 4.7: Cloning confirmation via restriction enzyme dugest**. After cloning of TFAR targets into VLuc and NLuc backbones, a BamH1 and XHO1 restriction enzyme digest of (lane 1) AP1-vLuc, (lane 2) NFkB-vLuc, (lane 3) pLNT-GW-vLuc-GFP-2A only, in comparison to inserts; (lanes 4/5/6) three separate colonies of NRF2-MP-nLuc, (lanes 7/8/9) three separate colonies of KLF2-MP-nLuc, (lanes 10/11/12) IRF3-MP-VLuc, XBP1-NLuc (lanes 13/14/15). Small bands of ~300bp represent TFAR inserts cut, with remaining larger 10kbp band remaining VLuc/NLuc backbone. Lanes with appropriate bands were chosen and sent for confirmational sanger sequencing.

4.2 Assessment of the dynamic range of TFARs

Three E-sense lines were created by transducing HCAECPro with lentiviral vectors containing pairs of TFARs. These were **E-Sense Red** containing KLF2-nLuc/AP1- vLuc, **E-Sense Green** containing NRF2-nLuc/NFκB-vLuc and **E-Sense Yellow** containing XBP1-nLuc/IRF3-vLuc. This facilitated the assessment of two signalling pathways by separate analysis of either vLuc or nLuc.

As an initial step, we quantified the dynamic range of each TFAR to know agonists for each signalling pathway that stimulated the quantified TF. Initial dose responses to each agonist were conducted under static culture in order to define an optimal concentration to subsequently test in either oscillatory or laminar flow.

After initial assessment of the new TFARs, the induction of luciferase was very high, resulting in up to 350,000-fold induction, as a raw value this was equal to an RLU value to the ninth power. As this caused issues with reading the assay in the luminometer, the data presented below is using a diluted substrate, resulting in a signal of approximately 20-fold less than if measured using luciferase reagents as directed by the manufacturer. This provides some scope for miniaturisation of the E-Sense system to create a higher throughput assay system.

4.2.1 Assessment of the dynamic range of Nrf2 TFAR

Transcriptional regulation of NRF2 is augmented in athero-protective regions of the endothelium by laminar shear stress (Zakkar *et al.*, 2009). Previous work by the White Lab has demonstrated that treatment of HCAECs with fresh aqueous cigarette smoke extract also induces the activation of NRF2, due to the exposure of free radicals within the cigarette smoke. We measured the response of the NRF2- NLuc TFAR to CSE at concentrations between 1 and 20% (Fig 4.8). Stimulation of our reporter under static conditions yields a maximal induction of 2720-fold ($p<0.0001$). In addition, the NRF2-nLuc TFAR was exposed to known NRF2 activator Sulforaphane at concentrations of 5-50µM (Figure 4.9). We see a maximal induction of the NRF2 reporter at a concentration of 50µM, with a 495-fold induction (Figure 4.10; $p<0.0001$). The reporter demonstrates an increased sensitivity when compared to currently available in literature where a maximal induction of 50-fold was observed (Motahari *et al.*, 2015). Given that the data presented here was generated using diluted luciferase assay reagents it supports the hypothesis that the alteration in spacing of NRF2 TF-binding sites has likely resulted in an increased dynamic range of the reporter.

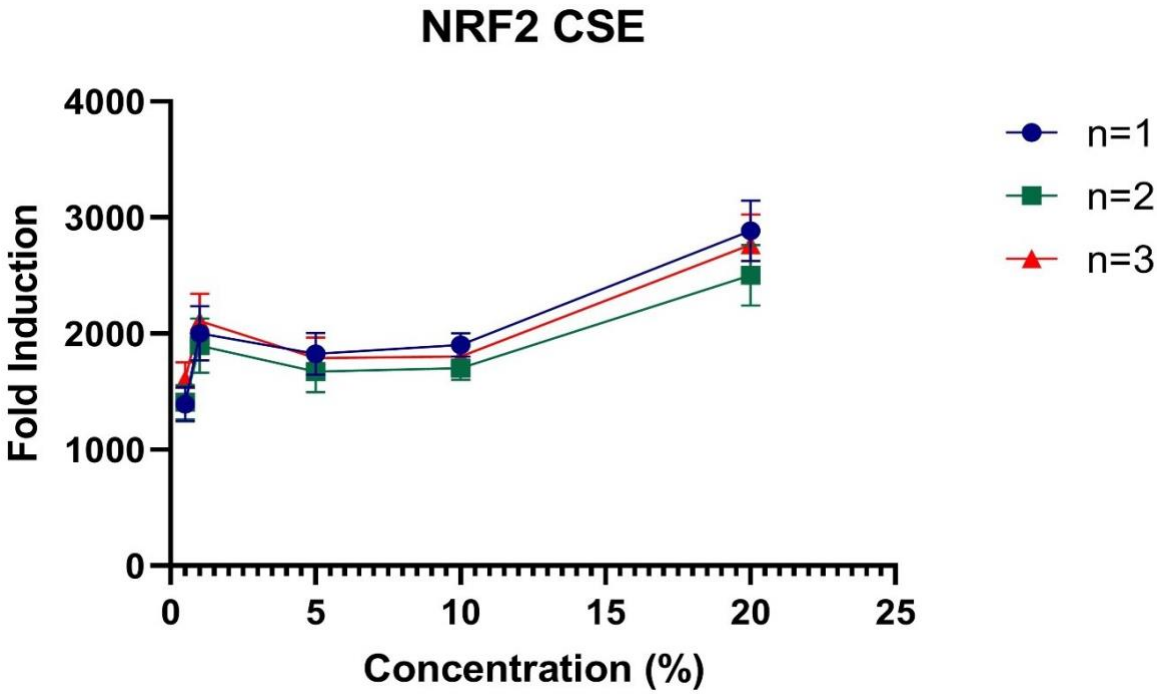

Figure 4.8 Dose Response of Cigarette smoke extract (CSE) on NRF2-nLuc in Static Culture.

HCAECPro Cells containing NRF2-nLuc reporter were cultured in 48-well plates until >90% confluent. Cells were treated with cigarette smoke extract at a concentration of 0.5%, 1%, 5%, 10% and 20% for 24 hours in Promocell MV2 endothelial cell media. Following treatment, media was collected for luciferase reaction. Reaction was incubated at room temperature for 5 mins before luminescence was measured using Promega GloMax Explorer plate reader using luciferase assay pre-set settings. All experiments were repeated three times, with each repeat pooling data from three technical replicates

.

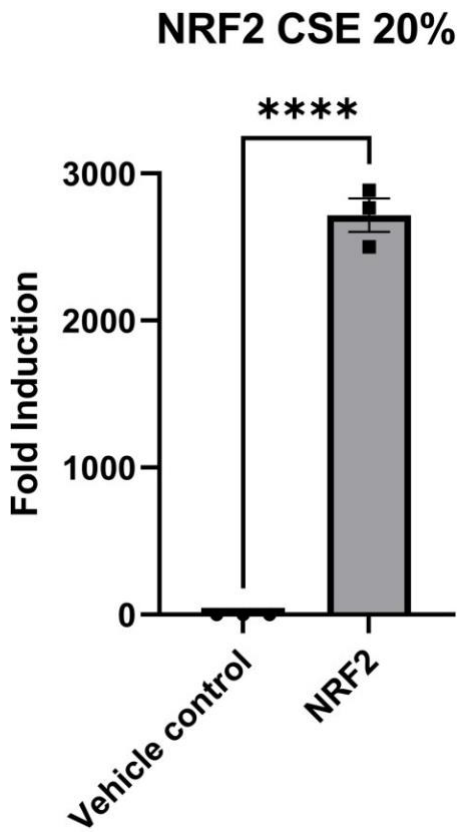

Figure 4.9 Response of NRF2-nLuc reporter in response to 20% CSE.

HCAECPro Cells containing Nrf2-nLuc reporter were cultured in 48-well plates until they had reached >90% confluency. Cells were stimulated with CSE at a concentration of 20% for 24 hours in triplicate for technical repeat in Promocell MV2 endothelial cell media. Following stimulation, media was collected for luciferase reaction. Reaction was incubated at room temperature for 5 mins before luminescence was measured using Promega GloMax Explorer plate reader using luciferase assay pre-set settings. N=3, T-test. *p= <0.05, **p<0.01, ***p<0.001, ±SEM.

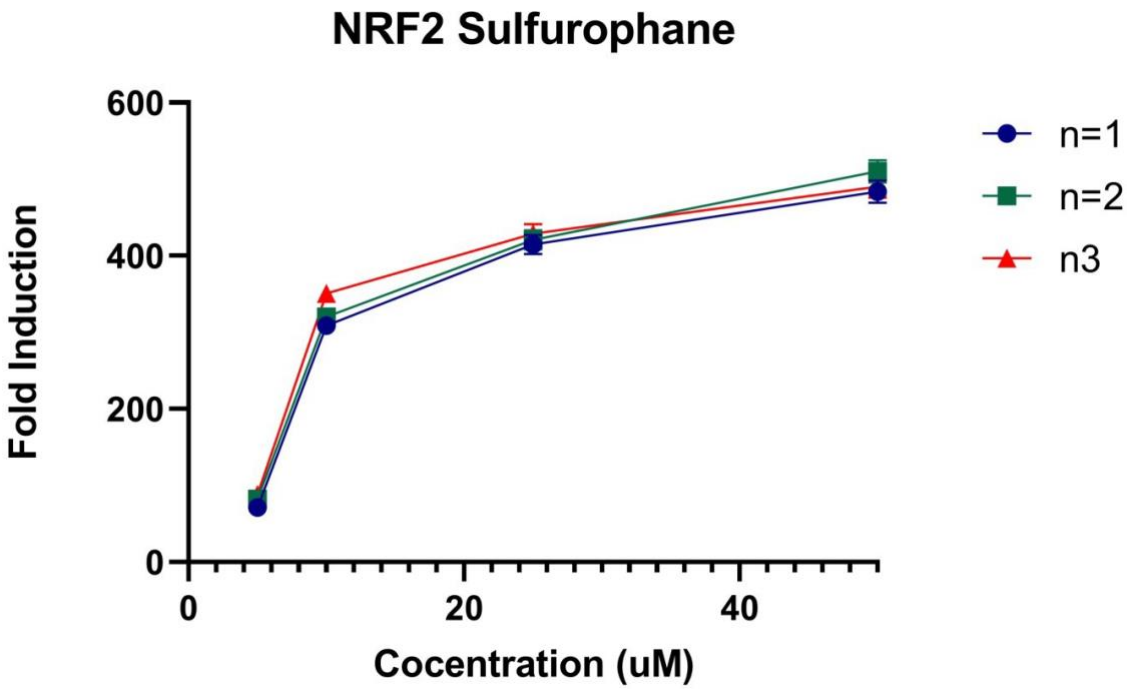

Figure 4.10 Dose Response of Sulforaphane on NRF2-nLuc in Static Culture.

HCAECPro Cells containing NRF2-nLuc reporter were cultured in 48-well plates until they had reached >90% confluency. Cells were stimulated with Sulforaphane at concentrations of 5µM, 10µM, 25µM and 50µM for 24 hours in triplicate for technical repeat in Promocell MV2 endothelial cell media. Following stimulation, media was collected for luciferase reaction. Reaction was incubated at room temperature for 5 mins before luminescence was measured using Promega GloMax Explorer plate reader using luciferase assay pre-set settings. Dose response curve is representative of n=3 and 3 technical repeats.

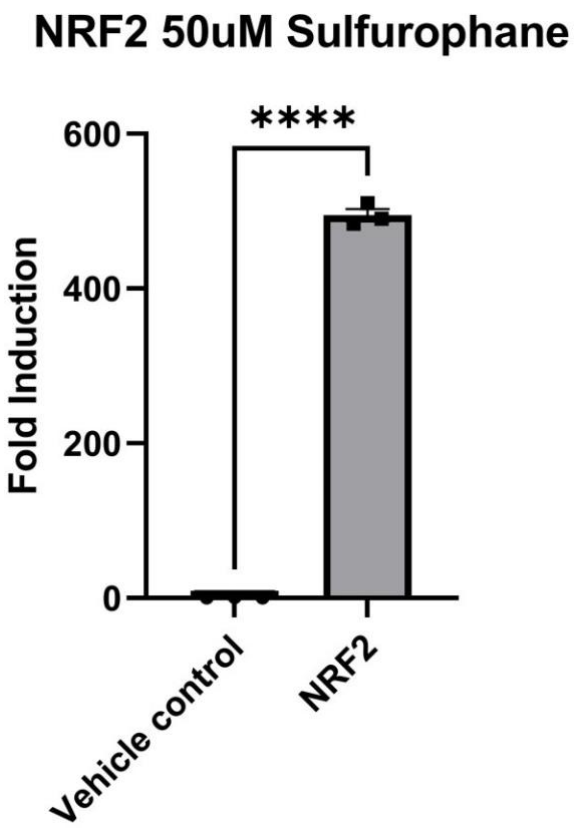

Figure 4.11 Response of NRF2-nLuc reporter in response to 20% CSE.

HCAECPro Cells containing Nrf2-nLuc reporter were cultured in 48-well plates until they had reached >90% confluency. Cells were stimulated with 50µM Sulforaphane for 24 hours in triplicate for technical repeat in Promocell MV2 endothelial cell media. Following stimulation, media was collected for luciferase reaction. Reaction was incubated at room temperature for 5 mins before luminescence was measured using Promega GloMax Explorer plate reader using luciferase assay pre-set settings. N=3, T-test. *p=<0.05, **p<0.01, ***p<0.001,

4.2.2 Assessment of the dynamic range of KLF2 TFAR

The laminar-shear stress modulated transcription factor, KLF2, is a crucial regulator protective signalling pathways in atherosclerosis development along with NRF2. KLF2 has been shown to be moderately induced by statin treatment, exerting an endothelial atheroprotective response (Sen-Banerjee *et al.*, 2005). To determine the maximal dynamic range of the KLF2-nLuc reporter, HCAECPro's were transduced E-Sense Red With a second lentiviral vector overexpressing KLF2 under the control of the PGK promoter, which resulted in a 3310-fold induction of NLuc expression ($p<0.001$) (fig 4.12). Statin-mediated increase in KLF2 and KLF2-dependent gene expression has been demonstrated in a number of studies (REFS). Therefore, a dose- response experiment was performed using Atorvastatin between 0.1µM and 10µM. We see a maximal induction of KLF2 of 387-fold ($p<0.0001$) when stimulated with 1µM Atorvastatin (fig 4.13 & 4.14). Previous studies have shown up to a 8-fold increase in KLF2- dependent gene expression with statin treatment (1µM Cerivastsin) (Parmar *et al.*, 2005). Therefore, our KLF2-Nluc TFAR provides much greater sensitivity of activation of KLF2 compared to measuring KLF-responsive gene expression changes, enabling the quantification of even small changes to KLF2 activity, even using diluted luciferase assay reagents.

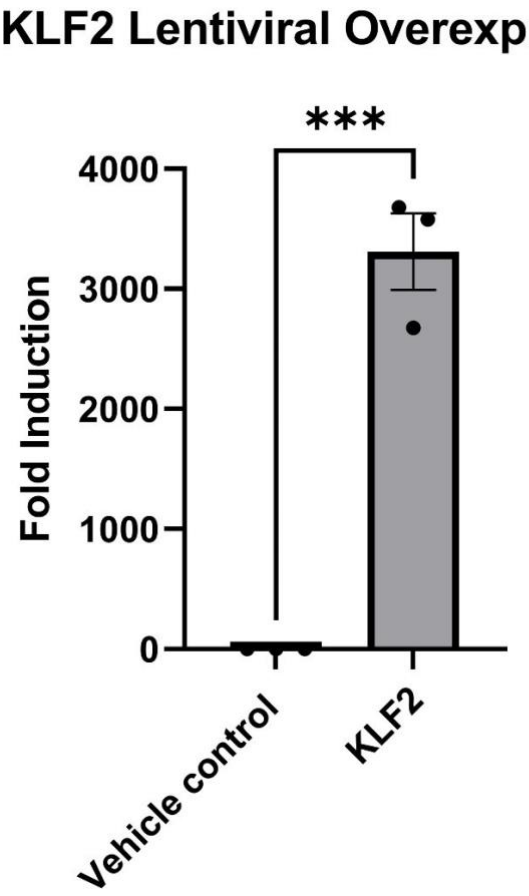

Figure 4.12 Response of KLF2-nLuc reporter in response to pGK-KLF2 overexpression Lentivirus.

HCAECPro Cells containing KLF2-nLuc reporter were cultured in 48-well plates until they had reached >90% confluency. Cells were stimulated with 100µL pGK-KLF2 overexpression lentivuirus. Following stimulation, media was collected for luciferase reaction. Reaction was incubated at room temperature for 5 mins before luminescence was measured using Promega GloMax Explorer plate reader using luciferase assay pre-set settings. n=3, T-test. *p= <0.05, **p<0.01, ***p<0.001, ±SEM

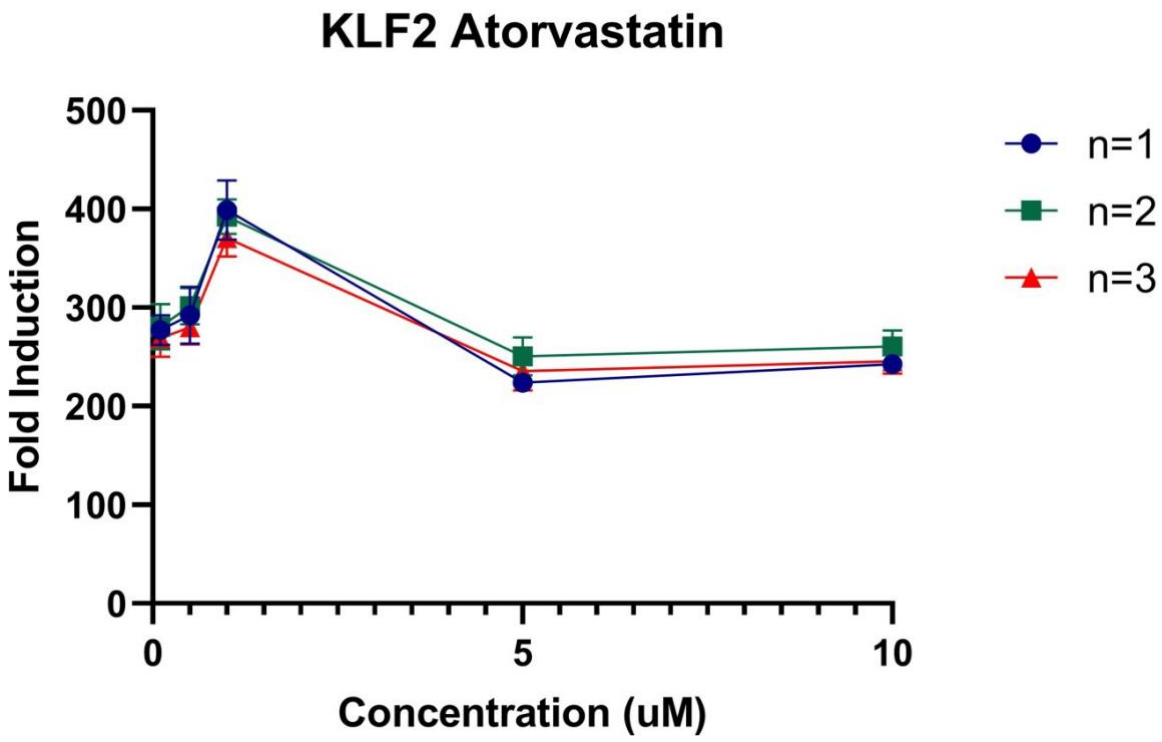

Figure 4.13 Dose Response of Atorvastatin on KLF2-nLuc in Static Culture.

HCAECPro Cells containing KLF2-nLuc reporter were cultured in 48-well plates until they had reached >90% confluency. Cells were stimulated Atorvastatin at concentrations of 0.1µM, 0.5µM, 1µM, 5µM and 10µM for 24 hours in triplicate for technical repeat in Promocell MV2 endothelial cell media. Following stimulation, media was collected for luciferase reaction. Reaction was incubated at room temperature for 5 mins before luminescence was measured using Promega GloMax Explorer plate reader using luciferase assay pre-set settings. Dose response curve is representative of n=3 and 3 technical repeats.

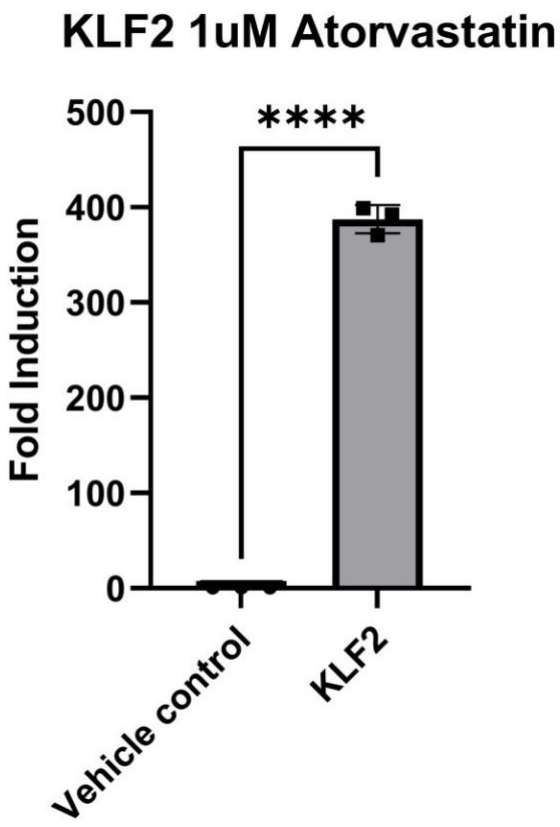

Figure 4.14 Response of KLF2-nLuc reporter in response to 1μM Atorvastatin.

HCAECPro Cells containing KLF2-nLuc reporter were cultured in 48-well plates until they had reached >90% confluency. Cells were stimulated with 10μM Atorvastatin for 24 hours in triplicate for technical repeat in Promocell MV2 endothelial cell media. Following stimulation, media was collected for luciferase rection. Reaction was incubated at room temperature for 5 mins before luminescence was measured using Promega GloMax Explorer plate reader using luciferase assay pre- set settings. n=3, T-test. *p= <0.05, **p<0.01, ***p<0.001, ±SEM

4.2.3 Assessment of the dynamic range of XBP1 TFAR

As mentioned in **1.5**, cell stress and the unfolded protein response present key factors in atherosclerosis disease progression and have been demonstrated to be shear stress responsive. We introduced the XBP1-nLuc and IRF3-vLuc reporters into the E-Sense system in order to monitor any modulation of transcriptional activity relating the cellular stresses.

We performed dynamic range testing of the two reporters in order to determine their range and maximal induction. For our XBP1-nLuc reporter, we used known ER stress inducers, Thapsigargin and Brefeldin A. Both Thapsigargin and Brefeldin A induce ER stress through different mechanisms; Thapsigargin is an inhibitor of sarco endoplasmic reticulum Ca2 ATPase (SERCA), while Brefeldin A (BFA) is an inhibitor of intracellular vesicle formation and protein trafficking between the endoplasmic reticulum (ER) and the Golgi apparatus (Ganley *et al.*, 2011)(de Galarreta *et al.*, 2016).

Treatment of E-Sense Yellow with 5-100nM Thapsigargin resulted in a dose-dependent increase in XBP1-nLuc activity, with a 515-fold induction of nLuc expression with 50nM Thapsigargin (Figure 4.16, $P<0.0001$). The reporter demonstrates high sensitivity, with 5nM Thapsigargin resulting in a 430-fold induction of Nluc. Interestingly, when stimulated with Brefeldin A, XBP1-nLuc had lower maximal induction of 102-fold (Figure 4.18, $p<0.0001$) at a concentration of 50µg/mL, suggesting Thapsigargin is a more potent inducer of XBP1.

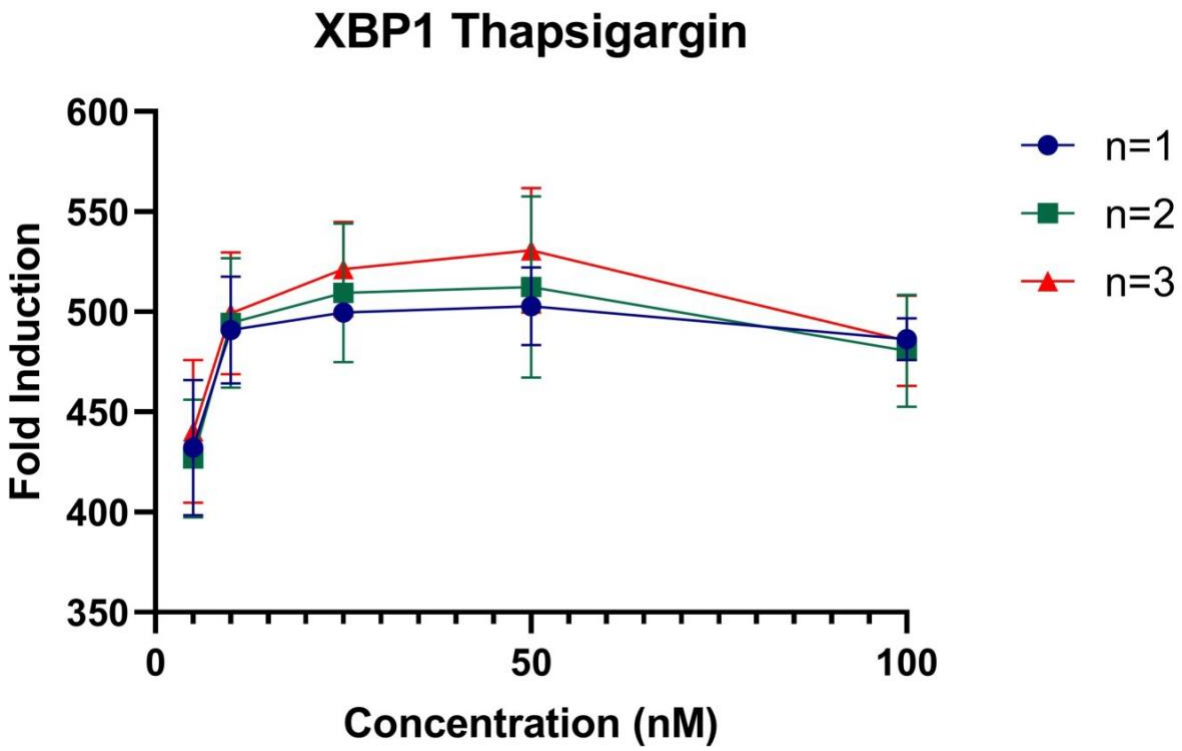

Figure 4.15 Dose Response of Thapsigargin on XBP1-nLuc in Static Culture.

HCAECPro Cells containing XBP1-nLuc reporter were cultured in 48-well plates until they had reached >90% confluency. Cells were stimulated with Thapsigargin at concentrations of 5nM, 10nM, 25nM, 50nM and 100nM for 24 hours in triplicate for technical repeat in Promocell MV2 endothelial cell media. Following stimulation, media was collected for luciferase reaction. Reaction was incubated at room temperature for 5 mins before luminescence was measured using Promega GloMax Explorer plate reader using luciferase assay pre-set settings. Dose response curve is representative of n=3 and 3 technical repeats.

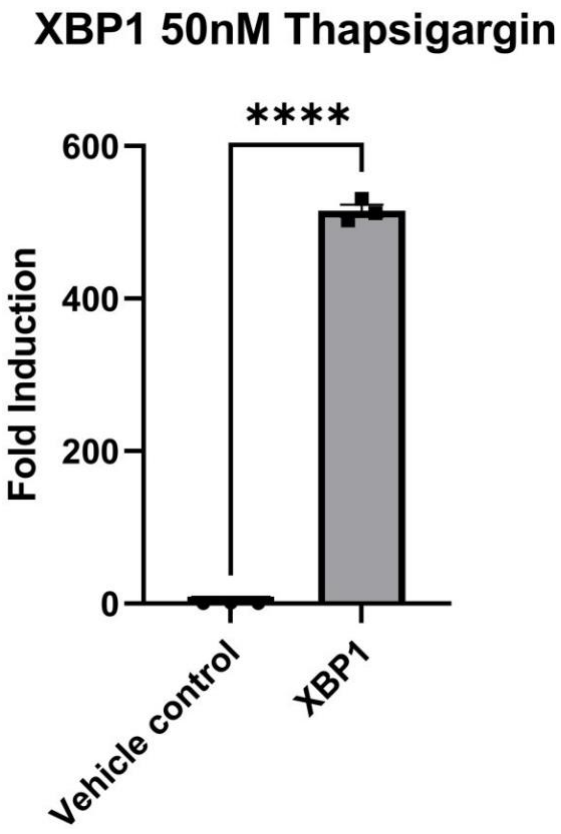

Figure 4.16 Response of XBP1-nLuc reporter in response to 50nM Thapsigargin in static culture.

HCAECPro Cells containing XBP1-nLuc reporter were cultured in 48-well plates until they had reached >90% confluency. Cells were stimulated with 50nM Thapsigargin for 24 hours in triplicate for technical repeat in Promocell MV2 endothelial cell media. Following stimulation, media was collected for luciferase reaction. Reaction was incubated at room temperature for 5 mins before luminescence was measured using Promega GloMax Explorer plate reader using luciferase assay pre-set settings. n=3, T-test. *p=<0.05, **p<0.01, ***p<0.001, ±SEM

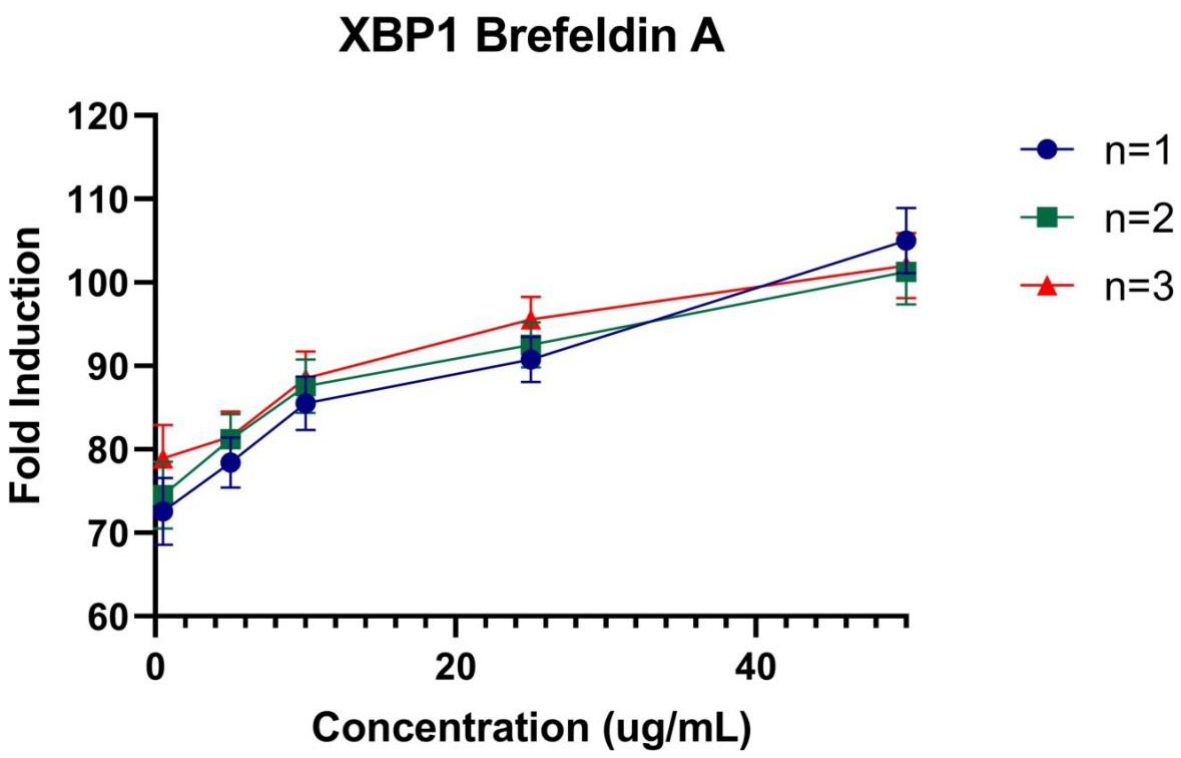

Figure 4.17 Dose Response of Brefeldin A on XBP1-nLuc in Static Culture.

HCAECPro Cells containing XBP1-nLuc reporter were in 48-well plates until they had reached >90% confluency. Cells were stimulated with Brefeldin A at concentrations of 0.5µg/mL, 5µg/mL, 10µg/mL, 25µg/mL and 50µg/mL for 24 hours in triplicate for technical repeat in Promocell MV2 endothelial cell media. Following stimulation, media was collected for luciferase reaction. Reaction was incubated at room temperature for 5 mins before luminescence was measured using Promega GloMax Explorer plate reader using luciferase assay pre-set settings. Dose response curve is representative of n=3 and 3 technical repeats.

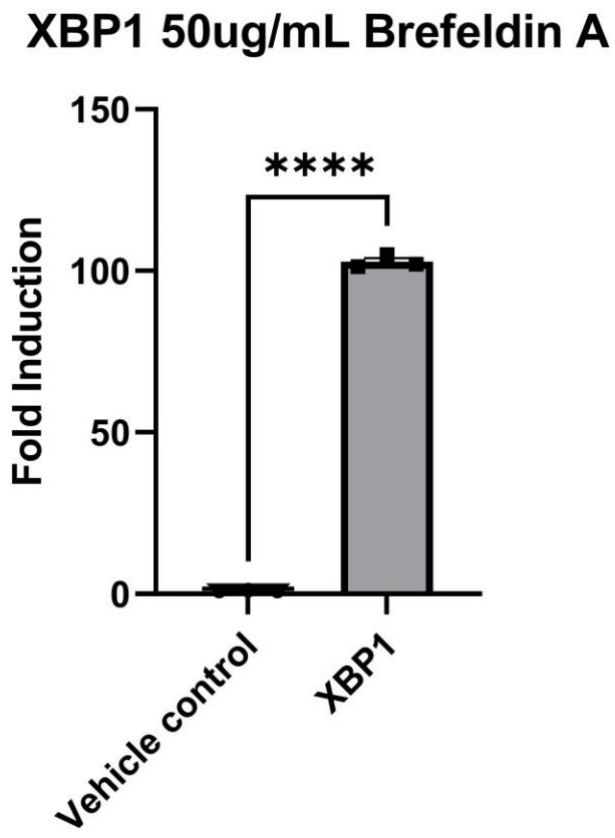

Figure 4.18 Response of XBP1-nLuc reporter in response to 50µg/mL Thapsigargin in static culture.

HCAECPro Cells containing XBP1-nLuc reporter were cultured in 48-well plates until they had reached >90% confluency. Cells were stimulated with 50µg/mL Brefeldin A for 24 hours in triplicate for technical repeat in Promocell MV2 endothelial cell media. Following stimulation, media was collected for luciferase reaction. Reaction was incubated at room temperature for 5 mins before luminescence was measured using Promega GloMax Explorer plate reader using luciferase assay pre-set settings. n=3, T-test. *p=<0.05, **p<0.01, ***p<0.001, ±SEM

4.2.4 Assessment of the dynamic range of IRF3 TFAR

In order to modulate IRF3 transcription, we stimulated our IRF3-vLuc reporter with 10-100µg/ml Oxidised low-density lipoprotein, purchased from Thermofisher Scientific (4.19, OxLDL) and lipopolysaccharide (LPS) both known induces of TLR4 (Cai, Li and Yan, 2013). Our data suggests a maximal induction of the IRF3-vLuc reporter of 35-fold induction (Figure 4.20), $p<0.0001$) when stimulated with OxLDL and a maximal induction of 27-fold (Figure 4.22, $p<0.0001$) when stimulated with 50ng/mL of LPS, using the diluted luciferase reagents.

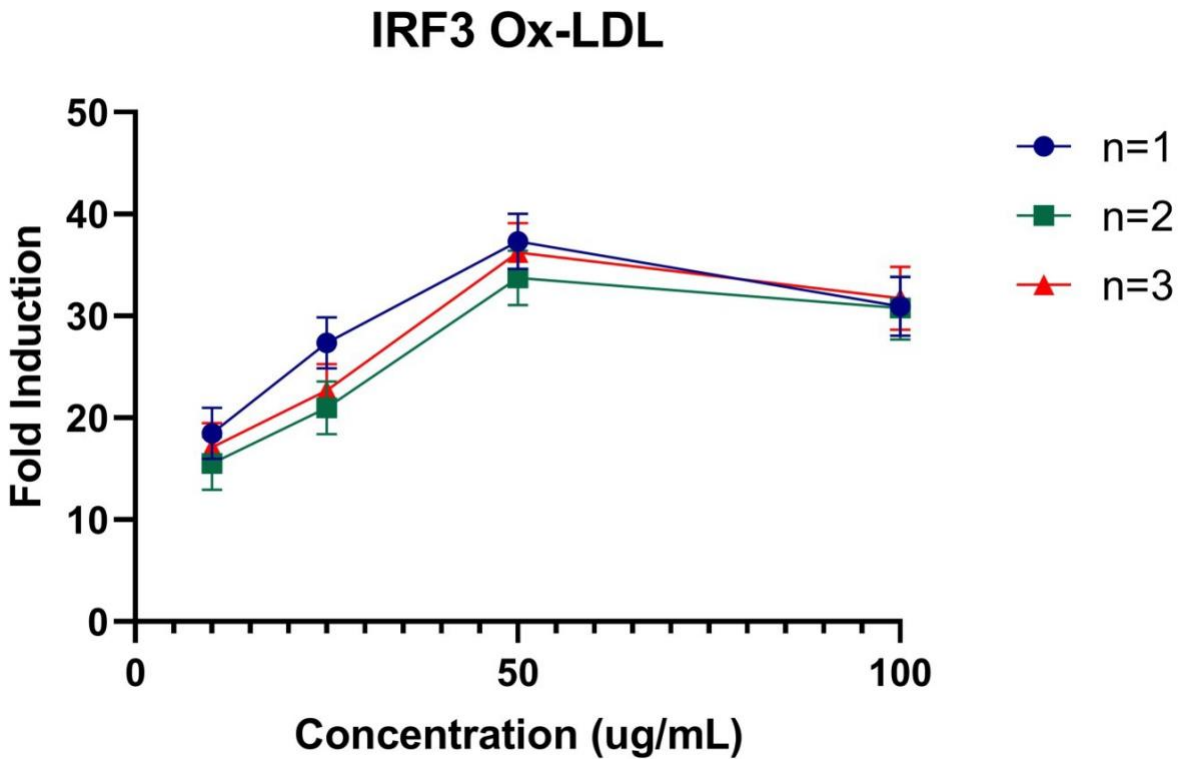

Figure 4.19 Dose Response of Ox-LDL on IRF3-vLuc in Static Culture.

HCAECPro Cells containing IRF3-vLuc reporter were cultured in 48-well plates until they had reached >90% confluency. Cells were stimulated Ox-LDL at concentrations of 10, 25, 50 and 100µg/mL for 24 hours in triplicate for technical repeat in Promocell MV2 endothelial cell media. Following stimulation, media was collected for luciferase reaction. Reaction was incubated at room temperature for 5 mins before luminescence was measured using Promega GloMax Explorer plate reader using luciferase assay pre-set settings. Dose response curve is representative of n=3 and 3 technical repeats.

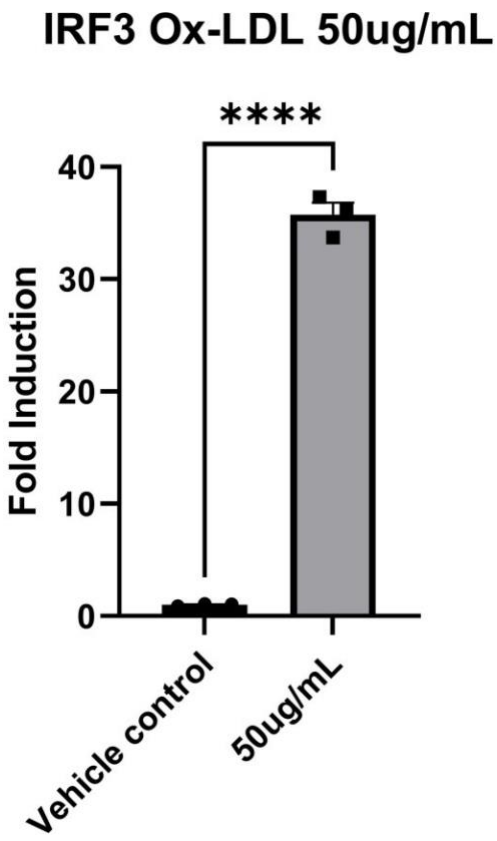

Figure 4.20 Response of IRF3-vLuc reporter in response to 50µg Ox-LDL in static culture.

HCAECPro Cells containing IRF3-vLuc reporter were cultured in 48-well plates until they had reached >90% confluency. Cells were stimulated with 50µg Ox-LDL for 24 hours in triplicate for technical repeat in Promocell MV2 endothelial cell media. Following stimulation, media was collected for luciferase reaction. Reaction was incubated at room temperature for 5 mins before luminescence was measured using Promega GloMax Explorer plate reader using luciferase assay pre-set settings n=3, T-test. *p=<0.05, **p<0.01, ***p<0.001, ±SEM

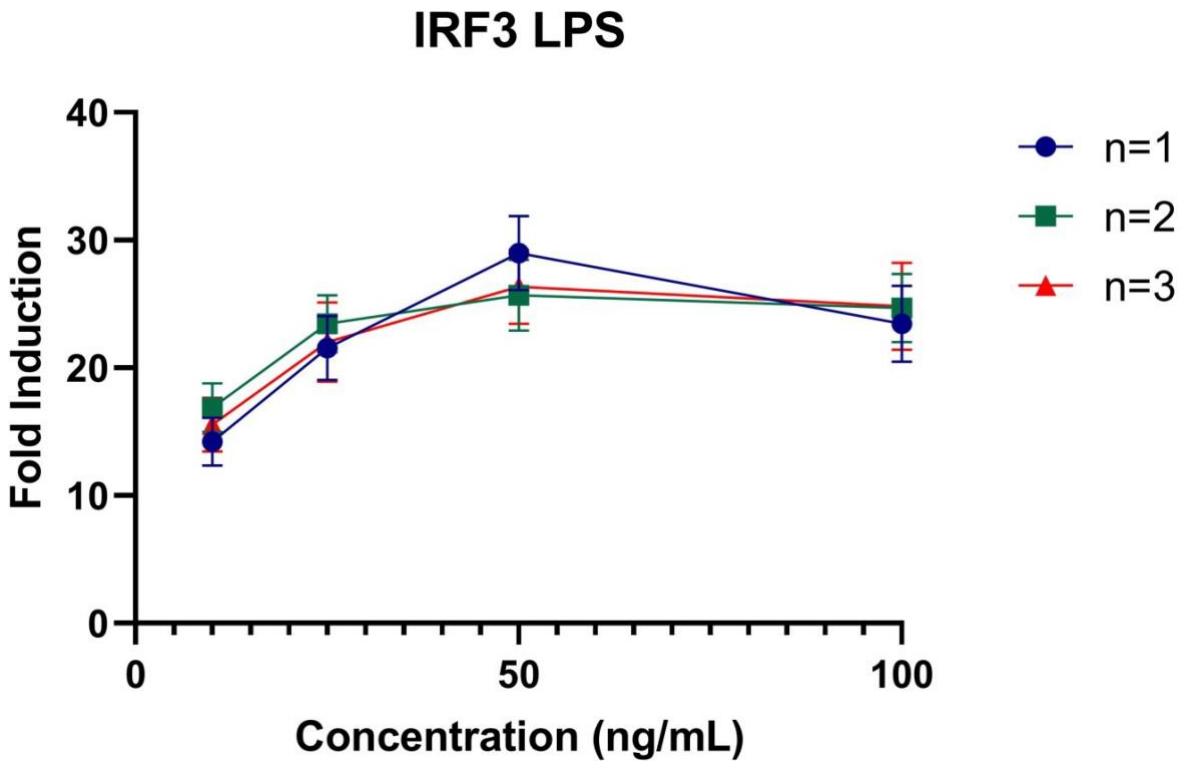

Figure 4.21 Dose Response of LPS on IRF3-vLuc in Static Culture.

HCAECPro Cells containing IRF3-vLuc reporter were cultured in 48-well plates until they had reached >90% confluency. Cells were stimulated LPS at concentrations of 10, 25, 50 and 100ng/mL for 24 hours in triplicate for technical repeat in Promocell MV2 endothelial cell media. Following stimulation, media was collected for luciferase reaction. Reaction was incubated at room temperature for 5 mins before luminescence was measured using Promega GloMax Explorer plate reader using luciferase assay pre-set settings. Dose response curve is representative of n=3 and 3 technical repeats.

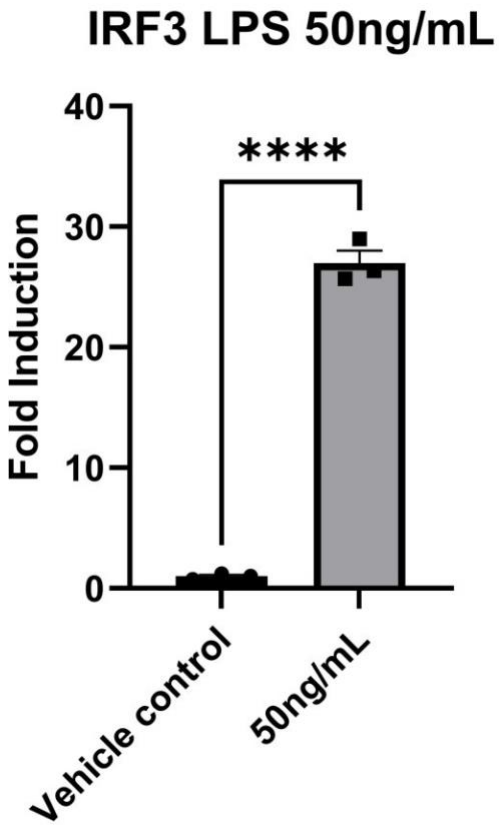

Figure 4.22 Response of IRF3-vLuc reporter in response to 50ng/ml LPS in static culture.

HCAECPro Cells containing IRF3-vLuc reporter were cultured in 48-well plates until they had reached >90% confluency. Cells were stimulated with 50ng/ml LPS for 24 hours in triplicate for technical repeat in Promocell MV2 endothelial cell media. Following stimulation, media was collected for luciferase reaction. Reaction was incubated at room temperature for 5 mins before luminescence was measured using Promega GloMax Explorer plate reader using luciferase assay pre-set settings n=3, T-test. *p=<0.05, **p<0.01, ***p<0.001, ±SEM

4.2.5 Assessment of the dynamic range of existing NFκB and AP1 TFARs

Pro-atherogenic environments of the endothelium result in dysfunction and dysregulation of endothelial cells. These regions are primed for inflammation and are predilected for plaque formations and subsequent atherosclerosis development (Nayak, Lin and Jain, 2011). The NFκB and AP1 pathways are known to play major roles in the inflammatory signalling cascade in atherosclerosis development, resulting in the modulation in a variety of both proinflammatory, but depending on the magnitude and signalling modifying pathways also pro-survival genes. The proinflammatory genes regulated by NFκB and AP1 are known to make a significant contribution to the development of atherosclerosis (Chistiakov, Orekhov and Bobryshev, 2017)(Boon and Horrevoers, 2009).

We used existing reporter constructs for NFκB-VLuc and AP1-vLuc and stimulated with the proinflammatory cytokine TNFα 0.1 to 5ng/ml, in order to ascertain the dynamic range of the two reporters and define the maximal induction.

When stimulated with 2ng/mL TNFα, NFκB-VLuc shows a maximal induction of 10.35-fold (fig 4.23 & 4.24, $p<0.0001$), with no observed increase in transcriptional activity when dosage of TNFα is increased to 5ng/ml. Interestingly, we see a near maximal induction of 9-fold when stimulated with only 0.1ng/mL TNFα.

The AP1-vLuc reporter demonstrates a slightly lower dynamic range than the NFκB- vLuc reporter, with a maximal induction of 7.9-fold at 2ng/ml TNFα (fig 4.25 & 4.26, $p<0.0001$) While with 0.1ng/ml TNFα treatment, the AP1-Vluc TFAR results in an approximate 50% induction of 4.2-fold of Vluc expression (figure

4.26).

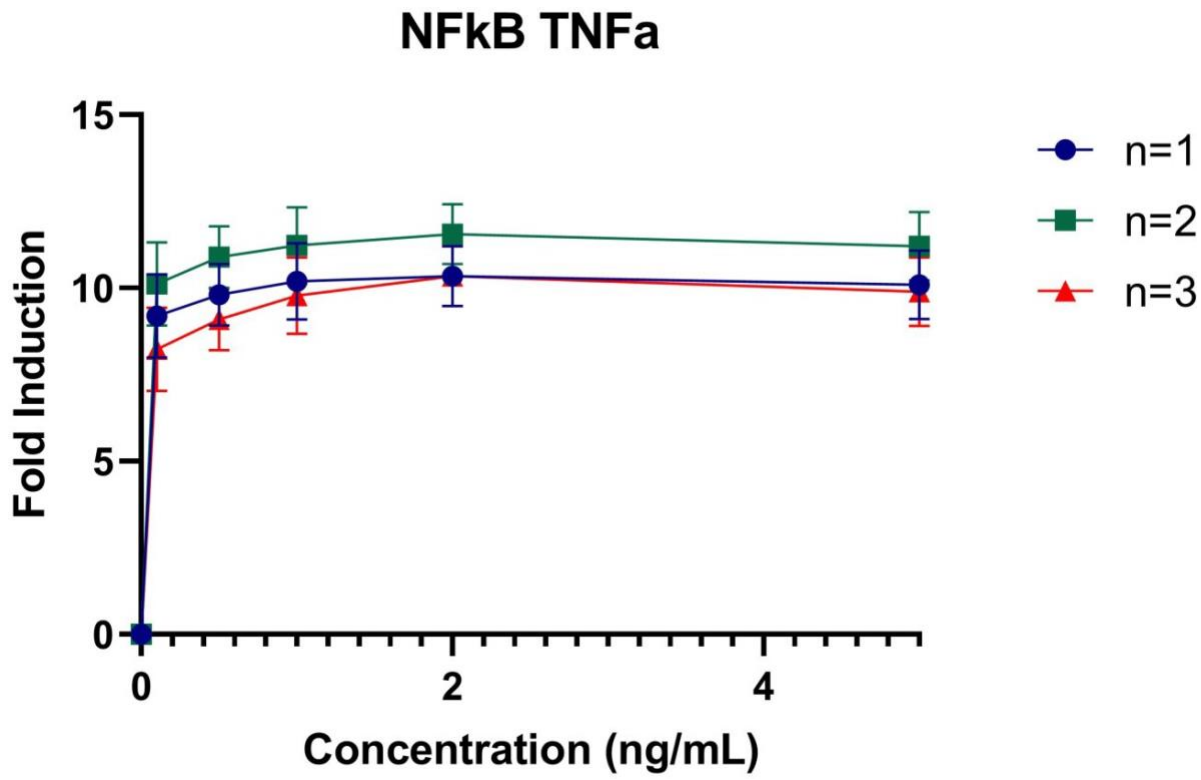

Figure 4.23 Dose Response of TNFa on NFkB-VLuc in Static Culture.

HCAECPro Cells containing NFkB-VLuc reporter were cultured in 48-well plates until they had reached >90% confluency. Cells were stimulated with TNFα at concentrations of 0.1ng/mL, 0.5ng/mL, 1ng/mL, 2ng/mL and 5ng/mL for 24 hours in triplicate for technical repeat in Promocell MV2 endothelial cell media. Following stimulation, media was collected for luciferase reaction. Reaction was incubated at room temperature for 5 mins before luminescence was measured using Promega GloMax Explorer plate reader using luciferase assay pre-set settings. Dose response curve is representative of n=3 and 3 technical repeats.

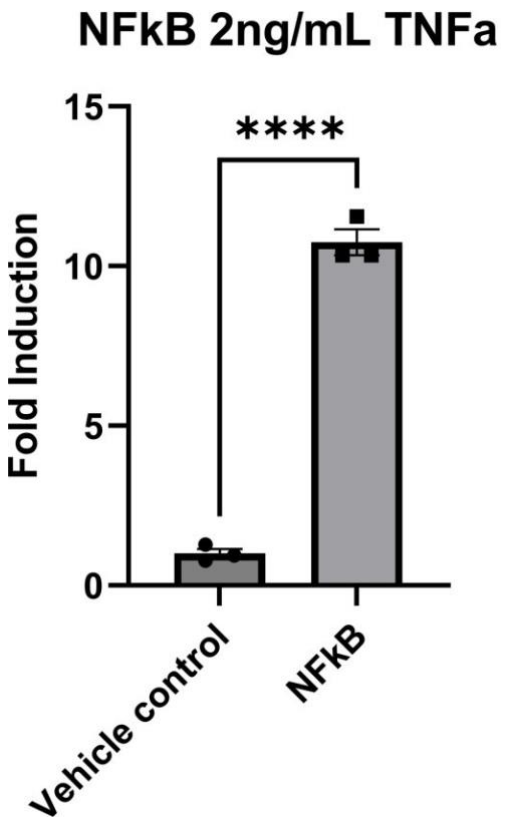

Figure 4.24 Response of NFkB-VLuc reporter in response 2ng/mL TNFa in static culture.

HCAECPro Cells containing NFkB-VLuc reporter were cultured in 48-well plates until they had reached >90% confluency. Cells were stimulated 2ng/mL TNFa for 24 hours in triplicate for technical repeat in Promocell MV2 endothelial cell media. Following stimulation, media was collected for luciferase reaction. Reaction was incubated at room temperature for 5 mins before luminescence was measured using Promega GloMax Explorer plate reader using luciferase assay pre-set settings. n=3, T-test. *p=<0.05, **p<0.01, ***p<0.001, ±SEM

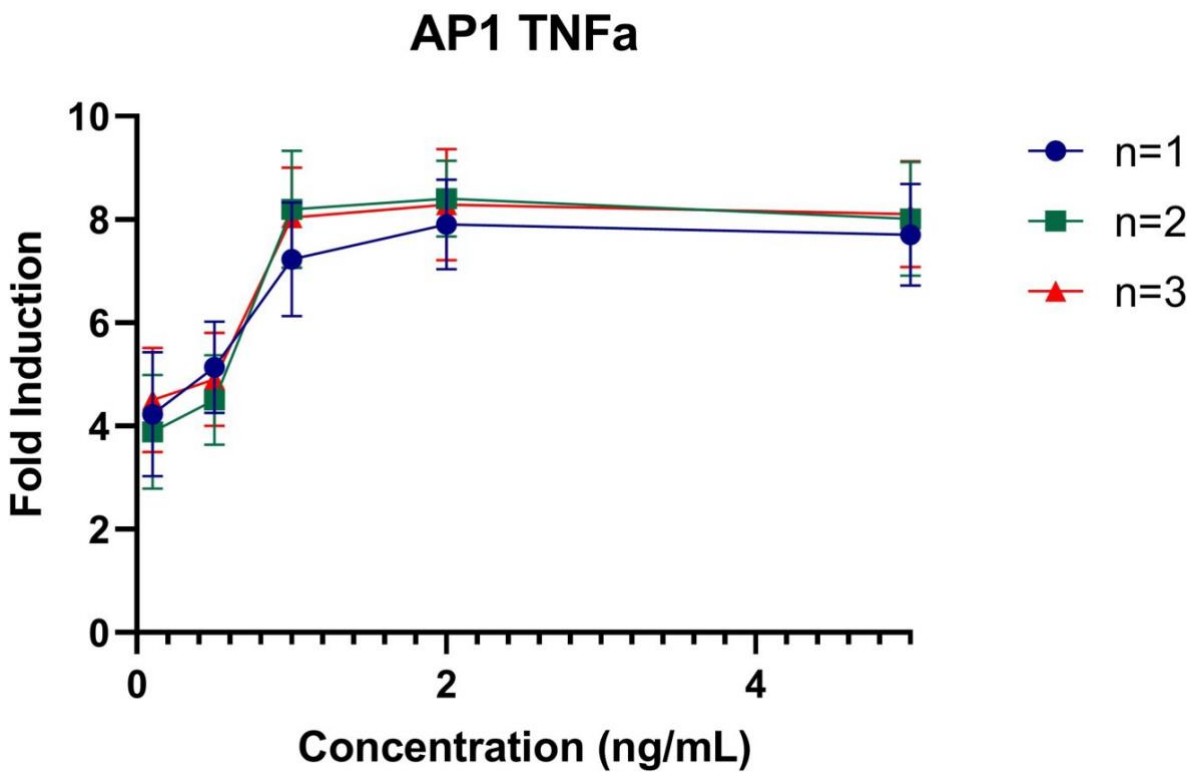

Figure 4.25 Dose Response of TNFa on AP1-VLuc in Static Culture.

HCAECPro Cells containing AP1-VLuc reporter were cultured in 48-well plates until they had reached
>90% confluency. Cells were stimulated with TNFa at concentrations of 0.1ng/mL, 0.5ng/mL, 1ng/mL, 2ng/mL and 5ng/mL for 24 hours in triplicate for technical repeat in Promocell MV2 endothelial cell media. Following stimulation, media was collected for luciferase reaction. Reaction was incubated at room temperature for 5 mins before luminescence was measured using Promega GloMax Explorer plate reader using luciferase assay pre-set settings. Dose response curve is representative of n=3 and 3 technical repeats.

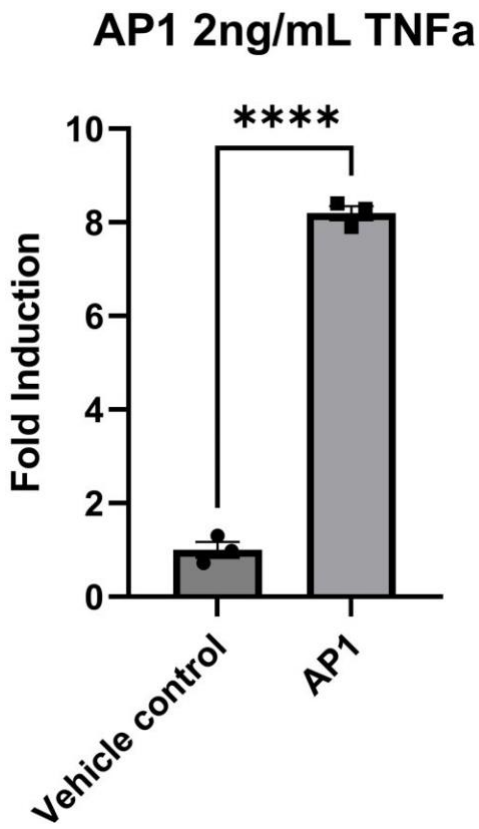

Figure 4.26 Response of AP1-vLuc reporter in response to 2ng/mL TNFa in static culture.

HCAECPro Cells containing AP1-vLuc reporter were cultured in 48-well plates until they had reached
>90% confluency. Cells were stimulated 2ng/mL TNFa for 24 hours in triplicate for technical repeat in Promocell MV2 endothelial cell media. Following stimulation, media was collected for luciferase reaction. Reaction was incubated at room temperature for 5 mins before luminescence was measured using Promega GloMax Explorer plate reader using luciferase assay pre-set settings. n=3, T-test. *p= <0.05, **p<0.01, ***p<0.001, ±SEM

4.2.5 Summary

- Altering the spacing of TF binding sites in our novel reporters seems to result in an enhanced dynamic range when compared to published and commercially available TFARs and TFARs using the same backbone, without optimal spacing (e.g. the AP1-vLuc and NFκB-VLuc used).
- Using a range of agonists and overexpression vectors, we defined the maximal response of the TFARs in HCAECPro under static culture.
- By using the combination of NLuc and VLuc luciferase reporters, we were able to create three E-Sense lines containing 6 TFARs:

➢ E-Sense green: NRF2-NLuc/NFκB-VLuc

➢ E-Sense Red: KLF2-NLuc/AP1-VLuc

➢ E-Sense Yellow: XBP1-NLuc/IRF3-VLuc

Table 4.1: Maximal inductions of reporters and agonist concentrations

TFAR	Agonist	Maximal induction
NRF2-nLuc	CSE (20%)	2717
KLF2-nLuc	pGK Overexpression	3310
XBP1-nLuc	Thapsigargin (50nM)	515.3
IRF3-vLuc	Ox-LDL (50µg/mL)	35.8
NFkB-vLuc	TNFa (2ng/mL)	10.8
AP1-vLuc	TNFa (2ng/mL)	8.2

4.3 Using E-sense to monitor endothelial signal transduction under flowed culture

The haemodynamic environment in which endothelial cells are cultured makes a significant difference to endothelial phenotype and response to dysfunctional stimuli. For instance, shear stress affects proliferation, apoptosis, inflammatory signalling ROS production, NO production and angiogenesis, all of which affect atherogenesis (Davis *et al.*, 2004). The TFARs contained within the E-sense lines are able to accurately quantify the transcriptional activity of the relevant TFs in HCAECPro to different flow environments and also generate data that help quantify the interaction of inflammatory and cell stress pathways with athero-protective KLF2 signalling. The data presented above was used to define a maximal or near-maximal dose of agonists to use in experiments performed under flow, using our in-house parallel plate flow apparatus. All experiments were performed for 72 hours, with analysis of luciferase expression every 24 hours. During the first 24 hours HCAECs adapt to their flow environment align with the direction of flow, therefore no agonists were added to the flow cells during this adaptation phase to prevent any disruption of the adaptation. Following this, agonists were introduced to the flow cell and transcriptional activity monitored at 24 at which point fresh agonist was applied with luciferase expression measured again at 48 hours after treatment and compared to vehicle controls. For these experiments the E-Sense lines were cultured under physiological laminar shear stress (LSS, 1.5Pa) and oscillatory shear stress (OSS,

±0.5Pa 1Hz). Once seeded, cells were exposed to 24h flow to allow endothelial cell adaptation under flow before exposed to a further 48h. After initial 24h, 1mL of media was extracted from flow rig and subsequently replenished, this was repeated at 48h mark, after 72h media was collected and flow model taken down. For experiments with treatments, the addition of compounds was administered at 24h and 48h timepoints. As the circulating volume under LSS is three times

greater than under OSS (30ml v 10 ml), the LSS media was diluted three-fold before analysis to allow direct comparisons to be made.

4.3.1 Monitoring the Transcriptional Regulation of NRF2-nLuc/NFκB-vLuc (E-Sense Green) under LSS and OSS

We exposed E-Sense green (HCAECPro containing NRF2-NLuc/NFκB-VLuc) to LSS and OSS for 72 hours. Cell lines were flowed for an initial 24 hours in order to allow HCAECPro cells to adapt to their flow conditions, after which either Sulforaphane (50μM) or TNFα (2ng/mL) were added. After an additional 24 hours (48 hours in total) Sulforaphane and TNFα were added again at the same concentration and culture continued under flow for an additional 24 hours. At each 24-hour timepoint, 1mL of media was collected in order to assay in a luciferase reaction, this resulted in the monitoring of the transcriptional activity of NRF2 and NFκB after the 24-hour adaptation period, and after 24 and 48 hours of agonist treatment and vehicle control for untreated comparisons.

Culture under LSS resulted in a large activation of Nrf2 during the first 24-hour adaption phase (~1370-fold), which increased further with continued culture under LSS (3720 at 48h, and 4828 at 72hr Figure 4.27), Nrf2 activation increased to 5313- fold with the addition of Sulforaphane (Figure 4.27, 4.29, 9% increase $P<0.05$). Interestingly, TNFα lowered the activation of Nrf2 by LSS, to 3089-fold (Figure 4.27, 4.29, 36% decrease $P<0.0001$).

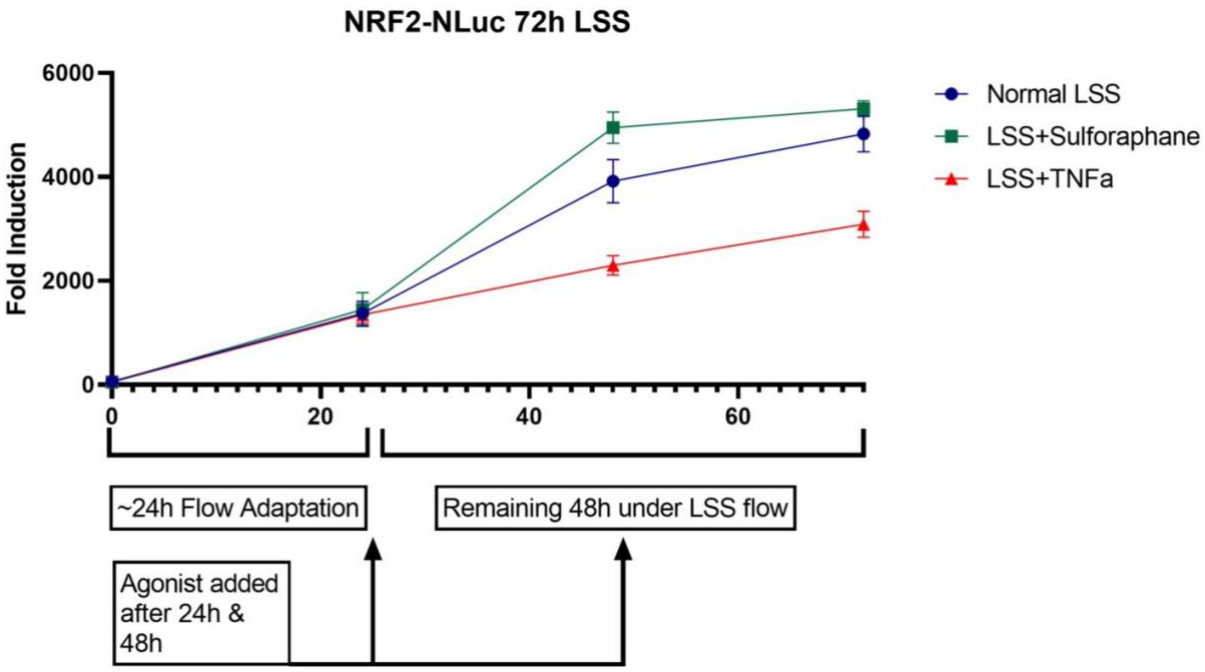

Figure 4.27 Response of NRF2-NLuc Reporter Under Laminar Shear Stress (LSS) for 72h

HCAECPro cells containing NRF2-NLuc/NFkB-VLuc were subjected to laminar shear stress (LSS, 1.5Pa for 72 hours. Cells were allowed to adapt to flow conditions for 24 hours. After 24h, cells continued LSS with the addition of TNFα(2ng/mL), Sulforaphane (50μM) or nothing else added and exposed for a further 48h. 1mL sample for luciferase assay was collected at 24, 48 and 72h. n=3 in triplicate for technical repeats.

OSS induced a much lower activation of Nrf2 over the first 24-hour adaptation phase compared to LSS (613-fold (OSS) v 1390-fold; Figure 4.28, 4.29). Unlike LSS, no further activation of Nrf2 was observed at 48 and 72 hours. Results show a significant reduction in Nrf2 activation under OSS v LSS after 72h (695-fold v 4828- fold, Figure 4.28, 4.29, $p<0.0001$). Sulforaphane (50μM) increased Nrf2 activation

in OSS from 695-fold to 984-fold, however this was not statistically significant (Figure 4.28, 4.29).

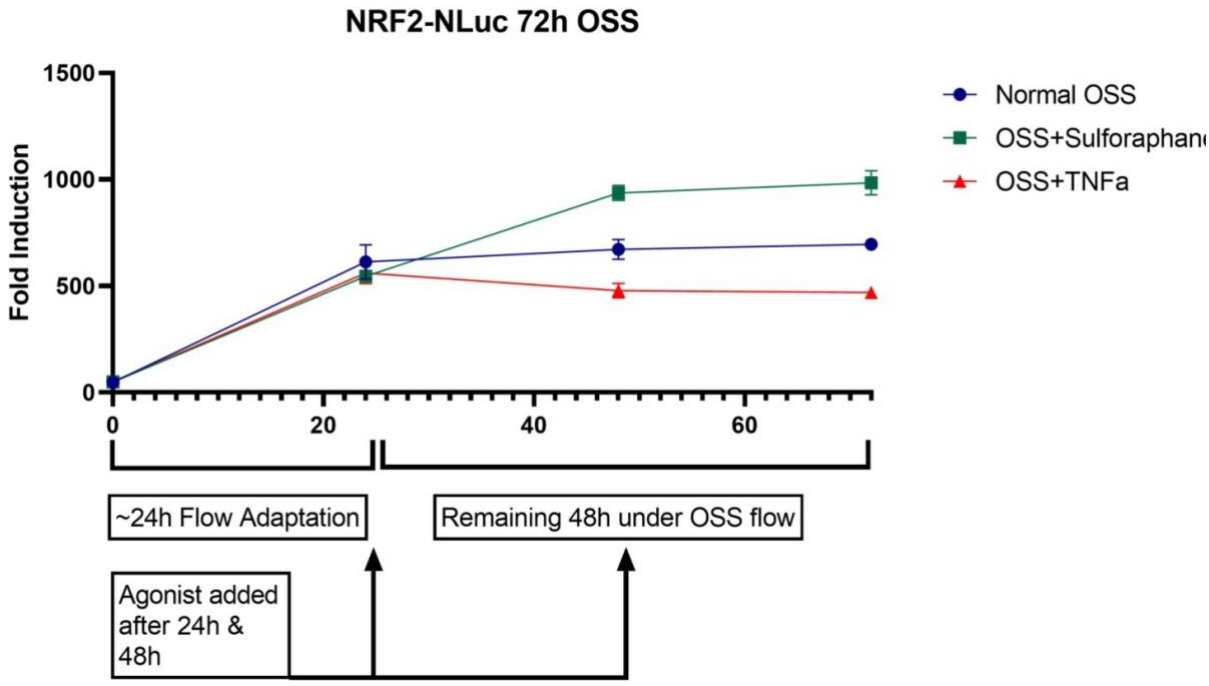

Figure 4.28 Response of NRF2-NLuc Reporter Under Oscillatory Shear Stress (OSS) for 72h

HCAECPro cells containing NRF2-NLuc/NFkB-VLuc were subjected to oscillatory shear stress (OSS, 0.5Pa) for 72 hours. Cells were allowed to adapt to flow conditions for 24 hours. After 24h, cells continued OSS with the addition of TNFα(2ng/mL), Sulforaphane (50μM) or nothing else added and exposed for a further 48h. 1mL sample for luciferase assay was collected at 24, 48 and 72h. n=3 in triplicate for technical repeats.

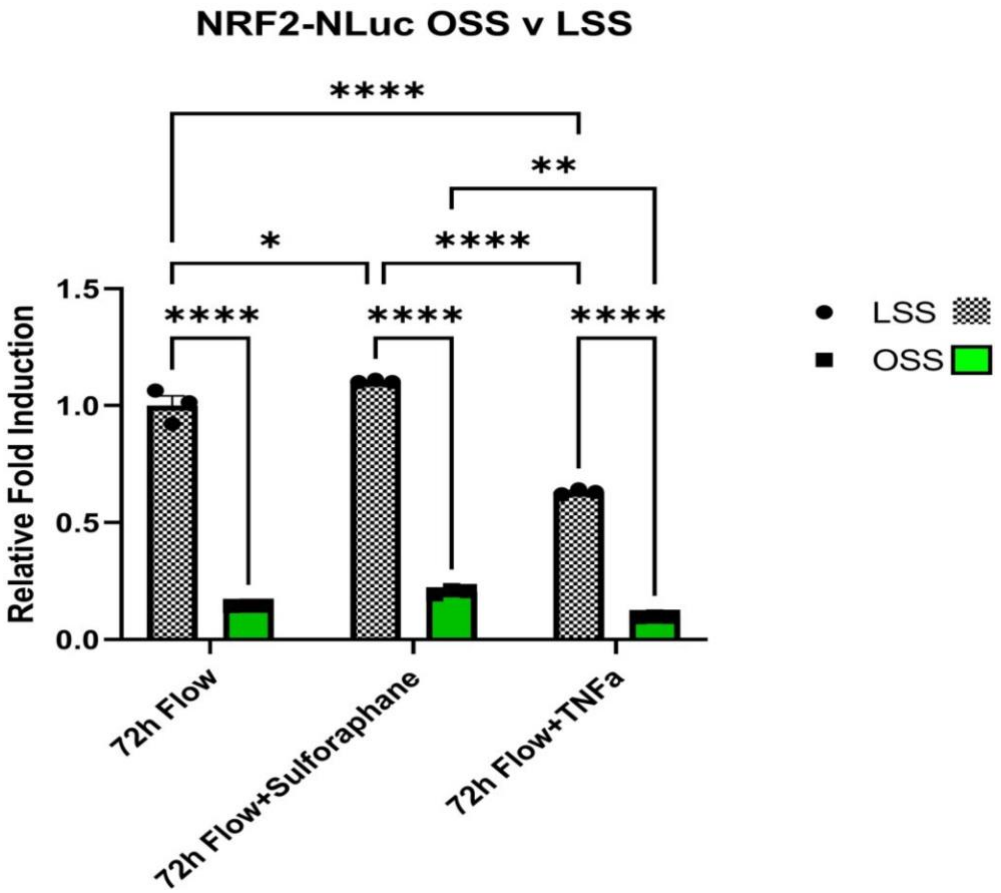

Figure 4.29 Response of NRF2-NLuc Under 72h Physiological LSS v OSS

HCAECPro cells containing NRF2-NLuc/NFkB-VLuc were subjected to laminar shear stress (LSS, 1.5Pa) and oscillatory shear stress (OSS, 0.5Pa) for 72 hours. Cells were allowed to adapt to flow conditions for 24 hours. After 24h, cells continued LSS and OSS with the addition of either TNFα(2ng/mL), Sulforaphane (50µM) or nothing else added and exposed for a further 48h. 1mL sample for luciferase assay was collected at 24, 48 and 72h. n=3 in triplicate for technical repeats. Statistics performed using Graphapad software, 2-way Anova *p<0.05, **p<0.01, ***p<0.001, ****p<0.0001

.

As expected, there was an observable reduced activation of NFκB during the adaptation phase under LSS compared to OSS (6.8-fold v 14.8-fold, Figure 4.30, 4.31. Under LSS, there was no further activation of NFκB after the first 24 hours. TNFα increased the activation of NFκB under both LSS and OSS conditions, synergising with flow, resulting in a larger induction of NFκB in OSS compared to LSS (32.7-fold v 22.9-fold, Figure 4.30, 4.31, 4.32 $P<0.0001$). There was an observed reduction in vLuc measurements in LSS conditions at 48hr and 72 in the control or Sulforaphane treatment. As the flow system is a sealed system and it is the same media circulating within the flow system, it suggests a slow degradation of VLuc in the absence of additional secretion into the media. Between 24 and 72 hours, vLuc reduced from 6.96-fold at 24 hours to 3.7-fold at 72 hours for control and sulforaphane treatment. Further experiments spiking in vLuc into a flow system and sequential measurements is required to quantify its stability in tissue culture conditions, so it can be determined if there is any additional activation of NFκB under control or sulforaphane treatment that is masked by degradation of the vLuc produced during the adaption phase.

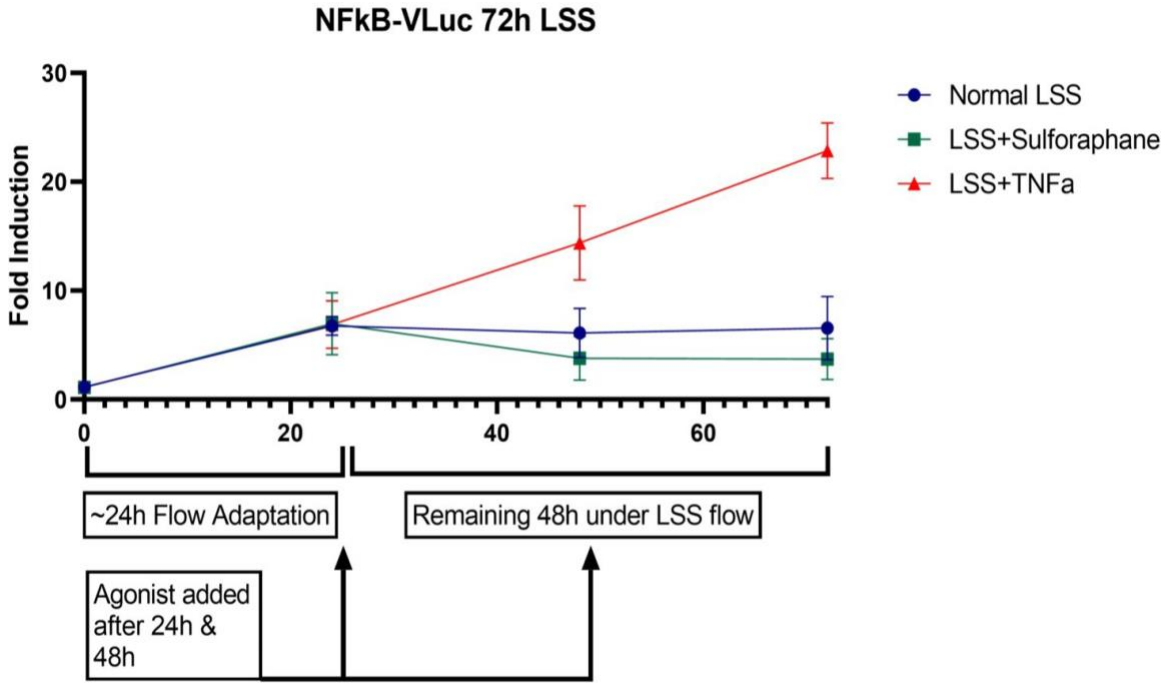

Figure 4.30 Response of NFκB-VLuc Reporter Under Laminar Shear Stress (LSS) for 72h

HCAECPro cells containing NRF2-NLuc/NFkB-VLuc were subjected to laminar shear stress (LSS, 1.5Pa for 72 hours. Cells were allowed to adapt to flow conditions for 24 hours. After 24h, cells continued LSS with the addition of TNFα(2ng/mL), Sulforaphane (50μM) or nothing else added and exposed for a further 48h. 1mL sample for luciferase assay was collected at 24, 48 and 72h. n=3 in triplicate for technical repeats.

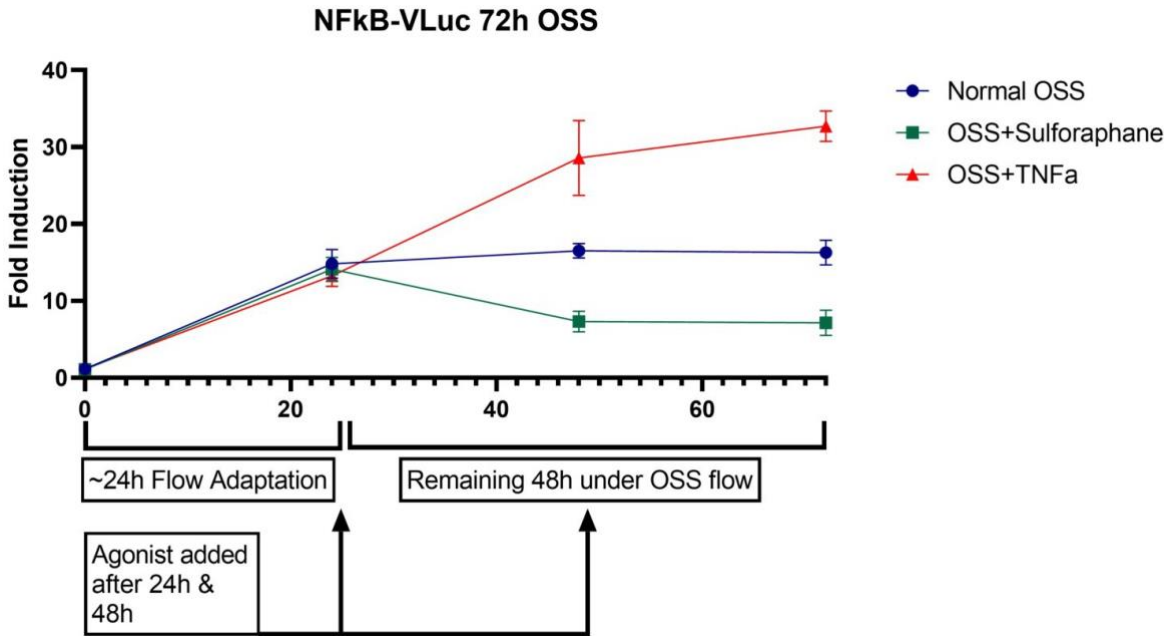

Figure 4.31 Response of NFκB-VLuc Reporter Under Oscillatory Shear Stress (OSS) for 72h

HCAECPro cells containing NRF2-NLuc/NFkB-VLuc were subjected to oscillatory shear stress (OSS, 0.5Pa) for 72 hours. Cells were allowed to adapt to flow conditions for 24 hours. After 24h, cells continued OSS with the addition of TNFα(2ng/mL), Sulforaphane (50μM) or nothing else added and exposed for a further 48h. 1mL sample for luciferase assay was collected at 24, 48 and 72h. n=3 in triplicate for technical repeats.

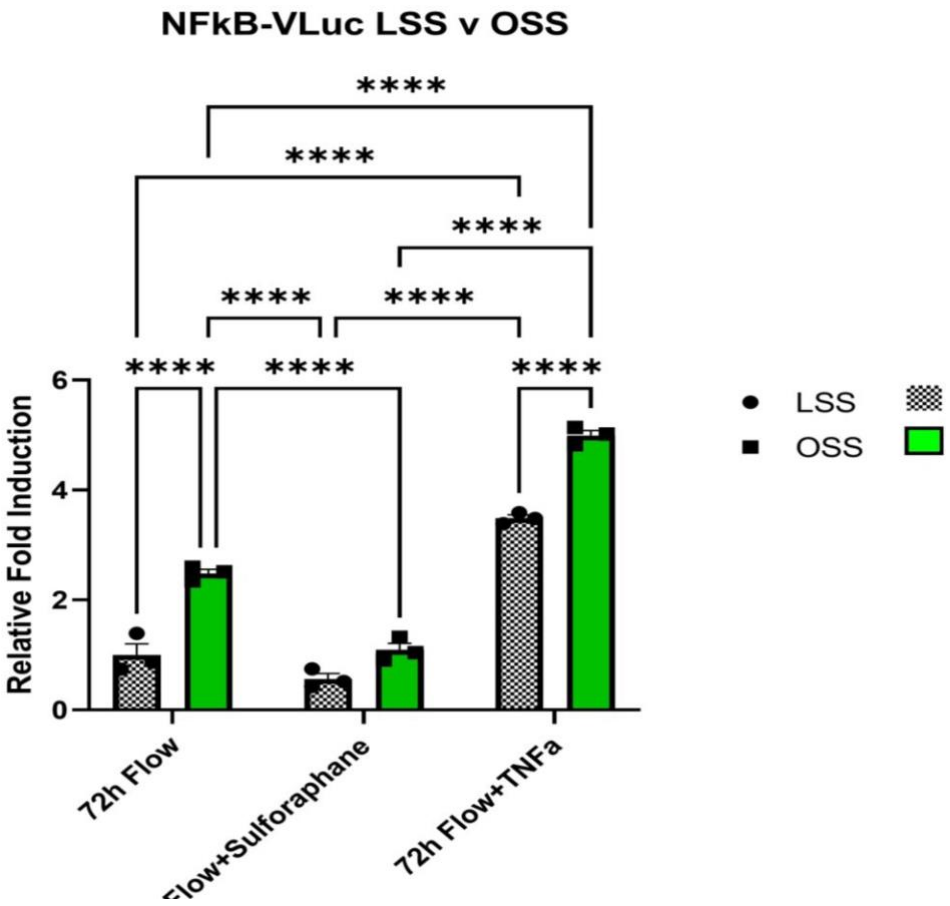

Figure 4.32 Response of NFκB-VLuc Under 72h Physiological LSS v OSS

HCAECPro cells containing NRF2-NLuc/NFkB-VLuc were subjected to laminar shear stress (LSS, 1.5Pa) and oscillatory shear stress (OSS, 0.5Pa) for 72 hours. Cells were allowed to adapt to flow conditions for 24 hours. After 24h, cells continued LSS and OSS with the addition of either TNFα(2ng/mL), Sulforaphane (50μM) or nothing else added and exposed for a further 48h. 1mL sample for luciferase assay was collected at 24, 48 and 72h. n=3 in triplicate for technical repeats. Statistics performed using Graphapad software, 2-way Anova *p<0.05, **p<0.01, ***p<0.001, ****p<0.0001 .

4.3.2 Monitoring the Transcriptional Regulation of KLF2-NLuc/AP1-VLuc (E-Sense Red) under LSS and OSS

As with E-Sense Green, E-Sense Red (HCAECPro containing KLF2-nLuc/AP1-VLuc) was cultured under LSS and OSS for 72 hours. After the initial 24 hour adaptation phase Atorvastatin (1µM), TNFα (2ng/mL) or vehicle control were added at 24 and 48 hours, with measurement of luciferase activity every 24 hours. At each 24-hour timepoint, 1mL of media was collected in order to assay in a luciferase reaction, this resulted in the quantification of the transcriptional activity of KLF2 and AP1 under physiological laminar or oscillatory shear stress.

At the end of the adaption phase, NLuc quantification demonstrated a difference between KLF2 activity under LSS and OSS (316-fold v 201-fold Figures 4.33, 4.34) with continued KLF2 activity resulting in further increases in NLuc measurements at 48 and 72 hours under LSS, but not OSS. Atorvastatin augmented KLF2 activation under LSS, but not OSS (LSS – 1223-fold v 950-fold, $p<0.01$; OSS 226-fold v 213- fold Figure 4.33, 4.34 & 4.35), suggesting that at atheroprone sites, statin treatment may not augment atheroprotective signalling. Interestingly, TNFα treatment reduced KLF2 activity under LSS but not OSS (LSS – 950-fold v 419-fold, $p<0.0001$; OSS, 226-fold v 191-fold Figure 4.33, 4.34 & 4.35)

.

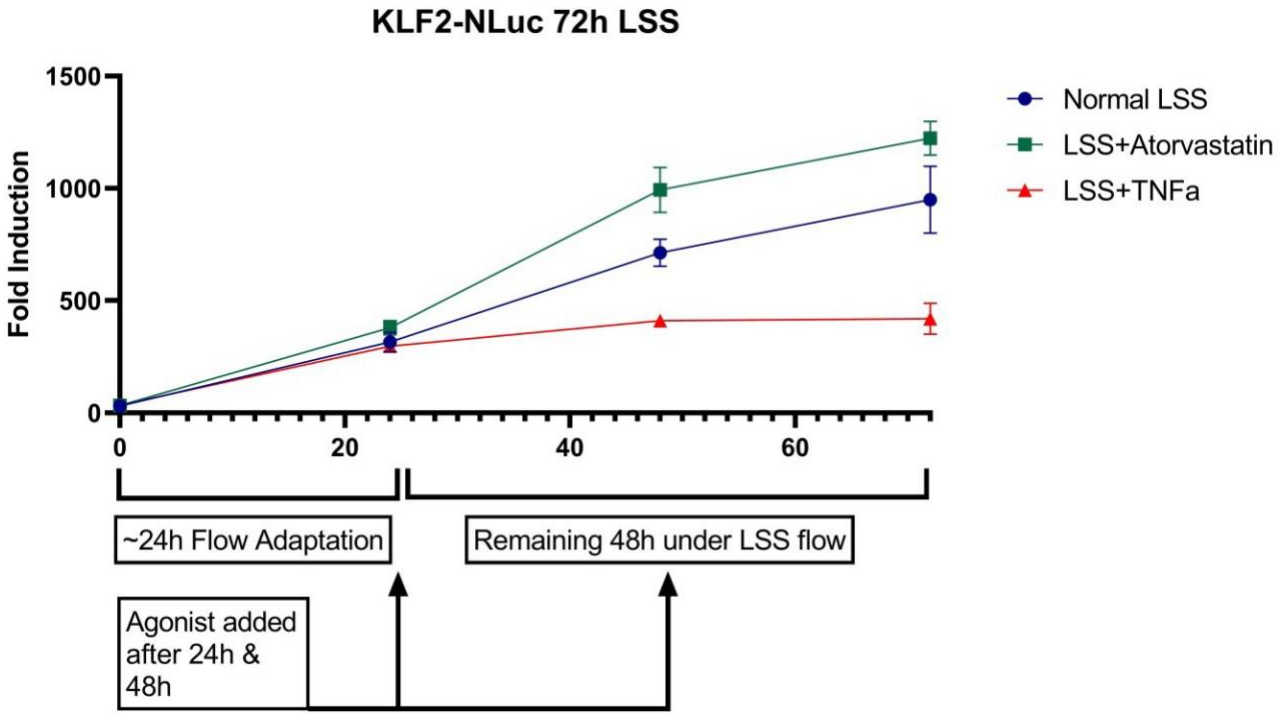

Figure 4.33 Response of KLF2-NLuc Reporter Under Laminar Shear Stress (LSS) for 72h

HCAECPro cells containing KLF2-NLuc/AP1-VLuc were subjected to laminar shear stress (LSS, 1.5Pa) for 72 hours. Cells were allowed to adapt to flow conditions for 24 hours. After 24h, cells continued LSS with the addition of either TNFα (2ng/mL), Atorvastatin (1μM) or nothing else added and exposed for a further 48h. 1mL sample for luciferase assay was collected at 24, 48 and 72h. n=3 in triplicate for technical repeats.

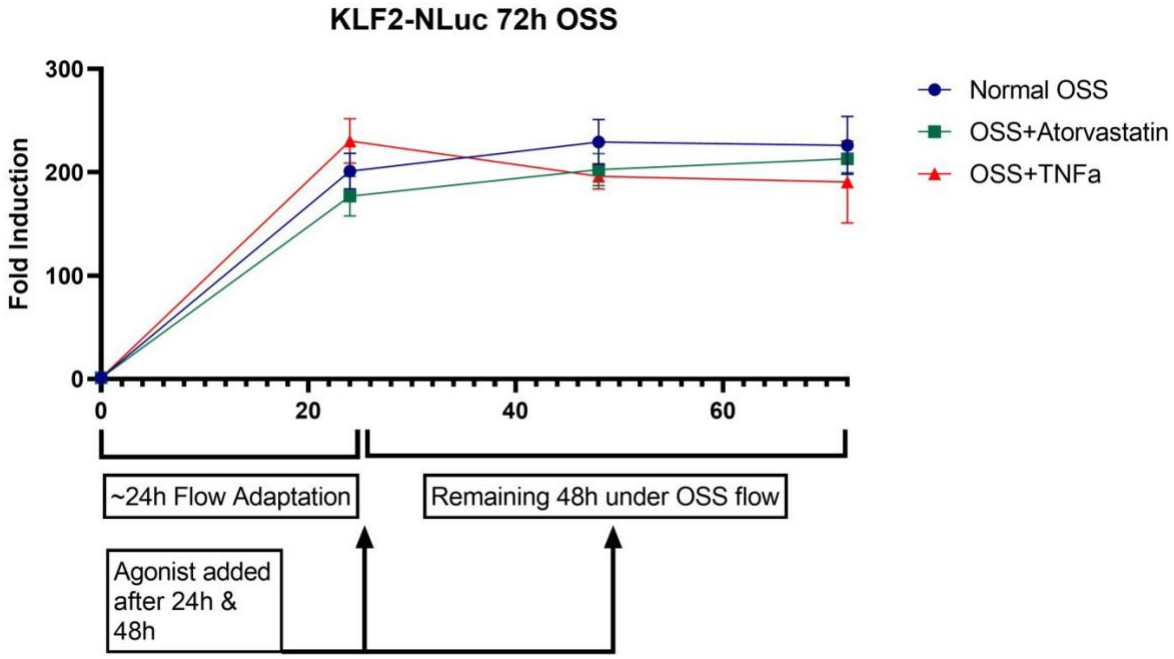

Figure 4.34 Response of KLF2-NLuc Reporter Under Oscillatory Shear Stress (OSS) for 72h

HCAECPro cells containing KLF2-NLuc/AP1-VLuc were subjected to oscillatory shear stress (OSS, 0.5Pa) for 72 hours. Cells were allowed to adapt to flow conditions for 24 hours. After 24h, cells continued OSS with the addition of either TNFα (2ng/mL), Atorvastatin (1μM) or nothing else added and exposed for a further 48h. 1mL sample for luciferase assay was collected at 24, 48 and 72h. n=3 in triplicate for technical repeats.

.

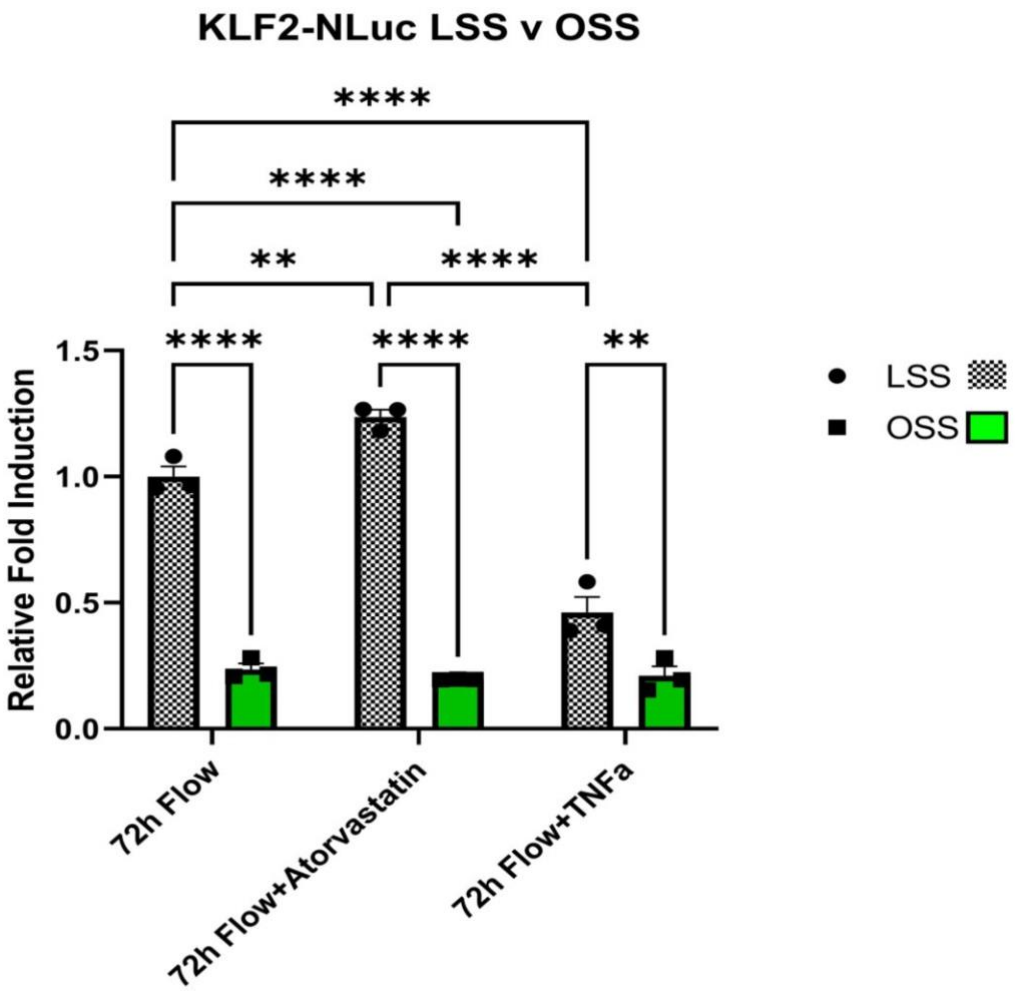

Figure 4.35 Response of KLF2-NLuc Under 72h Physiological LSS v OSS

HCAECPro cells containing KLF2-NLuc/AP1-VLuc were subjected to laminar shear stress (LSS, 1.5Pa) and oscillatory shear stress (OSS, 0.5Pa) for 72 hours. Cells were allowed to adapt to flow conditions for 24 hours. After 24h, cells continued LSS and OSS with the addition of either TNFα (2ng/mL), Atorvastatin (1μM) or nothing else added and exposed for a further 48h. 1mL sample for luciferase assay was collected at 24, 48 and 72h. n=3 in triplicate for technical repeats. Statistics performed using Graphapad software, 2-way Anova *p<0.05, **p<0.01, ***p<0.001, ****p<0.0001.

.

The activation of AP1 followed an identical pattern of induction compared to NFκB, quantified in E-Sense Green (Section 4.3.1). There was a reduced activation of AP1 during the adaptation phase under LSS compared to OSS (8.3-fold v 10.9-fold, Figure 4.36, 4.37). Under LSS, there was no further activation of AP1 after the first

24 hours. TNFα increased the activation of AP1 under both LSS and OSS conditions, synergising with flow, resulting in a larger induction of AP1 in OSS compared to LSS (26.5-fold v 12.9-fold, Figure 4.36, 4.37, 4.38, $P<0.001$). There was a trend towards a reduction in VLuc measurements in LSS conditions at 48hr and 72hr with Atorvastatin treatment but not OSS

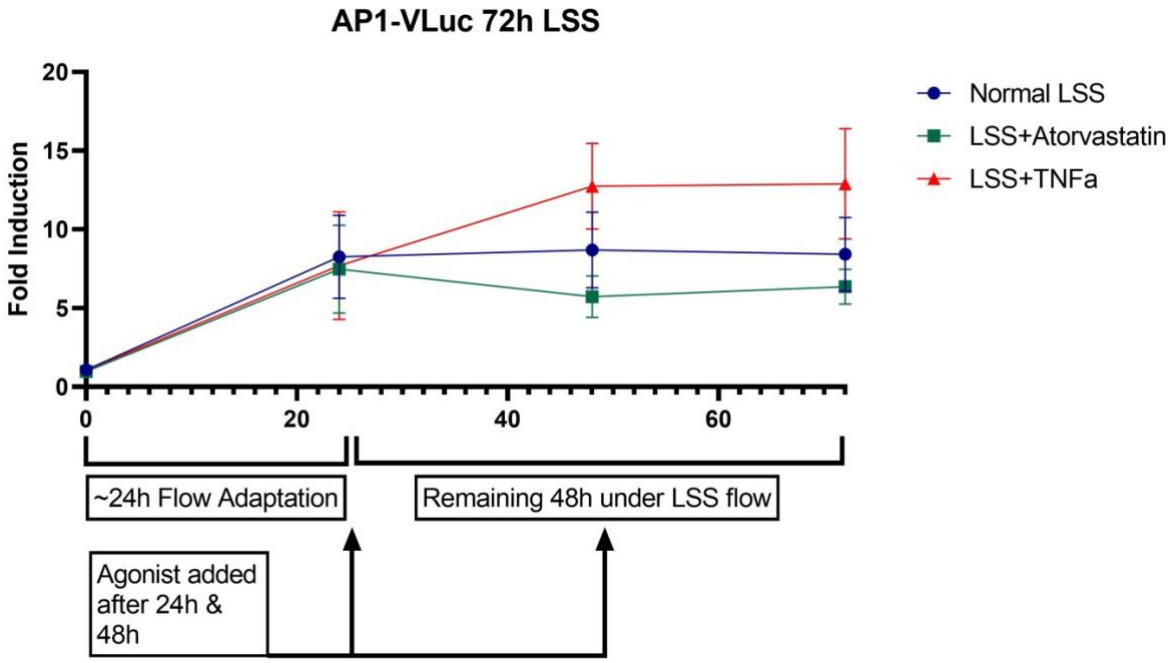

Figure 4.36 Response of AP1-VLuc Reporter Under Laminar Shear Stress (LSS) for 72h

HCAECPro cells containing KLF2-NLuc/AP1-VLuc were subjected to laminar shear stress (LSS, 1.5Pa) for 72 hours. Cells were allowed to adapt to flow conditions for 24 hours. After 24h, cells continued LSS with the addition of either TNFα (2ng/mL), Atorvastatin (1µM) or nothing else added and exposed for a further 48h. 1mL sample for luciferase assay was collected at 24, 48 and 72h. n=3 in triplicate for technical repeats.

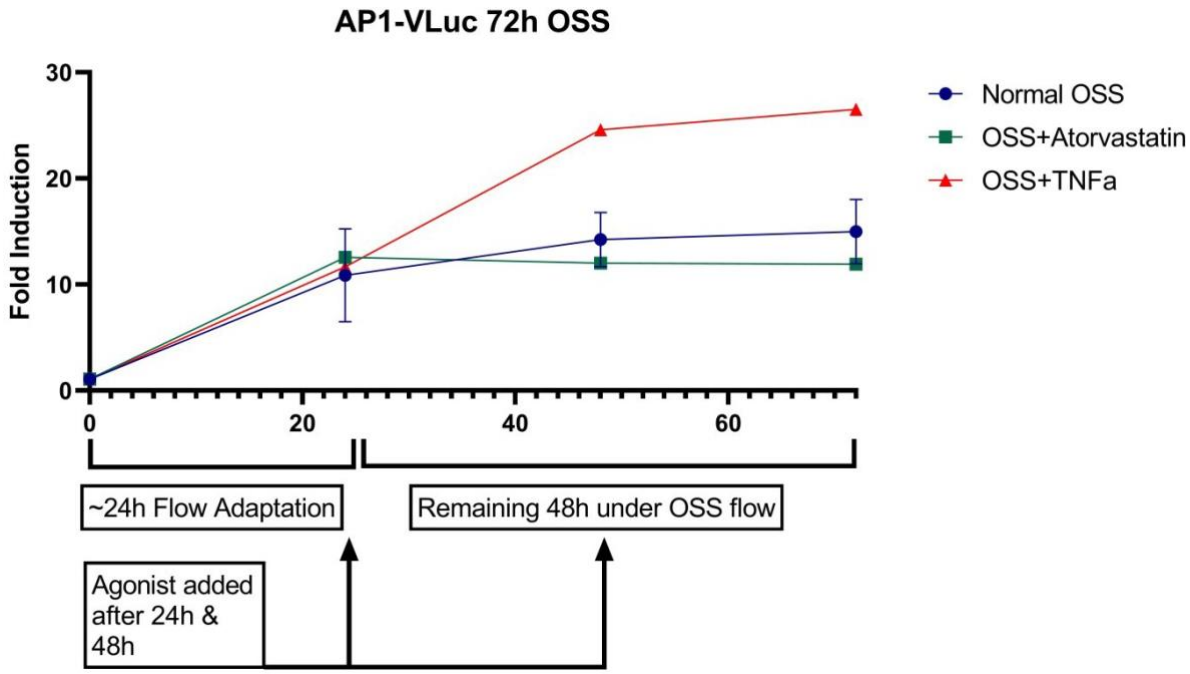

Figure 4.37 Response of AP1-VLuc Reporter Under Oscillatory Shear Stress (OSS) for 72h

HCAECPro cells containing KLF2-NLuc/AP1-VLuc were subjected to oscillatory shear stress (OSS, 0.5Pa) for 72 hours. Cells were allowed to adapt to flow conditions for 24 hours. After 24h, cells continued OSS with the addition of either TNFα (2ng/mL), Atorvastatin (1μM) or nothing else added and exposed for a further 48h. 1mL sample for luciferase assay was collected at 24, 48 and 72h. n=3 in triplicate for technical repeats.

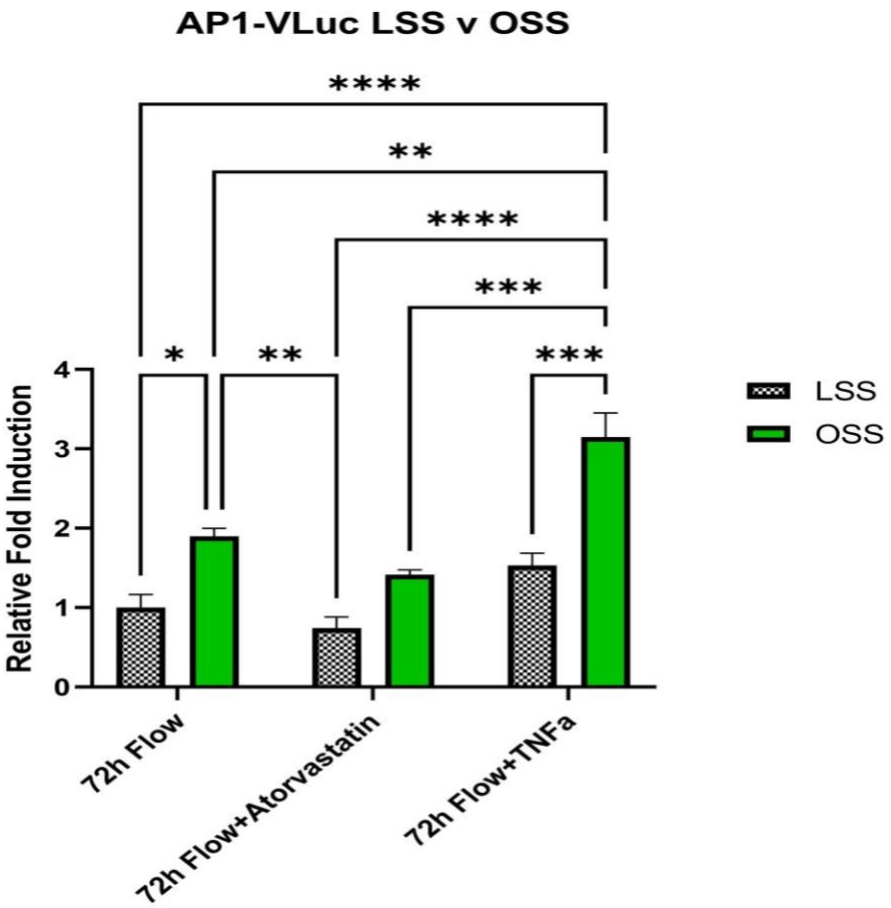

Figure 4.38 Response of AP1-VLuc Under 72h Physiological LSS v OSS

HCAECPro cells containing KLF2-NLuc/AP1-VLuc were subjected to laminar shear stress (LSS, 1.5Pa) and oscillatory shear stress (OSS, 0.5Pa) for 72 hours. Cells were allowed to adapt to flow conditions for 24 hours. After 24h, cells continued LSS and OSS with the addition of either TNFα (2ng/mL), Atorvastatin (1μM) or nothing else added and exposed for a further 48h. 1mL sample for luciferase assay was collected at 24, 48 and 72h. n=3 in triplicate for technical repeats. Statistics performed using Graphapad software, 2-way Anova *p<0.05, **p<0.01, ***p<0.001, ****p<0.0001.

4.3.3 Monitoring the Transcriptional Regulation of XBP1-nLuc/IRF3-vLuc (E-Sense Yellow) under LSS and OSS

Finally, as above, E-Sense Yellow (HCAECPro+XBP1-nLuc/IRF3-vLuc) was cultured under normal laminar shear stress (LSS) and oscillatory shear stress (OSS) for 72 hours with addition of Thapsigargin (50nM) or Lipopolysaccharide (LPS- 50ng/mL) or vehicle control at 24 hours and 48 hours in total. At each 24-hour timepoint, 1mL of media was collected in order to assay in a luciferase reaction, this resulted in the monitoring of the transcriptional activity of XBP1 and IRF3 under physiological laminar or oscillatory shear stress.

At the end of the adaption phase, NLuc quantification demonstrated a lower quantification of XBP1 activity under LSS and OSS (32.5-fold v 41-fold Figures 4.39,

4.40. Under LSS, XBP1 activity increased at 48 but not 72, while under OSS, XBP1 activity was sustained at 72 hours. Addition of both Thapsigargin and LPS increased XBP1 activity in both OSS and LSS, but to a greater extent under OSS (Figures 4.39, 4.40, 4.41).

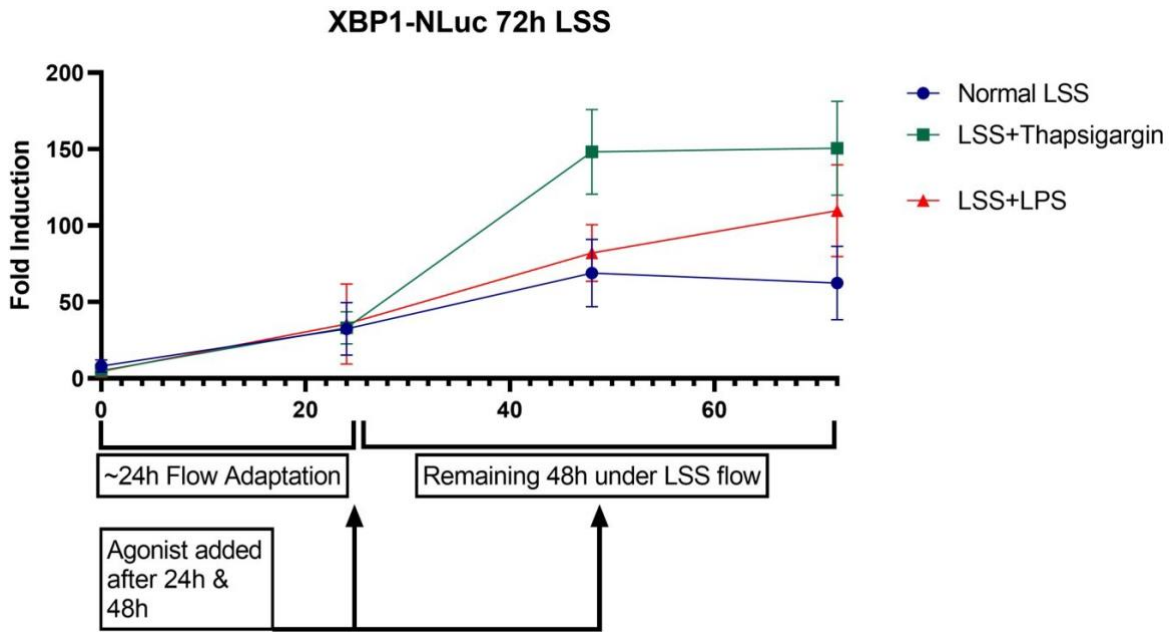

Figure 4.39 Response of XBP1-NLuc Reporter Under Laminar Shear Stress (LSS) for 72h

HCAECPro cells containing XBP1-NLuc/IRF3-VLuc were subjected to laminar shear stress (LSS, 1.5Pa) for 72 hours. Cells were allowed to adapt to flow conditions for 24 hours. After 24h, cells continued LSS and OSS with the addition of either Thapsigargin (50nM), LPS (50ng/mL) or nothing else added and exposed for a further 48h. 1mL sample for luciferase assay was collected at 24, 48 and 72h. n=3 in triplicate for technical repeats.

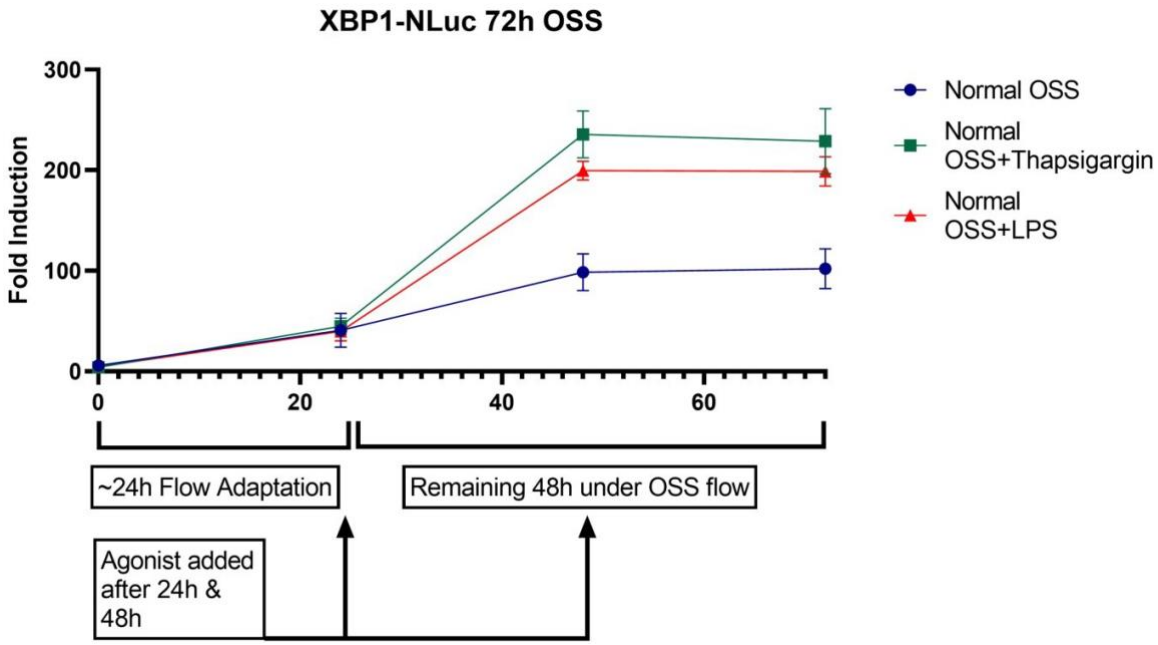

Figure 4.40 Response of XBP1-NLuc Reporter Under Oscillatory Shear Stress (OSS) for 72h

HCAECPro cells containing XBP1-NLuc/IRF3-VLuc were subjected to oscillatory shear stress (OSS, 0.5Pa) for 72 hours. Cells were allowed to adapt to flow conditions for 24 hours. After 24h, cells continued LSS and OSS with the addition of either Thapsigargin (50nM), LPS (50ng/mL) or nothing else added and exposed for a further 48h. 1mL sample for luciferase assay was collected at 24, 48 and 72h. n=3 in triplicate for technical repeats.

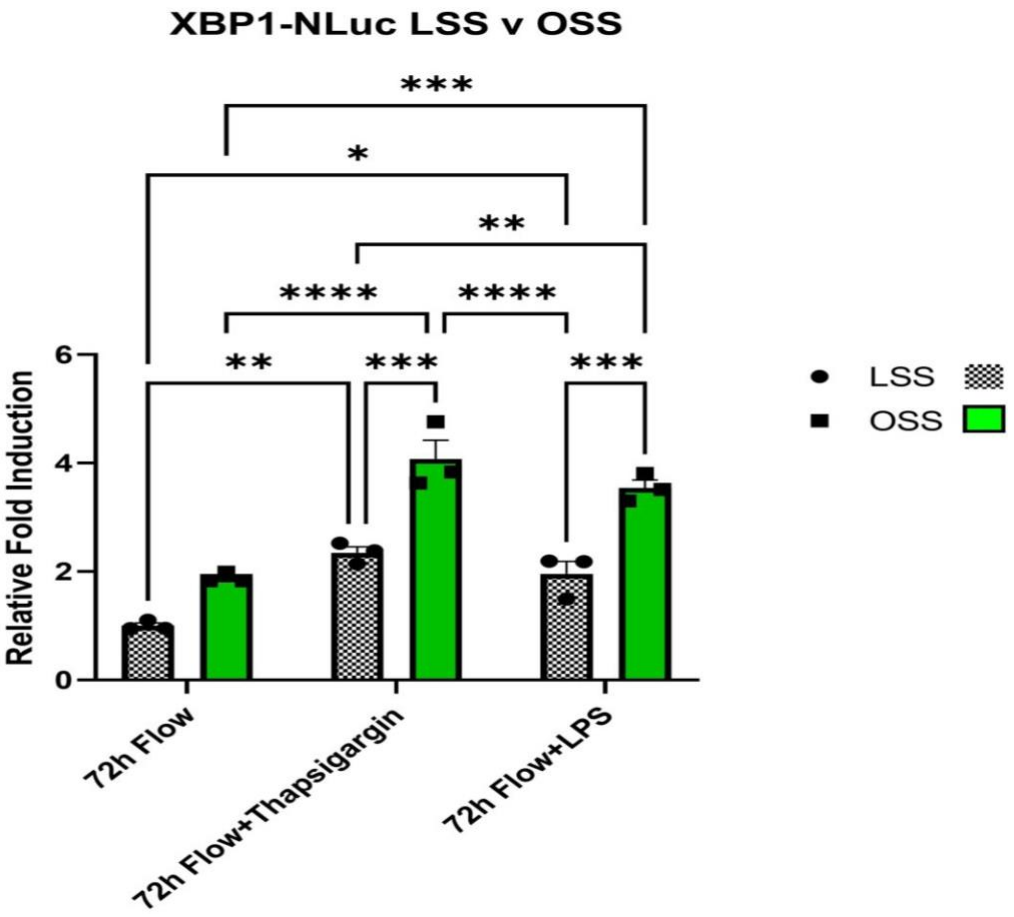

Figure 4.41 Response of XBP1-NLuc Under 72h Physiological LSS v OSS

HCAECPro cells containing XBP1-NLuc/IRF3-VLuc were subjected to laminar shear stress (LSS, 1.5Pa) and oscillatory shear stress (OSS, 0.5Pa) for 72 hours. Cells were allowed to adapt to flow conditions for 24 hours. After 24h, cells continued LSS and OSS with the addition of either Thapsigargin (50nM), LPS (50ng/mL) or nothing else added and exposed for a further 48h. 1mL sample for luciferase assay was collected at 24, 48 and 72h. n=3 in triplicate for technical repeats. Statistics performed using Graphapad software, 2-way Anova *p<0.05, **p<0.01, ***p<0.001, ****p<0.0001.

Similarly, measurement of IRF3 activity was lower after the adaptation phase under LSS compared to OSS (7.3-fold v 13.6-fold Figures 4.42, 4.43). Quantification of IRF3 response to LPS demonstrated a significantly greater activation under OSS compared to LSS (2.3-fold increase, $p<0.001$). Thapsigargin showed no additional activation of IRF3 above the differences observed by flow.

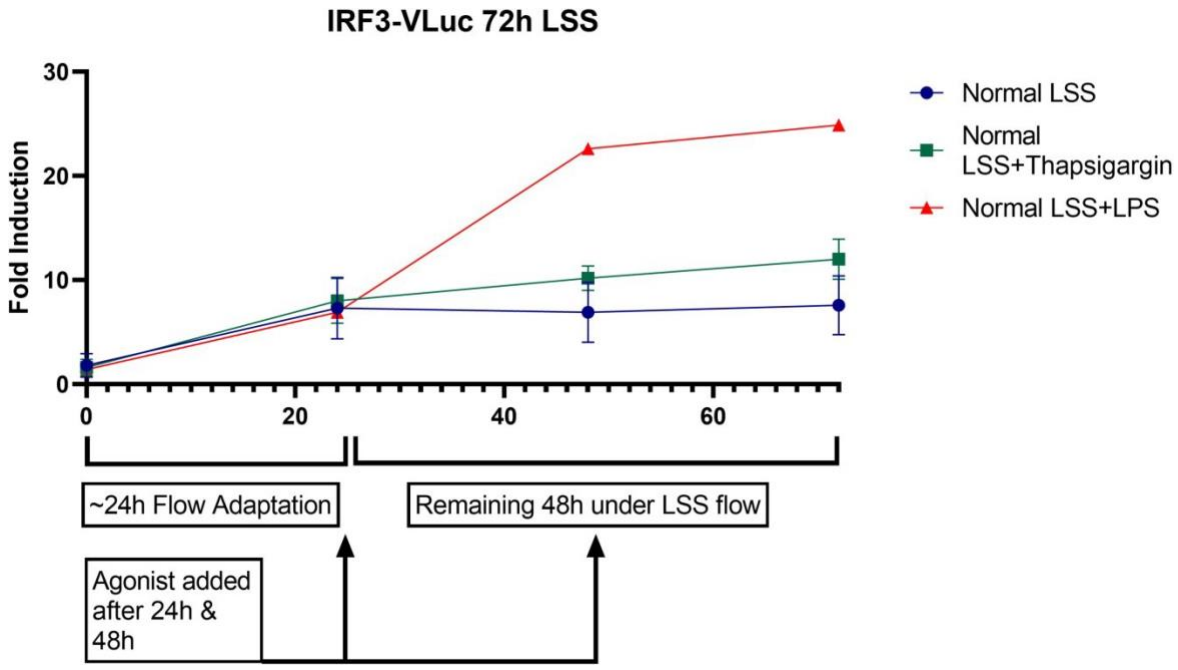

Figure 4.42 Response of IRF3-VLuc Reporter Under Laminar Shear Stress (LSS) for 72h

HCAECPro cells containing XBP1-NLuc/IRF3-VLuc were subjected to laminar shear stress (LSS, 1.5Pa) for 72 hours. Cells were allowed to adapt to flow conditions for 24 hours. After 24h, cells continued LSS and OSS with the addition of either Thapsigargin (50nM), LPS (50ng/mL) or nothing else added and exposed for a further 48h. 1mL sample for luciferase assay was collected at 24, 48 and 72h. n=3 in triplicate for technical repeats.

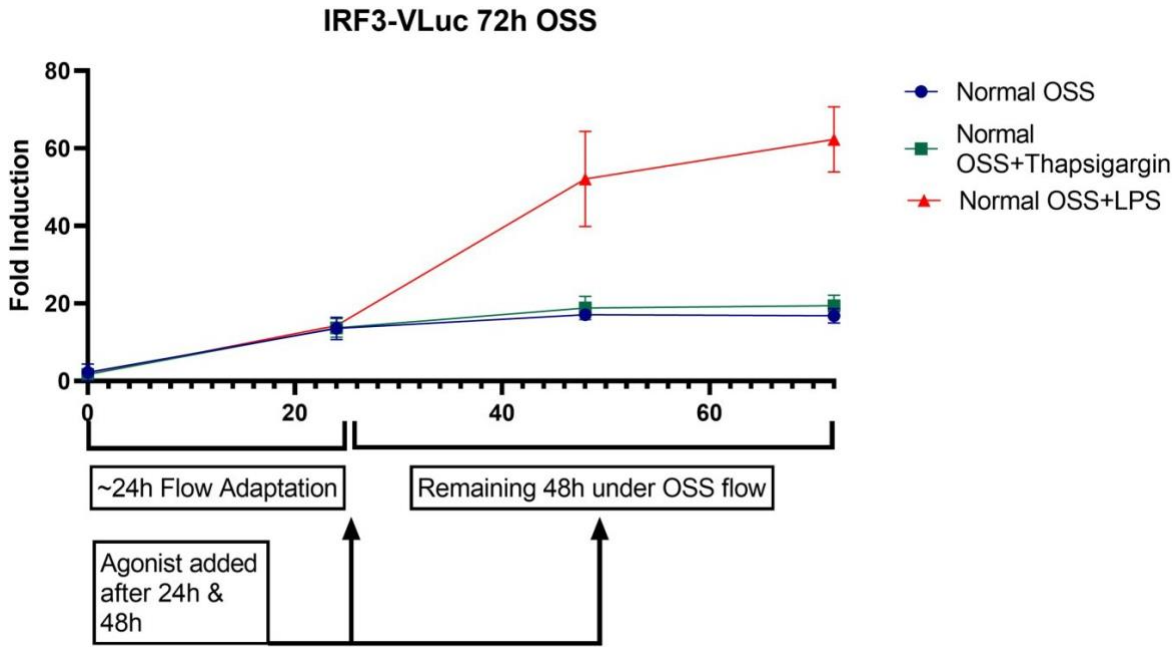

Figure 4.43 Response of IRF3-VLuc Reporter Under Oscillatory Shear Stress (OSS) for 72h

HCAECPro cells containing XBP1-NLuc/IRF3-VLuc were subjected to oscillatory shear stress (OSS, 0.5Pa) for 72 hours. Cells were allowed to adapt to flow conditions for 24 hours. After 24h, cells continued LSS and OSS with the addition of either Thapsigargin (50nM), LPS (50ng/mL) or nothing else added and exposed for a further 48h. 1mL sample for luciferase assay was collected at 24, 48 and 72h. n=3 in triplicate for technical repeats.

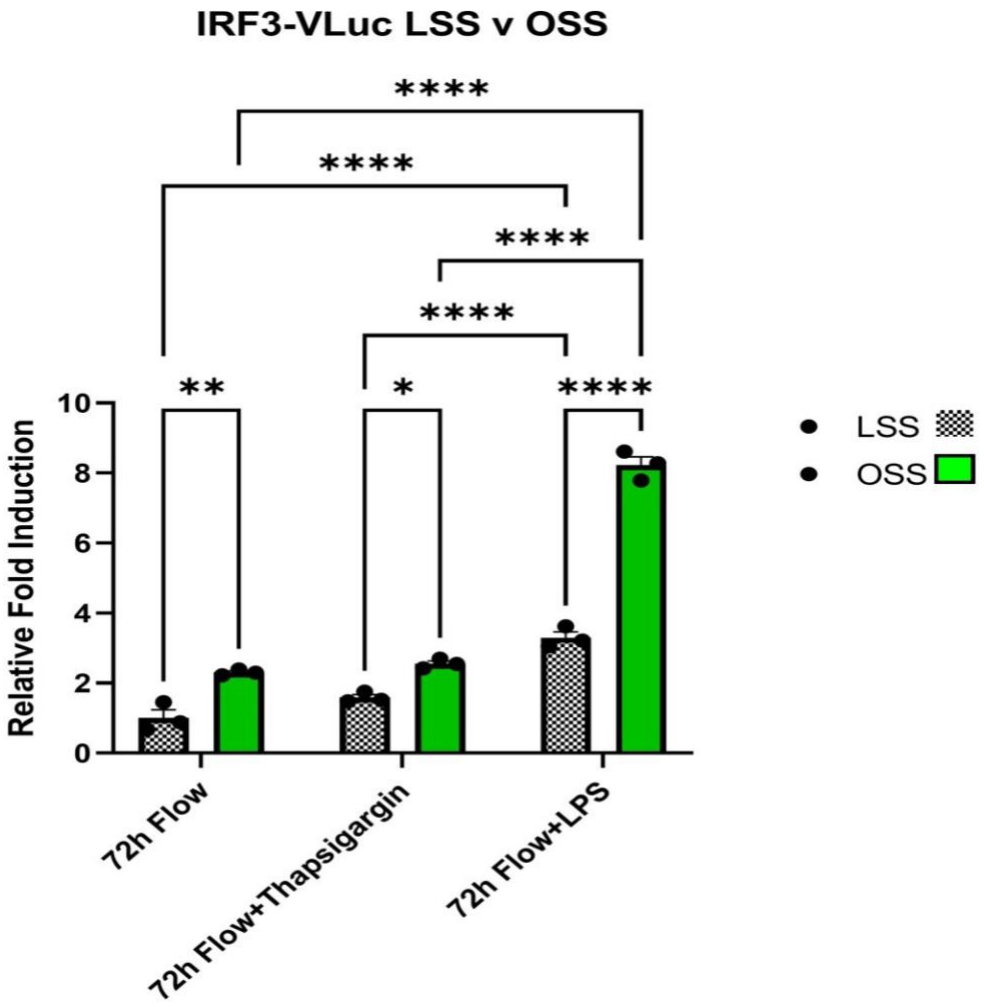

Figure 4.44 Response of IRF3-VLuc Under 72h Physiological LSS v OSS

HCAECPro cells containing XBP1-NLuc/IRF3-VLuc were subjected to laminar shear stress (LSS, 1.5Pa) and oscillatory shear stress (OSS, 0.5Pa) for 72 hours. Cells were allowed to adapt to flow conditions for 24 hours. After 24h, cells continued LSS and OSS with the addition of either Thapsigargin (50nM), LPS (50ng/mL) or nothing else added and exposed for a further 48h. 1mL sample for luciferase assay was collected at 24, 48 and 72h. n=3 in triplicate for technical repeats. Statistics performed using Graphapad software, 2-way Anova *p<0.05, **p<0.01, ***p<0.001, ****p<0.0001.

Summary

- Our E-Sense lines demonstrate shear responsiveness when exposed to normal laminar shear stress and oscillatory shear stress
- By utilising data from our E-Sense lines under static conditions, we were able to integrate agonists into our flow model, allowing us to determine the maximal induction of our reporters.
- This data provides a platform moving forwards, allowing us to monitor the modulation of transcriptional activity in our E-Sense lines to various compounds, enabling us to make observations in their affect in comparison to known agonists
- The table below summarises the responsiveness of our E-Sense lines to LSS and OSS in comparison to the maximal induction observed with key agonists.

TFAR	Max. fold Induction	LSS % Max. Induction	OSS % Max. Induction
NRF2 -nLuc	**5312.7** (LSS+Sulforaphane)	90.9	13.9
NFκB -vLuc	**32.7** (OSS+TNFα)	20.1	49.8
KLF2 -nLuc	**1223.4** (LSS+Atorvastatin)	77.6	18.5
AP1-vLuc	**26.5** (OSS+TNFα)	31.7	56.3
XBP1 -nLuc	**228.9** (OSS+Thapsigargin)	24.5	44.6
IRF3-vLuc	**62.3** (OSS+LPS)	12.2	27.9

4.5 Discussion

This chapter describes the creation of the E-Sense platform via integration of novel transcription factor activator reporter constructs into our HCAECPro cell line previously described in chapter 3. This enabled the production of three E-Sense lines for the monitoring of transcriptional regulation of six transcription factors well established to be involved in atherosclerosis. Our aim was to create a novel screening platform, capable of robust and reliable monitoring of the effects of potential pro-atherogenic compounds, achieved via a novel TFAR-centred model with an increased sensitivity compared to currently available both commercially and in literature (Minchin and Busby, 2013) (Motahari *et al.*, 2015). As previously discussed, atherosclerosis is a chronic condition, developing over several decades (Sena, Pereira and Seiça, 2013), it is therefore logical to assume even relatively small changes in the activity of certain transcription factors, would over the course of several decades relay alterations in endothelial dysfunction, plaque formation and propensity of subsequent acute coronary syndromes. TFARs with increased dynamic range would be capable of quantifying biologically significant regulation of atherosclerosis-modifying signalling pathways that might be predicted to affect the course of the disease, which are unmeasurable using animal models, because the effect size is too small to be significantly detected with the inherent variability in these models.

Using our novel spacing design of transcription binding motifs, we established four novel TFARs containing either nano-luciferase (nLuc) or Vargula luciferase (vLuc) (4.1). These included NRF2-nLuc and KLF2-nLuc for quantifying changes relating to atheroprotective pathways. Using XBP1-nLuc and IRF3-vLuc we were able to monitor alterations in ER stress and the unfolded protein response and Toll-Like Receptor signalling. Finally, we utilised the previously established TFARs; NFκB- vLuc and AP1-vLuc to quantify pro-inflammatory pathways,

produced by the McKay lab at Manchester Metropolitan University. By using two discreet luciferases, nLuc and vLuc, we were able to incorporate two different TFARs into once cell line, enabling us to create three distinct cell lines resulting in a higher throughput.

Initially, we implemented gateway cloning in order to create our E-Sense lines using nLuc and vLuc backbone plasmids (figure 4.4). However, we faced complications, the plasmid displaying instability during ligation resulting in an inability to create functional clones because of plasmid rearrangement. After extensive troubleshooting, it was decided to implement conventional cloning techniques. Ligated products obtained from cloning were appropriate size when implementing a restriction enzyme digest and subsequently TFARs were confirmed by sanger sequencing.

Following from the creation of our TFARs, we sort to measure the dynamic range and sensitivity of our reporter constructs. This provides a valuable benchmark for subsequent studies using novel compounds as we can relate any changes in TF activity to a known agonist and/or 'maximal' response. To achieve this, we performed a dose-response experiment for each TFAR with compounds known to induce transcriptional regulation of the signalling pathway that controlled the TF. By utilising this data under static conditions, we were able ascertain an optimal concentration of compound to use when testing our E-Sense lines under flow using our in-house parallel plate flow system.

As mentioned in chapter 1, the NRF2 antioxidant system plays a role in regulating atherosclerosis. Within the endothelium, flow-induced activation plays a role in reducing atherosclerosis, likely through enhancing protection against ROS insults (Zakkar *et al.*, 2009). Dysregulation and diminished activation of NRF2 has been well documented in atherogenesis (Satta *et al.*, 2017). NRF2-

nLuc was stimulated with cigarette smoke extract (CSE) at concentrations 5%-20% for 24 hours.

Cigarette smoke significantly induces oxidative stress resulting in the activation of Nrf2 and upregulation of antioxidant genes (Teasdale *et al.*, 2016) (Wang *et al.*, 2014). A study by Teasdale et al in 2016 demonstrated a significant upregulation in NRF2 activity and NRF2-regulated genes in human coronary artery endothelial cells in culture (Teasdale *et al.*, 2016). Our data demonstrates high sensitivity of the Nrf2 TFAR in response to this stimulus. Indeed, the dose response of NRF2 + CSE (figures 4.8 & 4.9), demonstrates a high fold induction compared to vehicle control at each concentration, with a 1469-fold induction at 5% CSE, and maximal induction of 2717-fold induction at 20% CSE. We compared CSE with Sulforaphane treatment at concentrations ranging from 5µM to 50µM for 24 hours in static conditions (figures 4.10 & 4.11). Sulforaphane has been demonstrated to directly interact with Keap1 and release NRF2 from Keap1-dependent repression, which in turn leads to nuclear translocation of NRF2 and regulation of genes containing functional Antioxidant Response Elements (AREs) in their promoters/enhancers (Hu *et al.*, 2011) (Houghton, Fassett and Coombes, 2016). The Nrf2 TFAR demonstrated a high sensitivity when stimulated with Sulforaphane, with a maximum induction of 495- fold at a concentration of 50µM. This is 5.5-fold lower than CSE, suggesting CSE more robustly activates Nrf2 than sulforaphane. In comparison, the commercially available ARE reporter kit (NRF2 antioxidant pathway) from BPS bioscience, advertises a 7-fold induction of its NRF2 reporter when treated with 10µM Sulforaphane, demonstrating the increased sensitivity of our NRF2 TFAR, even when using diluted luciferase reagents.

The KLF2 TFAR activity was assessed through lentiviral overexpression of KLF2 and by treatment with Atorvastatin. Overexpression of KLF2 under the control of

the PGK promoter resulted in a 3310-fold increase in NLuc activity showing a similar dynamic range as the Nrf2 TFAR. Statins have been shown to modestly upregulate KLF2, with this induction dependent on the inhibition of cholesterol synthesis he Rho pathway (Parmar *et al.*, 2005). The KLF2-nLuc TFAR demonstrated high sensitivity to statin treatment, with an induction of 276-fold compared to vehicle control at the lowest concentration of 0.1µM, and maximal induction of 387-fold at a concentration of 1µM, which is 11% of the activity induced by KLF2 overexpression. Having a theoretical understanding of a maximal activation allows an appreciation of the degree of activation achieved by a test compound. In this case, a 10% activation by atorvastatin fits with the literature (Sen-Banerjee *et al.*, 2005). The observation that atorvastatin upregulates KLF2 activity under LSS, but not OSS is intriguing and may limit the capacity of statins to augment atheroprotective signalling in endothelial cells at the sites most prone to disease development. Testing the effects of statins in E-Sense Red under elevated flow might illuminate if statins might increase atheroprotective signalling on the upstream surface of atherosclerotic plaques. This dynamic range demonstrates the effectiveness of our re-designed reporter system, as our atheroprotective reporters have shown a high sensitivity, it produces encouraging data to suggest we can discern the activity of novel compounds which may exhibit a modest effect on transcriptional activity.

XBP1 and IRF3 TFARs were created to quantify changes in ER stress and unfolded protein response (UPR) and Toll-Like Receptor (TLR) signalling respectively (Zeng *et al.*, 2009)(Lim and Staudt, 2013). Thapsigargin has been documented to induce ER stress resulting in the activation of IRE1α through dimerization, resulting in processing of XBP1 mRNA and translation of XBP1 (Tsuru *et al.*, 2016). The ER stress inducer, Brefeldin A, acts as an agonist for the induction of the unfolded protein response via IRE1α, PERK and ATF6

activation (de Galarreta *et al.*, 2016). Under static conditions, we demonstrate XBP1-nLuc was highly sensitivity to Thapsigargin treatment (5nM-100nM), with an induction of 433-fold at 5nM and a maximal induction of 515.-fold at a concentration of 50nM (figures 4.15 & 4.16). Stimulation with Brefeldin A (figures 4.17 & 4.18) resulted in significant induction of XBP1, albeit slightly diminished compared to Thapsigargin. Brefeldin A treatment at concentrations 0.5µg/mL – 50µg/mL, resulted in a 75- to 103-fold induction. Although we see a diminished induction following Brefeldin A treatment, the 103- fold induction still represents a large dynamic change in luciferase activity, and very easy to quantify. As described in chapter 1, IRF3 activity can be induced through the activation of the TLR3/TLR4 signalling (Lim and Staudt, 2013). Oxidized low- density lipoprotein (Ox-LDL) is recognised as a damage-associated molecular pattern (DAMPs) and is a key atherogen, in part by increasing proinflammatory signalling through binding to and activation of TLR4. In addition, bacterial-derived Lipopolysaccharides (LPS) are pathogen-associated molecular patterns (PAMPs) and also bind and activate TLR4 (Nogieć *et al.*, 2020) (Schnack *et al.*, 2019). Of the four newly designed TFARs, the IRF3-vLuc TFAR demonstrated the smallest dynamic range. This could be extended by not diluting the luciferase reagents, however we used the same dilution throughout these experiments to allow direct comparisons. Ox-LDL treatment (figures 4.19 & 4.20), resulted in a 17-fold induction at 10µg/ml and 36-fold induction at 50µg/ml. LPS treatment (figures 4.21 & 4.22) showed similar levels of activation of the IRF3-vLuc TFAR, between 16- and 27-fold induction, indicating that this probably does represent the highest level of activity achievable for induction of IRF3 activity and the maximum value to benchmark test compounds against.

Finally, we integrated previously established TFARs, NFκB-vLuc and AP1-vLuc into our HCAECPro cells and quantified their induction through TNFα activation

using the same dilution of luciferase reagents. The tumour necrosis factor (TNF) pathway plays a vital role in various physiological processes such as proliferation, differentiation, apoptosis and the modulation of immune responses and inflammation induction (Waters, Pober and Bradley, 2013). TNFα acts by binding to its receptors TNFR1 and TNFR2, which results in the recruitment of signal transducers activating three effectors. Through these complex signalling cascades and networks, it results in the activation of Caspases and two transcription factors; Activation Protein-1 (AP1) and Nuclear Factor-KappaB (NFκB) (Pires *et al.*, 2018) (Westwick *et al.*, 1994) (Kyriakis, 1999). We stimulated the NFκB-vLuc reporter with TNFα at concentrations ranging from 0.1ng/mL to 5ng/mL (figures 4.23 & 4.24), which resulted in a maximal induction of 10.8-fold compared to vehicle control and a fold induction of 9.2-fold at the lowest concentration of 01.ng/ml. AP1 activation via TNFα stimulation yielded similar results, with a maximal induction of 8.2-fold, however yielded a more diminished activation at the lowest concentration of 0.1ng/ml TNFα with a 4.2-fold induction.

On balance, our data suggests that by altering the spacing of the transcription factor binding motif, we have increased the dynamic range of TFARs. Indeed, when compared to existing TFARs based on the same vector backbone, (NFκB and AP1 TFARs), the dynamic ranges of between 36-fold (IRF3-vLuc TFAR) and 3310-fold induction (KLF2-nLuc TFAR), compare favourably with the maximal induction of 10.2-fold (NFκB-VLuc TFAR) under static cell culture.

We demonstrated in chapter 3 that our HCAECPro cell line retained mechanosensitivity, upregulating KLF2 and Nrf2-responsive genes in response to culture in OSS and LSS to a similar magnitude to p3 primary human coronary artery endothelial cells. Endothelial behaviour is profoundly affected by the

haemodynamic environment in which they exist. It is therefore important to quantify disease-related changes in TF activity under flow conditions that affect atherosclerosis. The phenotype adopted by ECs in LSS or OSS may also change the response to any test compound being used within the E-Sense system, so we quantified a single concentration of agonist that resulted in maximal, or near-maximal activation of each TFAR, to examine the ability of the three E-Sense lines to respond to agonist treatment while cultured under OSS or LSS (Table 4.1). By incorporating two distinct reporters into one cell line, we increase the throughput of the system, reducing both running and consumable costs as well as the time to perform experiments. For ease, we nominated these E-Sense Green (NRF2-nLuc/NFκB-vLuc), E-Sense Red (KLF2-nLuc/AP1-vLuc) and E-Sense Yellow (XBP1-nLuc/IRF3-vLuc).

As previously discussed in chapter 1, the activity NRF2 and NFκB have been demonstrated to be directly modulated by laminar and oscillatory shear stress (Simmons, Kumar and Jo, 2016). In line with the literature, the data presented here demonstrates that NRF2 activity is significantly upregulated under LSS compared to OSS. We flowed our E-Sense green line for 72h under LSS and OSS, with NRF2 under LSS exhibiting a 4828-fold induction observed (LSS) compared to 695-fold (OSS) ($p<0.0001$) (figures 4.27 & 4.28). NRF2 TFAR activity increased further by 10% ($p<0.05$) with the addition of Sulforaphane (50μM) under LSS and 41% under OSS ($p<0.01$). Interestingly, the addition of TNFα (2ng/mL) relaying a 37% reduction in Nrf2 TFAR activity compared to LSS ($p<0.0001$) (figure 4.27). Whilst the ability for Nrf2-depnedent gene expression to inhibit proinflammatory gene expression in ECs is well documented, the demonstration that inflammation inhibits Nrf2 activity has not previously been described (Teasdale *et al.*, 2017). Concurrent with this, E-Sense Green reports on NFκB activation. NFκB activity is reduced, both at the end of the adaptation

period and also at 72 hours, when cultured under LSS compared to OSS, with a 6.6-fold induction under LSS and 16.3-fold induction under OSS ($p<0.0001$) (figure 4.30 & 4.31). The stimulation using TNFα (2ng/mL) significantly increased NFκB under both LSS and OSS, resulting in a 3.48-fold ($p<0.0001$) and 4.99-fold ($p<0.0001$) increase compared to LSS respectively. Aligning with previous work from the White Lab (Teasdale *et al.*, 2017) (a diminished activation of the NFκB TFAR was observed under LSS and OSS when treated with Sulforaphane (50nM), highlighted above to activate Nrf2.

Analysing the data from E-Sense Red, we observed the expected greater activation of KLF2 under LSS for 72hr compared to OSS (950 v 226-fold, 67% reduction $P<0.0001$, figures 4.33 & 4.34). Stimulation with Atorvastatin (1μM) resulted in a 24% increase in KLF2 TFAR activation ($p<0.01$), however interestingly no significant change in KLF2 TFAR activity was observed under OSS. This suggests that the protective signalling downstream of statin-induced KLF2 activation would not ameliorate disease processes at sites vulnerable to plaque formation. Addition of TNFα under LSS reduced KLF2 TFAR activity by 54% ($p<0.0001$), however did not have any significant effect on the lower level of KLF2 TFAR activity observed in OSS (figure 4.34). Under OSS and LSS, we see significant alterations in the transcriptional activity of AP1, with a 8.4-fold induction observed under LSS and a 14.9-fold induction observed under OSS (figures 4.36 & 4.37). This induction of AP1 is significantly exacerbated under OSS with the addition of TNFα (figure 4.36), using AP1 LSS as the baseline we see a 315% increase in AP1 TFAR activity under OSS
+ TNFα ($p<0.0001$).

The data generated by E-Sense Yellow (XBP1-nLuc/IRF3-vLuc) demonstrates that both stress pathways are mechanosensitively regulated. While XBP1 activity

was not significantly elevated in OSS compared to LSS (p=0.054), once stimulated with either Thapsigargin or LPS, the response was significantly greater under OSS compared to LSS (figures 4.39 & 4.40) indicating that unfolded protein response signalling is likely increased at atheroprone sites. The enhanced response to agonists under OSS highlights the need to test endothelial response to novel compounds under different flow environments as the response to compound treatment may vary dependent on the different phenotypes adopted in response to flow. IRF3 activity was significantly increased in OSS compared to LSS, in the absence of exogenous agonists. At 72 hours, vLuc activity was 229% greater in OSS compared to LSS ($p<0.01$) (figure 4.44). Treatment with LPS increased IRF3 activity by 329% under LSS compared to LSS ($p<0.0001$), whilst OSS + LPS resulted in 830% increase in IRF3 activity compared to OSS ($p<0.0001$) (figure 4.4), again highlighting that the haemodynamic environment effects the endothelial response to dysfunctional stimuli. Stimulation with Thapsigargin did not produce any significant modulation of IRF3 activity.

4.6 Summary

Key Findings of the E-Sense System:

- The large dynamic range of the TFARs allow quantification of pathway activity in both static and under flowed culture
- Quantification of TFAR activity in OSS and LSS highlights flow-specific modulation of signalling activity
- Very low variability was observed between biological repeats of experiments

All TFs quantified showed some degree of mechanosensitive regulation

-

Known agonists were used to provide a benchmark for testing novel compounds

-

- We identified a novel suppression of Nrf2 activity by TNFα treatment.

Statin treatment increased KLF2 activation in LSS but not OSS

-

Conclusion

The data presented in this chapter details the creation of novel TFARs which demonstrate very high dynamic ranges, allowing sensitive quantification of TF activity. Integration of pairs of TFARs expressing either a NLuc or VLuc into HCAECPro allowed the creation of three E-Sense lines, which were assessed in both static and under physiological laminar and oscillatory flow environments conforming to atheroprotected 'straight' sections of coronary arteries (LSS) and sites of disturbed flow (OSS) predilected to develop atherosclerosis. This provides a secure foundation for the prediction of the pro- or anti-atherogenic effects of novel test compounds, with unknown effects on atherogenesis. The high sensitivity and reproducibility of TFAR quantification enables even small changes in TF activity to be quantified, which would be extremely hard, or impossible to quantify in preclinical animal models of atherosclerosis. Even small changes in TF activity may affect atherosclerotic plaque development in humans over the ~40+ year time course of plaque development, highlighting the utility of this system in capturing effects that may be relevant to human disease.

Chapter 5

Investigating the effect of microplastics on pathways known to regulate atherosclerosis

5.0 Introduction

The use of synthetic plastics has become ubiquitous in society since their invention in the early twentieth century, they represent a cost-efficient, versatile and readily- available resource that have become a mainstay in almost every aspect of human life. In the last few decades their effect on human health has become a cause for concern with ongoing research onto long term effects currently in its infancy. As with many facets of human invention, the effects of prolonged and increased use of these plastics may not become apparent for several decades due to the nature of human physiology.

One such plastic polymer that has become ever more widespread is the use of Bisphenol A (BPA), a monomer used in the production of polycarbonates, which accounts for around 70% of all BPA use (Sasso *et al.*, 2020). What makes BPA so prevalent is its versatility and unique combination of properties, including clarity, durability, heat and shatter resistance. These properties have resulted in widespread use, in everything from drinking bottles to medical equipment. Around 30% of all BPA use can be attributed to epoxy resin, this is of particular importance as these resins are used extensively in consumer-based products such as food containers, plastic bag manufacturing and even as a protective lining for aluminium food and drink cans (Thoene *et al.*, 2020). This factor has become a cause for concern, as studies have demonstrated BPA is able to leach into food and drink over a prolonged period of time, this is especially seen when BPA containers are exposed to heat, which may be accelerated in export and import of goods to and from countries with warmer climates (Nanjappa, Simon and Akingbemi, 2012). The widespread use of this particular plastic means that the majority of the population are continuously and increasingly exposed to BPA, with the production of the polycarbonate estimated to be 5-6 billion pounds, 2.3 billion in the US alone with

production ever increasing (Gerona *et al.*, 2016).

5.1 Monitoring the effect of Bisphenol A (BPA) on the protective signalling pathways

Previous results in chapter 4 demonstrate the novel TFARs within HCAECPro enable very sensitive quantification of TF activity. A dose-response study was performed in static culture to determine the biologically significant concentration of BPA and inform further experiments under flowed conditions. *In vivo* models, which have tested the effects of BPA exposure have discerned doses >1000ppm produce adverse effects on rats. Human exposure in urinary analysis studies were exposed to doses >100ug/kg (>100ppm) with excretion in urine noted to be as high as ~10ppm (Sasso *et al.*, 2020). TFAR activity was quantified to a range of doses (10ppm, 25ppm, 50ppm, 100ppm and 150ppm) for 24 hours in static culture (Hengstler *et al.*, 2011)

We demonstrated that the NRF2-nLuc TFAR increased in activity 2720-fold when treated with 20% CSE and 495-fold when treated with 50µM Sulforaphane in E-Sense Green. 24-hour BPA treatment at 10ppm increased Nrf2-nLuc TFAR activity by 42.5-fold compared to untreated E-Sense Green ($p<0.0001$) (fig 5.1 & 5.2). This represents a 1.56% activation compared to 20% CSE and 8.6% of the activity induced by 50µM sulforaphane. This increased to 51.4-fold with 25ppm BPA (fig 5.1, $p<0.001$ compared to untreated E-Sense Green) equivalent to a 10.4% of the maximal induction via Sulforaphane treatment. Interestingly, higher concentrations of BPA reduced the activation of Nrf2 TFAR. The acceptable level of BPA exposure has been estimated to be around 4µg/kg in humans, equivalent to 3-4 parts per million (ppm- the number of units of mass of BPA per million units of total mass e.g., 1mg/L) per day by the European Food Safety Authority. These figures are based on studies performed in 2008 Studies in the US by the National Health and Nutrition Examination Survey (NHANES) had shown that the mean concentration of BPA levels in human urine was 1.2ng/ml (Lang *et al.*, 2008). However, a study published in December 2019 by Gerona et al. measured the

geometric mean concentration in urine was 51.99ng/mL. This represents measurable concentrations of BPA circulating within the human body, 44 times higher than previously published (Gerona, vom Saal and Hunt, 2020).

The effects of Bisphenol A on the cardiovascular system are still poorly understood, with previous studies mainly focussing on the effect of BPA on the endocrine and neurological systems. The effect of BPA on the human endocrine system has been reported since the early 20th century. First synthesised in 1891, BPA was investigated as a synthetic oestrogen for potential commercial use in the 1930's (Jalal *et al.*, 2018). For this reason, it's not surprising that high levels of BPA exposure have been linked with an incidence of endocrine related abnormalities. Indeed, BPA exposure has been linked to an increase in miscarriages and increased number of premature births (Namat *et al.*, 2021). An increase in BPA levels was correlated with a decrease in peak oestradiol and reduction in oocyte retrieval numbers. The effects on the endocrine and reproductive system have not only shown to affect women; in men, elevated BPA concentrations in urine correlates with reduced sperm quality and increased sperm DNA damage (Wisniewski *et al.*, 2015). The effects of BPA during pregnancy have been associated with a variety of neurological and behavioural problems in children. High levels of BPA exposure is thought to disrupt hormone function in significant periods of prenatal development, thus inciting possible sex-specific and hormonally regulated behaviours. Mechanistically, BPA exposure during pregnancy leads to a reduction in total

thyroxine (T4) in pregnant women and a decrease in thyroid stimulating hormone in male neonates, thus suggesting that disruption of the maternal thyroid or gonadal hormones, imperative in normal foetal development may be due to BPA exposure and its effects. (Fouyet *et al.*, 2021)(Namat *et al.*, 2021)

In the current literature, there is evidence to suggest that high exposure to BPA is associated with the development of cardiovascular disease, however, the mechanisms by which this occurs has not been defined. In recent years the effects of pollutants, mainly those released into the air, heavy metals and organic pollutants have become a major area of cardiovascular research (Ohore and Songhe, 2019). However, BPA was not thought to persist in the body. Previously, it was speculated that the compound being metabolised in the liver and intestines before excretion through bile or urine, resulted in less influence on cardiovascular health (Genuis *et al.*, 2012). New evidence demonstrates that BPA and its metabolites concentrate in lipid-rich tissues due to its lipophilic trait and frequent human exposure (Li *et al.*, 2020). Experimental analysis determined that the metabolism of BPA induced oxidative stress in rat hepatocytes following 30-day oral exposure. More recently, BPA metabolite research suggests the half-life to be significantly greater than the 6 hours previously thought (Li *et al.*, 2020). The longer half-life and possibility of concentration of BPA and its metabolites to lipid-rich regions and tissues makes it plausible that long-term exposure could contribute to atherosclerosis. At sites predilected for atherosclerosis correlate with sites of disturbed flow, it is important to assess the effects of BPA on endothelial pathways that regulate atherosclerosis to determine if BPA may contribute to plaque formation in both OSS and LSS flow environments. This will add important information on the potential for BPA to increase pathological mechanisms related to plaque formation and also identify a concentration threshold that might inform a ‘safe exposure limit’ for BPA.

Aims and objectives:

Aim: Use the E-Sense platform to assess if BPA regulates pathways known to affect atherosclerosis

This will be addressed in the following objectives:

- Use the three E-Sense lines to determine the concertation of BPA that is biologically significant in endothelial cells, to predict a 'safe exposure limit'.
- Use the E-sense system to examine the regulation of transcriptional programmes known to regulate atherosclerosis to determine if there is a signature that highlights potential cardiovascular risk by BPA.
- Perform this analysis in both athero-protective (LSS) and atheroprone (OSS) flow environments to examine any differential effects of BPA under physiological flow.

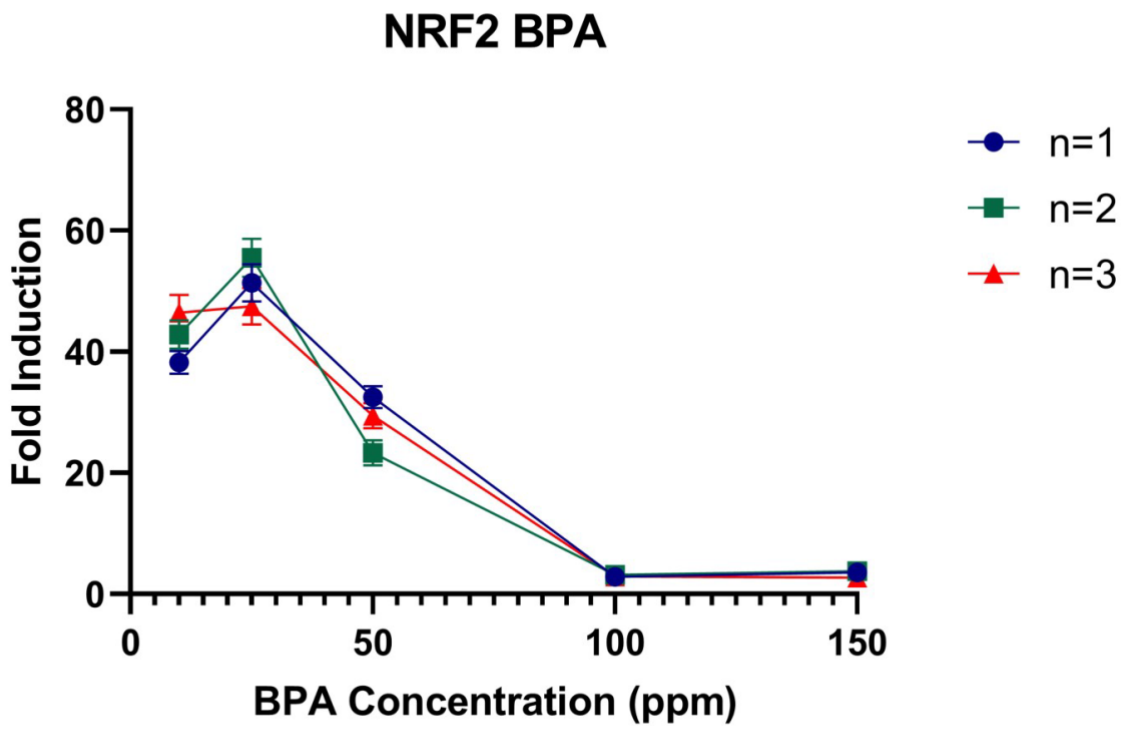

Figure 5.1 Dose Response of BPA on Nrf2-nLuc in Static Culture.

HCAECPro Cells containing Nrf2-NLuc reporter were cultured in 48-well plates and stimulated with BPA at a concentration of 10ppm, 25ppm, 50ppm, 100ppm and 150ppm for 24 hours in triplicate for technical repeat in Promocell MV2 endothelial cell media. Luciferase containing media was incubated at room temperature for 5 mins before luminescence was measured using Promega GloMax Explorer plate reader using luciferase assay pre-set settings. Dose response curve is representative of n=3 and 3 technical repeats.

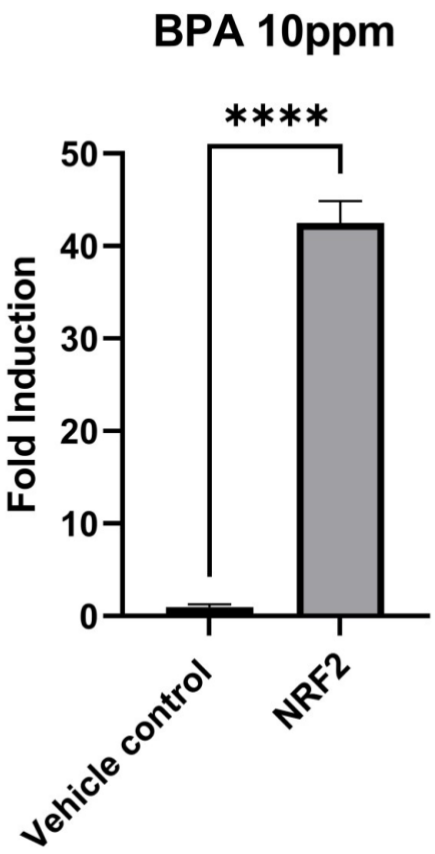

Figure 5.2 Response of NRF2-nLuc reporter in response to 10ppm BPA in static culture.

HCAECPro Cells containing Nrf2-NLuc reporter were cultured in 48-well plates and were stimulated with BPA at a concentration of 10ppm for 24 hours in triplicate for technical repeat in Promocell MV2 endothelial cell media. Following stimulation, media was collected. Media and luciferase reaction was incubated at room temperature for 5 mins before luminescence and was measured using Promega GloMax Explorer plate reader using luciferase assay pre set settings. n=3, T-test. *p= <0.05, **p<0.01, ***p<0.001, ±SEM

Using E-Sense Red, we previously demonstrated that the KLF2 TFAR increases activity by 3310-fold with KLF2 overexpression and 387-fold with 1µM Atorvastatin treatment. 10ppm BPA treatment induced KLF2 TFAR activity by 33.2-fold, ($p<0.01$ compared to vehicle-treated E-Sense Red, fig 5.3 & 5.4). This represents a 1.0% increase in TFAR activity compared to KLF overexpression and 8.8% of the effect induced by 1µM Atorvastatin treatment. Like Nrf2 TFAR activity, this non-significantly increased to 35.4-fold induction at 25 ppm, after which the KLF2 TFAR activity reduced (fig 5.3).

These results are indicative of a small ~1-2% activation of both protective signalling pathways, NRF2 and KLF2, at 10ppm BPA treatment. This demonstrates that 10ppm represents a biologically 'sensitive' dose of BPA and highlights the exquisite sensitivity of the E-sense system to measure even very small changes in TF activity. Nrf2 and KLF2 activation was lost at higher BPA concentrations.

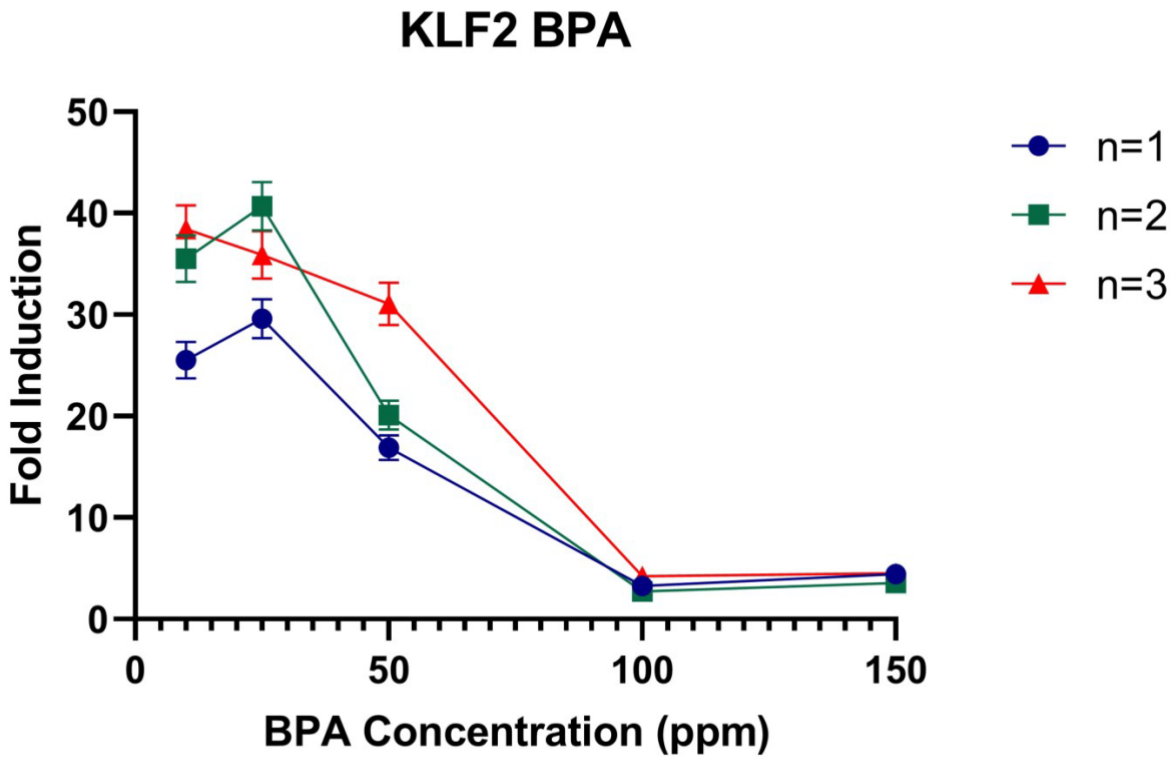

Figure 5.3 Dose Response of BPA on KLF2-nLuc in Static Culture.

HCAECPro Cells containing KLF2-NLuc reporter were cultured in 48-well plates and stimulated with BPA at a concentration of 10ppm, 25ppm, 50ppm, 100ppm and 150ppm for 24 hours in triplicate for technical repeat in Promocell MV2 endothelial cell media. Luciferase containing media was incubated at room temperature for 5 mins before luminescence was measured using Promega GloMax Explorer plate reader using luciferase assay pre-set settings. Dose response curve is representative of n=3 and 3 technical repeats.

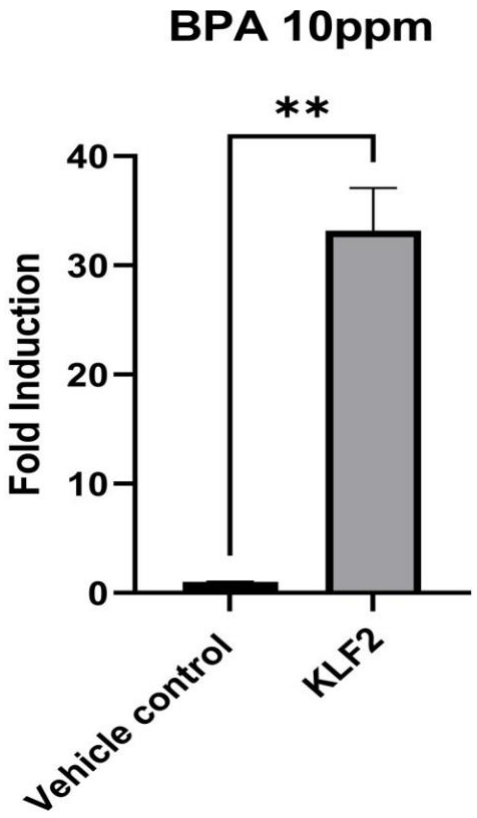

Figure 5.4 Response of KLF2-NLuc reporter in response to 10ppm BPA in static culture.

HCAECPro cells containing KLF2-NLuc reporter were cultured in 48-well plates and stimulated with BPA at a concentration of 10ppm for 24 hours in triplicate for technical repeat in Promocell MV2 endothelial cell media. Luciferase containing media was incubated at room temperature for 5 mins before luminescence was measured using Promega GloMax Explorer plate reader using luciferase assay pre-set settings. n=3 and 3 technical repeats. T-test. *p= <0.05, **p<0.01, ***p<0.001, ±SEM

5.2 Monitoring the effect of Bisphenol A (BPA) on the TLR/IRF3 signalling axes and unfolded protein response & ER Stress

Treatment of E-Sense Yellow with 50µg/mL Ox-LDL resulted in a 35.8-fold induction of the IRF3 TFAR. Treatment of E-Sense Yellow with 10ppm resulted in a 7.02-fold induction of TFAR activity (fig 5.5 & 5.6, $p<0.0001$, compared to vehicle control), representing 20% of the activity induced by 50µg/mL Ox-LDL. Induction of IRF3 activity remained between 5-7-fold above the vehicle control with increasing concentrations of BPA to 150ppm.

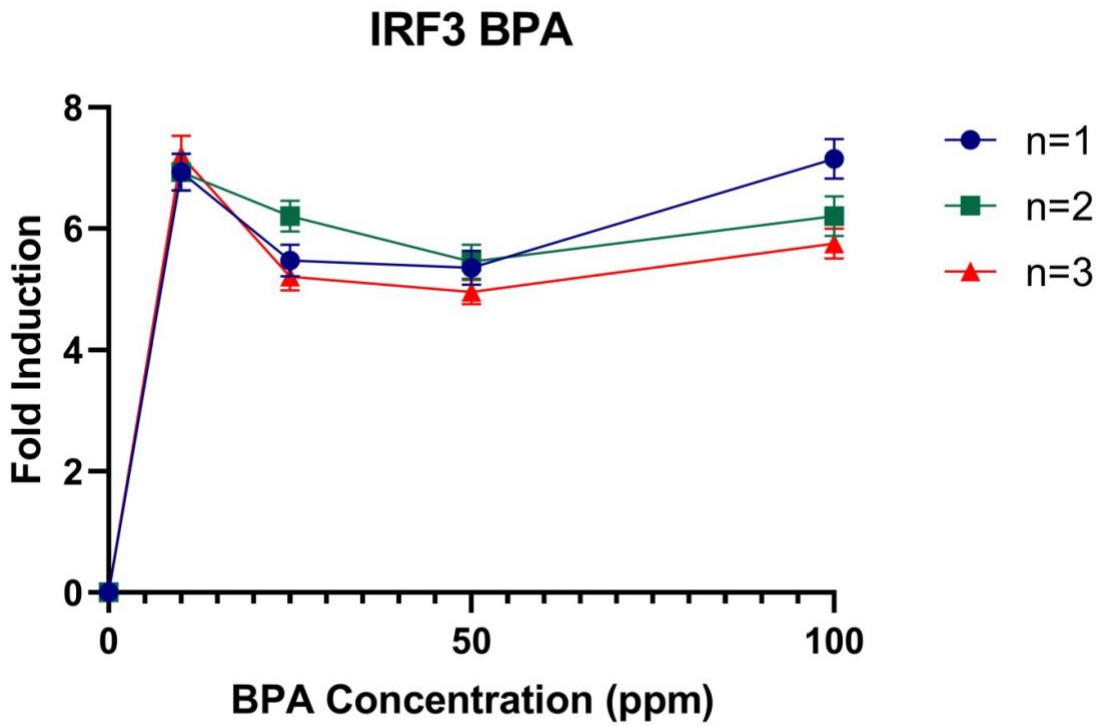

Figure 5.5 Dose Response of BPA on IRF3-vLuc in Static Culture.

HCAECPro Cells containing IRF3-vLuc reporter reporter were cultured in 48-well plates and stimulated with BPA at a concentration of 10ppm, 25ppm, 50ppm, 100ppm and 150ppm for 24 hours in triplicate for technical repeat in Promocell MV2 endothelial cell media. Luciferase containing media was incubated at room temperature for 5 mins before luminescence was measured using Promega GloMax Explorer plate reader using luciferase assay pre-set settings. Dose response curve is representative of n=3 and 3 technical repeats.

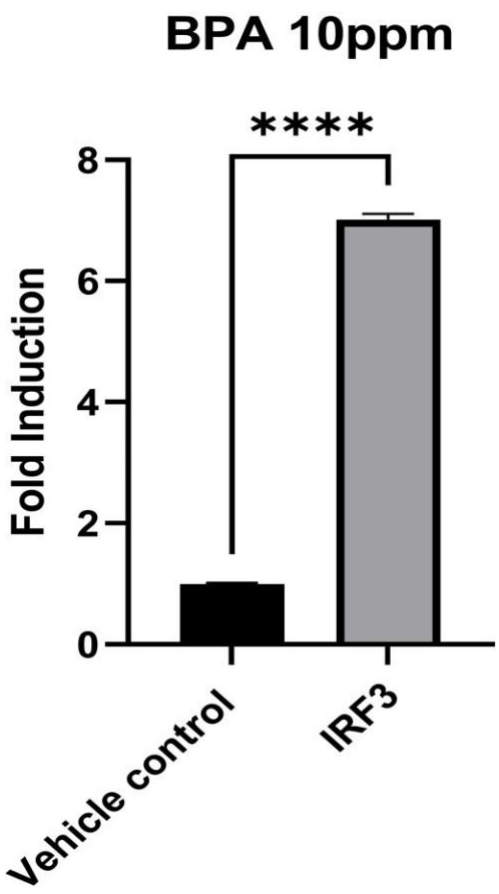

Figure 5.6 Response of IRF3-vLuc reporter in response to 10ppm BPA in static culture.

HCAECPro Cells containing IRF3-VLuc reporter were cultured in 48-well plates and stimulated with BPA at a concentration of 10ppm for 24 hours in triplicate for technical repeat in Promocell MV2 endothelial cell media. Luciferase containing media was incubated at room temperature for 5 mins before luminescence was measured using Promega GloMax Explorer plate reader using luciferase assay pre-set settings. n=3, T-test. *p= <0.05, **p<0.01, ***p<0.001, ±SEM

In addition, E-Sense Yellow quantified the activity of the XBP1 TFAR. Treatment with 50nM Thapsigargin resulted in a 515-fold induction of XBP1 TFAR activity, while treatment with 10ppm BPA resulted in a 23.7-fold induction of the XBP1 TFAR ($p<0.0001$ compared to vehicle control fig 5.7 & 5.8). This represents 4.4% of the activity induced by 50nM Thapsigargin. Unexpectedly, the XBP1 TFAR activity reduced with increasing BPA concentration.

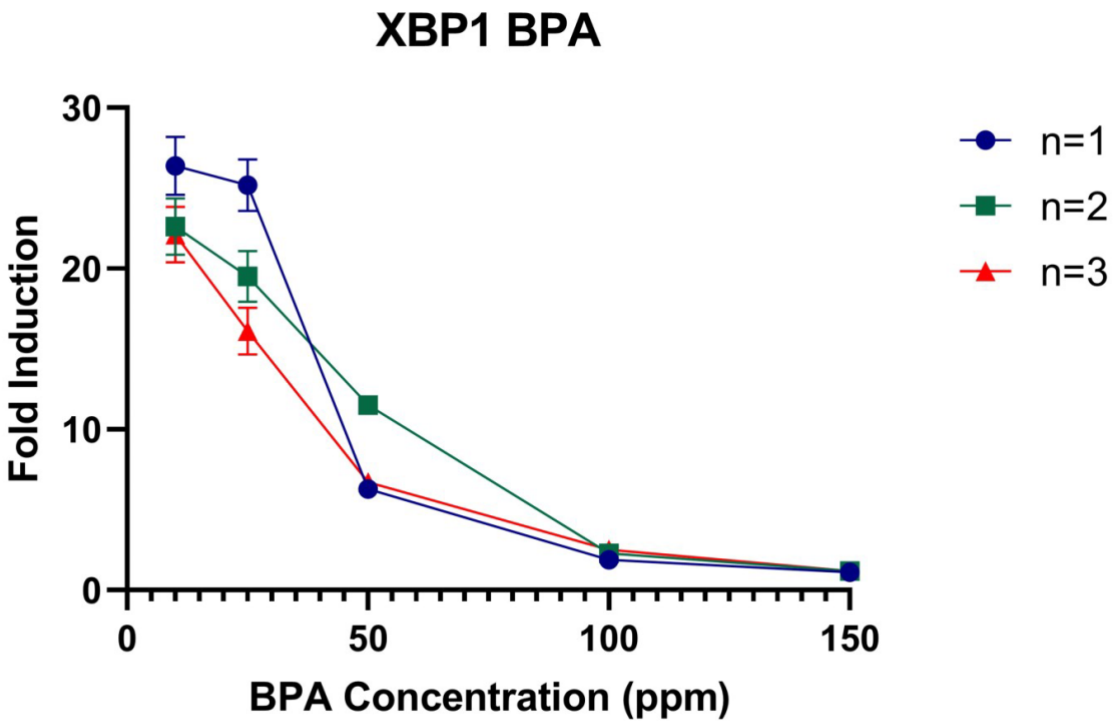

Figure 5.7 Dose Response of BPA on XBP1-nLuc in Static Culture.

HCAECPro Cells containing XBP1-NLuc reporter were cultured in 48-well plates and stimulated with BPA at a concentration of 10ppm, 25ppm, 50ppm, 100ppm and 150ppm for 24 hours in triplicate for technical repeat in Promocell MV2 endothelial cell media. Luciferase containing media was incubated at room temperature for 5 mins before luminescence was measured using Promega GloMax Explorer plate reader using luciferase assay pre-set settings. Dose response curve is representative of n=3 and 3 technical repeats.

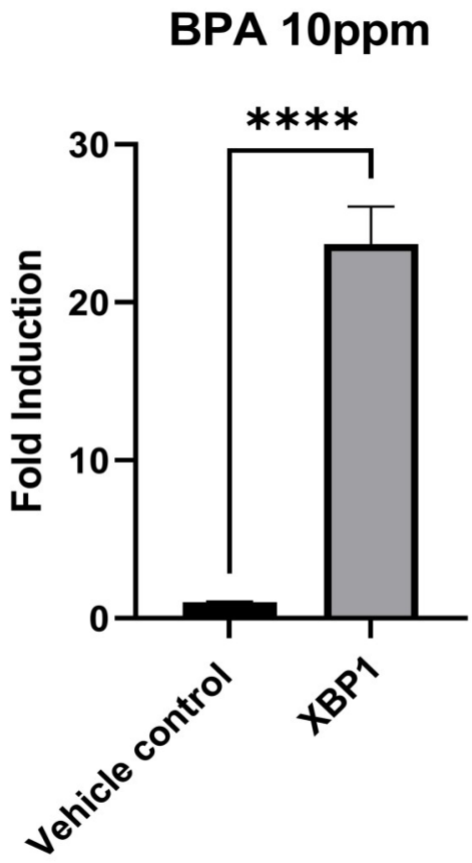

Figure 5.8 Response of XBP1-NLuc reporter in response to 10ppm BPA in static culture.

HCAECPro Cells containing XBP1-NLuc reporter were cultured in 48-well plates and stimulated with BPA at a concentration of 10ppm for 24 hours in triplicate for technical repeat in Promocell MV2 endothelial cell media. Luciferase containing media was incubated at room temperature for 5 mins before luminescence was measured using Promega GloMax Explorer plate reader using luciferase assay pre-set settings. n=3, T-test. *p= <0.05, **p<0.01, ***p<0.001, ±SEM

5.3 Monitoring the effect of Bisphenol A (BPA) on the Pro-Inflammatory Pathways

Treatment of E-Sense Green and E-Sense Red with 2ng/ml TNFα increased both the NFκB and AP1 TFAR activity, 10.8-fold and 8.2-fold respectively. BPA treatment increased both NFκB and AP1 TFAR activity by 1.3-fold, (fig 5.8 & 5.10, $p<0.05$ compared to vehicle control). NFκB TFAR activation peaks at 25ppm at 1.54-fold induction, while AP1 TFAR activity remains constant at ~1.3-fold above vehicle control (fig 5.9 & 5.11). The increase in NFκB TFAR activity relates to 3.1% at 10ppm and 5.5% at 25ppm BPA of the maximum NFκB activity at 2ng/ml TNFα. Similarly, treatment with 10 or 25 ppm BPA induced a 4.2% or 4.5% increase in the AP1 TFAR compared to the value induced by 2ng/ml TNFα. While the magnitude of these result could be increased by using more concentrated luciferase reagents, it should not affect the relative activation of either TFAR compared to the 2ng/ml TNFα positive control.

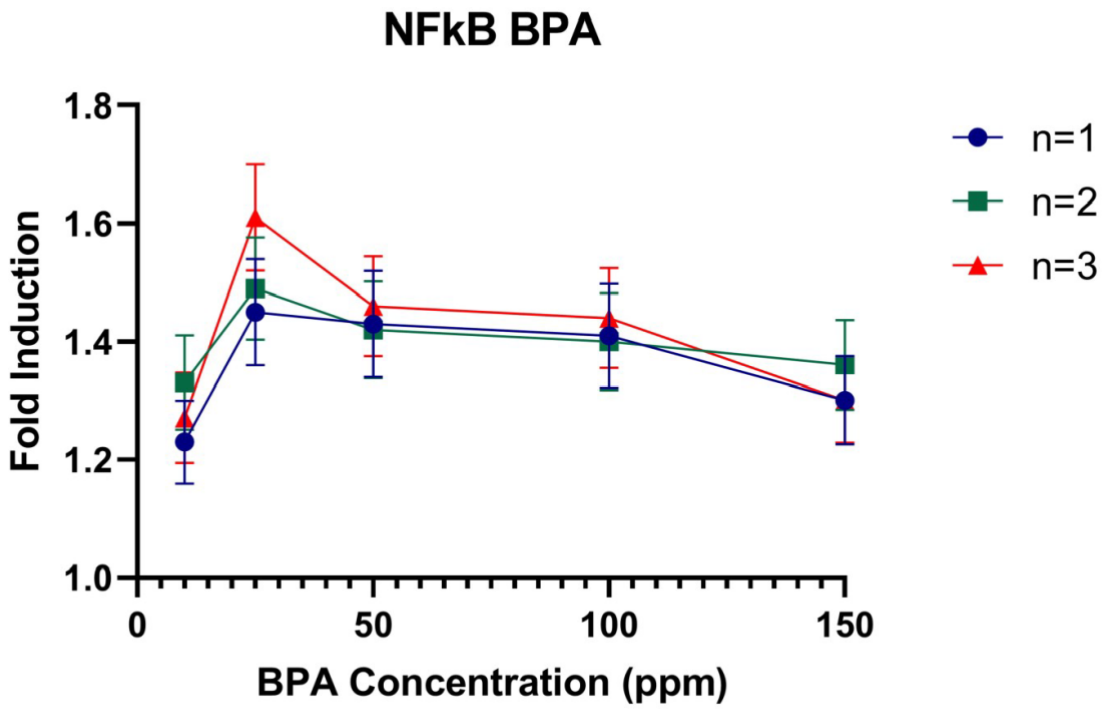

Figure 5.9 Dose Response of BPA on NFkB-vLuc in Static Culture.

HCAECPro Cells containing NFkB-VLuc reporter were cultured in 48-well plates and stimulated with BPA at a concentration of 10ppm, 25ppm, 50ppm, 100ppm and 150ppm for 24 hours in triplicate for technical repeat in Promocell MV2 endothelial cell media. Luciferase containing media was incubated at room temperature for 5 mins before luminescence was measured using Promega GloMax Explorer plate reader using luciferase assay pre-set settings. Dose response curve is representative of n=3 and 3 technical repeats.

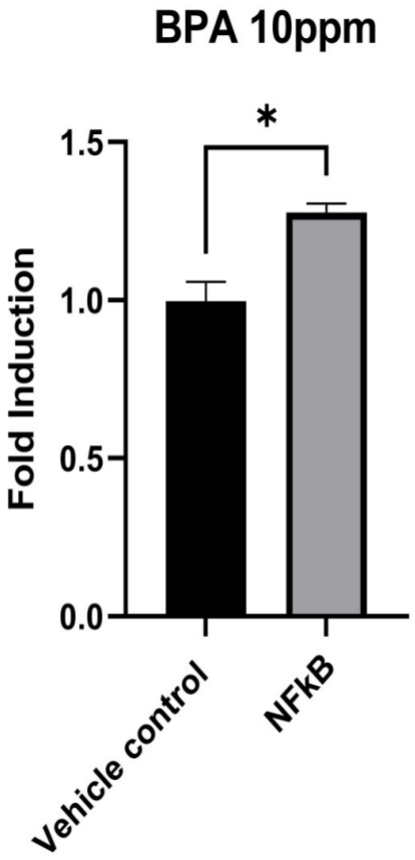

Figure 5.10 Response of NFkB-VLuc reporter in response to 10ppm BPA in static culture.

HCAECPro Cells containing NFkB-VLuc reporter were cultured in 48-well plates and stimulated with BPA at a concentration of 10ppm for 24 hours in triplicate for technical repeat in Promocell MV2 endothelial cell media. Luciferase containing media was incubated at room temperature for 5 mins before luminescence was measured using Promega GloMax Explorer plate reader using luciferase assay pre-set settings. n=3, T-test. *p= <0.05, **p<0.01, ***p<0.001, ±SEM

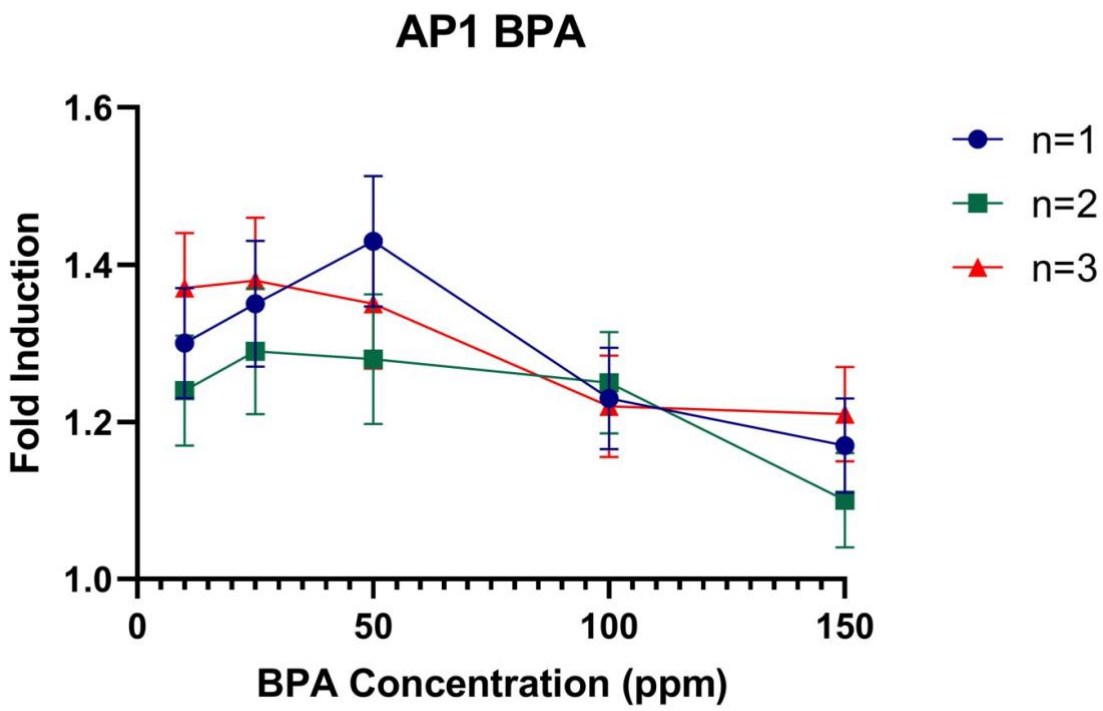

Figure 5.11 Dose Response of BPA on AP1-vLuc in Static Culture.

HCAECPro Cells containing AP1-vLuc reporter were cultured in 48-well plates and stimulated with BPA at a concentration of 10ppm, 25ppm, 50ppm, 100ppm and 150ppm for 24 hours in triplicate for technical repeat in Promocell MV2 endothelial cell media. Luciferase containing media was incubated at room temperature for 5 mins before luminescence was measured using Promega GloMax Explorer plate reader using luciferase assay pre-set settings. Dose response curve is representative of n=3 and 3 technical repeats.

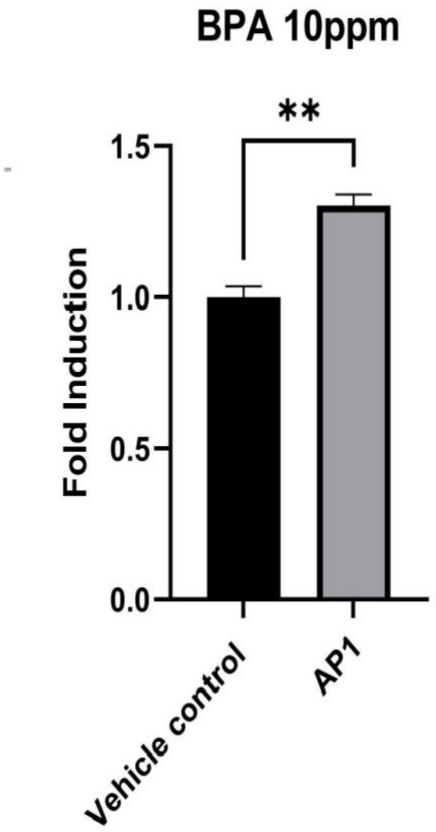

Figure 5.12 Response of AP1-vLuc reporter in response to 10ppm BPA in static culture.

HCAECPro Cells containing AP1-vLuc were cultured in 48-well plates and stimulated with BPA at a concentration of 10ppm for 24 hours in triplicate for technical repeat in Promocell MV2 endothelial cell media. Luciferase containing media was incubated at room temperature for 5 mins before luminescence was measured using Promega GloMax Explorer plate reader using luciferase assay pre-set settings. n=3, T-test. *p= <0.05, **p<0.01, ***p<0.001, ±SEM

Table 5.1 below summarises the effect of BPA on the activity on the repertoire of TFARs contained within the E-Sense lines. These are presented as a % activation of the known TFAR activators described in Chapter 4. In summary, the data presented here demonstrate the high sensitivity of the TFARs used in the E-sense system to quantify even very small changes in TF activation in response to BPA treatment. The ability to measure significant differences as low as 1% maximal activity change is almost impossible to achieve bay any other analytical method that uses a biological system for readout, for example a 1% change could not be quantified by qPCR or Western blotting, but is easily quantified ($P<0.001$) using the KLF2 TFAR. This allows quantification to a level that is probably not biologically significant, even in a disease course that takes 30-50 years.

Table 5.1: Activity of TFARs observed at 10ppm and 25ppm as a % of the induction of TFAR activity by known TFAR agonists.

TFAR	Induction 10ppm	Induction 25ppm	Agonist comparison
NRF2	1.6%	1.9%	20% CSE
KLF2	1.0%	3.2%	KLF2 overexpression
IRF3	17.3%	13.3%	50µg/ml Ox-LDL
XBP1	4.6%	3.9%	50nM Thapsigargin
NFkB	2.8%	5.3%	2ng/ml TNFa
AP1	4.2%	4.7	2ng/ml TNFa

5.4 Monitoring the effect of BPA on E-Sense Green cell line under oscillatory shear stress and laminar shear stress

Treatment of **E-Sense Green** with 10ppm BPA identified a much greater effect of BPA treatment under flowed culture, compared to static treatment. The most significant effect of BPA treatment was the downregulation of Nrf2 activity under LSS. As seen in Ch 4, LSS resulted in a ~7-fold increase in Nrf2 TFAR activity from 4828-fold activity compared to 695-fold under OSS, relative to a static control (Fig 5.13 $P<0.0001$). Sulforaphane treatment modestly increased Nrf2 TFAR activity under both flowed conditions ($P<0.05$) and TNFα treatment significantly suppressed Nrf2 TFAR activity under OSS ($p<0.05$) but not LSS. 10ppm BPA increased activity of the Nrf2 TFAR by 233% under OSS ($p<0.0001$, fig 5.13). This represents a 63% increase of TFAR activity ($p<0.0001$) compared to a known Nrf2 activator. By contrast Nrf2 TFAR activity was suppressed under LSS resulting in a 89% reduction ($p<0.0001$), which was even lower than the level observed under OSS with BPA treatment (OSS=322% increase Figure 5.13, $p<0.001$ OSS+BPA v LSS+BPA).

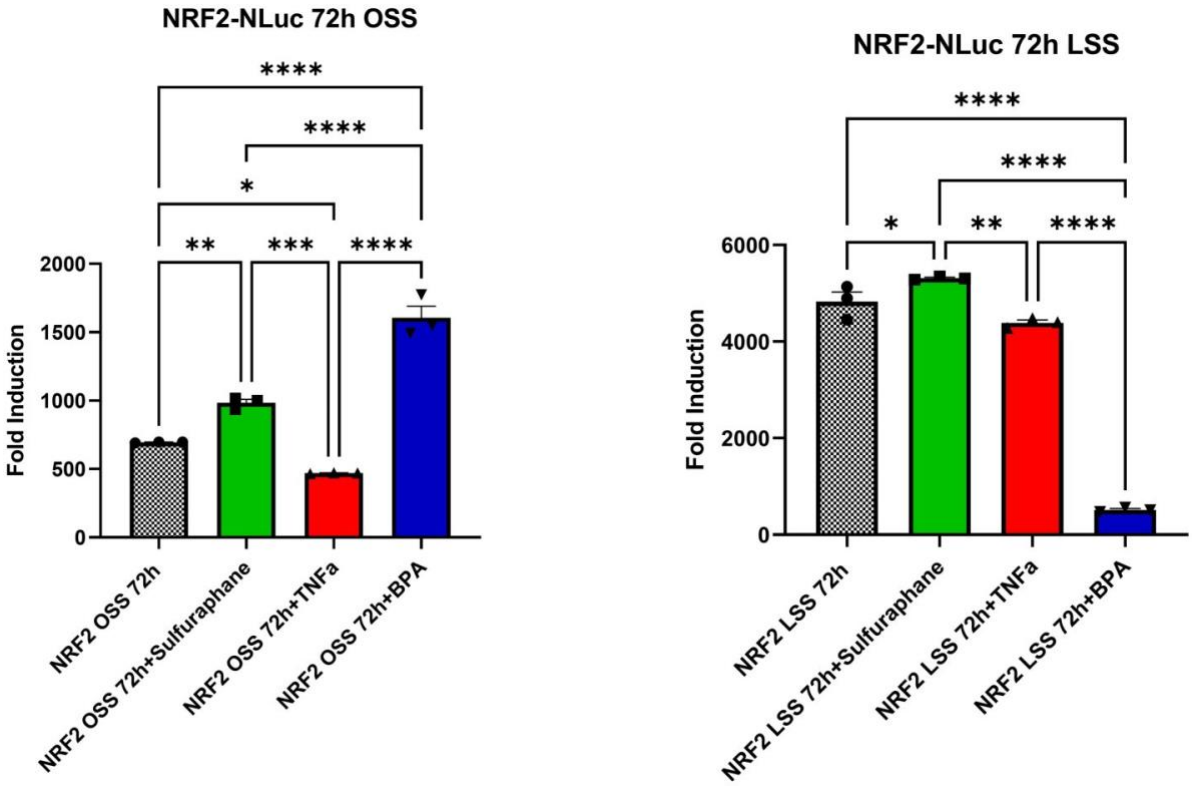

Figure 5.13 Comparison of Induction of NRF2-nLuc Under OSS Stimulated with BPA vs Induction under Normal OSS and OSS with Agonists

HCAECPro cells containing NRF2-nLuc/NFkB-vLuc reporters were cultured under physiological laminar shear stress (LSS, 1.5Pa) and oscillatory shear stress (OSS, ±0.5Pa 1Hz), in flow media containing BPA at a concentration of 10ppm, Sulforaphane (50µM), TNFα (2ng/mL) and nothing added. HCAECPro cells containing NRF2- nLuc/NFkB-vLuc reporter were flowed in triplicate for technical repeat. . Luciferase containing media was incubated at room temperature for 5 mins before luminescence was measured using Promega GloMax Explorer plate reader using luciferase assay pre set settings. n=3, ANOVA. *p= <0.05, **p<0.01, ***p<0.001, ±SEM.

Concomitant with this, quantification of the NFκB TFAR demonstrated an increase in NFκB activity by BPA under LSS, but not OSS (fig 5.14). As seen in Ch 4, culture under OSS resulted to a 214% elevation of NFκB activity under OSS compared to LSS (Figure 5.14, $p<0.01$), with a significant reduction in NFκB TFAR activity by sulforaphane treatment under OSS ($p<0.001$) and an increase in TFAR activity with TNFα treatment. By comparison, BPA did not increase NFκB TFAR activity under OSS, but significantly increased TFAR activity in LSS (240% LSS activity, Figure 5.14, $p<0.05$). Taken together, BPA treatment of E-Sense Green showed that 10ppm BPA increases Nrf2 TFAR activity under OSS, while under LSS, 10ppm BPA dramatically reduces Nrf2 TFAR activity while increasing NFκB activity.

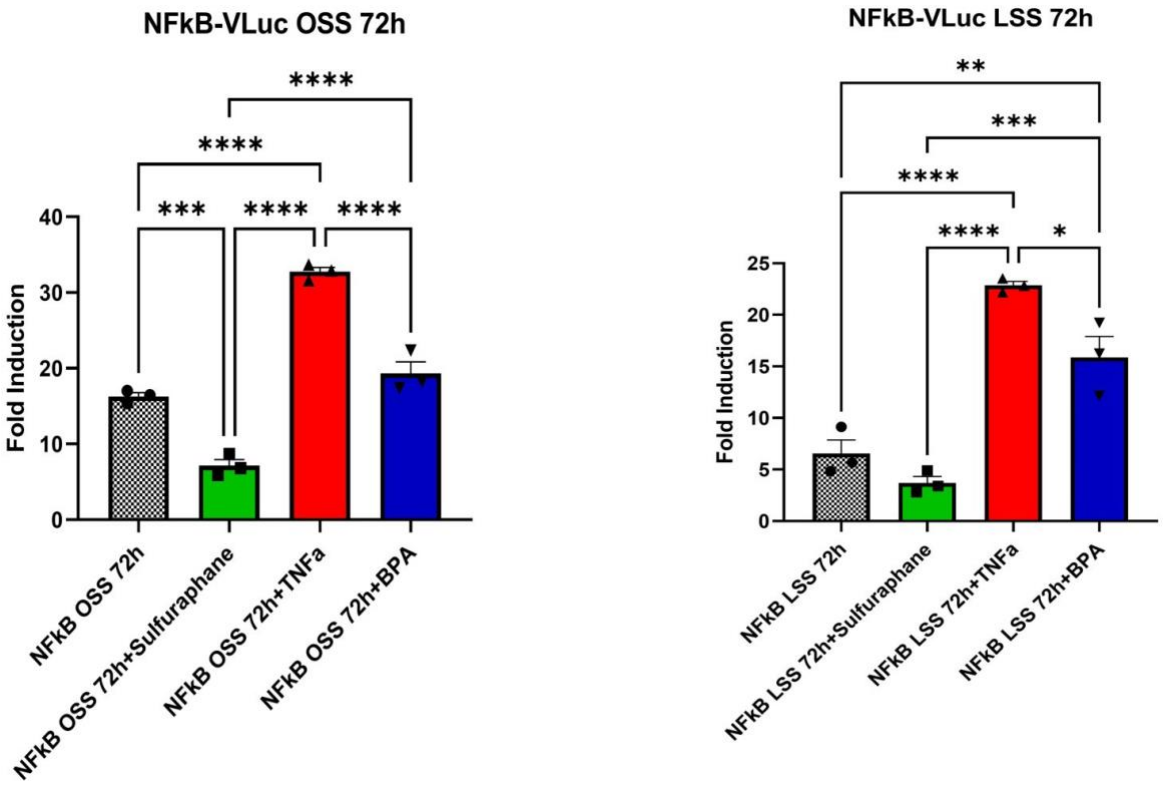

Figure 5.14 Comparison of Induction of NFκB-vLuc Under OSS Stimulated with BPA vs Induction under Normal OSS and OSS with Agonists

HCAECPro cells containing NRF2-nLuc/NFkB-vLuc were cultured under physiological laminar shear stress (LSS, 1.5Pa) and oscillatory shear stress (OSS, ±0.5Pa 1Hz), in flow media containing BPA at a concentration of 10ppm, Sulforaphane (50µM), TNFα (2ng/mL) and nothing added. HCAECPro cells containing NRF2- nLuc/NFkB-vLuc reporter were flowed in triplicate for technical repeat. Luciferase containing media was incubated at room temperature for 5 mins before luminescence was measured using Promega GloMax Explorer plate reader using luciferase assay pre set settings. n=3, ANOVA. *p= <0.05, **p<0.01, ***p<0.001, ±SEM.

5.5 Monitoring the effect of BPA on E-Sense Red cell line under physiological flow conditions; oscillatory shear stress and laminar shear stress

Treatment of **E-Sense Red** with 10ppm revealed a greater effect on KLF2 TFAR activity under LSS than compared to OSS. As seen in chapter 4, treatment of E-Sense red with Atorvastatin and TNFα did not reveal any significant modulation of KLF2 TFAR activity under OSS, our data (figure 5.15) also demonstrated no significant alteration to KLF2 activity when treated with KLF2. As with NRF2, the most significant effect of BPA treatment was the downregulation of KLF2 activity under LSS. As seen in flow data from chapter 4, it was observed that there was a 4.2-fold increase in KLF2 TFAR activity under LSS compared to OSS, relative to static control (Fig 5.15, $P<0.0001$). Atorvastatin treatment moderately increased KLF2 TFAR activity under LSS ($P<0.01$) but not under OSS, whilst TNFα treatment significantly reduced KLF2 TFAR activity under LSS ($P<0.0001$), however, we once again did not observe any significant alteration under OSS. 10ppm BPA treatment resulted in a 438% reduction in KLF2 under LSS compared to LSS 72h ($p<0.0001$). 10ppm BPA treatment also significantly reduced KLF2 TFAR activity compared to TNFα, resulting in a 241% reduction ($P<0.01$).

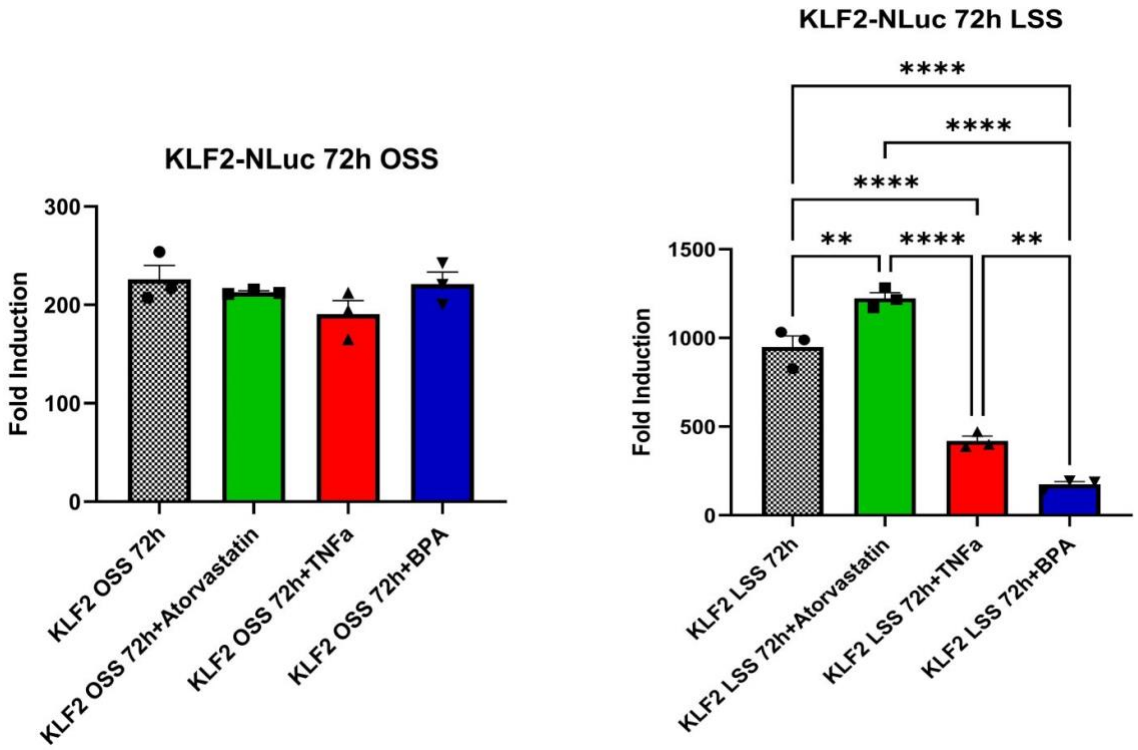

Figure 5.15 Comparison of Induction of KLF2-NLuc Under OSS Stimulated with BPA vs Induction under Normal OSS and OSS with Agonists

HCAECPro cells containing KLF2-NLuc/AP1-VLuc were cultured under physiological laminar shear stress (LSS, 1.5Pa) and oscillatory shear stress (OSS, ±0.5Pa 1Hz), in flow media containing BPA at a concentration of 10ppm, Atorvastatin (1µM), TNFα (2ng/mL) and nothing added. HCAECPro cells containing KLF2-NLuc/AP1-VLuc reporter were flowed in triplicate for technical repeat. Luciferase containing media was incubated at room temperature for 5 mins before luminescence was measured using Promega GloMax Explorer plate reader using luciferase assay pre-set settings. n=3, ANOVA. *p= <0.05, **p<0.01, ***p<0.001, ±SEM.

10ppm BPA treatment under both OSS and LSS does not appear to induce significant changes in AP1 transcriptional activity compared to physiological baselines (fig 5.16). Indeed, under OSS, BPA did not induce significant alterations in AP1 activity in comparison to normal OSS and OSS+Atorvastatin. This was also observed under LSS as no significant alterations were seen in AP1 transcriptional activity between LSS+BPA vs normal LSS as well as LSS+Atorvastatin. In both LSS and OSS, AP1 activity was significantly increased by TNFα stimulation, as previously demonstrated in chapter

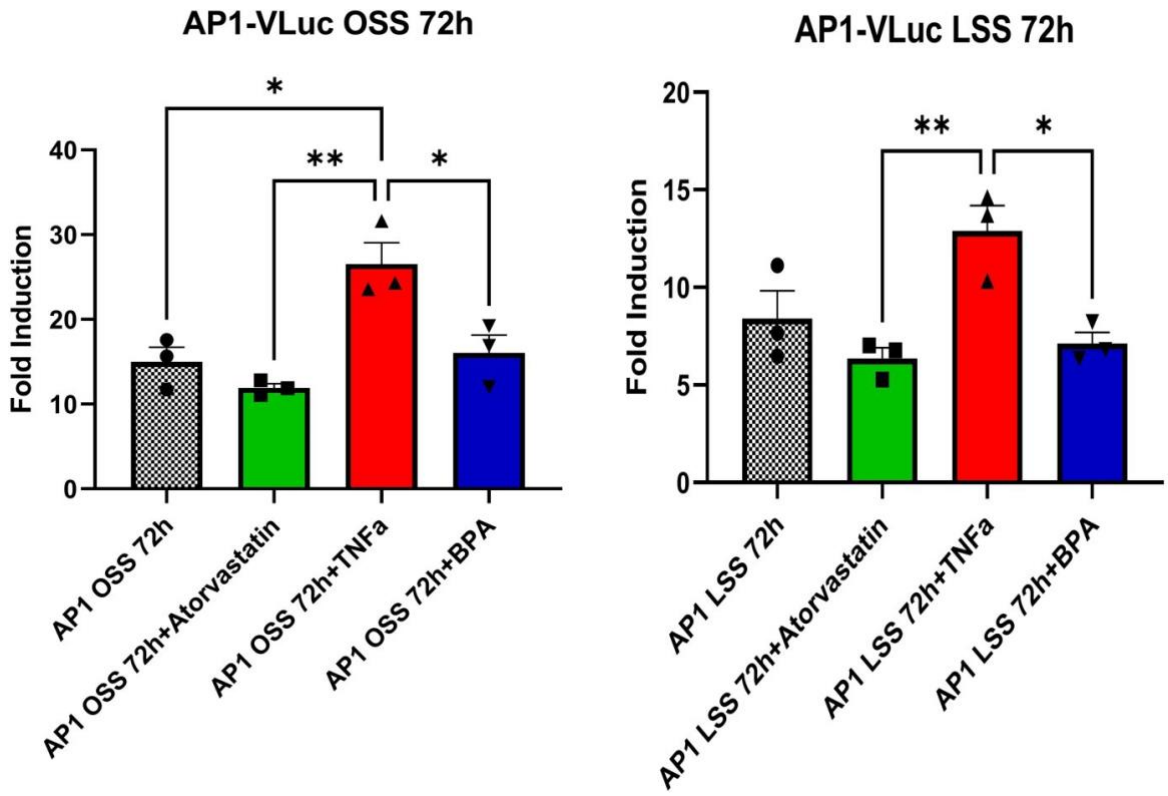

Figure 5.16 Comparison of Induction of AP1-vLuc Under OSS Stimulated with BPA vs Induction under Normal OSS and OSS with Agonists

HCAECPro cells containing KLF2-NLuc/AP1-VLuc reporters were cultured under physiological laminar shear stress (LSS, 1.5Pa) and oscillatory shear stress (OSS, ±0.5Pa 1Hz), in flow media containing BPA at a concentration of 10ppm, Atorvastatin (1µM), TNFα (2ng/mL) and nothing added. HCAECPro cells containing KLF2-NLuc/AP1-VLuc reporter were flowed in triplicate for technical repeat. Luciferase containing media was incubated at room temperature for 5 mins before luminescence was measured using Promega GloMax Explorer plate reader using luciferase assay pre-set settings. n=3, ANOVA. *p= <0.05, **p<0.01, ***p<0.001, ±SEM.

5.6 Monitoring the effect of BPA on E-Sense yellow cell line; oscillatory shear stress and laminar shear stress

Finally, treatment of **E-Sense yellow** with 10ppm BPA identified significant increase in IRF3 TFAR activity under OSS and LSS. As previously shown in chapter 4, OSS induces an 2.3-fold increase in IRF3 TFAR activity than LSS relative to static control (Fig. 5.17, $P<0.05$). Treatment of Thapsigargin did not present with any significant modulation in IRF3 TFAR activity under OSS or LSS. Treatment with LPS did significantly increase IRF3 TFAR activity under both LSS and OSS, with a 328% increase ($P<0.0001$) and 356% increase ($P<0.0001$) respectively. OSS + 10ppm BPA treatment resulted in a 147% increase in IRF3 TFAR activity vs OSS ($P<0.05$), whilst LSS + 10ppm BPA resulted in a 214% increase in IRF3 ($P<0.01$). Whilst these findings demonstrate a significant increase in IRF3 TFAR activity with 10ppm BPA treatment, they both represent a significantly lower induction than known TLR4 agonist, LPS.

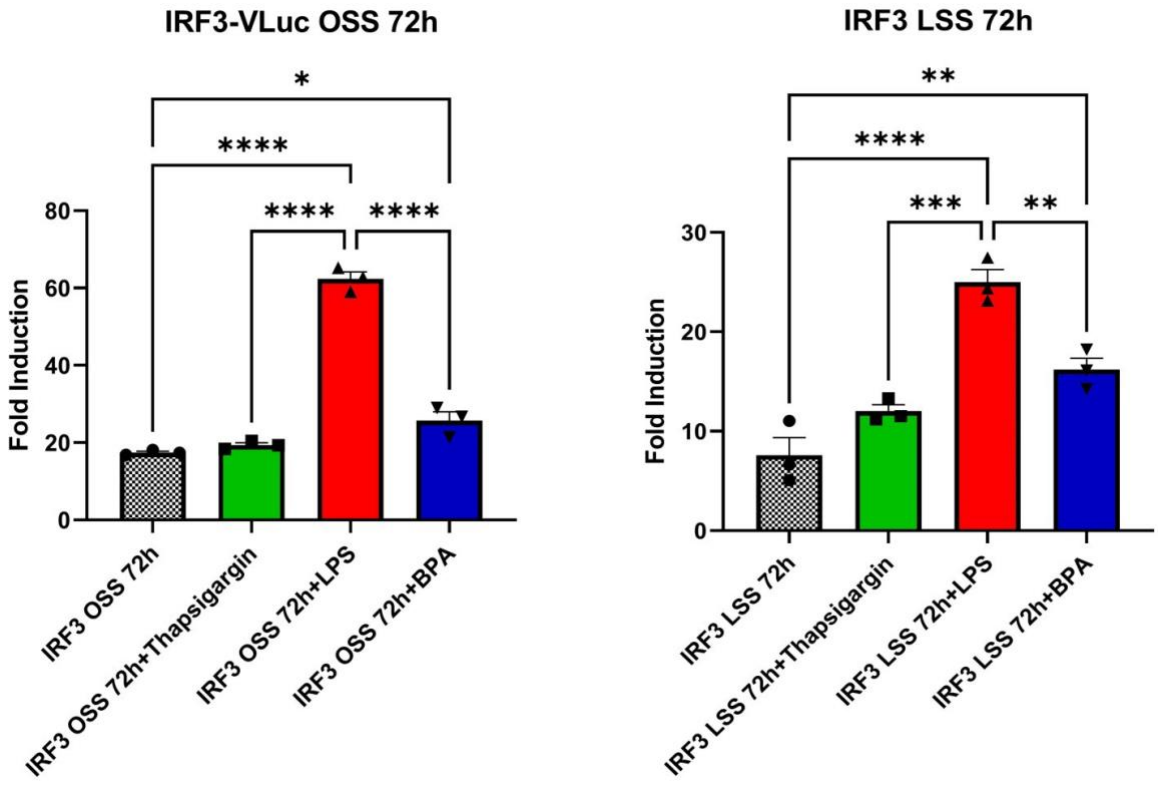

Figure 5.17 Comparison of Induction of IRF3-vLuc Under OSS Stimulated with BPA vs Induction under Normal OSS and OSS with Agonists

HCAECPro cells containing XBP1-NLuc/IRF3-VLuc were cultured under physiological laminar shear stress (LSS, 1.5Pa) and oscillatory shear stress (OSS, ±0.5Pa 1Hz), in flow media containing BPA at a concentration of 10ppm, Thapsigargin(50nM), LPS (50µg/mL) and nothing added. HCAECPro cells containing XBP1-NLuc/IRF3-VLuc reporter were flowed in triplicate for technical repeats. Luciferase containing media was incubated at room temperature for 5 mins before luminescence was measured using Promega GloMax Explorer plate reader using luciferase assay pre-set settings. n=3, ANOVA. *p= <0.05, **p<0.01, ***p<0.001, ±SEM

10ppm BPA treatment revealed a significant increase in XBP1 activity under LSS, however we did not see any significant induction under OSS. It has been previously demonstrated that OSS results in a 1.82-fold induction of XBP1 TFAR vs LSS (Fig 5.18, $P<0.05$). Thapsigargin treatment resulted in a significant increase in XBP1 TFAR activity under both conditions ($P<0.001$). A similar level of induction was observed with LPS treatment (OSS $P<0.001$), LSS $P<0.01$, Fig 5.18). 10ppm BPA treatment resulted in a 97% increase in XBP1 activity under LSS ($P<0.05$), representing 65% induction observed with Thapsigargin and 89% of the induction observed with LPS treatment.

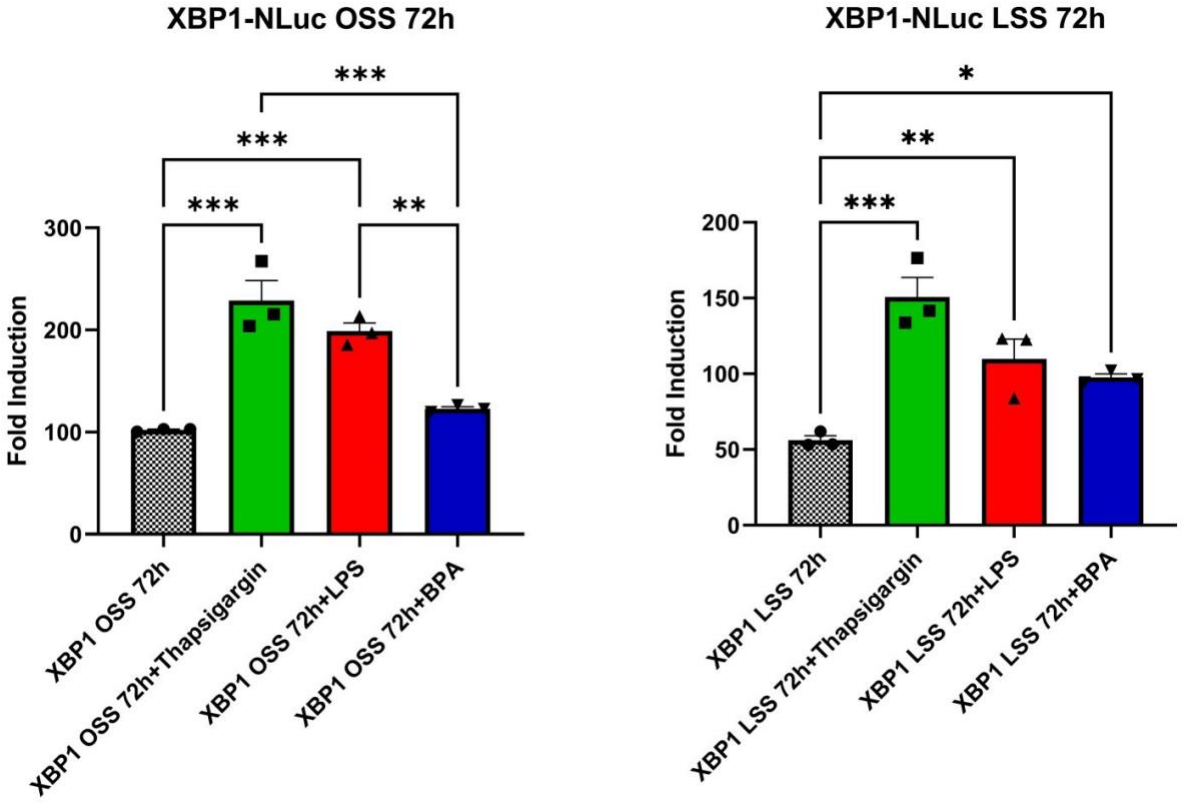

Figure 5.18 Comparison of Induction of XBP1-nLuc Under OSS Stimulated with BPA vs Induction under Normal OSS and OSS with Agonists

HCAECPro cells containing XBP1-NLuc/IRF3-VLuc reporters were cultured under physiological laminar shear stress (LSS, 1.5Pa) and oscillatory shear stress (OSS, ±0.5Pa 1Hz), in flow media containing BPA at a concentration of 10ppm, Thapsigargin(50nM), LPS (50µg/mL) and nothing added. HCAECPro cells containing XBP1-NLuc/IRF3-VLuc reporter were flowed in triplicate for technical repeat. Luciferase containing media was incubated at room temperature for 5 mins before luminescence was measured using Promega GloMax Explorer plate reader using luciferase assay pre-set settings. n=3, ANOVA. *p= <0.05, **p<0.01, ***p<0.001, ±SEM

Summary

- The addition of BPA to E-Sense lines results in several significant alterations in transcriptional activity of TFARs.

TFAR	% Induction observed with BPA compared to normal LSS	% Induction observed with BPA compared to normal OSS
NRF2	10.7%	231.9%
NFκB	240.3%	118.5%
KLF2	18.4%	97.8%
AP1	84.5%	107%
XBP1	173.9%	120%
IRF3	213.6%	147.7%

5.7 Monitoring the Effect of PVC Plasticizer, Dimethyl Phthalate on E-Sense Lines In Static Conditions

In addition to BPA, the plastic Polyvinyl Chloride (PVC) is a ubiquitous plastic readily available and currently implemented in many day to day uses such as pipes (drinking and waste), medical devices, windows and wire insulation. The material is a high strength thermoplastic and its widespread use has made it the second-largest thermoplastic material used by volume worldwide (Asadinezhad *et al.*, 2012).

In addition to observing the effects of BPA on our E-Sense cell lines, we stimulated our lines with PVC plasticiser, dimethyl phthalate (fig 5.19→5.24). We performed an n=3 experiment in triplicate for technical repeats at one dose of 0.01% under static conditions for 24 hours, dimethyl phthalate purchased at a concentration of >99%.

After stimulating our E-Sense lines with dimethyl phthalate, we observed modest, yet significant inductions in each our cell line compared to vehicle control. Indeed, when observing transcriptional activity in E-Sense green, we see a 1.8-fold induction of NRF2 compared to vehicle control ($p<0.0001$, fig 5.19), with a 3.3-fold induction of NFκB ($p<0.01$, fig 5.23) observed. Measuring the activity of E-Sense red, we observed a 1.2-fold induction of KLF2 ($p<0.01$, fig 5.20) after 24 hours stimulation, with dimethyl phthalate exhibiting a 1.1-fold increase in AP1 ($p<0.05$, fig 5.24). Finally, using our E-Sense yellow cell line, we were able to discern alterations in XBP1 and IRF3 activity, with dimethyl phthalate stimulation resulting in a 1.1-fold induction of XBP1 ($p<0.01$, fig 5.21) and a 1.15- fold induction of IRF3 ($p<0.01$, fig 5.22).

While these were significant changes in TFAR activity, they are unlikely to be biologically relevant when compared to the maximal changes in TFAR activity observed with agonist treatment and described in Chapter 4. Changes relative

to these agonists are described in Table 5.2.

Activation of the E-Sense lines with Dimethyl Phthalate resulted in only a modest induction of key transcriptional regulators. Due to time limitations and a small magnitude of observed changes, we did not move forward with full analysis under OSS or LSS.

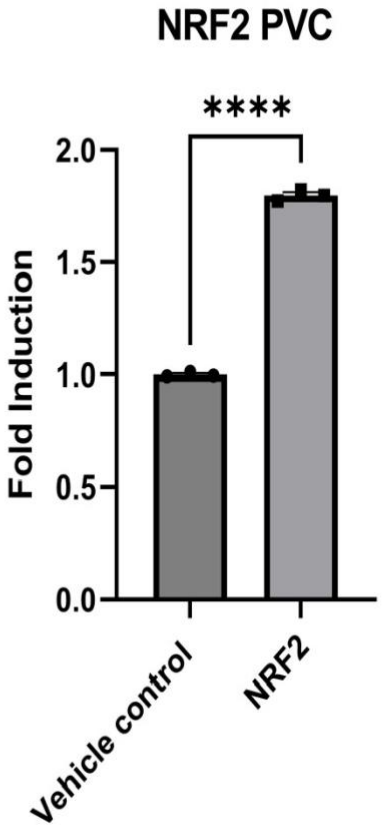

Figure 5.19: Response of NRF2-nLuc to PVC Plasticizer, Dimethyl Phthalate (0.01% concentration)

HCAECPro Cells containing NRF2-NLuc reporter were briefly cultured in a 48-well delta plate and were stimulated with 0.01% Dimethyl Phthalate for 24 hours in triplicate for technical repeat in Promocell MV2 endothelial cell media. Luciferase containing media was incubated at room temperature for 5 minutes before luminescence was measured using Promega GloMax Explorer plate reader using luciferase assay pre-set settings. n=3, T-test. *p= <0.05, **p<0.01, ***p<0.001, ±SEM

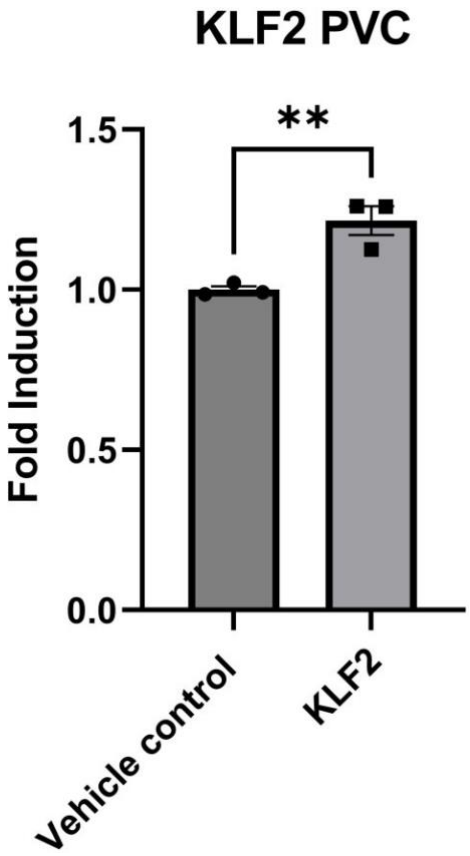

Figure 5.20: Response of KLF2-nLuc to PVC Plasticizer, Dimethyl Phthalate (0.01% concentration)

HCAECPro Cells containing KLF2-NLuc reporter were briefly cultured in a 48-well delta plate and were stimulated with 0.01% Dimethyl Phthalate for 24 hours in triplicate for technical repeat in Promocell MV2 endothelial cell media. Luciferase containing media was incubated at room temperature for 5 minutes before luminescence was measured using Promega GloMax Explorer plate reader using luciferase assay pre-set settings. n=3, T-test. *p= <0.05, **p<0.01, ***p<0.001, ±SEM

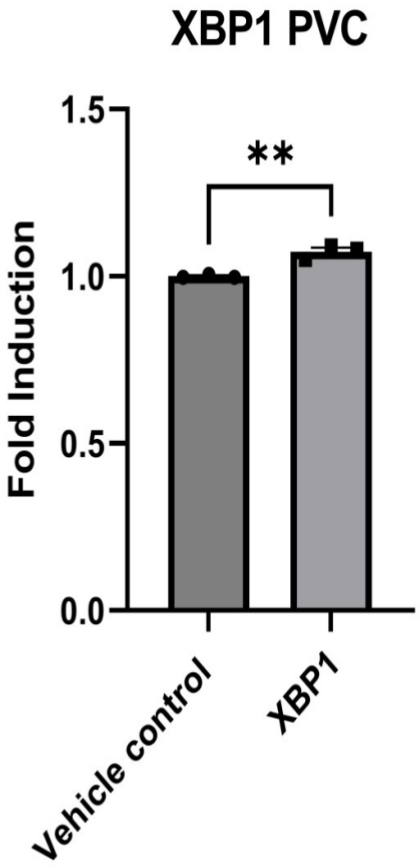

Figure 5.21: Response of XBP1-nLuc to PVC Plasticizer, Dimethyl Phthalate (0.01% concentration)

HCAECPro Cells containing XBP1-NLuc reporter were briefly cultured in a 48-well delta plate and were stimulated with 0.01% Dimethyl Phthalate for 24 hours in triplicate for technical repeat in Promocell MV2 endothelial cell media. Luciferase containing media was incubated at room temperature for 5 minutes before luminescence was measured using Promega GloMax Explorer plate reader using luciferase assay pre-set settings. n=3, T-test. *p= <0.05, **p<0.01,2***p<0.001, ±SEM

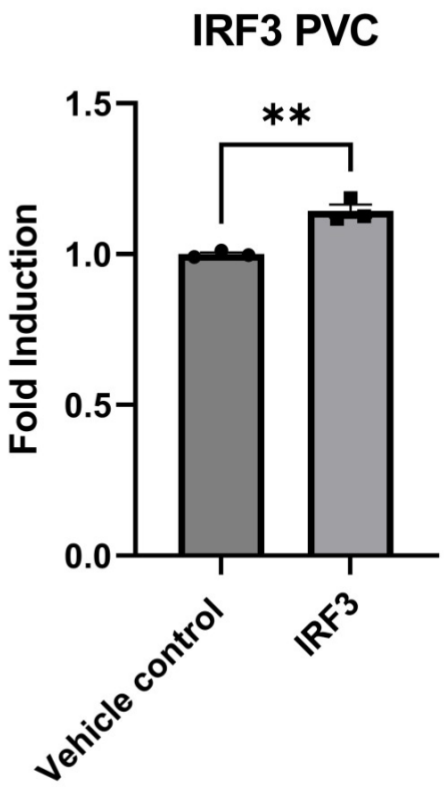

Figure 5.22: Response of IRF3-vLuc to PVC Plasticizer, Dimethyl Phthalate (0.01% concentration)

HCAECPro Cells containing IRF3-VLuc reporter were briefly cultured in a 48-well delta plate and were stimulated with 0.01% Dimethyl Phthalate for 24 hours in triplicate for technical repeat in Promocell MV2 endothelial cell media. Luciferase containing media was incubated at room temperature for 5 minutes before luminescence was measured using Promega GloMax Explorer plate reader using luciferase assay pre-set settings. n=3, T-test. *p= <0.05, **p<0.01, ***p<0.001, ±SEM

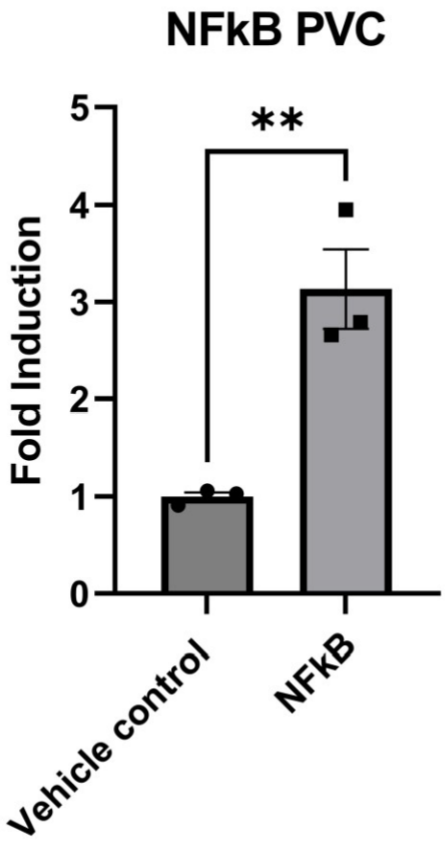

Figure 5.23: Response of NFkB-vLuc to PVC Plasticizer, Dimethyl Phthalate (0.01% concentration)

HCAECPro Cells containing NFkB-VLuc reporter were briefly cultured in a 48-well delta plate and were stimulated with 0.01% Dimethyl Phthalate for 24 hours in triplicate for technical repeat in Promocell MV2 endothelial cell media. Luciferase containing media was incubated at room temperature for 5 minutes before luminescence was measured using Promega GloMax Explorer plate reader using luciferase assay pre-set settings. n=3, T-test. *p= <0.05, **p<0.01, ***p<0.001, ±SEM

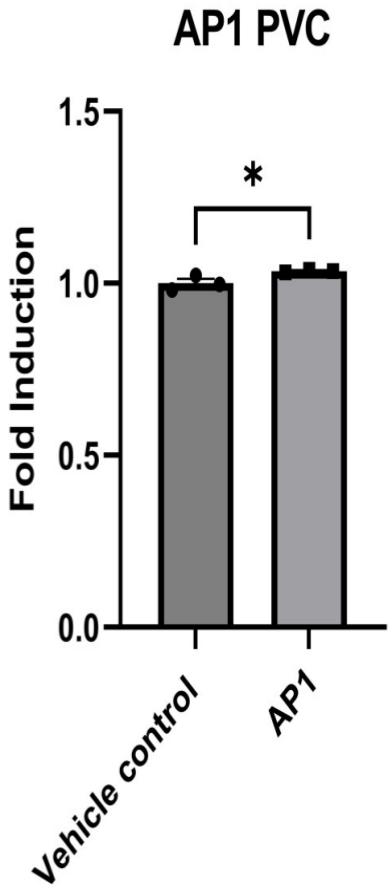

Figure 5.24: Response of AP1-vLuc to PVC Plasticizer, Dimethyl Phthalate (0.01% concentration)

HCAECPro Cells containing AP1-VLuc reporter were briefly cultured in a 48-well delta plate and were stimulated with 0.01% Dimethyl Phthalate for 24 hours in triplicate for technical repeat in Promocell MV2 endothelial cell media. Luciferase containing media was incubated at room temperature for 5 minutes before luminescence was measured using Promega GloMax Explorer plate reader using luciferase assay pre-set settings. n=3, T-test. *p= <0.05, **p<0.01, ***p<0.001, ±SEM

Summary of the effect of Dimethyl Phthalate on TFARs:

TFAR	Induction 0.1% Dimethyl Phthalate	Agonist Comparison
NRF2	0.07%	20% CSE
KLF2	0.04%	KLF2 overexpression
IRF3	0.4%	50µg/ml Ox-LDL
XBP1	0.01%	50nM Thapsigargin
NFκB	20%	2ng/ml TNFα
AP1	0.5%	2ng/ml TNFα

5.8 Discussion

Previous work in chapters 3 and 4 have described the generation and validation of the E-Sense system through integrating discreet, novel TFARs into our HCAECPro cell line. We have previously demonstrated the E-Sense system's ability to monitor changes in the activity of our discreet cell lines with a high degree of sensitivity. This line of work has enabled the monitoring of microplastics, namely BPA and Dimethyl phthalate (PVC) and their potentiation for atherogensis, via alterations in the transcriptional activity of pathways known to regulate atherosclerosis. The unique nature of our system allows us to make predictions on a compounds ability to result in a pro-atherogenic signalling within the endothelium by monitoring the six previously mentioned transcription factors. Due to its sensitivity, we were able to monitor changes even as small as a 1% of TFAR activity, which may be below the level of biological significance. These small changes in TF activity would be difficult to monitor by any other analytical method, or TFARs built with a different architecture.

Comparable to work carried out in chapter 4, we stimulated each of our E-Sense lines with BPA at varying, physiological concentrations in static conditions, in order to ascertain its ability to confer transcriptional alterations. By doing so we were able to optimise BPA concentration for full integration of the E-Sense system, monitoring the effects of BPA under physiological shear stress, LSS and OSS.

Initial work in this chapter aimed to determine the optimal concentration of BPA to be used moving forward integrating into the parallel plate flow apparatus. We subjected each of TFARs to BPA stimulation in a dose response experimental design, with dosages equal to 10ppm, 25ppm, 50ppm, 100ppm and 150ppm for 24 hours. Under static conditions, a significant induction of NRF2 in doses as low as 10ppm was observed, with a 42.4-fold induction compared to vehicle

control ($p<0.0001$) (figures 5.1 & 5.2). In comparison, the Nrf2 TFAR activity increased 495- fold with 50μM Sulforaphane treatment (figure 4.9), meaning in static culture BPA results in an increase in Nrf2 TFAR activity of 8.6%, relative to sulforaphane treatment. This indicates that BPA appears to induce a fairly modest, but significant activation of NRF2. Under these same conditions, we see a similar induction of KLF2 at 10ppm, resulting in a 33.2-fold induction in comparison to vehicle control (figure 5.3 & 5.4). The KLF2 activator, Atorvastatin, at a dose of 1μM results in a 387-fold induction of KLF2. With this in mind, we can observe BPA results in 8.6% of the induction seen with Atorvastatin treatment, the same level of activation seen in NRF2. These results indicate BPA has a small effect on these protective signalling pathways. To balance these observations, the transcriptional activity of IRF3 (figures 5.5 & 5.6), increased by 7-fold compared to vehicle control ($p<0.0001$). Comparing this with treatment of the TLR4 agonist LPS, which resulted in a 27-fold induction, 10ppm BPA treatment induces 26% of IRF3 TFAR activity, relative to LPS treatment. Furthermore, XBP1 activation via BPA treatment (figures 5.7 & 5.8) results in an induction equivalent to 23% of the XBP1 TFAR activity observed with Brefeldin A treatment (23.7-fold increase BPA vs 102-fold increase Brefeldin A) or 4.6% activity relative to Thapsigargin treatment (23.7-fold BPA vs 515-fold Thapsigargin). Finally, we were able to quantify significant alterations in the transcriptional activity of NFκB and AP1 in response to BPA stimulation (figures 5.9□5.12). At a concentration of 10ppm, we see a 1.28-fold induction of NFκB TFAR activity compared to vehicle control ($p<0.05$) and a 1.3-fold induction of AP1 TFAR activity ($p<0.01$). When analysing NFκB and AP1 activity with TNFα treatment (2ng/mL), this is equivalent to a 12.6% increase in NFκB TFAR and a 16.4% increase in AP1 TFAR activity.

Our analysis under static culture identified changes in TFAR activity in both athero- protective (Nrf2 and KLF2) and inflammatory and cell stress pathways (XBP1, IRF3, NFκB and AP1). By comparing the TFAR activation with the maximal values observed using known agonists of the signalling pathways that regulate the TFs we can generate an appreciation of the effects of BPA treatment on TF activity. On balance, the inflammatory and cell stress pathway activation are greater in magnitude than the atheroprotective pathways. This data supports the notion that BPA may promote atherosclerosis through activation of inflammatory and cell stress pathways in the endothelium.

As the haemodynamic environment induces a significant change in endothelial phenotype, we expanded our analysis to quantify TFAR activity under OSS and LSS, using the same protocol developed in chapter 4. This allows prediction of the effects of BPA treatment on endothelial signalling pathways at sites that experience atheroprotective flow and predilected sites at which the endothelium is primed for dysfunction and plaque formation that experience disturbed flow.

Previous work described in chapter 4 enabled us to define baseline values for transcriptional activity of the three E-Sense lines under physiological LSS and OSS as well as the regulation of TFAR activity by our panel of signalling agonists. We exposed our E-Sense lines to normal LSS and OSS with the addition of BPA at a concentration of 10ppm for 48h following the 24 hour period to allow the HCAECPro time to adapt to their flow environment. We observed significant changes in TFAR activity that denoted a strong pro-atherogenic signature within the endothelium.

Analysis of TFAR activity under atheroprotective flow identified profound downregulation of both atheroprotective transcriptional pathways regulated by KLF2 and Nrf2, reducing both to a level observed under OSS. This is an important

finding and effectively nullifies the 'atheroprotective' upregulation of both pathways by physiological laminar flow. Simultaneously, 10ppm BPA treatment induced the upregulation of XBP1 and IRF3 TFAR activity as well as activating the inflammatory cytokine pathway regulated by NFκB. Taken together, 10ppm treatment causes a shift in TF activity in HCAECPro that would promote endothelial dysfunction and atherosclerosis by inhibiting protective pathways while promoting cell stress pathways. The fact that these effects are observed with BPA treatment of 10ppm, highlights a potential contributor to increased risk of cardiovascular disease at levels found in the general population.

Under flow conditions that simulate atheroprone regions of the arterial tree, 10ppm BPA treatment has more modest effects. Significant upregulation of Nrf2 and IRF3 TFARs were observed. In contrast to culture under LSS, BPA treatment under OSS increased Nrf2 TFAR activity. The mechanism for this difference is unclear and is an opportunity for further study to dissect the mechanism behind this observation. IRF3 activity was also increased under OSS, however the other pathways related to inflammation and cell stress were not significantly changed.

Not only has the E-sense platform provided novel insight into the regulation of molecular pathways that are regulated by BPA treatment, it also informs further analysis and the design of any *in vivo* experiments that might be performed to further investigate the role that BPA might play in regulating atherosclerosis. The data presented here has implications for experimental design, both at defining a pathological dose, but also how to quantify changes in plaque development. The data suggests that analysis of plaque formation at predilected sites might be largely unaffected by BPA treatment, so analysis of the aortic root, inner curvature of the aortic arch, or proximal brachiocephalic artery may not identify a significant change in atherosclerotic plaque development, as these sites are all

dominated by disturbed flow (Chiu and Chien, 2011). The data suggests that a 'whole mount' en face oil red O stain of the aorta might provide a better opportunity to quantify changes in plaque formation as this would be exposed to laminar flow and therefore subject to a loss in atheroprotective signalling resulting in enhanced plaque formation (Ko *et al.*, 2017). This acts to 'refine' experimental design and ensure that the experimental design is optimised to prevent unnecessary use of animal for cardiovascular research.

The role of TLR4 signalling in252athogenenesis of atherosclerosis has been well established, linked with a major role in regulating the innate an adaptive immune response (Lim and Staudt, 2013). TLR4 recognises danger- and pathogen-associate molecular patterns, resulting in the activation of inflammatory cells. In addition, TLR4 signalling is intrinsically linked to downstream IRF3 and NFκB activation (Schnack *et al.*, 2019). Indeed, TLR4 signalling utilizes exogenous and endogenous ligands for activation, resulting in dimerization of the receptor and binding to the TIR domain-containing adaptor inducing interferon-β (TRIF)-dependent pathways leading to IRF3 activation (Yu, Wang and Chen, 2010) (Doyle *et al.*, 2002). Future work could establish if BPA treatment specifically regulates TLR2/4 signalling, and be responsible for the observed regulation of IRF3, or whether IRF3 activation is downstream of another regulatory pathway.

The role of NFκb in the transcriptional regulation of atherosclerosis is intrinsically linked to KLF2 inhibition. KLF2 and NFκB have been shown to compete for co-recruiting chromatin modulators p300/cyclic adenosine monophosphate response element binding protein (CBP)-associated factor (PCAF), resulting in KLF2 induction-dependent inhibition of NFκB via recruitment of crucial inflammatory co- factors (Jha and Das, 2017). Conversely NFκB induction is able to inhibit KLF2 expression via MADS box transcription enhancer factor 2 (MEF2)

factors interruption and preventing access of histone deacetylase (HDAC) molecules to the KLF2 promoter (Kumar *et al.*, 2005). These mechanisms demonstrate the effective interplay of the inflammatory signalling cascades between KLF2 and NFκB. There is also mounting evidence that NRF2 and NFκB play concomitant roles in redox balance through transcriptional and post-transcriptional mechanisms. Although there is significant evidence of functional interactions between NRF2 and NFκB, the exact molecular mechanisms and the dynamic nature of the interaction is still to be fully elucidated (Wardyn, Ponsford and Sanderson, 2015). Under LSS environments, we have also demonstrated a significant reduction in NRF2 protective signalling and increase in XBP1 expression. XBP1 splicing has been shown to be dependently induced via ER stress sensor, IRE1α, which is subsequently induced by ATF4 downstream of double-stranded RNA-dependent protein kinase (PKR)-like ER kinase (PERK) (Zeng *et al.*, 2009). PERK has been shown to play a role in NRF2 signalling, under ROS insults PERK is reported to phosphorylate NRF2. This induction of PERK signalling results in the dissociation of NRF2 from KEAP1 and further translocation allowing NRF2 to activate its downstream targets (Cullinan *et al.*, 2003).

Our results offer a valuable insight into the effects of BPA on the endothelium. Our data suggests BPA increases the activation of IRF3 possibly through activation of TLR4, this in conjunction with an increase in NFκB signalling implies an inflammatory mechanism central to TLR4 signalling. The induction of NFκB coincides with a reduction of protective signalling KLF2. Additionally, we observe a priming of the endothelium for dysfunction, with a clear induction of ER stress modulator, XBP1. The activation of ER stress may be further exacerbated with a concomitant reduction in NRF2. This may render the endothelium more

susceptible to oxidative stress without the normal programme of antioxidant gene expression controlled by NRF2 under laminar shear stress.

5.9 Summary

- BPA stimulation results in an increase in IRF3, NFκB, XBP1 under LSS, whist inhibiting KLF2 and NRF2 activity.
- Results indicate continual BPA exposure poses a possible risk to cardiovascular health by inhibiting key atheroprotective mechanism and increasing cellular stress pathways.
- Future work should aim to focus on how BPA exposure directly results in an increase in TLR4 signalling.

Chapter 6

General Discussion

6.0 Project Overview

Cardiovascular disease (CVD) and in particular coronary artery disease (CAD) represents the major leading cause of morbidity and mortality worldwide. The major underlying pathological process of in the potentiation of CAD is atherosclerosis. In the absence of severe predisposing genetic mutation (e.g. Hutchinson Gilford progeria syndrome or familial hypercholesterolaemia), atherosclerosis is a multifactorial, slow, clinically silent process with resultant plaque formation occurring over several decades (Virmani, Burke and Farb, 1999). The nature of the disease implicates the endothelium and its response to differing haemodynamic environments as a prime initiator of atherosclerosis. Indeed, studies have demonstrated the pathological processes leading to atherosclerotic plaque formation preferentially occur at predilected sites such as bifurcations where the endothelium is exposed to disturbed flow, leading to focal development of the disease (Teasdale *et al.*, 2017). Conversely, areas subjected to laminar shear flow are more athero-resistant. (Simmons, Kumar and Jo, 2016) Studies across decades of cardiovascular disease using *in vivo* models have provided great insight into the key transcriptional mechanisms in which atherosclerosis initiates and progresses. Intracellular signalling cascades from diverse cellular shear-sensors detect the haemodynamic environment and control a few key transcription factors, particularly KLF2 and NRF2 to elicit protective gene expression programmes whilst suppressing the activity of NFκB and other proinflammatory and cell stress signalling (Boon and Horrevoers, 2009).

The use of animal models has been a cornerstone in the study of atherosclerosis and coronary heart disease, with a variety of species throughout academic research. Although *in vitro* models provide useful insights into the innate immune response, it has proven difficult to accurately replicate the changing

haemodynamic environments produced in plaque formation. Previous *in vitro* studies have aimed to replicate the variance in the haemodynamic forces subjected to the arterial endothelium, with many of these producing a conservative estimation, which has resulted in the use of animal models, becoming a valuable asset to clinical and academic studies.

As previously mentioned, atherosclerosis is characterised as a chronic immune disease and remains asymptomatic until plaque formation becomes extensive enough to cause a stenosis leading to eventual rupture or erosion leading to myocardial infarction, ischemic stroke and subsequent morbidity or mortality (Lichtman *et al.*, 2013). In the earlier stages, the disease is driven by an increase in cholesterol-rich, apolipoprotein B-containing lipoproteins being retained at specific predilection sites (i.e., bifurcations). These mechanisms, in most part have required the use of animal models to mimic human disease, however, discerning an appropriate species has proved challenging. Recapitulating human disease perfectly is animal models is unrealistic, with best fit the current methodology, with different species chosen based on a specific area of research. The use of non- human primates provides the most appropriate in terms of similarities to human physiology and clinical significance, however, they are difficult to maintain due to

costs, ethical issues and time consumption, with disease developing over a longer period.

The overall aim of this project was to create and validate a cell-based *in vitro* physiological model to screen compounds for cardiovascular risk, utilising an endothelial cell-based platform to circumvent and refine some of the issues discussed in animal modelling. Previous research over the last 50-60 years utilising *in vivo* modelling, has elucidated many of the key modulators in atherosclerosis development. By utilising this data, it is possible to quantify the

effect of compounds on disease processes by observing the modulation of a few key transcription factors which control gene activity of a plethora of downstream targets. The platform was built on a human coronary artery endothelial cell line with enhanced proliferative capacity through the inhibition of senescence (HCAECPro). HCAECPro, were transduced with sensitive transcription activator reporters (TFARs) to create three distinct cell line; E-Sense Green (NRF2-nLuc/NFκB-vLuc), E-Sense Red (KLF2- nLuc/AP1-vLuc) and E-Sense Yellow (XBP1-nLuc/IRF3-vLuc). Finally, the E- Sense lines were assessed using our in-house parallel plate flow apparatus, in order to monitor transcriptional activity under physiological laminar shear stress (LSS) and representative disturbed flow-oscillatory shear stress (OSS).

The development of this model has demonstrated a number of key findings:

- Overexpressing BMI1 + hTERT results in a human coronary artery endothelial cell line with a proliferative potential which far exceeds that seen in primary cells.
- By adopting a novel spacing approach, we were able to create a TFAR-based system with a sensitivity several factorials higher than previous designs.
- Exposure to the widely-used microplastic, BPA, exerts a significant effect on the transcriptional regulation of the unfolded protein response under both OSS and LSS whilst also suppressing atheroprotective signalling normally upregulated in areas of laminar shear stress.
- The data obtained, implies BPA may increase the risk of atherosclerotic plaque development.

6.1 Extending HCAEC Proliferative Potential with BMI1 and hTERT

When utilising *in vitro* platforms for clinical and academic research purposes, human coronary artery endothelial cells remain the 'gold standard' in terms of primary cell lines used. Although they remain the most optimal cell line for disease modelling, they have some key drawbacks such as high cost and limitations on the number of passages before which they senesce, with most cell batches de-differentiating and senescing before p7. At this passage, a higher proportion of HCAECs enter full cycle arrest and cellular senescence, therefore unable to continue to proliferate and losing all phenotypical traits. Most researchers limit the use of primary cells to below passage five to prevent this skewing the data collected.

Cellular senescence represents critical process in the homeostatic response to prevent the propagation of damaged cells and neoplastic formation (Kuilman *et al.*, 2010). The process induces a stable cell cycle arrest accompanied by phenotypic changes such as metabolic reprogramming, chromatin remodelling, an increase in autophagy and the induction of a complex proinflammatory secretome (McHugh and Gil, 2018). Although a physiological process, crucial for normal development and tissue homeostasis, cellular senescence constitutes a stress response, characterised by proliferation limitation of aged or damaged cells triggered by events associated with aging such as telomere attrition and genomic instability (Sun, Youle and Finkel, 2016). As previously mentioned in chapter 3 (3.0), one of main regulators of cell cycle arrest is $p16^{INK4a}$/RB and $p52/p21^{CIP1}$ (figure 6.1, below). Another key regulator is DNA replication-induced telomere shortening, due to DNA polymerase α's inability to fully replicate ends of linear DNA molecules, thus telomere length shortens during each replicative cycle (Salama *et al.*, 2014)

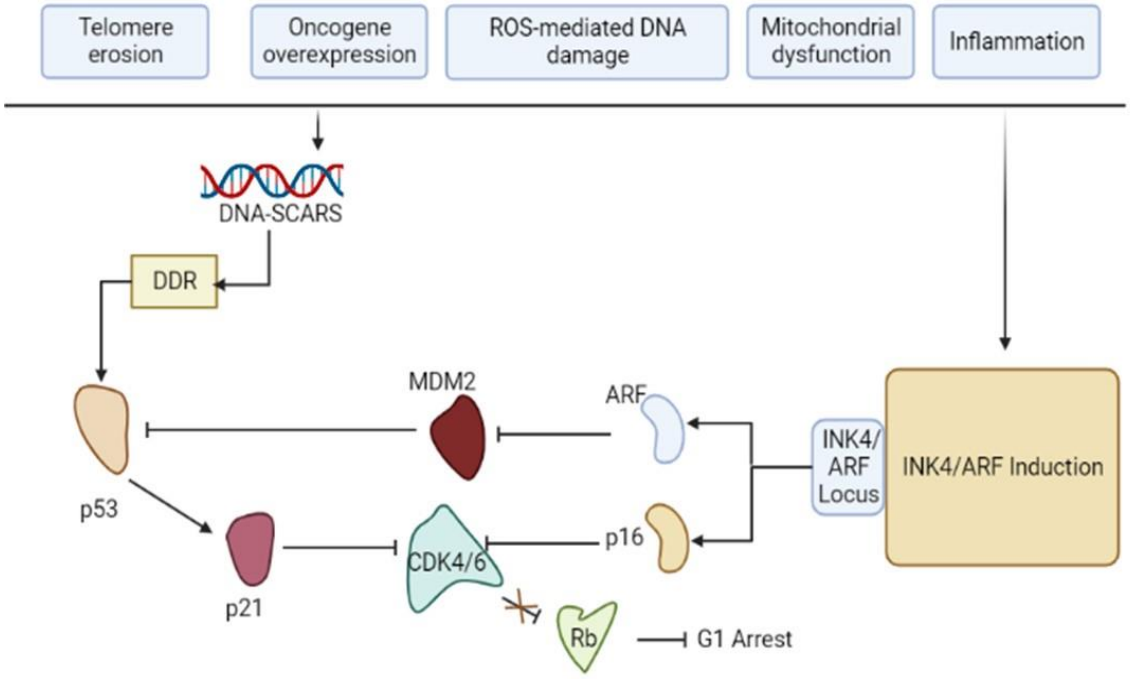

Figure 6.1 :Senescence-mediated arrest regulatory pathways. Cell cycle arrest, mediated by cellular senescence is regulated via the $p16^{INK4a}$/Rb and p53/p21 pathways, with both producing a repressive effect of CDK4/6. The p53/p21 pathway activates downstream of DDR from repair- resistant DNA segments, chromatin alterations also enable the reinforcement of senescence. Polycomb repressive complexes (PRCs) silence the INK4A/ARF locus and are activated during senescence (McHugh and Gil, 2018).

The lentiviral overexpression of BMI1 and hTERT inhibits the induction of senescence and allows the continued passage of transduced cells. Indeed, our BMI1 + hTERT cells (HCAECPro) demonstrate a reduction in the number of Senescent-associated β-galactosidase positive cells, demonstrating a significant reduction at passages p4, p5 and p15 in comparison to primary cell counterparts at same passage. As stated, senescence is known to be tightly regulated by p16, p21 and p53, mRNA expression indicates that HCAECPro cells have a diminished expression of both p16 and p21 at each aforementioned passages. BMI1 in a known repressor of the p16 encoding locus, *INK4a* thus inducing an extended proliferative effect, with hTERT expression known to be stably repressed via transient expression of p16, implicating a highly intricate role between hTERT expression and activation of the $p16^{INK4a}$ senescent pathway

(Bazarov *et al.*, 2010). DNA damage and erosion of telomeres results in the activation of the p53-p21 pathway, resulting in G1-phase arrest in mammalian cells via CDK2 inhibition (Qian and Chen, 2013). Our analysis indicates that overexpressing hTERT does not have a significant effect on p53 mRNA expression, however, does result in significant reduction of its downstream target p21. This relationship has been sparingly commented on previously, as hTERT protein expression and p21 protein expression was positively correlated in colorectal adenocarcinoma patients (Lam, Ong and Ho, 2008). Further work into the exact mechanisms by which hTERT affects the p53-p21 pathway in hTERT-overexpressed cells presents an interesting area of senescence associated research. Additionally, as previously mentioned, increased rates of cellular senescence within a cell culture will reduce the rate of proliferation. Flow cytometry demonstrated a higher proportion of HCAECPro cells remained in G2/S phase compared to primary cells, that remained elevated even at p15. BMI1 results in an inhibition of the $p16^{INK4A}$ pathway, which has been shown to mediate the permanent cell cycle arrest via CDK4 and CD6 inhibition, thus resulting in RB phosphorylation, blocking entry to S phase (Bazarov *et al.*, 2010). The two pronged approach to prevent cellular senescence used here proved particularly effective at extending the proliferative capacity of HCAECs.

Morphological studies did not identify any alterations in the phenotypic traits of HCAECPro, with HCAEPro cells maintaining the trademark ‘cobblestone’ phenotype at p15. Most notably, endothelial cells are known to store von Willebrand Factor (vWF) in Weibel palade bodies, which presents with punctuative staining of primary HCAECs. Immunofluorescent staining of primary HCAECs and HCAECPro’s did not present any clear differences in terms of size and number in positively stained cells.

As previously mentioned, endothelial cells are mechanosensitive, with changes in the haemodynamic environment known to result in the regulation of key transcription factors that modulate the atherosclerotic disease process. We monitored the mRNA expression of an array of key shear-regulated genes, utilising our in-house parallel plate flow apparatus. The response of both p3 primary HCAECs and p15 HCAECPro cultured under physiological laminar shear stress (LSS-15 dynes), oscillatory shear stress, representing disturbed flow (OSS - ±5 dynes, 1 Hz) or elevated shear stress (ESS – 75 dynes) for 72 hours was performed to ensure HCAECpro retained key endothelial traits needed for the E-Sense platform to be developed. Both phase contrast imaging and immunofluorescent cell staining of vinculin and phalloidin, show no clear differences in cell morphology between primary HCAECs (p4) and HCAECPro's (p9 & p15). This included the staining of focal adhesion component vinculin and actin filament marker phalloidin, which demonstrated a similar morphological response of HCAECPro under OSS, LSS and ESS comparable to p4 primary HCAECs. Each of the genes assessed responded in an identical manner to the different haemodynamic environments tested. Most notably, KLF2, KLF4 and NRF2 have been shown to be master regulators in the mechanosensitive response of the endothelium (Boon and Horrevoers, 2009). KLF2, KLF4 and NRF2 mRNA expression were all shown to be significantly upregulated in primary HCAECs (p4) and HCAECPro cells (p9 and p15) when exposed to LSS compared to OSS. Taken together, HCAECPro retain key endothelial traits, including mechanosensitivity and therefore represent an ideal cell platform to use to create the E-Sense system.

6.2 Novel TFAR Binding Sequence Spacing Results in Increased Sensitivity

The backbone of the project related to the use of transcription factor activator reporters as a method to quantify alterations in the TF activity known to regulate atherosclerosis. This approach has the potential to assess pro-atherosclerotic effects with a higher sensitivity and throughput than using alternative molecular techniques. As previously mentioned, decades of cardiovascular research has highlighted many signalling pathways and resultant transcriptional programmes that regulate atherosclerotic disease initiation and progression. Analysis of this research identified a few transcription factors, namely NRF2, KLF2, IRF3, XBP1, NFκB and AP1, which together have a plethora of downstream targets that control disease. Conventional methods for monitoring the activity of these transcription factors, such as quantitative PCR and western blot provide robust and well used methods, however, they have some major drawbacks when implementing drug screening which require repeated or continuous measurements. The utilisation of TFARs circumvent this issue, with luciferase continuously secreted into surrounding media which can be sensitively quantified and related to TF activity (Minchin and Busby, 2013).

Conventional methods for TFAR design incorporate transcription factor binding sequences spaced concurrently next to one another, upstream of a minimal promoter (Trifonov, 2016). We incorporated a novel binding sequence spacing corresponding to two double helical periods of 10.5bp, spacing the TF binding sites of 21bp apart – a feature frequently observed in eukaryotic gene promoters (Makeev *et al.*, 2003)(Huang *et al.*, 2012). This new design, which was implemented in our NRF2-NLuc, KLF2-NLuc, XBP1-NLuc and IRF3-VLuc reporters resulted in a sensitivity several orders of magnitude higher than normally observed for TFARs. Measuring transcriptional activity of our TFARs under static conditions, treated with known pathway agonists provided us with

the dynamic range of our reporters. As a consequence of the enhanced dynamic range of the developed TFARs, all the data presented here utilised luciferase reagents that were diluted 10-fold more than the recommended amount to ensure linearity of luciferase quantification. NRF2-NLuc provides an ideal example of the increase in sensitivity, displaying a 2719-fold induction compared to vehicle control ($p<0.0001$) when stimulated with 20% cigarette smoke extract. Previous work in the White lab has demonstrated that CSE treatment results in the hyperactivation of NRF2 and leads to endothelial detachment under flow conditions.

We produced three distinct E-Sense lines incorporating the developed TFARs within HCAECPro and exposed them to physiological laminar shear stress (LSS) as well oscillatory shear stress (representing disturbed flow - OSS). Our data demonstrates each of our cell lines are shear responsive with the upregulation of NRF2 and KLF2 under LSS when compared to OSS. Our data demonstrates that culture under OSS results in a significant upregulation of IRF3 and NFκB with reduction in KLF2 and Nrf2 activity. OSS has been previously demonstrated to promote activate TLR4 signalling in human endothelial cells (Wang *et al.*, 2019). Ligand induced dimerization of TLR4 results in TRIF-dependent activation of IRF3 and NFκB (Verstak *et al.*, 2014).

The data generated is concordant with the known competition between NFκB and KLF2 through the shared use of co-factor p300 (figure 6.2, below). Elevation of KLF2 TFAR activity under LSS was mirrored by a reduction in NFκB TFAR activity. Treatment with 2ng/ml TNFα resulted in a lower activation of NFκB TFAR under LSS compared to OSS and vice versa, KLF2 activity was reduced under LSS by TNFα treatment.

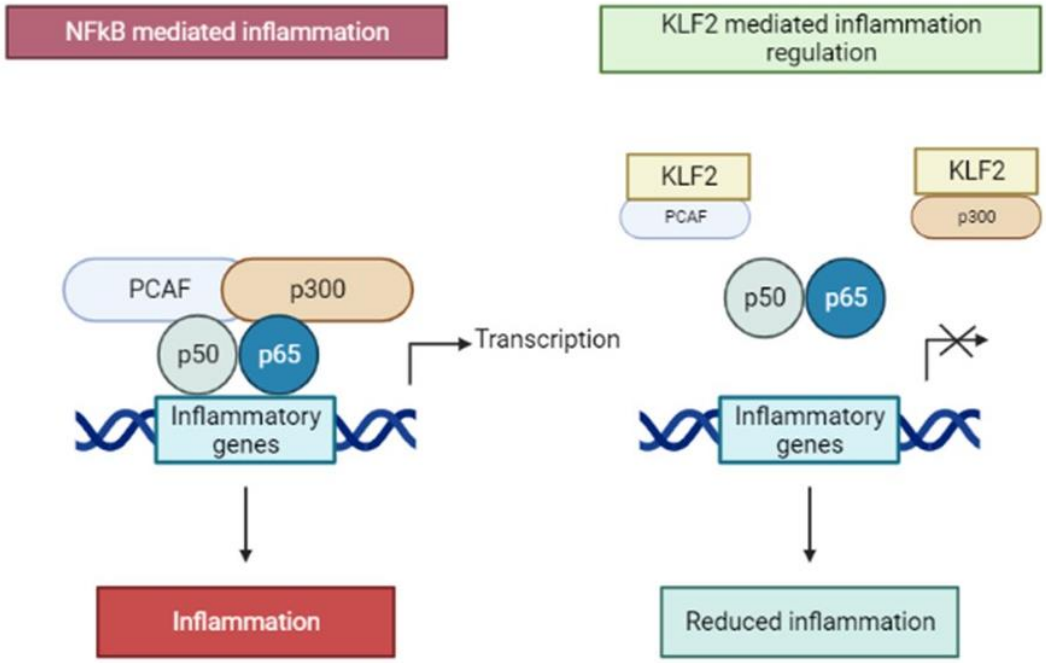

Figure 6.2: Transcriptional regulation of NFκB and KLF2. NFκB and KLF2 compete for transcriptional cofactors, PCAF and p300, with subsequent binding leading to transcriptional activity of corresponding transcription factor (Jha and Das, 2017).

TLR4 has also been shown to result in oxidative stress of human endothelial cells under OSS, with downstream effects on targets such as NOX2 and eNOS (Wang *et al.*, 2019). Under oxidative stress, NRF2 activation is known to upregulate a plethora of antioxidant response genes, which within the endothelium promotes athero- protection and endothelial homeostasis. However, under OSS, NRF2 TFAR activity is reduced compared to LSS. OSS dependent increases in oxidative stress promotes a redox imbalance and potentiates the unfolded protein response (UPR) (Saha *et al.*, 2020) (Lenna, Han and Trojanowska, 2014). Sustained oxidative stress leads to a disruption in the folding mechanism and enhances the production of misfolded protein giving rise to an

increase in ER stress. The UPR is a multifactorial signalling and transcriptional pathway, aimed at reducing ER stress via a reduction in transcription and translation to allow proper folding of proteins with the endoplasmic reticulum (Zhou and Tabas, 2013)(Civelek *et al.*, 2009). The UPR is mediated by ER-membrane-localised, Inositol-Requiring Protein 1 (IRE1). Under ER stress, IRE1 is activated leading to the sustained splicing and subsequent activation of X-box-binding protein 1 (XBP1), leading to translational frameshift and activated forms of XBP1 (Zeng *et al.*, 2009). This activation of the transcription factor XBP1 is crucial for the increased production of UPR target genes which facilitate protein folding within the ER. OSS has been shown to result in the sustained splicing of XBP1, resulting in increased rates of apoptosis in endothelial cells and subsequent cellular loss from blood vessels as demonstrated in ex-vivo cultures (Zeng *et al.*, 2009)(Tsuru *et al.*, 2016). Our data supports the notion of sustained XBP1 splicing and activation under OSS, potentially linked with the lower levels of NRF2 TFAR activity and subsequent gene expression that promotes a redox imbalance.

6.3 BPA Exposure May Result in an Increased Risk of Atherosclerosis via TLR4 Signalling

We have previously discussed the key interactions and the transcriptional regulation of atherosclerosis quantified by the TFARs included in E-Sense. Data discussed in this chapter thus far centred around the creation and validation of a high-throughput, flexible cell- based platform to determine cardiovascular risk. We opted to test the utility of this platform to determine the potential cardiovascular risk of microplastic BPA.

BPA is one of most widely used plastic worldwide due to its versatility and unique characteristics, with an estimated >5billion metric pounds (2.3 million tonnes)

produced each year (Fouyet *et al.*, 2021). It is becoming increasingly apparent, that due to ubiquitous exposure, BPA particulates have become a resident in circulating our body's Research into the effects of BPA have described it as a potential endocrine and neurological modulator, with effects on oestrogen levels widely described (Thoene *et al.*, 2020). However, little research into the effects of BPA on the cardiovascular system has been performed. Unlike historical research on risk factors such as cigarette use, the ubiquitous nature of BPA exposure will make associations with increased CVD hard to associate as there are few populations with low exposure to act as controls. Even so, direct evidence for a link between BPA exposure and adverse cardiovascular health may not be apparent for several decades. This highlights a potential niche for E-Sense to evaluate the potential cardiovascular risk posed by BPA exposure.

Quantification of TFAR activity demonstrates that BPA downregulates key atheroprotective signalling pathways in LSS, while promoting inflammatory and cell stress pathways. There is a potential signature that suggests TLR4 may act as a receptor for BPA and elevate IRF3 and NFκB signalling that interferes with the protective pathways controlled by KLF2 and Nrf2, however this requires further experiments to determine whether this is the case. As discussed previously, TLR4 signalling results in the activation of IRF3 and NFκB. Our results show a significant increase in IRF3 TFAR activity under both OSS and LSS conditions, and increase in NFκB TFAR activity under LSS. Concurrently with this a reduction in KLF2 and Nrf2 TFAR activity may in part result from increased NFκB-dependent signalling (as observed with TNFα treatment). The reduction in NRF2 TFAR activity and by implication reduced antioxidant gene expression may have secondary effects in elevating oxidative stress, that could promote ER stress and XBP1 TFAR activation (Ahmed *et al.*, 2017)(Park, Kang and So, 2021). Further experiments are required to confirm if these interactions

are correct, but highlight the utility of using a panel of TFARs for compound screening, not only to identify potential cardiovascular risk, but also for informing future studies to better understand the mechanism promoting this risk and possible interventions to mitigate risk.

6.4 Limitations and Future Work

While this study clearly implicates the potential risk of BPA on cardiovascular health using our E-Sense platform, it is not without its limits. One of main drawbacks demonstrated in our data and an ideal candidate for future refinement, is the use of the previously made TFARs, NFκB-VLuc and AP1-VLuc. Our data demonstrates a reduced dynamic range of these TFARs in comparison to the TFARs generated using the alternative spacing design, limiting the ability to quantify significant changes in TFAR activity. Our model implicates the potential mechanism of action of BPA on the transcriptional control of atherosclerosis via TLR4 signalling, however, the precise mechanism will require further study to define its role in mediating the observed effects of BPA. Further research into understanding the mechanism of action would aim to interfere with TLR4 signalling from our HCAECPro cell line and expose them to BPA. There are several avenues that could be used to achieve this. There are currently a variety of TLR4 inhibitors and peptides available commercially (e.g., TIRAP from NOVUSBIO), additionally siRNA knockdown of TLR4 could be implemented. My incorporating a TLR4 knockdown into our HCAECPro cell line, we would be able to observe any conformational changes in IRF3 and NFκB signalling. If IRF3 and NFκB signalling was reduced, it would provide a good indication the active transcriptional activity is being modulated via TLR4 and the MyD88-dependent and independent pathways.

A clear limitation of this body of work is the incorporation of only human coronary

artery endothelial cells. Atherosclerosis is a multifactorial disease incorporating a host of innate responses from a variety of cell types such as vascular smooth muscle cells. Although plaque formation occurs within the endothelium, clearly implying the role of human coronary artery endothelial cells as a prime target for research, atherosclerosis is generally termed a chronic inflammatory disease with intimal hyperplasia and leukocyte trafficking key mediators of the progression of the disease. Our model provides a good foundation for the prediction of a compounds ability to drive disease, however, future work could aim to build upon this model as with previously stated 3D models. Our model can be categorised as a 2D model with the addition of haemodynamic environments. Previous work in this area and improvements could be made in the areas of co-culture. Actin remodelling of the endothelium and therefore remodelling of the underlying extracellular matrix is a key component of atherosclerosis initiation and progression. The remodelling and alteration of the vascular smooth muscle bed has not been explored within our research and may confer additional changes which in turn may drive more profound changes.

The underlying aim of this project is to provide a model to predict a compounds ability to drive atherosclerosis plaque formation in an erosion model. However, atherosclerosis falls under two major categories of plaque rupture and plaque erosion. Many of the transcriptional hubs associated with plaque formation and its initiation are also present in ruptured plaques.

The E-Sense platform has the ability to contribute to the ‘3Rs’ in cardiovascular research of Replacement, Refinement and Reduction of *in vivo* preclinical models. Firstly, compound screening using E-Sense, can replace a proportion of experiments, if it results in no effect being observed. It can reduce and refine *in vivo* experiments, by defining a biologically relevant dose and highlighting the most appropriate therapeutic strategies to mitigate cardiovascular risk.

Additionally, it can provide a platform for screening therapeutic compound to take forward into preclinical models to alleviate cardiovascular risk. However, there will always be the necessity to perform targeted *in vivo* experiments to examine the complex interplay of the cells within the arterial wall that is responsible for the formation of atherosclerotic plaques. The modular design of the E-sense platform allows for further expansion as the understanding of disease increased, with additional TFARs to quantify novel disease-regulating pathways. Complimenting E-Sense with M(acrophage)-Sense and S(mooth muscle cell)-Sense may provide additional utility to evaluate cardiovascular risk, with tailored TFAR panels for each cell type relevant

to disease process. A combination of cell-based models may therefore provide a robust platform for further reducing and refining *in vivo* experiments.

6.5 Conclusions

In conclusion, this thesis has described the generation of a flexible endothelial-cell based platform capable of screening of compounds with a potential of effecting cardiovascular health. Innovation in TFAR design has increased the sensitivity in quantifying TF activity. The generation of the HCAECPro line provides a cost- effective approach for future research, proving to be a powerful and valuable resource. We defined the maximal responses of TFAR activity within the E-Sense platform to provide benchmarks for interpreting the modulation of TF activity. Finally, we have identified that BPA treatment induces a response in E-Sense that infers potential cardiovascular risk and a potential role for TLR4 revealing an area of further research and potential therapeutic target for mitigating the risk imposed by BPA exposure.

6.6 **Summary**

- Overexpressing BMI1 and hTERT in primary human coronary artery endothelial cells, resulted in a cell line (HCAECPro) with a reduction in senescent markers as well as an increase in proliferative capacity.
- HCAECPro cells appear indistinguishable from primary cell counterparts and retain key endothelial mechanosensing traits.
- Our novel TFAR design has resulted in the generation of reporters with a greatly enhanced dynamic range in comparison to currently available.
- Under laminar flow, TNFα suppresses Nrf2 upregulation, previously unknown.
- Under laminar flow, atorvastatin increases KLF2 upregulation, however, under oscillatory flow we see no significant aleration of KLF2 transcriptional activity.
- Under laminar flow, BPA at 10ppm significantly decreases the protective signalling pathway upregulation of NRF2 and KLF2 while simultaneously upregulating NFκB under LSS.
- BPA at 10ppm increases IRF3 transcriptional activity under LSS and OSS, implicating a TLR4 mechanism of action.

Table 7.1 Primers Used

Primer	Company	Sequence
cPPT FW	Merck	GATCTCGACGGTCGCCAAAT
NLuc Rev	Merck	GCCAGTCCCCAACGAAACTC
VLuc Rev	Merck	CAGCTGGTAGGCACGGTATT
CDKN2A (P16)	Merck	CGAGCTCGGCCCTGGAG TCGGGCGCTGCCCATCAT
CDKN1A (P21)	Merck	CTCAGGGTCGAAAACGGCGG GTGGGCGGATTAGGGCTTCCT
TP53 (P53)	Merck	TAGCGATGGTCTGGCCCCTCC GATGGGCCTCCGGTTCATGC
KLF2	Merck	TCACACCTGCAGCTACGCGG GAGCGCGCAAACTTCCAGCC
KLF4	Merck	TGGACCCCCTCTCAGCAATG CTCTTGGTAATGGAGCGGCG
eNOS	Merck	GCCGGAACAGCACAAGAGT GAGGATGCCAAGGCCGC
NOV	Merck	TGGTGCGGCCCTGTGAACAA AGCGGCCATCACTGCAGACC
PI16	Merck	ATGTGCGGCCACTACACGCA CCTTCACGTTCCCCGGAGGC
IκBα	Merck	CGCCCAAGCACCCGGATACA AACGTCAGACGCTGGCCTCC
OSGIN1	Merck	GGGAGCCTGGCACTCCATCG CCCGGCTGTTGCGAAGACCT
OSGIN2	Merck	TTGGTGACAACTTGGGGCGA GCCCTCAAGGCCCTCAGACA

Table 7.2 Antibodies Used

Antibody	Company	Species
Vinculin	**Merck**	**Mouse**
Phalloidin (stain)	**Merck**	**-**
VE-Cadherin	**Cell Signalling**	**Rabbit**
β-catenin	**BD Transduction**	**Mouse**
vWF	**Abcam**	**Mouse**
Thrombomodulin	**Abcam**	**Rabbit**

7.1 Transcript Variants

KLF2 binding site from eNOS promoter confirmed by gel shift studies (CACCC consensus) [1]

Wild type probe:
5’ GTCATGGGGGTGTGGGGGTTCCAGGAAAT
5’ ATTTCCTGGAACCCCCACACCCCCATGAC (matches if you reverse…)

Mutant probe (no binding):
5’ GTCATGGTATTTTAAGGGTTCCAGGAAAT
5’ ATTTCCTGGAACCCTTAAAATACCATGAC

Separate centres of the binding sites by 21 bp to make the proteins align on the
helical pitch of the DNA. Red highlight for centre marker…

ATT sites at each end
XXCCCCACACCCCCATXXXXXXXCCCCACACCCCCATXXXXXXXCCCCACACCCCCATXXXXXXXCCCCACACCCCCATXXXXX XXCCCCACACCCCCATXX

KLF1 consensus appears to be (G/A)CCACACCC(A/T/C) [2]
CCCCACACCCCCAT
Therefore we can introduce more wobble in the blue highlighted sections to reduce the GC content of the binging site for second attempt.

ACAAGTTTGTACAAAAAAGCAGGCTTCATCACCACACCCTCATTAGACAACCCCACACCCCCATATACGATCGCCACACCCACATTAATCGAACCCACACCCACATAATACTACGCCACACCCTCATATTTACACACCACACCCCCATAAGACCCAGC TTTCTTGTACAAAGTGGT

Nrf2

Function	Species	Gene	Element	Orientation	Sequence	Position of 5′ T in 'core' from TSS	Reference
Antioxidant enzymes	Human	*GCLC*	ARE-4/AP1	reverse	TCcccGTGACtcaGCG	−3118	227
	Human	*GCLM*	EpRE	reverse	agAcaATGACtaaGCA	−291 (ATG)	217
			ARE (var)	forward	TAAcgGTtACgaaGCA	−330 (ATG)	70
	Human	*GPX2*	ARE-1	reverse	cCAggATGACttaGCA	−76	13
			ARE-2	reverse	gtAcaGTGAgaggGCA	−387	13
	Mouse	*Gsr1*	ARE-1	reverse	TCgccGTGACtaaGCA	−35	100
			ARE-2	reverse	TCAcaGTGACcaaGCG	−804	100
	Human	*PRDX1*	EpRE-1	forward	TgtaacTGAatcaGCc	−3429 (ATG)	163
			EpRE-2	forward	TtctccTGcCtcaGCc	−4322 (ATG)	163
	Human	*PRDX6*	ARE	forward	gCAacGTGACcgaGCc	−349 (ATG)	38
	Mouse	*Slc7a11*	EpRE-2	reverse	cCAgctTGAgaaaGCG	−440 (ATG)	272
	Rat	*SRXN1*	ARE-1/AP1	forward	TCAcccTGAgtcaGCG	−247	285
	Human	*TRX*	ARE/AP1	forward	TCAccGTtACtcaGCA	−416	162
	Human	*TXNRD1*	ARE	reverse	TCAgaATGACaaaGCA	−301	268
Metal-binding proteins	Mouse	*Fth1*	FER1	forward	cCtccATGACaaaGCA	−4076	305
			AP1/NF-E2	reverse	cCAccGTGACtcaGCA	−4023	305
	Mouse	*Ftl1*	EpRE	forward	TCAgcGTGACtcaGCA	−1118	116
	Human	*FTL*	MARE/ARE	forward	TCAgcATGACtcaGCA	−1565 (ATG)	116
	Mouse	*Mt1*	ARE	forward	ggcgcGTGACtatGCG	−69	46
	Human	*MT1B*	ARE	reverse	gAgcaGTGACctgGCc	−99	46
	Mouse	*Mt2*	ARE/AP1	forward	ggggtGTGACtcaGCG	−214	46
Detoxication proteins	Mouse	*Akr1b3*	ARE-1	forward	ggAgcATGACccaGCA	−925	241
	Human	*AKR1C2*	ARE	reverse	TCAggGTGACtcaGCA	−5522	200
	Mouse	*Gsta1*	EpRE	forward	TAAtgGTGACaaaGCA	−728	84
	Rat	*GSTA2*	ARE	forward	TAAtgGTGACaaaGCA	−696	270
	Mouse	*Gsta3*	ARE	forward	cAggcATGACattGCA	−147	143
	Rat	*GSTP1*	GPEI/AP1	forward	TCActATGATtcaGCA	−2528	245
	Human	*MGST1*	EpRE	forward	aCAtcGTGACaaaGCA	−499	153
	Mouse	*Mrp2*	ARE-1	forward	ctgggATGACataGCA	−94	312
	Mouse	*Nqo1*	ARE	forward	TCAcaGTGAgtcgGCA	−435	239
	Rat	*NQO1*	ARE	forward	TCAcaGTGACttgGCA	−421	77
	Human	*NQO1*	ARE/AP1	forward	TCAcaGTGACtcaGCA	−463	140
	Human	*UGT1A1*	ARE	forward	aAAcccgGACttgGCc	−3296	341
			ARE 'core'		TGACnnnGC		270
			ARE 'consensus'		TMAnnRTGAYnnnGCR		319
			AP1-binding site		TGAStca		7

[3]

So the consensus is: TMAnnRTGAYnnnGCR
T(A/C)Ann(A/G)TGA(C/T)nnnGC(A/G)

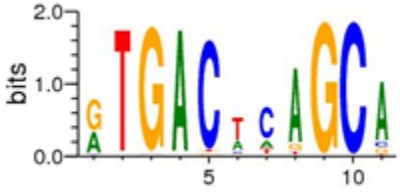

from motifmap So
T(A/C)Ann(A/G)TGA(**C)**TCAGC(**A**)
Therefore use this:
XXTAAnnATGACTCAGCAXXXXXTCAnnGTGACACAGCAXXXXXTAAnnGTGAC
TCAGCAXXXXXTCAnnATGACTCAGCAXXXXXTAAnnATGACTCAGCAXXXXX
T CAnnGTGACACAGCAXX

IRF3

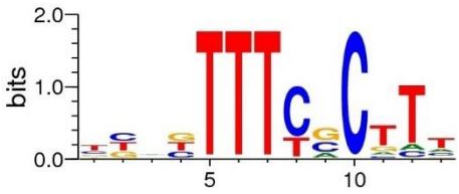

motifmap is different from these

J. Leukoc. Biol. 98: 119–128; 2015

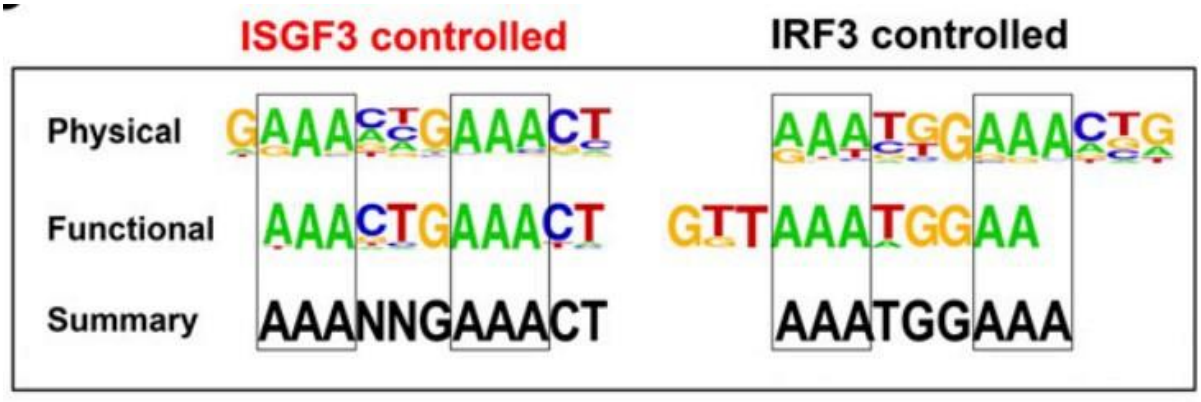

This is close to the reverse complement of motifmap TTTCCATTT

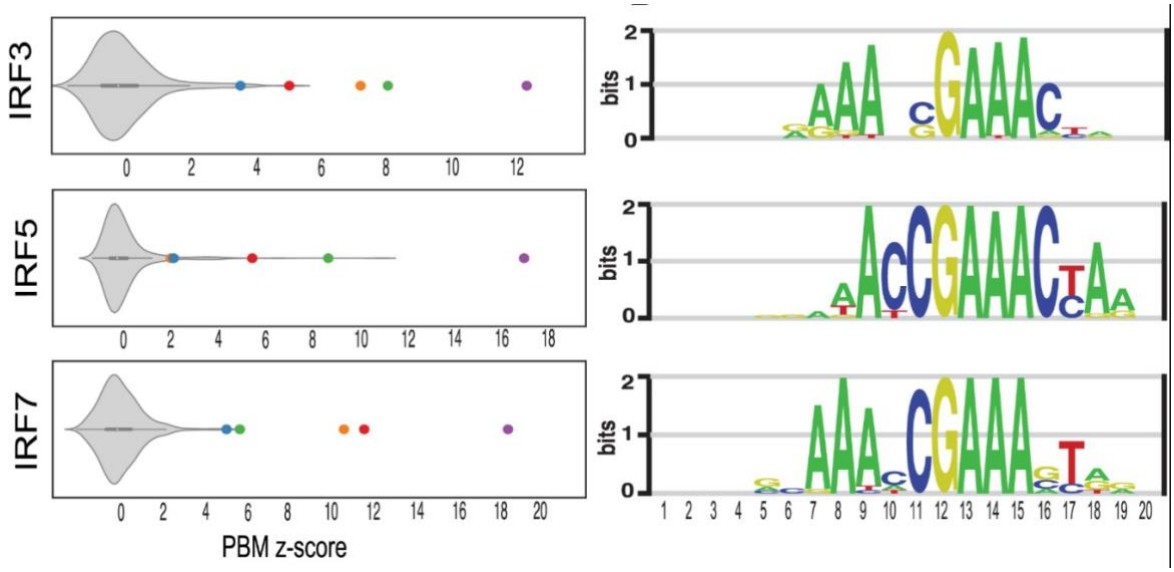

[4]
IRF3 and IRF7 are downstream of TLR4, so not a problem if you get overlap in binding.
So Go for GAAATCGAAA as the cores site. With flanking bp:
AACCGAAATCGAAACTG

XXAACCGAAATCGAAACTGXXXXAACCGAAATCGAAACTGXXXXAACCGAAAT
CGAAACTGXXXXAACCGAAATCGAAACTGXXXXAACCGAAATCGAAACTGXX XAACCGAAATCGAAACTGXX

Page Break
XBP-1

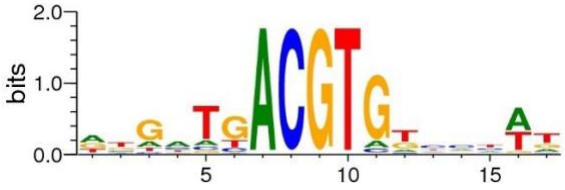

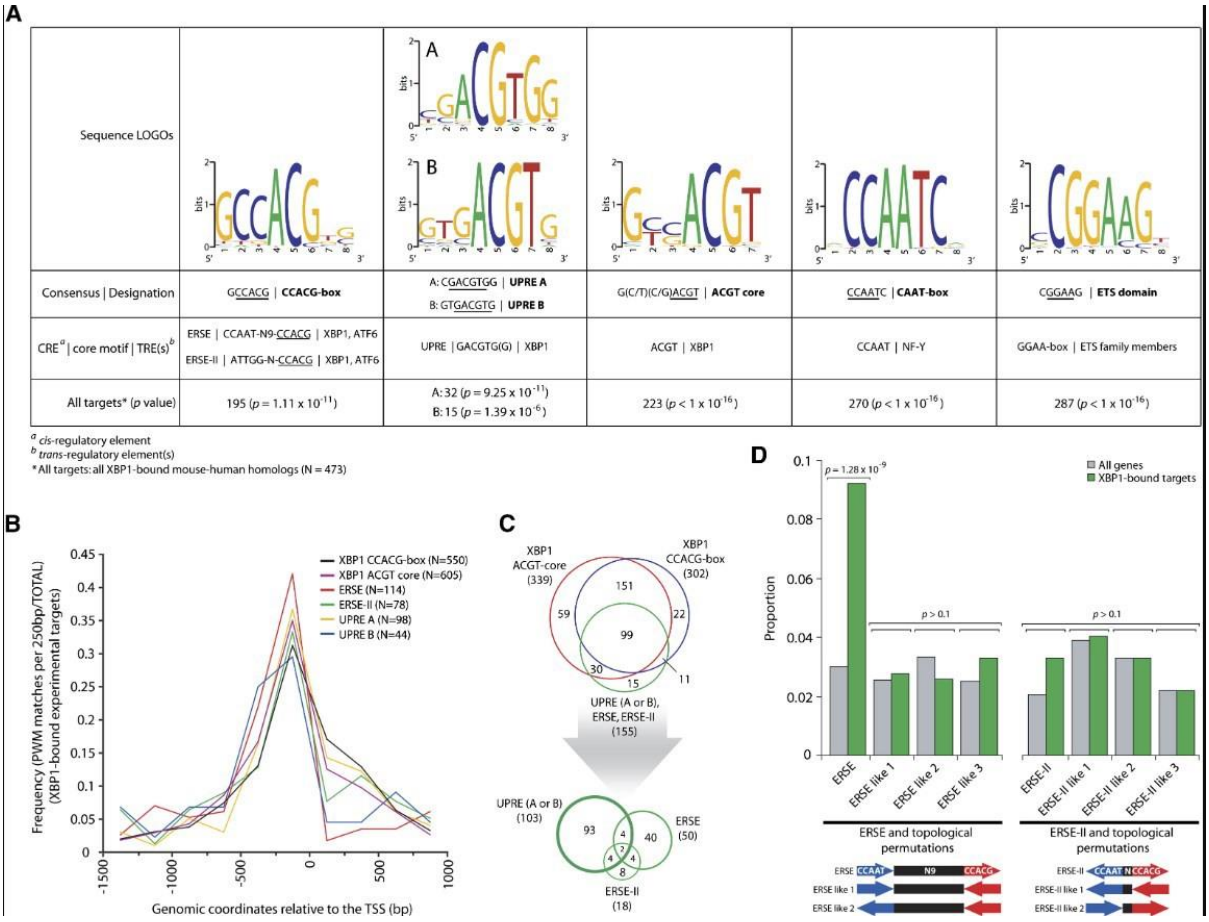

[5]

Taken together the core is ACGT

From ERSE-II you would have ATTGGnCCACGTG (ERSE would introduce a CCAAT box)

UPRE A CGACGTGG UPRE B GTGACGTG ACGT core G(C/T)(C/G)ACGT

ATTGGnCCACGTG

CGACGTGG GTGACGTG

G(C/T C/G)ACGT

so a consensus would be the ACGT core which also has the largest number of genes it that group.

XXATTGGGCCACGTGTXXXATXXATTGGGCGACGTGTXXXATXXATTGGGTGA

CGTGTXXXATXXATTGGGCCACGTGTXXXATXXATTGGGCGACGTGTXXXATX XATTGGGTGACGTGTXXXATXX

Be careful not to create any ATGs

8.0 References

Ahmed, S. M. U. *et al.* (2017) 'Nrf2 signaling pathway: Pivotal roles in inflammation', *Biochimica et Biophysica Acta - Molecular Basis of Disease*. doi: 10.1016/j.bbadis.2016.11.005.

Alhayaza, R. *et al.* (2020) 'The Relationship Between Reactive Oxygen Species and Endothelial Cell Metabolism', *Frontiers in Chemistry*. doi: 10.3389/fchem.2020.592688.

Asadinezhad, A. *et al.* (2012) 'Recent progress in surface modification of polyvinyl

chloride', *Materials*. doi: 10.3390/ma5122937.

Baird, L. and Yamamoto, M. (2020) 'The Molecular Mechanisms Regulating the KEAP1-NRF2 Pathway', *Molecular and Cellular Biology*. doi: 10.1128/mcb.00099- 20.

Baker, D. J. *et al.* (2016) 'Naturally occurring p16 Ink4a-positive cells shorten healthy lifespan', *Nature*. doi: 10.1038/nature16932.

Bazarov, A. V. *et al.* (2010) 'p16INK4a-mediated suppression of telomerase in normal and malignant human breast cells', *Aging Cell*. doi: 10.1111/j.1474-9726.2010.00599.x.

Bentzon, J. F. *et al.* (2014) 'Mechanisms of plaque formation and rupture', *Circulation Research*. doi: 10.1161/CIRCRESAHA.114.302721.

Boon, R. A. *et al.* (2010) 'KLF2-induced actin shear fibers control both alignment to flow and JNK signaling in vascular endothelium', *Blood*. doi: 10.1182/blood-2009- 06-228726.

Boon, R. A. and Horrevoers, A. J. G. (2009) 'Key transcriptional regulators of the vasoprotective effects of shear stress', *Hamostaseologie*. doi: 10.1055/s-0037- 1616937.

Cai, Y., Li, J. D. and Yan, C. (2013) 'Vinpocetine attenuates lipid accumulation and atherosclerosis formation', *Biochemical and Biophysical Research Communications*. doi: 10.1016/j.bbrc.2013.03.092.

Chan, K., Han, X. D. and Kan, Y. W. (2001) 'An important function of Nrf2 in combating oxidative stress: Detoxification of acetaminophen', *Proceedings of the National Academy of Sciences of the United States of America*. doi: 10.1073/pnas.081082098.

Chen, B. *et al.* (2015) 'The role of Nrf2 in oxidative stress-induced endothelial injuries', *Journal of Endocrinology*. doi: 10.1530/JOE-14-0662.

Chien, S. (2008) 'Effects of disturbed flow on endothelial cells', *Annals of Biomedical Engineering*. doi: 10.1007/s10439-007-9426-3.

Chistiakov, D. A., Orekhov, A. N. and Bobryshev, Y. V. (2017) 'Effects of shear stress on endothelial cells: go with the flow', *Acta Physiologica*. doi: 10.1111/apha.12725.

Chiu, J. J. and Chien, S. (2011) 'Effects of disturbed flow on vascular endothelium: Pathophysiological basis and clinical perspectives', *Physiological Reviews*. doi: 10.1152/physrev.00047.2009.

Civelek, M. *et al.* (2009) 'Chronic endoplasmic reticulum stress activates unfolded protein response in arterial endothelium in regions of susceptibility to atherosclerosis', *Circulation Research*. doi: 10.1161/CIRCRESAHA.109.203711.

Conway, D. E. *et al.* (2013) 'Fluid shear stress on endothelial cells modulates mechanical tension across VE-cadherin and PECAM-1', *Current Biology*. doi: 10.1016/j.cub.2013.04.049.

Cullinan, S. B. *et al.* (2003) 'Nrf2 Is a Direct PERK Substrate and Effector of PERK-Dependent Cell Survival', *Molecular and Cellular Biology*. doi: 10.1128/mcb.23.20.7198-7209.2003.

D'Auria, F. *et al.* (2015) 'Tumor Necrosis Factor Related Apoptosis Inducing Ligand (Trail) in Endothelial Response to Biomechanical and Biochemical Stresses in Arteries', *Journal of Cellular Biochemistry*. doi: 10.1002/jcb.25223.

Dabravolski, S. A. *et al.* (2022) 'The Role of KLF2 in the Regulation of Atherosclerosis Development and Potential Use of KLF2-Targeted Therapy', *Biomedicines*. doi: 10.3390/biomedicines10020254.

Dang, D. T., Pevsner, J. and Yang, V. W. (2000) 'The biology of the mammalian Krüppel-like family of transcription factors', *International Journal of Biochemistry and Cell Biology*. doi: 10.1016/S1357-2725(00)00059-5.

Davignon, J. and Ganz, P. (2004) 'Role of endothelial dysfunction in atherosclerosis', *Circulation*. doi: 10.1161/01.cir.0000131515.03336.f8.

Davis, M. E. *et al.* (2004) 'Shear Stress Regulates Endothelial Nitric-oxide Synthase Promoter Activity through Nuclear Factor κB Binding', *Journal of Biological Chemistry*. doi: 10.1074/jbc.M307528200.

den Dekker, W. K. *et al.* (2010) 'Toll like receptor 4 in atherosclerosis and plaque destabilization', *Atherosclerosis*. doi: 10.1016/j.atherosclerosis.2009.09.075.

Deshmukh, P. *et al.* (2017) 'The Keap1–Nrf2 pathway: promising therapeutic target to counteract ROS-mediated damage in cancers and neurodegenerative diseases', *Biophysical Reviews*. doi: 10.1007/s12551-016-0244-4.

Doddaballapur, A. *et al.* (2015) 'Laminar shear stress inhibits endothelial cell metabolism via KLF2-mediated repression of PFKFB3', *Arteriosclerosis,*

Thrombosis, and Vascular Biology. doi: 10.1161/ATVBAHA.114.304277.

Dolan, J. M., Kolega, J. and Meng, H. (2013) 'High wall shear stress and spatial gradients in vascular pathology: A review', *Annals of Biomedical Engineering*. doi: 10.1007/s10439-012-0695-0.

Doyle, S. E. *et al.* (2002) 'IRF3 Mediates a TLR3/TLR4-Specific Antiviral Gene

Program', *Immunity*. doi: 10.1016/S1074-7613(02)00390-4.

Emini Veseli, B. *et al.* (2017) 'Animal models of atherosclerosis', *European Journal of Pharmacology*. doi: 10.1016/j.ejphar.2017.05.010.

Fan, J. *et al.* (2015) 'Rabbit models for the study of human atherosclerosis: From pathophysiological mechanisms to translational medicine', *Pharmacology and Therapeutics*. doi: 10.1016/j.pharmthera.2014.09.009.

Fouyet, S. *et al.* (2021) 'Bisphenol A, bisphenol F, and bisphenol S: The bad and

the Ugly. where is the good?', *Life*. doi: 10.3390/life11040314.

Fuster, V. and Kovacic, J. C. (2014) 'Acute coronary syndromes: Pathology, diagnosis, genetics, prevention, and treatment', *Circulation Research*. doi: 10.1161/CIRCRESAHA.114.302806.

de Galarreta, M. R. *et al.* (2016) 'Unfolded protein response induced by Brefeldin A increases collagen type I levels in hepatic stellate cells through an IRE1α, p38 MAPK and Smad-dependent pathway', *Biochimica et Biophysica Acta - Molecular Cell Research*. doi: 10.1016/j.bbamcr.2016.05.002.

Gangnuss, S. *et al.* (2004) 'Regulation of MAPK activation, AP-1 transcription factor expression and keratinocyte differentiation in wounded fetal skin', *Journal of Investigative Dermatology*. doi: 10.1111/j.0022-202X.2004.22319.x.

Ganley, I. G. *et al.* (2011) 'Distinct Autophagosomal-Lysosomal Fusion Mechanism Revealed by Thapsigargin-Induced Autophagy Arrest', *Molecular Cell*. doi: 10.1016/j.molcel.2011.04.024.

Gareus, R. *et al.* (2008) 'Endothelial cell-specific NF-kappaB inhibition protects mice from atherosclerosis', *Cell Metabolism*.

Gaziano, T. A. *et al.* (2010) 'Growing Epidemic of Coronary Heart Disease in Low- and Middle-Income Countries', *Current Problems in Cardiology*. doi: 10.1016/j.cpcardiol.2009.10.002.

Genuis, S. J. *et al.* (2012) 'Human excretion of bisphenol A: Blood, urine, and sweat (BUS) study', *Journal of Environmental and Public Health*. doi: 10.1155/2012/185731.

Gerona, R. R. *et al.* (2016) 'Direct measurement of Bisphenol A (BPA), BPA glucuronide and BPA sulfate in a diverse and low-income population of pregnant women reveals high exposure, with potential implications for previous exposure estimates: A cross-sectional study', *Environmental Health: A Global Access Science Source*. doi: 10.1186/s12940-016-0131-2.

Gerona, R., vom Saal, F. S. and Hunt, P. A. (2020) 'BPA: have flawed analytical techniques compromised risk assessments?', *The Lancet Diabetes and Endocrinology*. doi: 10.1016/S2213-8587(19)30381-X.

Getz, G. S. and Reardon, C. A. (2006) 'Diet and murine atherosclerosis', *Arteriosclerosis, Thrombosis, and Vascular Biology*. doi: 10.1161/01.ATV.0000201071.49029.17.

Getz, G. S. and Reardon, C. A. (2012) 'Animal models of Atherosclerosis', *Arteriosclerosis, Thrombosis, and Vascular Biology*. doi: 10.1161/ATVBAHA.111.237693.

Getz, G. S. and Reardon, C. A. (2016) 'Do the Apoe-/- and Ldlr-/- mice yield the same insight on atherogenesis?', *Arteriosclerosis, Thrombosis, and Vascular Biology*. doi: 10.1161/ATVBAHA.116.306874.

Ghim, C. M. *et al.* (2010) 'The art of reporter proteins in science: Past, present and future applications', *BMB Reports*. doi: 10.3858/BMBRep.2010.43.7.451.

Gimbrone, M. A. and García-Cardeña, G. (2016) 'Endothelial Cell Dysfunction and the Pathobiology of Atherosclerosis', *Circulation Research*. doi: 10.1161/CIRCRESAHA.115.306301.

Gonzalez, L. *et al.* (2018) 'Hyperglycemia aggravates diet - Induced coronary artery disease and myocardial infarction in SR -B1 -Knockout/ApoE - Hypomorphic mice', *Frontiers in Physiology*. doi: 10.3389/fphys.2018.01398.

Hahn, C. and Schwartz, M. A. (2009) 'Mechanotransduction in vascular physiology and atherogenesis', *Nature Reviews Molecular Cell Biology*. doi: 10.1038/nrm2596.

Haldar, S. M., Ibrahim, O. A. and Jain, M. K. (2007) 'Kruppel-like Factors (KLFs) in muscle biology', *Journal of Molecular and Cellular Cardiology*. doi: 10.1016/j.yjmcc.2007.04.005.

Harhaj, E. W. and Dixit, V. M. (2011) 'Deubiquitinases in the regulation of NF-κB signaling', *Cell Research*. doi: 10.1038/cr.2010.166.

Hazell, G. G. J. *et al.* (2016) 'PI16 is a shear stress and inflammation-regulated inhibitor of MMP2', *Scientific Reports*. doi: 10.1038/srep39553.

He, F., Ru, X. and Wen, T. (2020) 'NRF2, a transcription factor for stress response and beyond', *International Journal of Molecular Sciences*. doi: 10.3390/ijms21134777.

He, G. *et al.* (2005) ‘Induction of p21 by p53 following DNA damage inhibits both Cdk4 and Cdk2 activities’, *Oncogene*. doi: 10.1038/sj.onc.1208474.

Hengstler, J. G. *et al.* (2011) ‘Critical evaluation of key evidence on the human health hazards of exposure to bisphenol A’, *Critical Reviews in Toxicology*. doi: 10.3109/10408444.2011.558487.

Hoogendoorn, A. *et al.* (2019) ‘Multidirectional wall shear stress promotes advanced coronary plaque development: comparing five shear stress metrics’, *Cardiovascular Research*. doi: 10.1093/cvr/cvz212.

Houghton, C. A., Fassett, R. G. and Coombes, J. S. (2016) ‘Sulforaphane and Other Nutrigenomic Nrf2 Activators: Can the Clinician’s Expectation Be Matched by the Reality?’, *Oxidative Medicine and Cellular Longevity*. doi: 10.1155/2016/7857186.

Hu, C. *et al.* (2011) ‘Modification of Keap1 cysteine residues by sulforaphane’, *Chemical Research in Toxicology*. doi: 10.1021/tx100389r.

Huang, J. *et al.* (2021) ‘KLF2 Mediates the Suppressive Effect of Laminar Flow on Vascular Calcification by Inhibiting Endothelial BMP/SMAD1/5 Signaling’, *Circulation Research*. doi: 10.1161/CIRCRESAHA.120.318690.

Huang, Q. *et al.* (2012) ‘Distance and helical phase dependence of synergistic transcription activation in cis-regulatory module’, *PLoS ONE*. doi: 10.1371/journal.pone.0031198.

Ishii, T., Warabi, E. and Mann, G. E. (2021) ‘Mechanisms underlying unidirectional laminar shear stress-mediated Nrf2 activation in endothelial cells: Amplification of low shear stress signaling by primary cilia’, *Redox Biology*. doi: 10.1016/j.redox.2021.102103.

Ishikawa, K. *et al.* (2001) 'Heme oxygenase-1 inhibits atherosclerotic lesion formation in LDL-receptor knockout mice', *Circulation Research*. doi: 10.1161/01.RES.88.5.506.

Jain, M. *et al.* (2017) 'The rabbit model of accelerated atherosclerosis: A methodological perspective of the iliac artery balloon injury', *Journal of Visualized Experiments*. doi: 10.3791/55295.

Jain, M. K., Sangwung, P. and Hamik, A. (2014) 'Regulation of an Inflammatory Disease', *Arteriosclerosis, Thrombosis, and Vascular Biology*. doi: 10.1161/atvbaha.113.301925.

Jalal, N. *et al.* (2018) 'Bisphenol A (BPA) the mighty and the mutagenic', *Toxicology Reports*. doi: 10.1016/j.toxrep.2017.12.013.

Jha, P. and Das, H. (2017) 'KLF2 in regulation of NF-κB-mediated immune cell function and inflammation', *International Journal of Molecular Sciences*. doi: 10.3390/ijms18112383.

Jo, H. *et al.* (1997) 'Differential effect of shear stress on extracellular signal-regulated kinase and N-terminal jun kinase in endothelial cells: G(i)2- and Gβ/γ-dependent signaling pathways', *Journal of Biological Chemistry*. doi: 10.1074/jbc.272.2.1395.

Juckett, M. B. *et al.* (1995) 'Ferritin protects endothelial cells from oxidized low density lipoprotein in vitro', *American Journal of Pathology*.

Juers, D. H., Matthews, B. W. and Huber, R. E. (2012) 'LacZ β-galactosidase: Structure and function of an enzyme of historical and molecular biological importance', *Protein Science*. doi: 10.1002/pro.2165.

Kishimoto, Y., Kondo, K. and Momiyama, Y. (2019) 'The protective role of heme

oxygenase-1 in atherosclerotic diseases', *International Journal of Molecular Sciences*. doi: 10.3390/ijms20153628.

Ko, K. A. *et al.* (2017) 'En face preparation of mouse blood vessels', *Journal of*

Visualized Experiments. doi: 10.3791/55460.

Kuilman, T. *et al.* (2010) 'The essence of senescence', *Genes and Development*. doi: 10.1101/gad.1971610.

Kumar, A. *et al.* (2005) 'Tumor Necrosis Factor Alpha-Mediated Reduction of KLF2 Is Due to Inhibition of MEF2 by NF-κB and Histone Deacetylases', *Molecular and Cellular Biology*. doi: 10.1128/mcb.25.14.5893-5903.2005.

Kumar, V. (2020) 'Toll-like receptors in sepsis-associated cytokine storm and their endogenous negative regulators as future immunomodulatory targets', *International Immunopharmacology*. doi: 10.1016/j.intimp.2020.107087.

Kyriakis, J. M. (1999) 'Activation of the AP-1 transcription factor by inflammatory cytokines of the TNF family', in *Gene Expression*.

Lago, C. U. *et al.* (2011) '"'Go With the Flow'": How Kru¨ppel-Like Factor 2 Regulates the Vasoprotective Effects of Shear Stress', *Metabolism Clinical And Experimental*. doi: 10.1089/ars.2010.3647.

Lam, A. K. Y., Ong, K. and Ho, Y. H. (2008) 'hTERT expression in colorectal adenocarcinoma: Correlations with p21, p53 expressions and clinicopathological features', *International Journal of Colorectal Disease*. doi: 10.1007/s00384-008-0455-7.

Lang, I. A. *et al.* (2008) 'Association of Urinary Bisphenol A concentration with medical disorders and laboratory abnormalities in adults', *JAMA*. doi: 10.1001/jama.300.11.1303.

Lenna, S., Han, R. and Trojanowska, M. (2014) 'Endoplasmic reticulum stress and

endothelial dysfunction', *IUBMB Life*. doi: 10.1002/iub.1292.

Li, M. *et al.* (2020) 'Effects of bisphenol A at the safe reference dose on

abdominal
fat deposition in aged hens', *Ecotoxicology and Environmental Safety*. doi: 10.1016/j.ecoenv.2020.111398.

Lichtman, A. H. *et al.* (2013) 'Adaptive immunity in atherogenesis: New insights and therapeutic approaches', *Journal of Clinical Investigation*. doi: 10.1172/JCI63108.

Lieb, W. and Vasan, R. S. (2013) 'Genetics of coronary artery disease', *Circulation*. doi: 10.1161/CIRCULATIONAHA.113.005350.

Lim, K. H. and Staudt, L. M. (2013) 'Toll-Like receptor signaling', *Cold Spring Harbor Perspectives in Biology*. doi: 10.1074/jbc.R300028200.

Lin, B., Xu, D. and Leaman, D. W. (2016) 'X-linked inhibitor of apoptosis-associated factor 1 regulates TNF receptor 1 complex stability', *FEBS Letters*. doi: 10.1002/1873-3468.12467.

Linton, M. F. *et al.* (2019) 'The Role of Lipids and Lipoproteins in Atherosclerosis - Endotext - NCBI Bookshelf', *Endotext*.

Liu, H. *et al.* (2017) 'Ablation of interferon regulatory factor 3 protects against atherosclerosis in apolipoprotein e-deficient mice', *Hypertension*. doi: 10.1161/HYPERTENSIONAHA.116.08395.

Magid, R. and Davies, P. F. (2005) 'Endothelial protein kinase C isoform identity and differential activity of PKCζ in an athero-susceptible region of porcine aorta', *Circulation Research*. doi: 10.1161/01.RES.0000179767.37838.60.

Makeev, V. J. *et al.* (2003) 'Distance preferences in the arrangement of binding motifs and hierarchical levels in organization of transcription regulatory information', *Nucleic Acids Research*. doi: 10.1093/nar/gkg799.

Mankan, A. K. *et al.* (2009) 'NF-κB regulation: The nuclear response', *Journal of*

Cellular and Molecular Medicine. doi: 10.1111/j.1582-4934.2009.00632.x.

McHugh, D. and Gil, J. (2018) 'Senescence and aging: Causes, consequences, and therapeutic avenues', *Journal of Cell Biology*. doi: 10.1083/jcb.201708092.

Meir, K. S. and Leitersdorf, E. (2004) 'Atherosclerosis in the apolipoprotein E-deficient mouse: A decade of progress', *Arteriosclerosis, Thrombosis, and Vascular Biology*. doi: 10.1161/01.ATV.0000128849.12617.f4.

Meyne, J., Ratliff, R. L. and Moyzis, R. K. (1989) 'Conservation of the human telomere sequence (TTAGGG)(n) among vertebrates', *Proceedings of the National Academy of Sciences of the United States of America*. doi: 10.1073/pnas.86.18.7049.

Minchin, S. D. and Busby, S. J. W. (2013) 'Transcription Factors', in *Brenner's Encyclopedia of Genetics: Second Edition*. doi: 10.1016/B978-0-12-374984-0.01552-7.

Moi, P. *et al.* (1994) 'Isolation of NF-E2-related factor 2 (Nrf2), a NF-E2-like basic leucine zipper transcriptional activator that binds to the tandem NF-E2/AP1 repeat of the β-globin locus control region', *Proceedings of the National Academy of Sciences of the United States of America*. doi: 10.1073/pnas.91.21.9926.

Motahari, P. *et al.* (2015) 'Generation of stable ARE- driven reporter system for monitoring oxidative stress', *DARU, Journal of Pharmaceutical Sciences*. doi: 10.1186/s40199-015-0122-9.

Namat, A. *et al.* (2021) 'Association of BPA exposure during pregnancy with risk of preterm birth and changes in gestational age: A meta-analysis and systematic review', *Ecotoxicology and Environmental Safety*. doi: 10.1016/j.ecoenv.2021.112400.

Nandakumar, J. and Cech, T. R. (2013) 'Finding the end: Recruitment of

telomerase

to telomeres', *Nature Reviews Molecular Cell Biology*. doi: 10.1038/nrm3505.

Nanjappa, M. K., Simon, L. and Akingbemi, B. T. (2012) 'The industrial chemical bisphenol A (BPA) interferes with proliferative activity and development of steroidogenic capacity in rat Leydig cells', *Biology of Reproduction*. doi: 10.1095/biolreprod.111.095349.

Nayak, L., Lin, Z. and Jain, M. K. (2011) '"go with the flow": How Krüppel-like factor 2 regulates the vasoprotective effects of shear stress', *Antioxidants and Redox Signaling*. doi: 10.1089/ars.2010.3647.

De Nisco, N. J. *et al.* (2021) 'Manipulation of IRE1-Dependent MAPK Signaling by a Vibrio Agonist-Antagonist Effector Pair', *mSystems*. doi: 10.1128/msystems.00872-20.

Nogieć, A. *et al.* (2020) 'Phenotype and Response to PAMPs of Human Monocyte- Derived Foam Cells Obtained by Long-Term Culture in the Presence of oxLDLs', *Frontiers in Immunology*. doi: 10.3389/fimmu.2020.01592.

Oeckinghau, A. and Sankar, G. (2009) 'The NF-κB Family of Transcription Factors and Its Regulation', *Cold Spring Harbor perspectives in biology*.

Oh, Y. S. and Jun, H. S. (2018) 'Effects of glucagon-like peptide-1 on oxidative stress and Nrf2 signaling', *International Journal of Molecular Sciences*. doi: 10.3390/ijms19010026.

Ohore, O. E. and Songhe, Z. (2019) 'Endocrine disrupting effects of bisphenol A exposure and recent advances on its removal by water treatment systems. A review', *Scientific African*. doi: 10.1016/j.sciaf.2019.e00135.

Ouguerram, K. *et al.* (2004) 'Apolipoprotein B100 metabolism in autosomal-

dominant hypercholesterolemia related to mutations in PCSK9', *Arteriosclerosis, Thrombosis, and Vascular Biology*. doi: 10.1161/01.ATV.0000133684.77013.88.

Papadakis, E. *et al.* (2005) ‘Promoters and Control Elements: Designing Expression Cassettes for Gene Therapy’, *Current Gene Therapy*. doi: 10.2174/1566523044578077.

Park, S. M., Kang, T. Il and So, J. S. (2021) ‘Roles of XBP1s in transcriptional regulation of target genes’, *Biomedicines*. doi: 10.3390/biomedicines9070791.

Park, Y. *et al.* (2014) ‘The ubiquitin system in immune regulation’, in *Advances in Immunology*. doi: 10.1016/B978-0-12-800147-9.00002-9.

Parmar, K. M. *et al.* (2005) ‘Statins exert endothelial atheroprotective effects via the KLF2 transcription factor’, *Journal of Biological Chemistry*. doi: 10.1074/jbc.C500144200.

Passerini, A. G. *et al.* (2004) ‘Coexisting proinflammatory and antioxidative endothelial transcription profiles in a disturbed flow region of the adult porcine aorta’, *Proceedings of the National Academy of Sciences of the United States of America*. doi: 10.1073/pnas.0305938101.

Pasterkamp, G. *et al.* (2016) ‘Human validation of genes associated with a murine atherosclerotic phenotype’, *Arteriosclerosis, Thrombosis, and Vascular Biology*. doi: 10.1161/ATVBAHA.115.306958.

Pendse, A. A. *et al.* (2009) ‘Apolipoprotein E knock-out and knock-in mice: Atherosclerosis, metabolic syndrome, and beyond’, *Journal of Lipid Research*. doi: 10.1194/jlr.R800070-JLR200.

Pires, B. R. B. *et al.* (2018) ‘NF-kappaB: Two sides of the same coin’, *Genes*. doi: 10.3390/genes9010024.

Plump, A. S. *et al.* (1992) ‘Severe hypercholesterolemia and atherosclerosis in

apolipoprotein E-deficient mice created by homologous recombination in ES

cells', *Cell*. doi: 10.1016/0092-8674(92)90362-G.

Ponjavic, J. *et al.* (2006) 'Transcriptional and structural impact of TATA-initiation site spacing in mammalian core promoters', *Genome Biology*. doi: 10.1186/gb-2006-7- 8-r78.

Pua, L. J. W. *et al.* (2022) 'Functional Roles of JNK and p38 MAPK Signaling in Nasopharyngeal Carcinoma', *International Journal of Molecular Sciences*. doi: 10.3390/ijms23031108.

Qian, Y. and Chen, X. (2013) 'Senescence regulation by the p53 protein family',

Methods in Molecular Biology. doi: 10.1007/978-1-62703-239-1_3.

Roberts, R. (2014) 'Genetics of coronary artery disease', *Circulation Research*. doi: 10.1161/CIRCRESAHA.114.302692.

Saha, S. *et al.* (2020) 'An Overview of Nrf2 Signaling Pathway and Its Role in Inflammation', *Molecules (Basel, Switzerland)*. doi: 10.3390/molecules25225474.

Salama, R. *et al.* (2014) 'Cellular senescence and its effector programs', *Genes and Development*. doi: 10.1101/gad.235184.113.

Sangwung, P. *et al.* (2017) 'KLF2 and KLF4 control endothelial identity and vascular integrity', *JCI Insight*. doi: 10.1172/jci.insight.91700.

Sasso, A. F. *et al.* (2020) 'Pharmacokinetics of bisphenol A in humans following dermal administration', *Environment International*. doi: 10.1016/j.envint.2020.106031.

Satta, S. *et al.* (2017) 'The Role of Nrf2 in Cardiovascular Function and Disease',

Oxidative Medicine and Cellular Longevity. doi: 10.1155/2017/9237263.

Schnack, L. *et al.* (2019) 'Mechanisms of trained innate immunity in oxLDL

primed human coronary smooth muscle cells', *Frontiers in Immunology*. doi: 10.3389/fimmu.2019.00013.

Sen-Banerjee, S. *et al.* (2005) 'Kruppel-like factor 2 as a novel mediator of statin effects in endothelial cells', *Circulation*. doi: 10.1161/CIRCULATIONAHA.104.525774.

Sena, C. M., Pereira, A. M. and Seiça, R. (2013) 'Endothelial dysfunction - A major mediator of diabetic vascular disease', *Biochimica et Biophysica Acta - Molecular Basis of Disease*. doi: 10.1016/j.bbadis.2013.08.006.

Silvestre-Roig, C. *et al.* (2014) 'Atherosclerotic plaque destabilization: Mechanisms, models, and therapeutic strategies', *Circulation Research*. doi: 10.1161/CIRCRESAHA.114.302355.

Simmons, R. D., Kumar, S. and Jo, H. (2016) 'The role of endothelial mechanosensitive genes in atherosclerosis and omics approaches', *Archives of Biochemistry and Biophysics*. doi: 10.1016/j.abb.2015.11.005.

Sun, N., Youle, R. J. and Finkel, T. (2016) 'The Mitochondrial Basis of Aging', *Molecular Cell*. doi: 10.1016/j.molcel.2016.01.028.

Suzuki, T. *et al.* (2005) 'Vascular implications of the Krüppel-like family of transcription factors', *Arteriosclerosis, Thrombosis, and Vascular Biology*. doi: 10.1161/01.ATV.0000165656.65359.23.

Teasdale, J. E. *et al.* (2016) 'Cigarette smoke but not electronic cigarette aerosol activates a stress response in human coronary artery endothelial cells in culture', *Drug and Alcohol Dependence*. doi: 10.1016/j.drugalcdep.2016.04.020.

Teasdale, J. E. *et al.* (2017) 'Cigarette smoke extract profoundly suppresses TNFα- mediated proinflammatory gene expression through upregulation of ATF3 in human coronary artery endothelial cells', *Scientific Reports*. doi:

10.1038/srep39945.

Tebay, L. E. *et al.* (2015) 'Mechanisms of activation of the transcription factor Nrf2 by redox stressors, nutrient cues, and energy status and the pathways through which it attenuates degenerative disease', *Free Radical Biology and Medicine*. doi: 10.1016/j.freeradbiomed.2015.06.021.

Thoene, M. *et al.* (2020) 'Bisphenol S in food causes hormonal and obesogenic effects comparable to or worse than bisphenol a: A literature review', *Nutrients*. doi: 10.3390/nu12020532.

Thygesen, K. *et al.* (2019) 'Fourth universal definition of myocardial infarction (2018)', *European Heart Journal*. doi: 10.1093/eurheartj/ehy462.

Trifonov, E. N. (2016) 'Transcription factors operate TATA switches via rotational remodeling of local columnar chromatin structure', *Journal of Biomolecular Structure and Dynamics*. doi: 10.1080/07391102.2015.1134348.

Tsuru, A. *et al.* (2016) 'Novel mechanism of enhancing IRE1α-XBP1 signalling via the PERK-ATF4 pathway', *Scientific Reports*. doi: 10.1038/srep24217.

Ve, T. *et al.* (2017) 'Structural basis of TIR-domain-assembly formation in MAL- and MyD88-dependent TLR4 signaling', *Nature Structural and Molecular Biology*. doi: 10.1038/nsmb.3444.

Vergallo, R. *et al.* (2013) 'Correlation between degree of neointimal hyperplasia and incidence and characteristics of neoatherosclerosis as assessed by optical coherence tomography', *American Journal of Cardiology*. doi: 10.1016/j.amjcard.2013.05.076.

Verstak, B. *et al.* (2014) 'The TLR signaling adaptor TRAM interacts with TRAF6 to mediate activation of the inflammatory response by TLR4', *Journal of Leukocyte Biology*. doi: 10.1189/jlb.2a0913-487r.

Victorelli, S. and Passos, J. F. (2017) ‘Telomeres and Cell Senescence - Size

Matters Not’, *EBioMedicine*. doi: 10.1016/j.ebiom.2017.03.027.

Virmani, R., Burke, V. P. and Farb, A. (1999) ‘Plaque rupture and plaque erosion’,

in *Thrombosis and Haemostasis*. doi: 10.1055/s-0037-1615543.

Wan, F. and Lenardo, M. J. (2010) ‘The nuclear signaling of NF-κB: Current knowledge, new insights, and future perspectives’, *Cell Research*. doi: 10.1038/cr.2009.137.

Wang, L. *et al.* (2014) ‘Nrf2 signaling modulates cigarette smoke-induced complement activation in retinal pigmented epithelial cells’, *Free Radical Biology and Medicine*. doi: 10.1016/j.freeradbiomed.2014.01.015.

Wang, Z. *et al.* (2019) ‘Oscillatory shear stress induces oxidative stress via TLR4 activation in endothelial cells’, *Mediators of Inflammation*. doi: 10.1155/2019/7162976.

Warboys, C. M. *et al.* (2011) ‘The role of blood flow in determining the sites of atherosclerotic plaques’, *F1000 Medicine Reports*. doi: 10.3410/M3-5.

Wardyn, J. D., Ponsford, A. H. and Sanderson, C. M. (2015) ‘Dissecting molecular cross-talk between Nrf2 and NF-κB response pathways’, *Biochemical Society Transactions*. doi: 10.1042/BST20150014.

Waters, J. P., Pober, J. S. and Bradley, J. R. (2013) ‘Tumour necrosis factor and cancer’, *Journal of Pathology*. doi: 10.1002/path.4188.

Weber, C. and Noels, H. (2011) ‘Atherosclerosis: Current pathogenesis and

therapeutic options’, *Nature Medicine*. doi: 10.1038/nm.2538.

Westwick, J. K. *et al.* (1994) ‘Tumor necrosis factor α stimulates AP-1 activity

through prolonged activation of the c-Jun kinase', *Journal of Biological Chemistry*.

doi: 10.1016/s0021-9258(18)47207-9.

White, S. J., Newby, A. C. and Johnson, T. W. (2016) 'Endothelial erosion of plaques as a substrate for coronary thrombosis', *Thrombosis and Haemostasis*. doi: 10.1160/TH15-09-0765.

Wisniewski, P. *et al.* (2015) 'Adult exposure to bisphenol A (BPA) in Wistar rats reduces sperm quality with disruption of the hypothalamic-pituitary-testicular axis', *Toxicology*. doi: 10.1016/j.tox.2015.01.002.

Wong, A. K. *et al.* (2016) 'A Parallel-Plate Flow Chamber for Mechanical Characterization of Endothelial Cells Exposed to Laminar Shear Stress', *Cellular and Molecular Bioengineering*. doi: 10.1007/s12195-015-0424-5.

World Health Organization (2022) *Cardiovascular Diseases*, *Health topics*. Available at: https://www.who.int/health-topics/cardiovascular-diseases#tab=tab_1.

Xu, J. and Zou, M. H. (2009) 'Molecular insights and therapeutic targets for diabetic endothelial dysfunction', *Circulation*. doi: 10.1161/CIRCULATIONAHA.108.835223.

Xu, Y. Z. *et al.* (2013) 'Promoter deletion analysis using a dual-luciferase reporter

system', *Methods in Molecular Biology*. doi: 10.1007/978-1-62703-284-1_7.

Yariv Greenshpan, Omri Sharabi , Ksenia M Yegodayev, Ofra Novoplansky , Moshe Elkabets, R. G. A. P. (2022) 'The Contribution of the Minimal Promoter Element to the Activity of Synthetic Promoters Mediating CAR Expression in the Tumor Microenvironment', *International Journal of Molecular Sciences*.

Yu, L., Wang, L. and Chen, S. (2010) 'Endogenous toll-like receptor ligands and their biological significance', *Journal of Cellular and Molecular Medicine*. doi: 10.1111/j.1582-4934.2010.01127.x.

Zakkar, M. *et al.* (2008) 'Increased endothelial mitogen-activated protein kinase phosphatase-1 expression suppresses proinflammatory activation at sites that are resistant to atherosclerosis', *Circulation Research*. doi: 10.1161/CIRCRESAHA.108.183913.

Zakkar, M. *et al.* (2009) 'Activation of Nrf2 in endothelial cells protects arteries from exhibiting a proinflammatory state', *Arteriosclerosis, Thrombosis, and Vascular Biology*. doi: 10.1161/ATVBAHA.109.193375.

Zeng, L. *et al.* (2009) 'Sustained activation of XBP1 splicing leads to endothelial apoptosis and atherosclerosis development in response to disturbed flow', *Proceedings of the National Academy of Sciences of the United States of America*. doi: 10.1073/pnas.0903197106.

Zhang, J. and Friedman, M. H. (2013) 'Adaptive response of vascular endothelial cells to an acute increase in shear stress frequency', *American Journal of Physiology - Heart and Circulatory Physiology*. doi: 10.1152/ajpheart.00174.2013.

Zhou, A. X. and Tabas, I. (2013) 'The UPR in atherosclerosis', *Seminars in Immunopathology*. doi: 10.1007/s00281-013-0372-x.

Zhu, X., Huang, H. and Zhao, L. (2022) 'PAMPs and DAMPs as the Bridge Between Periodontitis and Atherosclerosis: The Potential Therapeutic Targets', *Frontiers in Cell and Developmental Biology*. doi: 10.3389/fcell.2022.856118.